

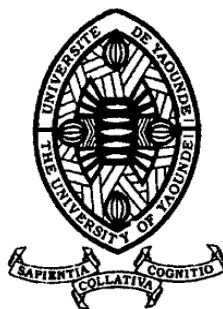
REPUBLIQUE DU CAMEROUN
Paix-Travail-Patrie

UNIVERSITE DE YAOUNDE I

CENTRE DE RECHERCHE ET DE
FORMATION DOCTORALE EN
SCIENCES, TECHNOLOGIES ET
GEOSCIENCES

UNITE DE RECHERCHE ET DE
FORMATION DOCTORALE
PHYSIQUE ET APPLICATIONS
B.P 812 Yaoundé

Email: crftstg@uyi.uninet.cm



REPUBLIC OF CAMEROON
Peace-Work-Fatherland

THE UNIVERSITY OF YAOUNDE I

POSTGRADUATES SCHOOL OF
SCIENCE, TECHNOLOGY AND
GEOSCIENCES
RESEARCH AND POSTGRADUATE
TRAINING UNIT FOR PHYSICS AND
APPLICATIONS

P.O.BOX 812 Yaoundé
Email: crftstg@uyi.uninet.cm

DEPARTMENT OF PHYSICS
LABORATORY OF NUCLEAR, ATOMIC, MOLECULAR PHYSICS
AND BIOPHYSICS

**NONLINEAR DYNAMICS OF MARCKS PROTEIN
BETWEEN CYTOPLASMIC MEMBRANE AND
CYTOSOL: INHOMOGENEITY EFFECT**

THESIS

Submitted and defended in Fulfillment of the Requirements for the
award of the Degree of **Doctorate/Ph.D** in Physics

Option: Atomic, Molecular Physics and Biophysics

By:

FOUEDJI Chenceline

Registration number: 12W0734

Master in Physics

**Under the supervision of
EKOBENA FOU DA Henri Paul**

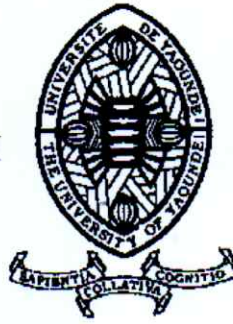
Professor

University of Yaoundé I



YEAR : 2024

UNIVERSITE DE YAOUNDE I
UNIVERSITY OF YAOUNDE I



FACULTE DES SCIENCES
FACULTY OF SCIENCE

DEPARTEMENT DE PHYSIQUE
DEPARTMENT OF PHYSICS

ATTESTATION DE CORRECTION DE LA THESE DE DOCTORAT/Ph.D

Nous, Professeur **MVOGO Alain** et Professeur **BEN-BOLIE Germain**, respectivement Examineur et Président du jury de la Thèse de Doctorat/Ph.D de Madame **FOUEDJI Chenceline**, Matricule **12W0734**, préparée sous la direction du Professeur **EKOBENA FOUA Henri Paul**, intitulée : « **NONLINEAR DYNAMICS OF MARCKS PROTEIN BETWEEN CYTOPLASMIC MEMBRANE AND CYTOSOL: INHOMOGENEITY EFFECT** », soutenue le **mercredi 31 Juillet 2024**, en vue de l'obtention du grade de Docteur/Ph.D en Physique, Spécialité Physique Nucléaire, Atomique, Moléculaire et Biophysique, option Physique Atomique, Moléculaire et Biophysique, attestons que toutes les corrections demandées par le jury de soutenance ont été effectuées.

En foi de quoi, la présente attestation lui est délivrée pour servir et valoir ce que de droit.

Fait à Yaoundé, le **28.06.2024**.....

Examineur


Px. Mvogo Alain
Maitre de Conférences

Le Président du jury


Ben-Bolie Germain Hubert
Professeur

Le Chef de Département de Physique



Jean-Marie Biemvema
Professeur

Dedication

I dedicate this thesis to :

*My late father, **NGUEFFO Martin** and my mother **AZONLEFACK Melanie**.*

Acknowledgements

At the end of this Ph.D. thesis, I am grateful and honored to have walked the steps of intellectual challenges amongst brilliant minds below. Under their guidance, I have gained insights. I hereby reiterate my utmost appreciations to all of you:

- ♣ To The **Almighty God, the Father** maker of all living and intelligent creatures.
- ♣ My Supervisor, **Professor Henri Paul EKOBENA FOUA**, for his guidance, advices and critical analysis during this thesis .
- ♣ The esteemed members of the jury of this dissertation and to the anonymous reviewers of the publications on which this dissertation is based.
- ♣ **Professor Luc Calvin OWONO OWONO**, Vice Rector of the University of Yaounde 1 for his teaching specially in atomics, molecular physics.
- ♣ **Professor Jean-Marie Bienvenu DJAKA**, Head of the Physics Department and **Professor Germain Hubert BEN-BOLIE**, Head of the Nuclear, Atomic, Molecular Physics and Biophysics Laboratory, I am grateful for their relentless and combined efforts providing to students.

♣ The teaching staff of the Physics Department for advice, as well as the highly instructive challenges thrown at us since our undergraduate studies.

♣ **Professor Conrad Bertrand TABI** and **Doctor Armand Sylvain ETEME** for our invaluable discussions. Their timely suggestions shaped in great detail my scientific aptitudes.

♣ My teachers: **Professor Timoléon Crépin KOFANE**, **Professor Paul WOAFU**, **Professor Serge ZEKENG**, **Professor Clement TCHAWOUA**, **Professor Alain MVOGO**, **Professor Germaine DJUDJE**, **Professor Debortini VONDOU**, **Professor Bertrand BODO**, **Professor Jacques HONA**, **Professor Blaise Roméo NANA NBENJO**, and **Dr ABDOURAHIMI**.

♣ I hereby thank **Doctor Didier BELOBO BELOBO**, **Doctor Adamou DANG KOKO**, **Doctor Carlos GNINZANLONG**, **Doctor Dieudonné ZANGA**, for their continue input over the years of my Ph.D studies.

♣ I thank the **African Centre for Advanced Studies (ACAS)** that gave me the opportunities

to performed my numerical resolutions of ordinary and partial differential equations.

♣ My friends: **Doctor Armstrong FORWAH TAH, Doctor Arnold Pavel NDJAWA YOMI, Franky Kévin NANDO TEZOH, Blaise DZOU TABI, Eric M SIGNE, S.N MUNDIH, Aïcha GBOULIE** for our constructive discussions.

♣ I also wish to thank my classmates and the Biophysics laboratory who have been of tremendous moral support during my research studies.

♣ My late father **Martin NGUEFFO**, my mother, **Melanie AZONLEFACK**, my brothers and my sisters for their love, advice, and care throughout my Ph.D. studies.

♣ My husband, **Guy LEKEUFACK**, and my children **Helena LEKEUFACK, Rowan LEKEUFACK, Fredy LEKEUFACK** and **Cheguy LEKEUFACK**.

♣ I am deeply grateful to **Professor KEKEUNOU Sevilor** for all his support and kind attention during this thesis.

♣ Mr and Mrs **ANANFACK**, Mrs **Colette ZITSA** and Mrs **Helene ANOUMEDEM** for all their support.

♣ All those from who near or far have accompanied me during these doctoral years.

Contents

Dedication	i
Acknowledgments	ii
Abstract	xi
Résumé	xii
List of Abbreviations	xiii
GENERAL INTRODUCTION	1
1 Literature review on protein kinase C and traveling waves	4
1.1 Introduction	4
1.2 Generality on Proteins	4
1.2.1 Cell membrane	6
1.2.2 Phosphorylation of protein	7
1.3 Structure and function of MARCKS protein	8
1.3.1 Function of protein kinase C in the cell	8
1.3.2 Pathophysiological roles of MARCKS in hematological malignancies	12
1.3.3 Inhomogeneity effect in MARCKS protein dynamics	12
1.4 Mechanical models for generating pattern and form in development	13
1.4.1 Karin John and Markus Bär model	13
1.4.2 Sergio and Markus model	15
1.4.3 Sergio and Dietrich model	21
1.4.4 Turing model	23
1.5 The soliton concept in the protein media	25
1.6 Conclusion	27

2	Mathematical Background and Methodology	28
2.1	Introduction	28
2.2	Reaction Diffusion model	28
2.2.1	MARCKS dynamics diagram	29
2.2.2	MARCKS protein model with homogenous diffusion coefficients	30
2.2.3	MARCKS protein model with the inhomogeneity effect	31
2.3	Analytical methods	32
2.3.1	The reductive perturbation method	32
2.3.2	The Hirota Bilinear Method (HBM)	42
2.3.3	Leon and Manna method	45
2.4	Numerical schemes	49
2.4.1	Finite difference Method	49
2.4.2	The fourth order Runge-Kutta method (RK4)	50
2.5	Conclusion	51
3	RESULTS AND DISCUSSION	52
3.1	Introduction	52
3.2	Multisolitons-like patterns in homogeneous MARCKS protein cyclic model	52
3.2.1	Domain formation of MARCKS protein through modulational instability	52
3.2.2	Multisolitons-like MARCKS patterns based on analytical predictions	57
3.2.3	Multisolitons-like MARCKS patterns based on numerical experiments	58
3.3	Traveling wave with inhomogeneous diffusion effect in MARCKS protein dynamic	66
3.3.1	Linear stability analysis	66
3.3.2	Weakly nonlinear solutions	67
3.4	Conclusion	69
	GENERAL CONCLUSION AND OUTLOOKS	70
	Appendices	72
3.4.1	Appendix A_1 : Coefficients of Eqs.(3.1)	72
3.4.2	Appendix A_2 : Coefficients of Eq.(3.5)	73
3.4.3	Appendix A_3 : Coefficients of Eq.(3.6)	74
	Bibliography	75

List of Figures

1.1	Protein structure [40].	5
1.2	Girl with kwashiorkor [40]	6
1.3	Molecular view of the cell membrane with examples of different types of proteins embedded into the lipid bilayer. Figure taken from [40].	7
1.4	The phosphorylation of a protein can make it active or inactive. Phosphorylation can either activate a protein (orange) or inactivate it (green). Kinase is an enzyme that phosphorylates proteins. Phosphatase is an enzyme that dephosphorylates proteins [42].	8
1.5	Model of the regulation of cytoskeletal rigidity by MARCKS, protein kinase C and calmodulin Ca^{2+} [40].	10
1.6	MARCKS structure and the electrostatic switch mechanism. (A) MARCKS contains three highly conserved domains: an N-terminal myristoylation domain, <i>MH2</i> domain of unknown function, and the ED which contains three serines that are phosphorylated by PKC. (B) When the ED of MARCKS is unphosphorylated, positively charged amino acid residues interact with negatively charged phospholipids in the inner leaflet to the plasma membrane, and the N-terminal myristate inserts into the plasma membrane. Phosphorylation by PKC or association with Ca^{2+} /calmodulin abolishes the affinity between the ED and the plasma membrane, and MARCKS translocates to the cytosol [53].	11
1.7	Linear stability of the uniform steady-state solution of equations Eq.(1.1) in the $k_{PKC} - u$ plane. [18].	15
1.8	Dependence of the values of the physical solutions (m, c, p) of Eq.(1.2) for $\gamma_1 = 6s^{-1}$ (a) and $\gamma_1 = 14s^{-1}$ (b). The solid and dashed lines correspond to stable and unstable solutions, respectively. Parameters of the model: $\gamma_2 = 10s^{-1}$, $\gamma_3 = 100s^{-1}$, $km = 0.01$, $D = 25\mu m^2 s^{-1}$ and $D_m = 0.5\mu m^2 s^{-1}$. [18].	16

1.9	Sketches of the mechanisms. a) Sketch of the Goldbeter-Koshland mechanism of protein phosphorylation and dephosphorylation applied to MARCKS protein. b) Sketch of the myristoyl-electrostatic switch. The binding and unbinding of MARCKS and PKC proteins, and the phosphorylation and dephosphorylation of MARCKS proteins by kinase (PKC) and phosphatase (PPA) is shown [90].	17
1.10	Effects of an spike of Ca^{2+} on the distribution of MARCKS and PKC. a) Evolution of Ca^{2+} concentration Eq.(1.6). b) Evolution of PKC at the membrane and in the cytoplasm Eq.(1.5). c) Evolution of MARCKS at the membrane and in the cytoplasm: free and phosphorylated Eq.(1.4) [90].	20
1.11	Sketch of the attachment-detachment mechanism of MARCKS and PKC and of the phosphorylation of MARCKS by PKC [86].	21
1.12	Temporal evolution of m (solid line) and θ (dashed line) at the monolayer (a), and of the fractions ϕ_M (solid line) in the subphase (b). Parameters of the numerical simulations: $D_M = 160\mu m^2 s^{-1}$, $K_m^+ = 1s^{-1}$, $k_1 = 1$, $K_m^- = 2 \times 10^{-5} s^{-1}$, $\phi_M = 3$. [86].	24
1.13	Expression of kinetics for the Gierer Meinhardt activator inhibitor system [102]. . .	25
1.14	Small amplitude of travelling wave solution [81].	27
2.1	Sketch of the myristoyl-electrostatic switch. The red objects represent membrane proteins (M), green objects phosphorylated proteins (P) and yellow objects free cytosolic proteins (C). Reaction rates are correspondingly noted [18].	30
2.2	The membrane structure and protein attachment during different phases ($a - d$) of the oscillation. The bright parts of the background symbolize the disordered phase of the membrane and the dark parts the ordered phase. The green dots indicate MARCKS molecules while the red dots stand for PKC. The right figure shows the membrane associated variables amount of membrane bound MARCKS in green, the amount of membrane bound PKC in red [47].	32
2.3	The dispersion relation of Eq.2.8. Parameters are chosen as $k_m = 0.1$, $D_m = 0.5\mu m^2 s^{-1}$, $D = 10.0\mu m^2 s^{-1}$, $\gamma_1 = 6.0s^{-1}$, $\gamma_2 = 1.0s^{-1}$, $\gamma_3 = 5.0s^{-1}$	36
2.4	The group velocity of Eq.2.9. Parameters are chosen as $k_m = 0.1$, $D_m = 0.5\mu m^2 s^{-1}$, $D = 10.0\mu m^2 s^{-1}$, $\gamma_1 = 6.0s^{-1}$, $\gamma_2 = 1.0s^{-1}$, $\gamma_3 = 5.0s^{-1}$	38
3.1	Qualitative characterization of MI through 3D view of stability/instability regions according to the criteria given in Eq.(3.8). The products $P \times Q_r$ on the left columns and $Q_i \times R_r$ on the right columns are plotted in: $k - \gamma_1$ plane in the first row while taking $\gamma_3 = 25s^{-1}$ and $D = 10\mu m^2 s^{-1}$; $k - \gamma_3$ plane in the second row while taking $\gamma_1 = 10s^{-1}$ and $D = 10.0$; $k - D$ plane in the third row while taking $\gamma_1 = 10s^{-1}$ and $\gamma_3 = 25s^{-1}$. The other parameters are $k_m = 0.1$, $D_m = 0.5\mu m^2 s^{-1}$, $\gamma_2 = 1.0s^{-1}$. Instability regions appear when both products are simultaneous positive.	56

3.2 Quantitative characterization of MI through features of the maximal MI growth rate Γ_{max} . In panels (a_j), Γ_{max} is plotted versus γ_1 while fixing $\gamma_3 = 25.0s^{-1}$ and $D = 10.0\mu m^2s^{-1}$. In panels (b_j), Γ_{max} is plotted versus γ_3 while fixing $\gamma_1 = 10.0s^{-1}$ and $D = 10.0\mu m^2s^{-1}$. In panels (c_j), Γ_{max} is plotted versus D while fixing $\gamma_1 = 10.0s^{-1}$ and $\gamma_3 = 25.0s^{-1}$. The left panels correspond to the long wavelength instability ($k = 0.05\pi$), while the right panels correspond to the mean wavelength instability ($k = 0.25\pi$). The other parameters are: $k_m = 0.1$, $D_m = 0.5\mu m^2s^{-1}$, $\gamma_2 = 1.0s^{-1}$ 57

3.3 The spatiotemporal dynamics of MARCKS protein obtained from analytical solutions of Eq.(2.23). Parameters are chosen as $k_m = 0.1$, $D_m = 0.5\mu m^2s^{-1}$, $D = 10.0\mu m^2s^{-1}$, $\gamma_1 = 10.0s^{-1}$, $\gamma_2 = 1.0s^{-1}$, $\gamma_3 = 25.0s^{-1}$ and $k = 0.05\pi\mu m^{-1}$ 58

3.4 The spatiotemporal dynamics of MARCKS protein obtained from analytical solutions of Eq.(2.23). Parameters are chosen as $k_m = 0.1$, $D_m = 0.5\mu m^2s^{-1}$, $D = 10.0\mu m^2s^{-1}$, $\gamma_1 = 10.0s^{-1}$, $\gamma_2 = 1.0s^{-1}$, $\gamma_3 = 25.0s^{-1}$ and $k = 0.05\pi\mu m^{-1}$ 59

3.5 The spatiotemporal dynamics of MARCKS protein obtained from numerical simulations of Eqs.(2.3 - 2.4). Parameters are chosen as $k_m = 0.1$, $D_m = 0.5\mu m^2s^{-1}$, $D = 10.0\mu m^2s^{-1}$, $\gamma_1 = 10.0s^{-1}$, $\gamma_2 = 1.0s^{-1}$, $\gamma_3 = 25.0s^{-1}$ and $k = 0.05\pi\mu m^{-1}$ 60

3.6 The spatiotemporal dynamics of MARCKS protein obtained from numerical simulations of Eqs.(2.3 - 2.4). Parameters are chosen as $k_m = 0.1$, $D_m = 0.5\mu m^2s^{-1}$, $D = 10.0\mu m^2s^{-1}$, $\gamma_1 = 10.0s^{-1}$, $\gamma_2 = 1.0s^{-1}$, $\gamma_3 = 25.0s^{-1}$ and $k = 0.05\pi\mu m^{-1}$ 61

3.7 The spatial multisolitons-like patterns of MARCKS protein obtained from numerical simulations of Eqs.(2.3 - 2.4) using solutions of Eq.(2.23) as initial conditions. The increasing of phosphorylation rate γ_1 for $k_m = 0.1$, $D_m = 0.5\mu m^2s^{-1}$, $D = 10.0\mu m^2s^{-1}$, $\gamma_2 = 1.0s^{-1}$ is observed. This feature is depicted at $t = 5ms$ in the long wavelength instability case, i.e., $k = 0.05\pi\mu m^{-1}$ 62

3.8 The spatial multisolitons-like patterns of MARCKS protein obtained from numerical simulations of Eqs.(2.3 - 2.4). The increasing of binding rate γ_3 is observed while $k_m = 0.1$, $D_m = 0.5\mu m^2s^{-1}$, $D = 10.0\mu m^2s^{-1}$, $\gamma_1 = 10.0s^{-1}$ and $\gamma_2 = 1.0s^{-1}$. This feature is depicted at $t = 5ms$ in the long wavelength instability case, i.e., $k = 0.05\pi\mu m^{-1}$ 63

3.9 The spatial multisolitons-like patterns of MARCKS protein obtained from numerical simulations of Eqs.(2.3 - 2.4). The increasing of the cytosolic diffusion coefficient D is observed while $k_m = 0.1$, $D_m = 0.5\mu m^2s^{-1}$, $\gamma_1 = 10.0s^{-1}$, $\gamma_2 = 10s^{-1}$ and $\gamma_3 = 25.0s^{-1}$. This feature is depicted at $t = 5ms$ in the long wavelength instability case, i.e., $k = 0.05\pi\mu m^{-1}$ 64

3.10 Time series for MARCKS protein at the position $x = 75\mu m$. Panels (a), (b) and (c) correspond, respectively to the concentration of MARCKS in membrane bound, in cytosol and in phosphorylated site. Space parameters are given by $k_m = 0.1$, $D_m = 0.5\mu m^2s^{-1}$, $\gamma_1 = 10.0s^{-1}$, $\gamma_2 = 1.0s^{-1}$, $\gamma_3 = 25.0s^{-1}$, $D = 10.0\mu m^2s^{-1}$ 65

- 3.11 The plot of the critical amplitude versus the wave number q of the carrier wave. We have fixed $D_0 = 1.1, D_1 = 0.09, D_2 = 0.05, \gamma_1 = 2, \gamma_2 = 10, \gamma_3 = 50, k_m = 0.1, D = 10$ as the model parameters. 68
- 3.12 The panels show the critical amplitude versus the wave number q . In panel (a) we have fixed $D_0 = 1.1, D_1 = 0.09, D_2 = 0.05$ and increase γ_1 . In panel (b) we fixed $\gamma_1 = 2.0$ and increased the diffusion coefficients (see legend for more readability). The remaining parameters of the model are: $\gamma_2 = 10.0, \gamma_3 = 50.0, k_m = 0.1, D = 10$. 68

List of Tables

1.1	Parameter values related to MARCKS dynamic of the model	18
1.2	Parameter values related to PKC dynamic of the model	19
1.3	Parameter values related to Ca^{2+} dynamic of the model	20

ABSTRACT

This thesis describes the nonlinear dynamics of myristoylated alanine-rich C kinase substrate (MARCKS) in the cell. The study model is based on a system of three reaction diffusion equations describing the concentration of myristoylated alanine-rich C kinase substrate protein from the cytoplasmic membrane to the cytosol and from the cytosol to the cytoplasmic membrane. We use analytical methods like the reductive perturbation techniques, and numerical methods such as the Runge kutta order 4 and the finite difference methods, to describe the formation and propagation of nonlinear waves in homogeneous and inhomogeneous media in the cells.

In the homogeneous medium, we transform the generic reaction diffusion model into a cubic complex Ginzburg-Landau equation. The analysis of stability leads to the derivation of the modulational instability (MI) criteria. On the basis of these criteria, we find the domains of some parameter space where nonlinear patterns are expected in the model. Analytical results on the growth rate instability predicts that the rate of phosphorylation and binding affect MARCKS protein dynamics. The rate of phosphorylation tends to support highly localized structures of the MARCKS protein, unlike the binding rate. We also notice that the increasing of the diffusion coefficient amplifies the appearance of patterns. Analytical predictions are confirmed by numerical simulations. These results show that, the cyclic transport of the MARCKS protein from the cytoplasmic membrane to the cytosol can be performed by means of a multisoliton wave.

In the inhomogeneous media, we take into account the effect of inhomogeneous diffusion modeled by an inhomogeneous diffusion coefficient, we show that unstable patterns are expected in the short wavelength domain. Additionally the increase of inhomogeneous diffusion coefficients induced a increasing in critical amplitude and expansion of instability regions . The results obtained during this thesis contribute to improved cell regeneration, regulation of the homeostasis of body fluids, secretion as well as mediation of the inflammatory response and in hematological malignancies.

Keywords: *MARCKS protein, phosphorylation, inhomogeneous diffusion, binding, multi-solitons, traveling waves, horizontal stripes, oblique stripes, modulational instability, dephosphorylation.*

RÉSUMÉ

Cette thèse décrit la dynamique non linéaire de la molécule myristoylée de substrat kinase C riche en alanine(MARCKS) dans la cellule. Le modèle d'étude est basé sur un système de trois équations de réaction diffusion décrivant la concentration de la protéine myristoylée riche en alanine, de la membrane cytoplasmique vers le cytosol et du cytosol vers la membrane. Nous utilisons des méthodes analytiques telle que l'approche des techniques de perturbations et les méthodes numériques dont la méthode de Runge Kutta d'ordre 4 et la méthode des différences finies pour décrire la formation et la propagation des ondes non linéaires en milieu homogène et en milieu inhomogène dans la cellule.

Dans le milieu homogène, nous transformons le modèle générique de réaction diffusion en une équation cubique complexe de Ginzburg-Landau. L'analyse de la stabilité linéaire nous conduit à la dérivation des critères de l'instabilité modulationnelle(IM). Sur la base de ces critères, nous trouvons les domaines de certains paramètres du système où des motifs non linéaires peuvent apparaître. Les résultats analytiques le taux de phosphorylation tend à soutenir des structures hautement localisées de la protéine MARCKS, contrairement au taux de liaison. On remarque également que l'augmentation du coefficient de diffusion amplifie l'apparition des motifs. Les prédictions analytiques sont confirmées par des simulations numériques. Ces résultats montrent que le transport cyclique de la protéine MARCKS de la membrane cytoplasmique au cytosol peut être effectué au moyen d'une onde de type multisolitons.

Dans les milieux inhomogènes, nous montrons que des motifs instables sont attendus dans le domaine des courtes longueurs d'onde. En outre, l'augmentation des coefficients de diffusion inhomogène induit une augmentation de l'amplitude critique et une expansion des régions d'instabilité. Nos études ont aussi révélé que l'effet de diffusion inhomogène modifie les structures du système. Les résultats obtenus au cours de cette thèse contribuent à l'amélioration de la régénération cellulaire, de la régulation de l'homéostasie des fluides corporels, la sécrétion ainsi que la médiation de la réponse inflammatoire et dans les des hémopathies malignes.

Mots clés: *protéine MARCKS, phosphorylation, diffusion inhomogène, liaison, multi-solitons, train d'ondes, ondes progressives, rayures horizontales, rayures obliques, instabilité modulationnelle, déphosphorylation.*

List of Abbreviations

ATP: Adenosine Triphosphate

MARCKS: Myristoylated Alanine-Rich C-Kinase Substrate

PKC: Protein Kinase C

DNLS: Discrete Nonlinear Schrödinger

PDE: Partial Differential Equation

GAP43: Growth Associated Protein

CAP23: Neuronal Protein

CCGL: Cubic Complex Ginzburg-Landau

MI: Modulational instability

HBM: Hirota Bilinear Method

AML: Acute Myeloid Leukemia

GENERAL INTRODUCTION

The Myristoylated Alanine-Rich C-Kinase Substrate (MARCKS) is a peripheral membrane protein, particularly abundant in the nervous system. It plays an important role in embryonic development, adult brain plasticity, regeneration, and the inflammatory response. In adult vertebrates, MARCKS proteins are very important for multiple regenerative processes, including the regeneration of peripheral nerves in the appendages and tail [1]. MARCKS protein has recently emerged as an important component of cellular map, governing a wide variety of protein interactions in every cell type within the brain. The experimental study of the interactions between the MARCKS protein, phospholipids and protein kinase C PKC was carried out at three levels: in vitro experiments where MARCKS interacts with vesicles composed of neutral and acidic phospholipid [2–6,47], in vitro experiments where MARCKS and PKC interact with a monolayer. Langmuir formed from a mixture of acidic and neutral phospholipid [7–10], and in vivo experiments with living cells subjected to external disturbances [11–14]. In vitro experiments make it possible to control the distributions of phospholipid on vesicles and in Langmuir monolayers. The above allow the characterization of the protein response to different concentrations of phospholipid acid and the performance of dynamic experiments by the introduction of activated PKC [5, 10]. A recent study on the interaction of MARCKS and PKC with a Langmuir monolayer [10] shows oscillations based on the nonlinear nature of protein-phospholipid interactions. In vivo experiments are more realistic, however, additional components in the cell can alter the dynamics. Other experiments show similar results for functionally related MARCKS proteins, like growth associated protein 43 (GAP43) and neuronal protein CAP23 [15].

Understanding the formation of spatiotemporal patterns in biological systems is relevant for regulatory processes in cells. This implies that, the ability to detect and analyze spatiotemporal patterns is essential for understanding how neural circuits function. Formation of spatiotemporal patterns in reaction-diffusion systems is also a common feature of self-organized chemical [16] and biological media [17]. Turing patterns in activator-inhibitor systems, traveling waves in excitable media are obtained in such nonlinear systems outside of equilibrium. Alonso and Bär [18] proposed a model which describes the spatio-temporal evolution of the concentration of the MAR-

CKS protein at the biomembrane involving: binding, phosphorylation and dephosphorylation of the MARCKS protein when the total number of proteins is conserved. Thus, conserved reaction-diffusion equations, have been discussed recently in references [19–23]. The pioneers have shown by using numerical simulations that the model presents two qualitatively different mechanisms of protein domain formation namely: phase separation linked to the long-wave instability of a membrane state with homogeneous protein coverage and stable coexistence of two states with protein coverage different homogeneous in bistable media.

Given the complexity of this model to be solved theoretically, no analytical study has been proposed up to date to compare the previous results. One of our main motivation in the present thesis is to highlight the implication of multi-solitons in the process of the transport of MARCKS protein from the membrane to cytosol and vice versa. In fact, since the suggestion of the nonlinear solitons mechanism for the localization and transport of vibrational energy and charges in proteins by Davydov and Kislukha [24], their study in biomolecules has become very active. Modulational instability (MI) is considered, to some extent, to be a precursor of soliton formation. In recent years, nonlinear systems have received considerable attention by researchers from different scientific domains such as biophysics, Bose-Einstein condensates, hydrodynamics, and magnetostatics [25–28]. Generally, MI is the direct way through which localized patterns emerge in nonlinear systems. It has been widely shown in recent contributions that it gives more generalized solitonic structures and is the best mechanism by which energy can be localized and transported in biological molecules such as DNA and proteins [29, 30]. By exploring Sergio and Markus model in continuous media, and showed that multi-solitons is a solution of coupled nonlinear equations. Kuramoto [31] demonstrated that all reaction-diffusion systems with a reaction dynamic close to the start of oscillations, can be reduced to an universal envelope equation, with a great predictive power, which is the cubic complex Ginzburg-Landau (CCGL) equation. This equation has therefore become an appropriate setup for the search and characterization of patterns in oscillatory media [32, 33].

MARCKS protein has been found to interact with a number of other proteins involved in processes ranging from intracellular signaling to process outgrowth. In fact, biological processes in nature are carried out in the presence of inhomogeneities [34]. Thus, the impact of inhomogeneous diffusion effect on MARCKS proteins patterns formation constitutes the second main motivation of this thesis. These inhomogeneities are due to defects caused by the presence of additional molecules in the cytoplasmic membrane and in the cytosol. During the last decades, effects of inhomogeneity on the regulation of some biological processes have been increasingly studied in different biological systems such as, alpha-helix proteins [34, 35], cardiac tissue [36], embryonic development [37], cellular automaton model for tumor [38], and Turing model [39]. It is well known that degenerative diseases are caused by incorrect protein folding. Also, biological processes in nature are carried out in a medium full of inhomogeneities.

During MARCKS protein dynamics, the main source of energy is ATP. However, for this

energy to be effective, it must be localized. So what are the necessary conditions to induce this localization of energy in homogeneous and inhomogeneous media? In this thesis, we will study the energy localization processes induced by ATP hydrolysis during MARCKS protein dynamics in the membrane and cytosol, in both continuous and discrete environments.

The rest of the work is outlined as follows: The first part is devoted to the literature review on PKC and traveling waves. We briefly present the role of Proteins Kinase *C*, in general, and of MARCKS, in particular, in the living cell. We also give the function of MARCKS in the cells and in the brain. We explain the origin of the soliton concept and give some applications of solitons. The second part is devoted to the methodology of investigations such as the analytical and numerical methods that are used to achieve our objectives. In the third part, we show by the means of MI that in the homogeneous media, the cyclic transport of MARCKS protein from membrane to cytosol may be done by means of multisolitons-like patterns. Instead, taking into account the inhomogeneities effects, we perform that an increase of spatial inhomogeneities effects leads to a transition from a spatial patterns of horizontal stripes to a spatial pattern of oblique stripes. Finally, we end this work with a general conclusion in which we present our main results and give some perspectives for the future works.

LITERATURE REVIEW ON PROTEIN KINASE C AND TRAVELING WAVES

1.1 Introduction

This chapter aims to present a literature review on PKC in general and on MARCKS in particular, then we would also present a type of mathematical model that describes this process. It is organized as follows: *In section 1.2*, we give a brief generality on protein. *Section 1.3* gives a brief review of the structure and the function of MARCKS in the brain. *Section 1.4* presents the mechanical models for generating pattern and form in development. *Section 1.5* reviews the soliton concept in the protein media. The chapter ends with a conclusion.

1.2 Generality on Proteins

To ensure their survival, cells must regulate a wide range of cellular functions, such as cell migration, cell growth, DNA synthesis, and cell division. For example, in order to produce two viable daughter cells, a cell must precisely coordinate cell growth with the duplication and segregation of DNA, and with subsequent cell division. These cellular functions, in turn, are controlled and coordinated by proteins. Proteins are biopolymeric structures composed of amino acids, of which are 20 common and found in biological chemistry, participating in nearly all cellular activities see Fig.(1.1). There are seven types of proteins: antibodies, contractile proteins, enzymes, hormonal proteins, structural proteins, storage proteins, and transport proteins. Proteins serve crucial roles in human biochemistry. The major role is to provide the body's building blocks. Protein helps repair and build body's tissues. It drives metabolic reactions, maintains pH and fluid balance, and keeps the immune system strong. Proteins transport, store nutriment and can act as an energy source. It is results of long chains repeating the same motif. These chains fold to form the secondary structure of the proteins, which is stabilized by the formation of hydrogen bonds between the different motifs.

Proteins are the precursors of several biologically relevant molecules, to realized their functions proteins should get the form depicted by Figure (1.1). Proteins control many vital functions in

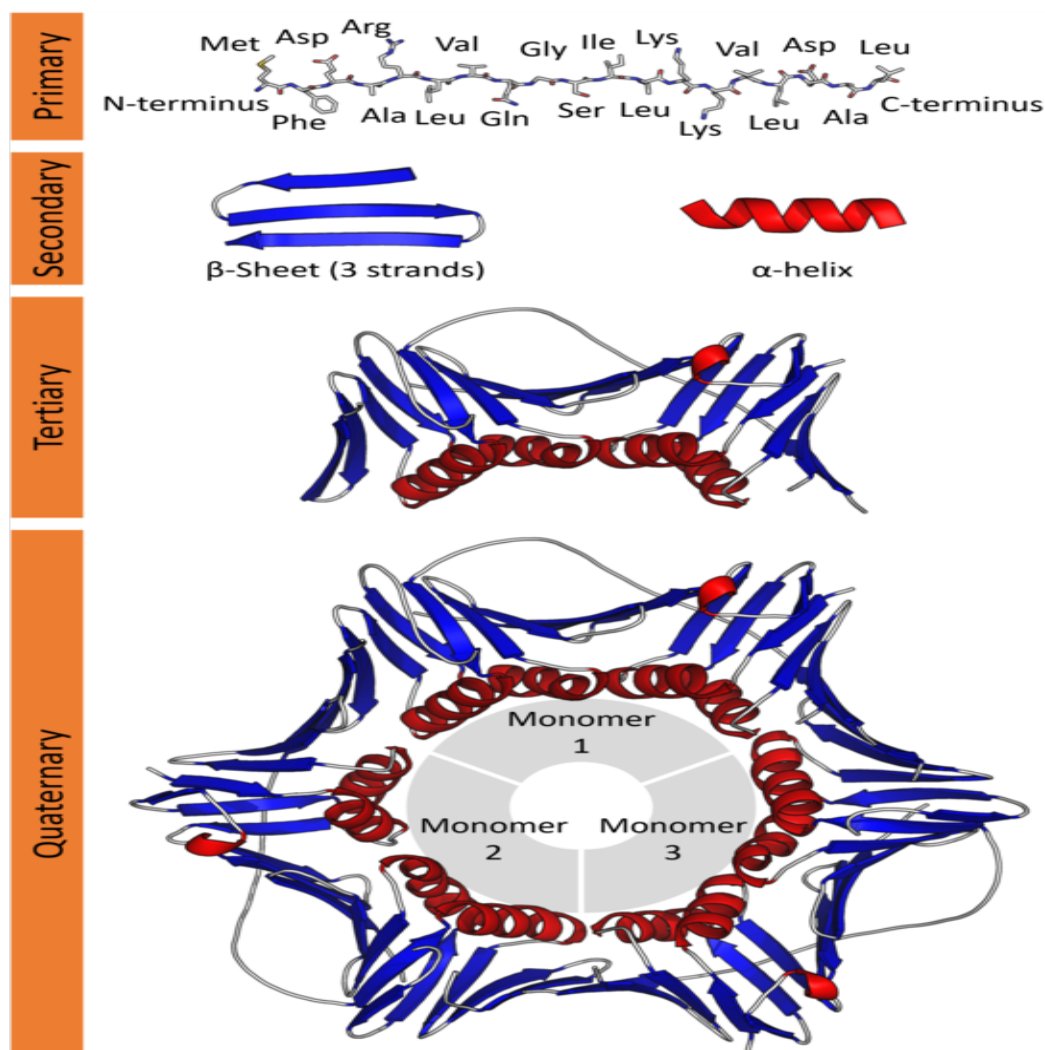


Figure 1.1: Protein structure [40].

living cells, such as cell growth and cell division. Reliable coordination of these functions requires the spatial and temporal organization of proteins within the cells, which encodes information about the cell's geometry and the cell-cycle stage. The idea that the collective organization of chemical reactions in an initially homogeneous medium can give rise to spatial patterns dates back to Turing's seminal work on spontaneous pattern formation in reaction-diffusion systems [41]. Such protein patterns arise from protein transport and reaction kinetics, and they can be controlled by various guiding cues within the cell. Therefore, either the excess or deficiency of protein can lead to disease in the nervous system, metabolic problems, organ failure, and even death. Protein deficiency can lead to kwashiorkor (Anorexia Nervosa) as showing in Fig.(1.2).



Figure 1.2: Girl with kwashiorkor [40]

1.2.1 Cell membrane

Membrane is a highly specialized compartment, which acts as a multiphysics scaffold holding many essential cellular functions including transport of molecules, communication, and metabolic properties. Mammalian cell membranes consist of a lipid bilayer composed of amphiphilic lipid molecules arranged in a $2D$ assembly, and proteins embedded or associated with it, which include ion channels as can be seen in Fig.(1.3). The plasma membrane is a dynamic structure that undergoes various changes across time and length scales. Cell membranes provide a barrier between cells and organelles that serves to maintain differences in chemical and electrical potentials by separating molecules and ions. The composition of cell membranes is very diverse: each membrane can contain from 500 to 1000 different types of lipids and its composition varies from cell to cell and from organism to organism. Furthermore, every membrane presents asymmetry, *i.e.*, the lipid

composition is different in each of the two leaflets. In particular, the inner monolayer contains more charged lipids than the outer one, the extra and intra-cellular fluid typically consists of sodium ions Na^+ , potassium ions K^+ , and Chloride Cl^- ions. Sodium ions Na^+ and Chloride Cl^- ions are at high concentrations in the extra-cellular region and low in the intracellular regions whereas potassium ions K^+ is at a high concentration inside the nerve cell and low outside. Since all charged lipids are negatively charged, the inside of the membrane is negatively charged with respect to the outside. The differences in the concentration of ions on each side of the membrane leads to a voltage called Membrane potential. The proteins act as selective ion transporters and lead to this concentration difference. The existing negatively charged fixed molecules inside the cell must be counterbalanced by cations, which is why the concentration of cations is higher inside than outside the cell. However, this high concentration of solutes inside the cell would lead to the continuous movement of water into the cell by osmosis. In order to establish an osmotic balance, the cell maintains a low concentration of cations inside the cell. In the membrane, there are also the presence of leak channels that are continuously open and allow the flow across the membrane. Nevertheless, due to the high number of leak channels, the flow out of the cell through the leak channels cannot be counteracted by the flow of pumped into the cell. In this situation, we find a net flow of cations out of the cell (down its concentration gradient), leaving an excess of negative charges inside the cell.

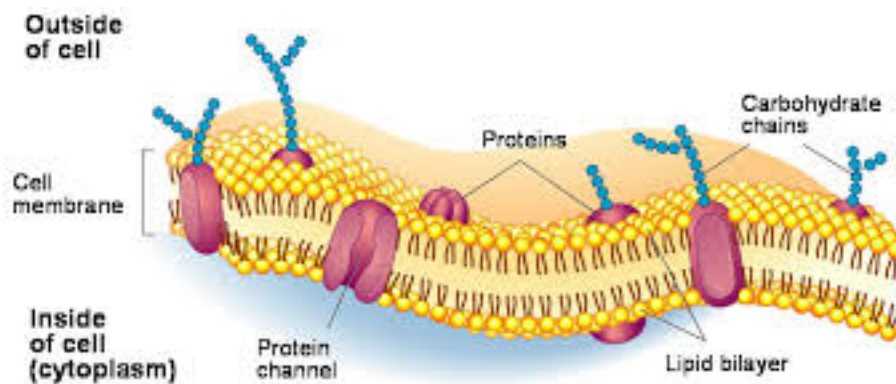


Figure 1.3: Molecular view of the cell membrane with examples of different types of proteins embedded into the lipid bilayer. Figure taken from [40].

1.2.2 Phosphorylation of protein

Proteins are sometimes altered after translation and folding are complete. In such cases, so-called transferase enzymes add small modifier groups, such as phosphates or carboxyl groups, to the protein. These modifications often shift protein conformation and act as molecular switches that turn the activity of a protein on or off. Many post-translational modifications are reversible, although different enzymes catalyze the reverse reactions. For example, enzymes called kinases

add phosphate groups to proteins, but enzymes called phosphatases are required to remove these phosphate groups Fig.(1.4).

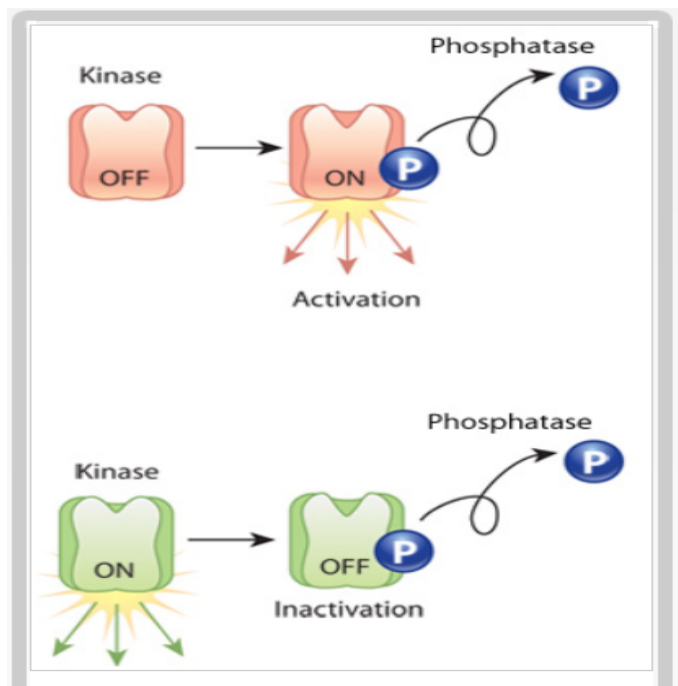


Figure 1.4: The phosphorylation of a protein can make it active or inactive. Phosphorylation can either activate a protein (orange) or inactivate it (green). Kinase is an enzyme that phosphorylates proteins. Phosphatase is an enzyme that dephosphorylates proteins [42].

Phosphorylation and dephosphorylation, catalysed by protein kinases and protein phosphatases, can modify the function of a protein in almost every conceivable way; for example by increasing or decreasing its biological activity, by stabilizing it or marking it for destruction, by facilitating or inhibiting movement between subcellular compartments, or by initiating or disrupting protein-protein interactions. Phosphorylation of MARCKS by PKC occurs at the membrane, while dephosphorylation of MARCKS in the cytosol. The simplicity, flexibility and reversibility of phosphorylation, coupled with the ready availability of ATP as a phosphoryl donor, explains its selection as the most general regulatory device adopted by eukaryotic cells [42]. It is thought that perhaps 30% of the proteins encoded by the human genome contain covalently bound phosphate, and abnormal phosphorylation is now recognized as a cause or consequence of many human diseases.

1.3 Structure and function of MARCKS protein

1.3.1 Function of protein kinase C in the cell

Protein kinase activity was first observed in 1954 when Gene Kennedy described a liver enzyme that catalysed the phosphorylation of casein in [43]. Soon after, Fischer and Krebs [44] as well as Wosilait

and Sutherland [45], found that the inter conversion of phosphorylase b to phosphorylase a involved a phosphorylation/dephosphorylation mechanism. In particular, Fischer and Krebs demonstrated that the b form could be converted to the a form in the presence of ATP. Phosphorylase kinase was subsequently shown to catalyse the transfer of the γ -phosphoryl group of ATP to a specific serine residue on phosphorylase b. The reconversion of phosphorylase a to phosphorylase b was therefore catalysed by a 'phosphate-releasing' enzyme, today called protein phosphatase 1 to reflect its much wider use in cell regulation.

Protein kinase C (PKC) is a family of related serine/threonine kinases and plays a key role in cellular responses such as neurotransmission, gene expression, regulation of cytoskeletal rigidity Fig.(1.5) cell growth and differentiation. It is a multimodule protein that is under acute conformational regulation. Myristoylated alanine-rich protein kinase C substrate (MARCKS) is a major PKC substrate that is distributed in various cell types. MARCKS has been implicated in cell motility, phagocytosis, membrane traffic and mitogenesis. Both phosphorylation and binding of cofactors induce long-range conformational changes that regulate inter domain interactions, of which the most central is the binding of the auto inhibitory pseudo substrate sequence to the substrate-binding cavity. Protein kinase C is the receptor for the tumor-promoting phorbol esters [46].

MARCKS is a 32 kDa protein with two functional domains that mediate interactions with the plasma membrane, the N-terminus and the effector domain (ED) [47]. It is a protein which binds to the membrane by electrostatic interaction, translocated from the membrane and phosphorylated by Protein Kinase C. Back into the cytoplasm the translocated MARCKS proteins are dephosphorylated by the enzyme phosphatase and can reattach to the membrane Fig.(1.6). These three processes (membrane binding, translocation, dephosphorylation) give rise to a cyclic dynamics known as the myristoyl-electrostatic switch. Salli *et al* [48] confirm the existence of MARCKS protein in bovine large luteal cells and demonstrate that phosphorylation of the protein is essential for initiation of the exocytotic process. It appears from these observations that phosphorylation of MARCKS protein is involved with the generation of a signal propagated via the interior cytoskeletal matrix to ensure mobilization of secretory vesicles. The similar affinities for calmodulin of MARCKS, considering both the theoretical differences between their calmodulin binding domains and the structural features of known calmodulin binding domains. Calmodulin generally binds to basic, amphiphilic α -helices of approximately 20 amino acids [49].

MARCKS is localized on the plasma membrane, and the binding of MARCKS to the plasma membrane requires hydrophobic insertion of its myristate chain into the bilayer and also electrostatic interaction of the cluster, of the basic residues in the effector domain with acidic lipids Fig.(1.6). Phosphorylation of MARCKS by PKC introduces negative charges into the basic cluster, reducing the electrostatic interaction with acidic lipids. In many cell types, this results to the translocation of MARCKS from the membrane to the cytoplasm. Mutation of N-terminal glycine results in a non-myristoylated form of MARCKS being localized in the cytosol [50].

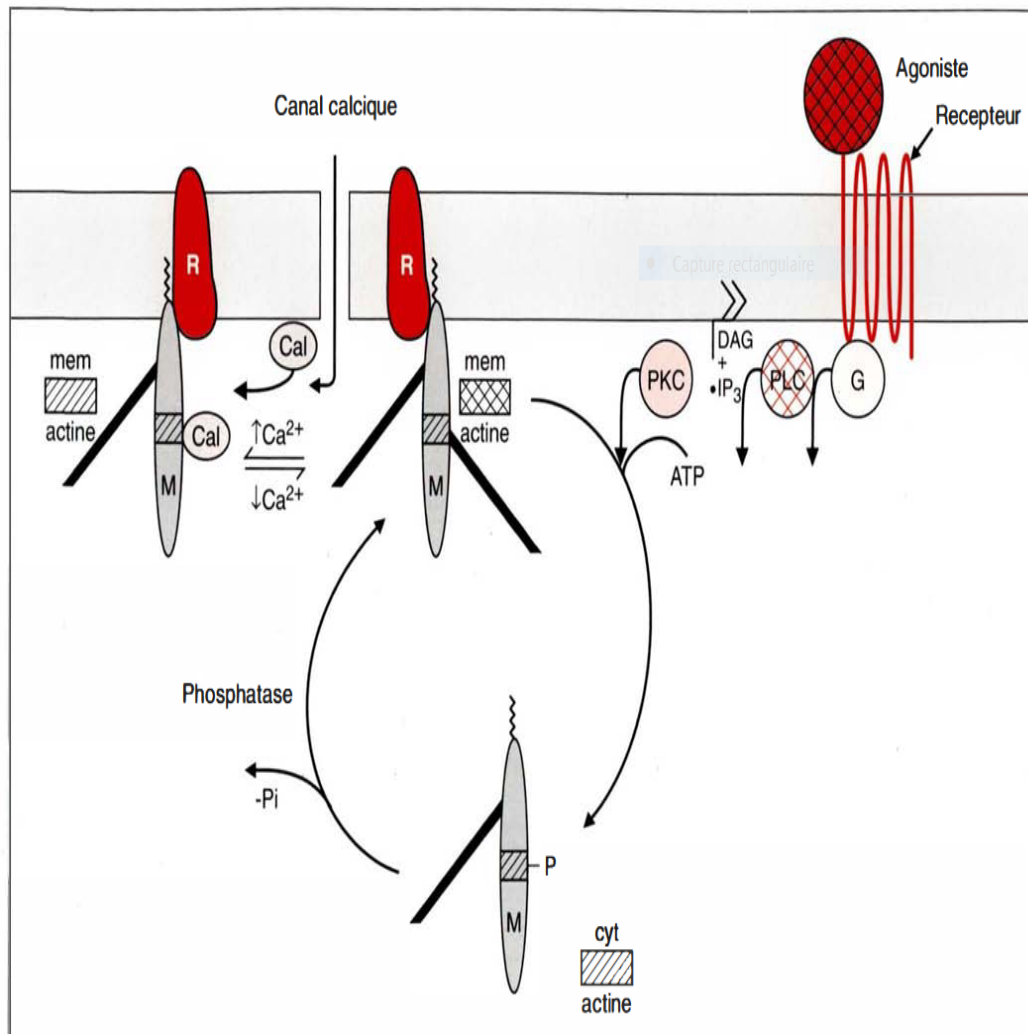


Figure 1.5: Model of the regulation of cytoskeletal rigidity by MARCKS, protein kinase C and calmodulin Ca^{2+} [40].

MARCKS, a major cellular substrate for protein kinase C plays an important role in the living world: it is involved in the regulation of the homeostasis of body fluids, blood coagulation, cell motility, vesicular traffic, secretion as well as mediation of the inflammatory response. Since MARCKS was first identified as a primary target of protein kinase C [51], it has emerged as an essential regulator of the dynamic actin cytoskeleton, membrane phosphoinositides, and many highly localized molecular interactions, with diverse roles in a variety of cell types, tissues, and organs. These roles have been heavily investigated in the brain, where the modulation of these pathways is critical for fundamental processes such as neurite outgrowth, exocytosis, and synaptic plasticity. These varied functions have revealed MARCKS as an integral player in a host of physiological processes and novel etiologies, ranging from development of the cerebral cortex [15, 52]. Recently, it has also been identified as important players in regeneration and inflammatory response. The ability of MARCKS to induce cellular migration underlies its effects on regeneration and cancer. It

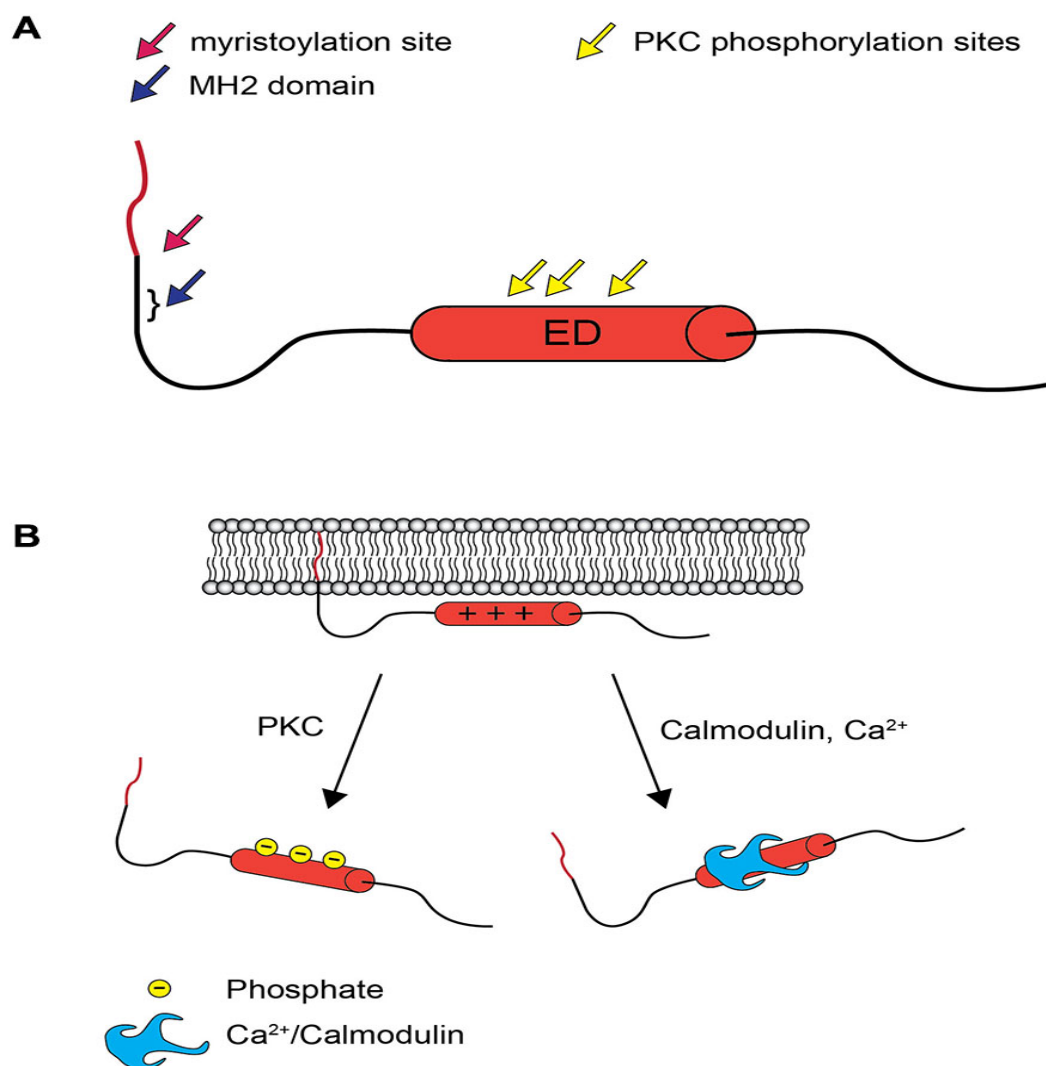


Figure 1.6: MARCKS structure and the electrostatic switch mechanism. (A) MARCKS contains three highly conserved domains: an N-terminal myristoylation domain, *MH2* domain of unknown function, and the ED which contains three serines that are phosphorylated by PKC. (B) When the ED of MARCKS is unphosphorylated, positively charged amino acid residues interact with negatively charged phospholipids in the inner leaflet to the plasma membrane, and the N-terminal myristate inserts into the plasma membrane. Phosphorylation by PKC or association with Ca^{2+} /calmodulin abolishes the affinity between the ED and the plasma membrane, and MARCKS translocates to the cytosol [53].

is involved in the regulation of cell migration, secretion, proliferation and differentiation in many different tissues. For example, mice carrying loss of function mutations when MARCKS genes die shortly after birth due to multiple deficiencies including detrimental neural tube closure defects. In adult vertebrates, MARCKS continue to be important for multiple regenerative processes including peripheral nerve, appendage, and tail regeneration [1].

1.3.2 Pathophysiological roles of MARCKS in hematological malignancies

Among several other functions, MARCKS protein has been identified as a vital controller of secretion in various cell types. Moreover, phosphorylated MARCKS has a recognized role in the migration of inflammatory leukocytes such as neutrophils and macrophages, besides secretion of inflammatory cytokines [54–57]. Indeed, within the hematological system, several such regulatory roles of MARCKS have been observed. By modulating the availability of free PIP₂, MARCKS or MRP adjusts the epithelial sodium channel open probability that has a remarkable role in the regulation of total body fluid homeostasis and blood pressure control [58, 59]. Whereas the functional influence of MARCKS on cellular systems extends beyond developmental and maintenance workflow, numerous studies have now indicated that anomalous expression of MARCKS is often associated with several cancers. Extensive data suggest that dysregulated MARCKS expression drives the development and progression of several solid tumors including melanoma [60–62], glioma [63–65], renal cell carcinoma [66], lung cancer [67, 68], colorectal cancer [69, 70], liver cancer [71, 72], and breast cancer [73–75]. Similarly, aberrant MARCKS has been observed to contribute to increased cell proliferation, reduced cell death, higher rates of cell migration, invasion, and motility, and malignant transformation in several hematological malignancies. In addition to its role in the development and progression of hematological malignancies, MARCKS has been implicated in defining the overall outcome in several blood cancers. A high expression of MARCKS has been reported to be associated with an overall poor disease prognosis in AML [76]. Hence, patients with MARCKS-driven blood cancers have a higher risk of disease progression or recurrence and an overall worse prognosis [77–79]. Consequently, targeting MARCKS, whether directly or indirectly, is a viable therapeutic alternative with landmark clinical repercussions for the treatment of several solid and blood cancers.

1.3.3 Inhomogeneity effect in MARCKS protein dynamics

Inhomogeneity in MARCKS protein may occur due to different reasons. It may arise due to defects caused by the presence of additional molecules such as drugs, carcinogens, mutants and dyes in specific sites of the protein sequence [80]. Also the reasons for inhomogeneity or site dependence in exchange interactions may be one of the following reasons: The distance between neighbouring atoms may vary along the protein lattices, and the concentration of myristoylated alanine-rich C kinase substrate protein from the cytoplasmic membrane to the cytosol and from the cytosol to the cytoplasmic membrane .

1.4 Mechanical models for generating pattern and form in development

Development of spatial pattern and form is one of the central issues in embryology. The formation of structure in embryology is known as morphogenesis. Population level brain activity is often organized into propagating waves that are structured in both space and time. Such spatiotemporal patterns have been linked to brain function and observed across multiple recording methodologies and scales. Pattern generation models are generally grouped together as morphogenetic models. These models provide the embryologist with possible scenarios as to how pattern is laid down and how the embryonic form might be created. Broadly speaking the two prevailing views of pattern generation that have dominated the thinking of embryologists in the past few years are the long standing Turing chemical pre-pattern approach, and the mechanochemical approach developed by Oster and Murray [81]. The two approaches are basically quite different. In the chemical pre-pattern approach, pattern formation and morphogenesis take place sequentially. First the chemical concentration pattern is laid down, then the cells interpret this pre-pattern and differentiate accordingly. In this approach, morphogenesis is essentially a slave process which is determined once the chemical pattern has been established. Meanwhile, in the mechanochemical approach, pattern formation and morphogenesis is considered to go on simultaneously as a single process. Here the chemical patterning, the form-shaping movements of the cells and the embryological tissue interact continuously to produce the observed spatial pattern. The principal use of any theory is in its predictions. In this thesis we will be concerned by the chemical pre-pattern approach.

1.4.1 Karin John and Markus Bär model

The second potential mechanism for structure formation in membranes may be provided by reaction-diffusion processes involving the membrane. The living cell constitutes an open system that is kept out of thermodynamical equilibrium by its metabolism, which in turn is a basic requirement for reaction-diffusion induced pattern formation. Several studies have applied the RD mechanism to model the polarization of Dictyostelium cells. Therein, pattern formation in the cytoplasmic membrane requires reactive transformations of lipids involving a positive or negative feedback [82]. Karin and Markus propose a mathematical model wherein the molecular interactions between proteins and lipids are crucial for pattern formation in the membrane. It is desirable that mathematical models are based on experimentally well-studied systems, so that parameters and rate constants can be taken from experimental data, and quantitative predictions become possible. As a biologically important and welldocumented example authors chose the family of GMC proteins (*GAP43*, *MARCKS*, *CAP23*) [83], whose interactions with acidic lipids are regulated by a protein kinase C (PKC).

The model consists of four continuous mass balance equations, which describe reaction-diffusion

processes relevant for the myristolate electrostatic switch and take into account the diffusive transport of acidic lipids and GMC proteins in the presence of lipid-protein interactions at the membrane. We assume that GMC proteins can exist in three states, such as membrane bound unphosphorylated (m), cytosolic unphosphorylated (c) and cytosolic phosphorylated proteins (cp). Furthermore, we assume that the status of the membrane is described by the area fraction of acidic lipids p . The evolution equations of these four variables are then given by:

$$\begin{aligned}\frac{\partial P}{\partial t} &= -\nabla \cdot \vec{j}_p, \\ \frac{\partial m}{\partial t} &= R_m - \nabla \cdot \vec{j}_m, \\ \frac{\partial C}{\partial t} &= R_C + D_C \nabla^2 C, \\ \frac{\partial C_P}{\partial t} &= R_{CP} + D_C \nabla^2 C_P,\end{aligned}\tag{1.1}$$

where the reaction terms R_m, R_c and R_{cp} describe membrane binding and unbinding of the protein as well as its phosphorylation-dephosphorylation cycle. The vectorial quantities \vec{j}_m and \vec{j}_p denote the fluxes of acidic lipids and membrane bound GMC proteins in the plane of the membrane, where the reaction terms are:

$$\begin{aligned}R_m &= k_{ad}(1-m)c - k_{de}m \exp(-N_{up}) - k_{pkc} \frac{m}{k_m + m}, \\ R_c &= -k_{ad}(1-m)c + k_{de}m \exp(-N_{up}) + k_{ph}c_p \\ R_{cp} &= k_{pkc}^* \frac{m}{k_m + m} - k_{ph}c_p,\end{aligned}$$

with:

$$k_{pkc}^* = k_{pkc}(1-m) \frac{p^n}{k_p^n + p^n},$$

The results of the linear stability analysis of the uniform state of Eq.(1.1) are summarized in the phase diagram Fig.((1.7)).

Stationary domains as expected due to protein-lipid interactions for low or zero PKC activity. This case corresponds to quiescent cells, where GMC proteins are mainly membrane bound and colocalize with acidic lipids. Therefore, the resulting patterns described below are the phenomena that require the cooperation of non equilibrium chemistry and physical interactions. They have investigated mechanisms for pattern formation in bio membranes and shows that the cooperative action of intermolecular forces (here protein-lipid interactions) and biochemical reaction- diffusion

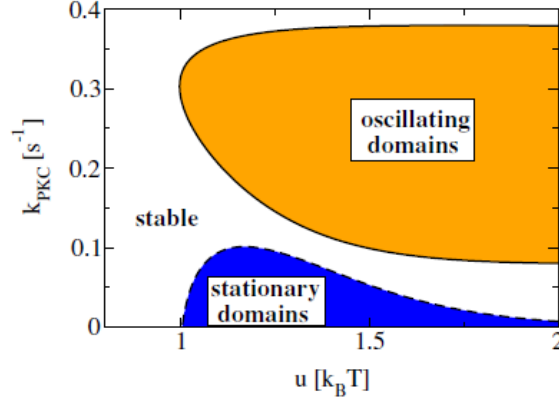


Figure 1.7: Linear stability of the uniform steady-state solution of equations Eq.(1.1) in the $k_{PKC} - u$ plane. [18].

processes is required for the appearance of oscillatory non equilibrium patterns in the membrane

1.4.2 Sergio and Markus model

Different approaches have been proposed to study the movements involved in the MARCKS molecule. These attempts have been appreciated in various ways in biology. Many authors focus their research in experimental studies [2, 84–86], meanwhile just a few focus on theoretical approach of this phenomenon. Phosphorylation and dephosphorylation of proteins are mechanisms of activation and deactivation which regulate many cellular processes; phosphorylation and dephosphorylation of proteins are usually modeled by the Goldbeter-Koshland mechanism [87]. MARCKS is a protein which binds to the membrane by electrostatic interaction. It is translocated from the membrane and phosphorylated by Protein Kinase C. Back in the cytoplasm the translocated MARCKS proteins are dephosphorylated by the enzyme phosphatase and can reattach to the membrane Fig.(1.10). These three processes (membrane binding, translocation, dephosphorylation) give rise to a cyclic dynamics known as the myristoyl-electrostatic switch. The first mathematical model of the interactions between the MARCKS protein, phospholipids and PKC was proposed in [88]. Authors start from a reaction-diffusion model taking into account mass conservation of the MARCKS proteins.

$$\begin{aligned}
 \frac{\partial m}{\partial t} &= \gamma_3 c(1 - m) - \gamma_1(1 - m) \frac{m}{k_m + m} + D_m \frac{\partial^2 m}{\partial x^2}, \\
 \frac{\partial c}{\partial t} &= -\gamma_3 c(1 - m) + \gamma_2 p + D \frac{\partial^2 c}{\partial x^2} \\
 \frac{\partial p}{\partial t} &= \gamma_1(1 - m) \frac{m}{k_m + m} - \gamma_2 p + D \frac{\partial^2 p}{\partial x^2},
 \end{aligned} \tag{1.2}$$

Eq.(1.2) is a non-dimensional version of a general model.

Some theoretical computation have been done in homogeneous media and they show that, one can have two different types of mechanisms that are: related to a long-wave instability of a membrane state with homogeneous protein coverage and stable coexistence of two states with different homogeneous protein coverage in bistable media. The mechanisms of wave instability is knowing to lead to traveling or standing waves, which will be of great interest in this thesis. They also evaluate the impact of the cytosolic volume on the occurrence of protein pattern formation by simulations in a three-dimensional model. And show that the explicit treatment of the volume in the model leads to an effective rescaling of the reaction rates.

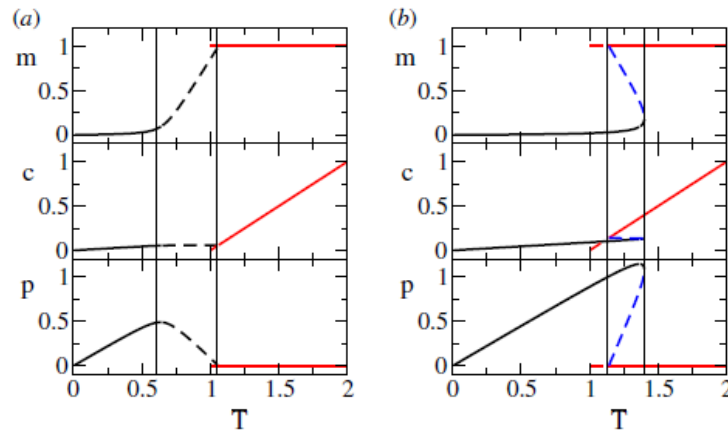


Figure 1.8: Dependence of the values of the physical solutions (m, c, p) of Eq.(1.2) for $\gamma_1 = 6s^{-1}$ (a) and $\gamma_1 = 14s^{-1}$ (b). The solid and dashed lines correspond to stable and unstable solutions, respectively. Parameters of the model: $\gamma_2 = 10s^{-1}$, $\gamma_3 = 100s^{-1}$, $km = 0.01$, $D = 25\mu m^2s^{-1}$ and $D_m = 0.5\mu m^2s^{-1}$. [18].

For low concentrations of proteins, there is only one physically meaningful solution which is stable. While for fixed $\gamma_1 = 6s^{-1}$ this solution may become unstable to long-wavelength perturbations, see Fig.(1.8) (a), and phase separation may develop, for $\gamma_1 = 14s^{-1}$ this solution coexists with the solution corresponding to a complete coverage of the membrane, see Fig.(1.8) (b).

Authors founded in this model of domain formation of MARCKS proteins at biomembranes that, there are three main ingredients in the model which facilitate protein domain formation. The difference between the diffusion constants of the proteins in the cytosol and on the membrane permits the formation of spatial structures in the membrane without any dynamical interaction with other proteins. The complex interaction among molecules in the membrane, requiring intermediate processes, induces nonlinearities in binding and unbinding rates. The nonlinearities are responsible for pattern formation and may give rise to oscillations and complex dynamics in membranes [89]. Furthermore, the third ingredient which determines many of the properties of the model is the conservation of the total number of proteins.

1.4. MECHANICAL MODELS FOR GENERATING PATTERN AND FORM IN DEVELOPMENT

Four years later, authors extended this studies by including the dynamics of binding and unbinding of PKC enzymes. Furthermore, they show that the model fits previous experimental results well and predicts, in addition, the formation of domains with high concentration of MARCKS proteins at the membrane. Using a quasi-steady approximation of the intermediate complexes, the original dynamics can be simplified to a couple of equations for the free and phosphorylated MARCKS (respectively $[MRK]_f$, and $[MRK]_p$) using Michaelis-Menten rates [17]:

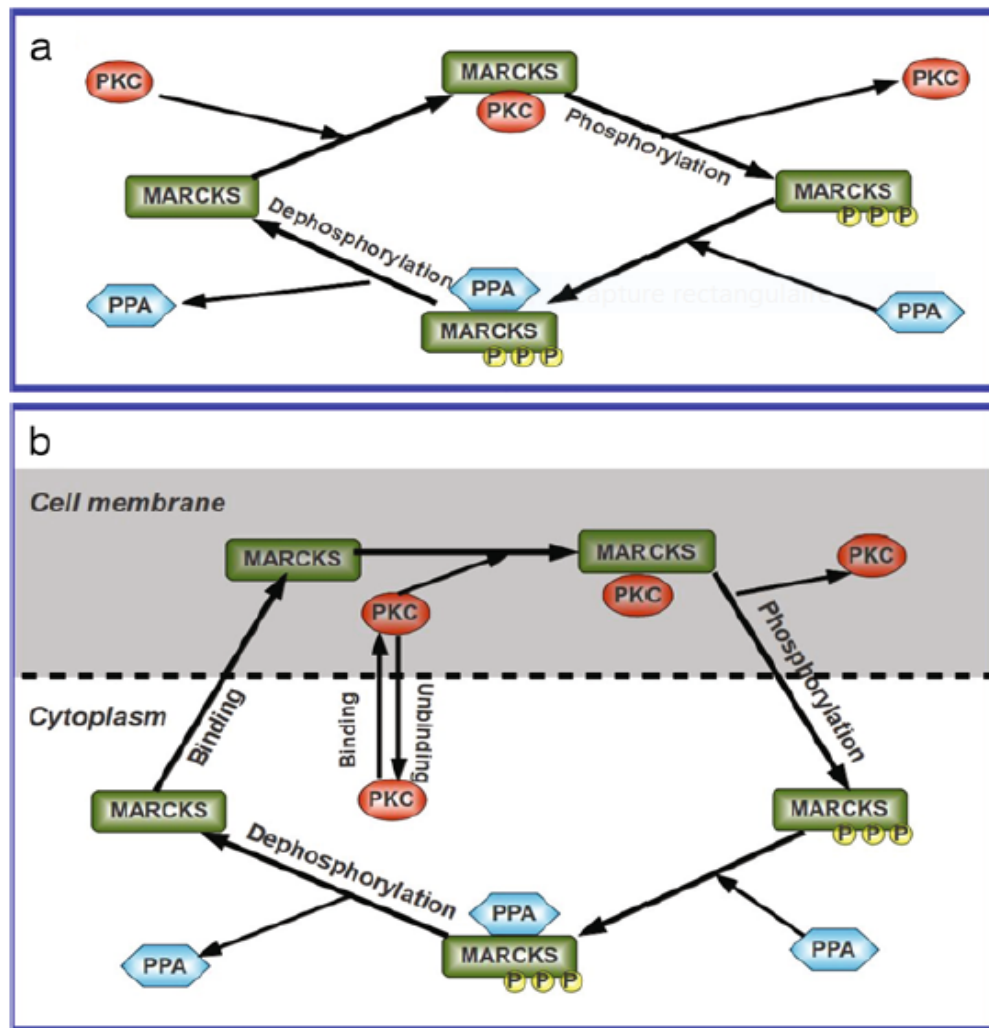


Figure 1.9: Sketches of the mechanisms. a) Sketch of the Goldbeter-Koshland mechanism of protein phosphorylation and dephosphorylation applied to MARCKS protein. b) Sketch of the myristoyl-electrostatic switch. The binding and unbinding of MARCKS and PKC proteins, and the phosphorylation and dephosphorylation of MARCKS proteins by kinase (PKC) and phosphatase (PPA) is shown [90].

MARCKS dynamics

Phosphorylation and dephosphorylation of proteins are usually modeled by the Goldbeter-Koshland mechanism. Using a quasi-steady approximation of the intermediate complexes, the original dynamics can be simplified to a couple of equations for the free and phosphorylated MARCKS (*respectively* $[MRK]_f$, *and* $[MRK]_p$) using Michaelis-Menten rates :

$$\begin{aligned}\frac{\partial [MRK]_m}{\partial t} &= -k_{pkc}^{mrk} \frac{[MRK]_f}{k_{mrk} + [MRK]_f} [PKC] + K_{ppa}^{mrk} \frac{[MRK]_p}{k_1 + [MRK]_p} [PPA] \\ \frac{\partial [MRK]_p}{\partial t} &= k_{pkc}^{mrk} \frac{[MRK]_f}{k_{mrk} + [MRK]_f} [PKC] - K_{ppa}^{mrk} \frac{[MRK]_p}{k_1 + [MRK]_p} [PPA],\end{aligned}\quad (1.3)$$

where $[PKC]$ and $[PPA]$ are respectively, the concentrations of the kinase and phosphatase, see sketch Fig.((1.9))(a). However, the phosphorylation of MARCKS is controlled by a binding-unbinding process. After considering $k_1 \gg [MRK]_p$ and defining $k_{ppa}^{mrk} = \frac{k_{ppa}^{mrk} [PPA]}{k_1}$, they extend Eq.(1.3) to a more adequate model of the evolution of the membrane, cytosolic and phosphorylated MARCKS (respectively $[MRK]_m$, $[MRK]_c$ and $[MRK]_p$), see sketch in Fig.((1.9))(b):

$$\begin{aligned}\frac{\partial [MRK]_m}{\partial t} &= S_m k_b^{mrk} [MRK]_c - k_u^{mrk} [MRK]_m - k_{pkc}^{mrk} \left(\frac{[MRK]_m}{k_{mrk} + [MRK]_m} \right) [PKC]_m, \\ \frac{\partial [MRK]_c}{\partial t} &= -S_m k_b^{mrk} [MRK]_c + k_u^{mrk} [MRK]_m + k_{ppa}^{mrk} [MRK]_p, \\ \frac{\partial [MRK]_p}{\partial t} &= k_{pkc}^{mrk} \left(\frac{[MRK]_m}{k_{mrk} + [MRK]_m} \right) [PKC]_m - k_{ppa}^{mrk} [MRK]_p,\end{aligned}\quad (1.4)$$

where the total concentration of MARCKS is preserved. The terms k_b^{mrk} and k_u^{mrk} are the binding and unbinding rates of MARCKS. The rate of phosphorylation at the membrane and dephosphorylation in the cytoplasm are determined by the parameters k_{pkc}^{mrk} and k_{ppa}^{mrk} .

Table 1.1: Parameter values related to MARCKS dynamic of the model .

Molecules	Parameter	value	Meaning	References
MARCKS	$[MRK]$	$75\mu M$	concentration	[91]
	$[MRK]_0$	$15\mu M$	coverage	[18, 89]
	k_b^{mrk}	$4 \times 10^3 s^{-1}$	binding	[92]
	k_u^{mrk}	$0.1 s^{-1}$	unbinding	[92]
	k_{pkc}^{mrk}	$0.25 s^{-1}$	phosphorylation	[92]
	k_{mrk}	$0.15\mu M$	Michaelis-menten binding	[5]
	k_{ppa}^{mrk}	$0.031 s^{-1}$	dephosphorylation	[93, 94]
	D_c	$5\mu m^2 s^{-1}$	cytoplasmic diffusion	[95]
	D_m	$0.1\mu m^2 s^{-1}$	membrane diffusion	[96]

The phosphorylation depends on the concentration of PKC at the membrane $[PKC]_m$ and,

therefore, indirectly on Ca^{2+} . The dephosphorylation is assumed to be independent of $[Ca^{2+}]$ [18]. The binding of MARCKS depends on the surface term: $S_m = (1 - \frac{[MRK]_m}{[MRK]_o})$, where the concentration $[MRK]_o$ is the saturation concentration, and corresponds to the theoretical concentration of MARCKS which completely covers the membrane. Assuming that $[MRK] \gg [PKC]$, S_m is the fraction of accessible space at the membrane.

PKC dynamics

The simple binding and unbinding dynamics of the PKC enzymes at the membrane is considered. The total concentration of enzymes is conserved giving rise to the next two coupled equations:

$$\begin{aligned} \frac{d[PKC]_m}{dt} &= -S_m K_b^{pkc} \left(\frac{[Ca^{2+}]_f}{k_{ca} + [Ca^{2+}]} \right) [PKC]_c - K_u^{pkc} [PKC]_m, \\ \frac{d[PKC]_c}{dt} &= S_m K_b^{pkc} \left(\frac{[Ca^{2+}]_f}{k_{ca} + [Ca^{2+}]} \right) [PKC]_c + K_u^{pkc} [PKC]_m. \end{aligned} \quad (1.5)$$

Table 1.2: Parameter values related to PKC dynamic of the model .

Molecules	Parameter	value	Meaning	References
PKC	[PKC]	$0.5\mu M$	concentration	[97]
	k_b^{pkc}	$150s^{-1}$	binding	[92]
	k_u^{pkc}	$1s^{-1}$	unbinding	[92]
	k_{ca}	$0.4\mu M$	Michaelis-menten binding Ca^{2+}	[92]
	D_c	$5\mu m^2 s^{-1}$	cytoplasmic diffusion	[98]
	D_m	$0.1\mu m^2 s^{-1}$	membrane diffusion	[99]

Ca^{2+} dynamics

Usually, $[Ca^{2+}]$ is constant and stays at rest, however external signals or internal processes produce random spikes of large $[Ca^{2+}]$. In such case, the global dynamics of $[Ca^{2+}]$ is simply modeled by a relaxation dynamics to the rest state and random spike generation:

$$\frac{d[Ca^{2+}]_m}{dt} = - \left(\frac{[Ca^{2+}] - [Ca^{2+}]_0}{\tau} \right) + I(t); \quad (1.6)$$

where τ is the characteristic relaxation time to the rest state $[Ca^{2+}]_0$. This time is controlled by the concentration of buffers in the cell. The term $I(t)$ represents the random spikes.

The concentration of PKC, MARCKS at the membrane and in the cytoplasm, and the evolution of Ca^{2+} concentration are represented in Fig.((1.12)).

The absolute responses of MARCKS and PKC proteins to the Ca^{2+} spike are shown in Fig.(1.10). The concentration of PKC at the membrane increases, see Fig.(1.10)(b), and phospho-

Table 1.3: Parameter values related to Ca^{2+} dynamic of the model .

Molecules	Parameter	value	Meaning	References
Ca^{2+}	τ	8s	Relaxation time	[100]
	$[Ca^{2+}]$	$0.1\mu M$	rest concentration	[101]

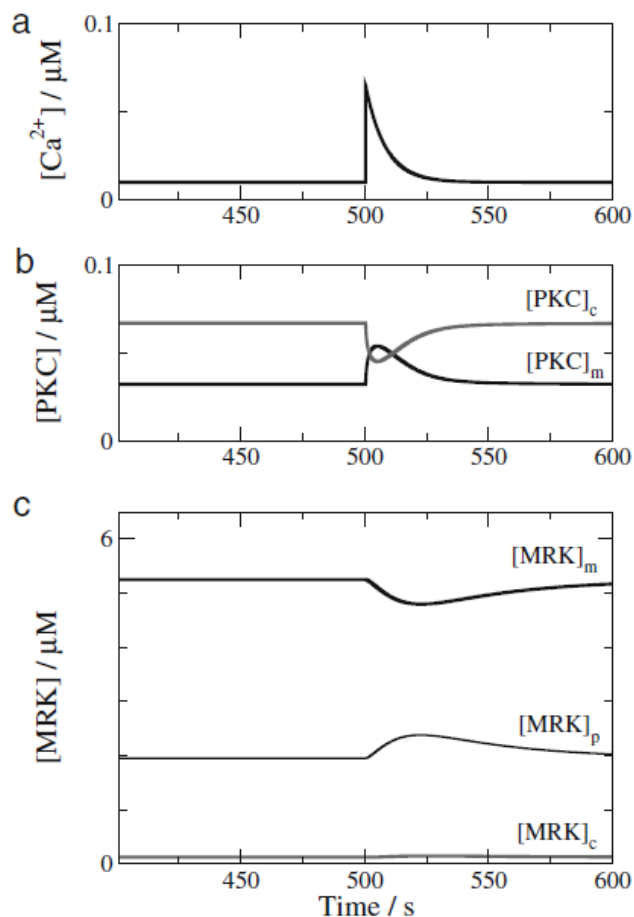


Figure 1.10: Effects of an spike of Ca^{2+} on the distribution of MARCKS and PKC. a) Evolution of Ca^{2+} concentration Eq.(1.6). b) Evolution of PKC at the membrane and in the cytoplasm Eq.(1.5). c) Evolution of MARCKS at the membrane and in the cytoplasm: free and phosphorylated Eq.(1.4) [90].

rylates some membrane MARCKS proteins. It produces an increase of phosphorylated MARCKS, Fig.(1.10)(c), and the subsequent dephosphorylation in the cytoplasm. Note that the low dephosphorylation rate produces a delay in the increase of free MARCKS proteins on the cytoplasm with respect the phosphorylated MARCKS. It increases the recovery time of MARCKS to the initial state with respect to the PKC dynamics.

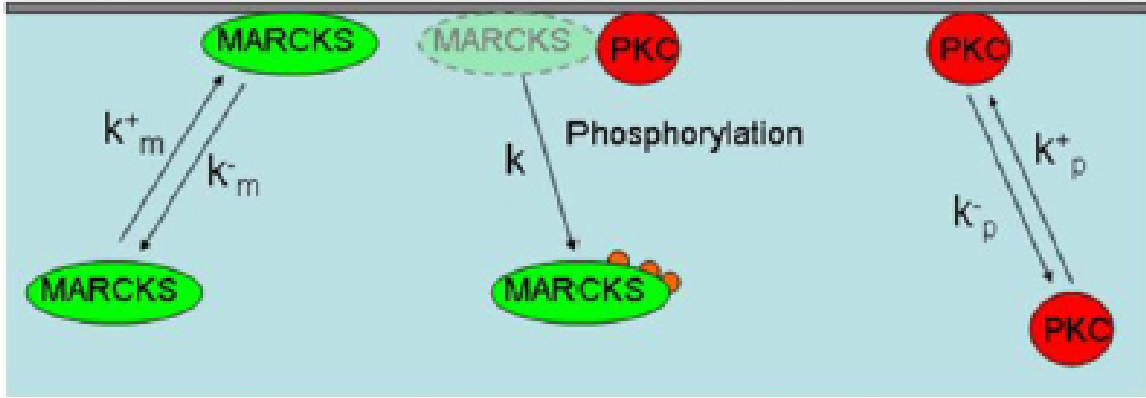


Figure 1.11: Sketch of the attachment-detachment mechanism of MARCKS and PKC and of the phosphorylation of MARCKS by PKC [86].

1.4.3 Sergio and Dietrich model

A mathematical model to explain changes in the physical structure of the monolayer by the translocation of MARCKS peptide had been developed Fig.(1.11). The model is extended to an open system that sustains chemical oscillations. They have restrict the modeling to the computation of one-dimensional profiles along the z -coordinate describing the direction orthogonal to the membrane plane. To derive the model, the system has been divided into two compartments. A narrow layer, where all the reactions take place ($0 < z < l$); and a passive subphase ($l < z < L$), where l is the size of narrow layer and L the vertical size of the system. Three chemical species: MARCKS peptides (M), PKC enzymes (P), and phosphorylated MARCKS peptides (M_P) diffuse in the subphase ($l < z < L$),

$$\begin{aligned}
 \frac{\partial M(z, t)}{\partial t} &= D_M \frac{\partial^2 M(z, t)}{\partial z^2}, \\
 \frac{\partial P(z, t)}{\partial t} &= D_P \frac{\partial^2 P(z, t)}{\partial z^2}, \\
 \frac{\partial M_P(z, t)}{\partial t} &= D_M \frac{\partial^2 M_P(z, t)}{\partial z^2},
 \end{aligned} \tag{1.7}$$

where D_M and D_P are the diffusion coefficients of MARCKS and PKC, respectively. The reactions occur only near the monolayer ($0 < z < l$),

$$\begin{aligned}\frac{\partial M(z, t)}{\partial t} &= -R_M + D_M \frac{\partial^2 M(z, t)}{\partial z^2}, \\ \frac{\partial P(z, t)}{\partial t} &= -R_P + D_P \frac{\partial^2 P(z, t)}{\partial z^2}, \\ \frac{\partial M_p(z, t)}{\partial t} &= R_{MP} + D_M \frac{\partial^2 M_p(z, t)}{\partial z^2},\end{aligned}\tag{1.8}$$

where the terms R_i ($i = M, P, MP$) correspond to the nonlinear reaction rates and attachment-detachment processes and in general may depend on the MARCKS and PKC concentrations in the subphase and at the monolayer. Then the concentration of monolayer-bound proteins is define as

$$\frac{\partial \check{m}(z, t)}{\partial t} = R_M - R_{MP} D_{\check{m}} \frac{\partial^2 \check{m}(z, t)}{\partial z^2},\tag{1.9}$$

where the average is define as $m(t) = \frac{1}{l} \int_0^l \check{m}(z, t) dz$.

The reaction rates is giving by: $\frac{1}{l} \int_0^l R_i dz \approx \frac{1}{l} R_i l = R_i$.

The corresponding equations for the averaged concentration of MARCKS peptides (m) and PKC enzymes (p) at the monolayer are obtained from an approximation and read

$$\dot{m}(t) = R_M - R_{MP} \text{ and } \dot{p}(t) = R_p.$$

To model the interaction between the monolayer and the subphase, the narrow layer from which proteins bind and into which proteins are released from the monolayer is considered. This layer is diffusively coupled to the subphase. The integral quantities is define as:

$$\phi_M = (L - l) \int_0^l M dz \text{ and } \phi_{MP} = (L - l) \int_0^l M_P dz,$$

which represent the total amount of free and phosphorylated MARCKS peptides in the subphase, respectively. Equivalently we define the total amount of PKC in the subphase as:

$\phi_P = (L - l) \int_0^l P dz$. The total amount of peptides $\phi_{M,T} = m + \phi_M$ and of enzymes $\phi_{P,T} = P + \phi_P$ are conserved quantities. In order to take into account the structure of the monolayer upon the binding of the peptides, which in turn affects the attachment rates, the variable θ should be consider. The value of θ is related with the accessible quantity of *PIP2*. A simple phenomenological equation to describe the dependence of the variable θ on the monolayer-bound MARCKS is: $\dot{\theta}(t) = R_\theta$.

The concentration M of the peptide in the subphase is described by:

$$\frac{\partial M(z, t)}{\partial t} = D_m \frac{\partial^2 M(z, t)}{\partial z^2},\tag{1.10}$$

The equations describing translocation dynamics of the peptide close to the monolayer reads

$$\frac{\partial M(z, t)}{\partial t} = -[1 - m(t)]K_m^+(\theta)M(z, t) + K_m^-m(t) + D_m \frac{\partial^2 M(z, t)}{\partial z^2}, \quad (1.11)$$

and the corresponding equations at the monolayer,

$$\dot{m} = [1 - m(t)]K_m^+(\theta)M(z, t) + K_m^-m(t), \dot{\theta} = k_\theta[m(t) - \theta(t)], \quad (1.12)$$

where the variables M and m correspond to the fractions of MARCKS in the subphase and the fraction of MARCKS bound to the monolayer, respectively. The attachment and detachment of the peptide to the monolayer is accounted by $k_m^+(\theta)$ and $k_m^-(\theta)$. Authors integrate Eq.(1.12) to study the dynamics of MARCKS peptides interacting with the monolayer. Based on an initially homogeneous distribution M of MARCKS in the subphase, there is a monotonous increase of the concentration of monolayer-bound peptides m Fig.(1.14)(a). It implies an increase of the monolayer pressure due to the binding of MARCKS because the lateral pressure is assumed to be proportional to m . The translocation to the monolayer produces a decrease of concentration in the subphase region near the membrane. This, in turn, induces a concentration gradient of free peptide in the subphase, which induces the transport of more peptide to the monolayer. If the system remains undisturbed, the peptide accumulates at the monolayer until saturation is reached (*see Fig.4*).

1.4.4 Turing model

The potential for pattern formation of reaction-diffusion processes has first been introduced theoretically by Turing who argued for a physicochemical basis of morphogenesis. Because of their supposed role in morphogenesis, the possible emergence of Turing structures in single phase chemical systems maintained far from equilibrium by a permanent supply of reactants, first asserted in [41]. Turing structures are stationary concentration patterns, originating in the sole coupling of reaction and diffusion processes. The Turing patterns result from spontaneous symmetry breaking phenomena associated with bifurcations of steady states often known as non equilibrium phase transitions or self-organization phenomena. He proposed that pattern formation during morphogenesis might arise through a diffusion-driven instability in a systems of reacting chemicals. Two or more chemicals are required to interact in a well defined manner in order that an heterogeneous distribution in their concentrations is generated. They correspond to stable stationary solutions of a set of reaction diffusion equations,

$$\frac{\partial c_i}{\partial t} = f_i(\dots, c_j, \dots) + D_i \Delta c_i, \quad (1.13)$$

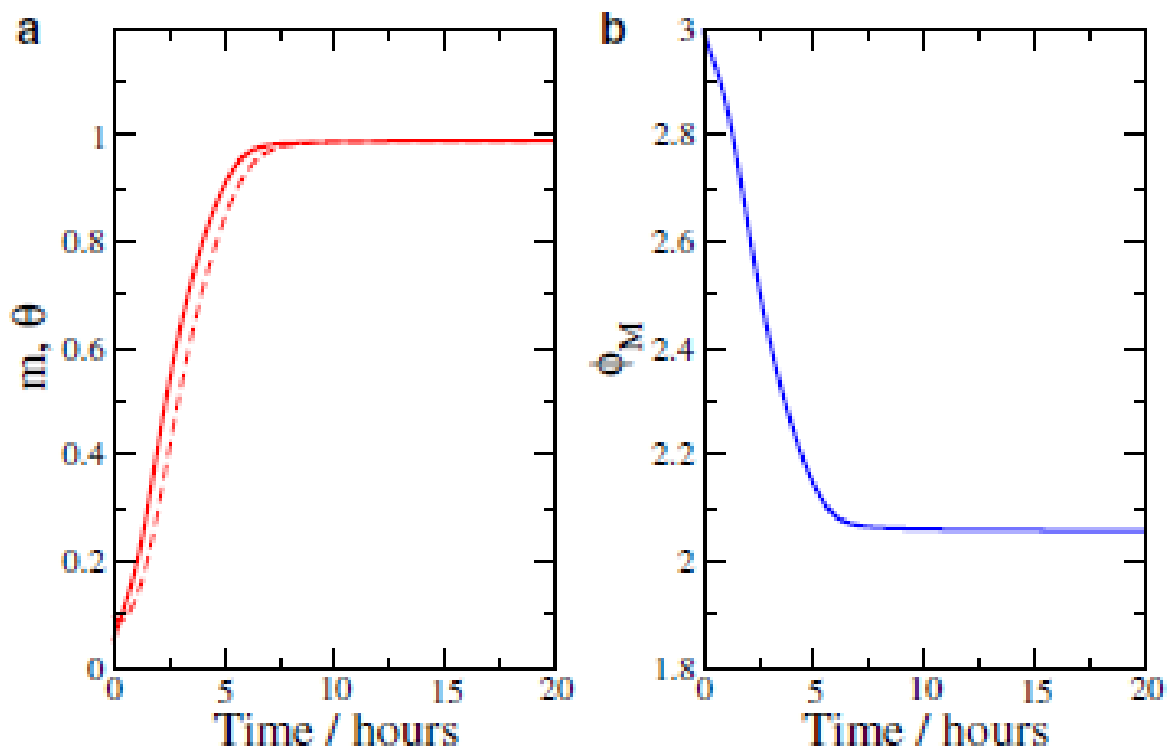


Figure 1.12: Temporal evolution of m (solid line) and θ (dashed line) at the monolayer (a), and of the fractions ϕ_M (solid line) in the subphase (b). Parameters of the numerical simulations: $D_M = 160\mu m^2 s^{-1}$, $K_m^+ = 1s^{-1}$, $k_1 = 1$, $K_m^- = 2 \times 10^{-5}s^{-1}$, $\phi_M = 3$. [86].

where the nonlinear functions f_i of the concentrations c_i , represents the contribution of reactive processes, the D_i are the diffusion coefficients, and Δ is the Laplacian operator which brings in the spatial dependence Fig.(1.13). The patterns are characterized by an intrinsic wavelength which does not depend on the geometrical parameters but only on the concentrations or input rates of the reactants, the diffusion coefficients, and the macroscopic reaction rates. The necessary conditions for Turing patterns are: the kinetics should include a positive feedback such as autocatalysis on a species called activator and an inhibitory process; the inhibitor should diffuse much faster than the activator so that $D_h \gg D_a$. Clearly it depends on the present reaction kinetics. Periodic patterns in reaction-diffusion systems can be broadly defined in three categories:

- (I) patterns that are homogeneous throughout space and change periodically in time, which happens when a steady state loses stability in favor of a limit cycle (a Hopf bifurcation);
- (II) patterns that are stationary in time but do have some periodicity in space, which, for instance, can come from an instability due to differential diffusion as first described by Turing;
- and (III) patterns that are periodic in both space and time, like traveling waves.

Turing described an instability that generates traveling or standing waves, which is known as wave instability. Traveling waves are patterns that are periodic in both space and time and this

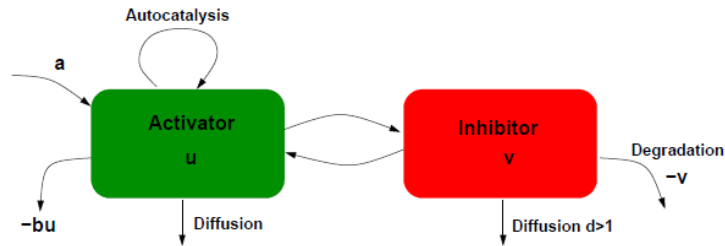


Figure 1.13: Expression of kinetics for the Gierer Meinhardt activator inhibitor system [102].

type of moving patterns will be of great interest in the cases of this thesis.

1.5 The soliton concept in the protein media

The energy required for protein activity usually comes from the hydrolysis of the ATP molecule. But it can only be effective if it is not rapidly distributed to all the protein's degrees of freedom by equipartition of energy, *i.e.* if it remains localized.

Three physical processes play a key role in the functioning of biological molecules such as proteins and DNA.

- Energy storage and transfer: the energy could be temporarily stored in electronic form, but it is also possible that it could be localized by nonlinear effects and even transported in the form of nonlinear-excitation.
- Changes in molecular conformation, which are essential to many of their functions: Changes in the conformation of molecules are involved in protein in the dynamics of proteins, particularly in the functioning of enzymes, but they are even more fundamental for DNA, for example, the reading of the genetic code could not take place without unfolding of local molecule.
- Charge transport (electrons and protons): It is possible to consider transport along chains of hydrogen bonds that extend from one side of the membrane to the other, either because they belong to transmembrane proteins, or because certain proteins, such as gramicidin, form veritable one-dimensional channels containing chains of water molecules.

The ATP hydrolysis reaction releases an energy close to two quanta $\hbar\omega$ of the vibration mode of binding $C = O$. This vibration is therefore a natural candidate for the storage of ATP hydrolysis energy. This is what Davydov model propose, which considers that the energy transmitted to the $C = O$ binding, contributes to local deformation of the helix [24].

This distortion tends slightly modify the vibrational frequency of the excited $C = O$ bond, which ceases to be resonant with other $C = O$ bonds in the vicinity. This reduces the rate of

energy transfer to these neighboring $C = O$ bonds, and thus maintains the hydrolysis energy of ATP in a localized form. So this process of energy self-localization works on principles quite analogous to those encountered in optics [103]. The energy injected into the environment modifies the characteristics of the environment and this modification of the medium tends to reinforce the localization.

The soliton mechanism for the storage and transport of energy in biological systems, suggested by Davydov and Kislukha [104] in 1973, consists in the interaction of collective excitations of molecules in a one-dimensional chain (peptide groups in the case of proteins) with their longitudinal displacements, and leads to the formation of a self-consistent soliton state. The Davydov mechanism for energy localization and transport in proteins concerns the *helix* – α , often found in membranes. According to this hypothesis, the energy stored in the Amid-I vibration of the CO stretching of the peptide group, becomes autolocalized due to the interaction with the local deformation of the relatively soft polypeptide chains formed by weak hydrogen bonds along the α -helical protein molecules. This is applied widely to studying energy and charge transport processes. It is experimentally estimated that in a number of processes the transfer of charges takes place by pairs. As an example, we can refer to biological oxidation, which is the source of energy stored in ATP molecules and necessary for all metabolic processes.

There is a vast number of phenomena in biology where a key element or precursor to a developmental process seems to be the appearance of a travelling wave of chemical concentration. In fact, self-organization among different proteins processes can give rise to the formation of traveling waves in lipid bilayers mimicking the membranes of bacteria [105]. Looking at almost any film of a developing embryo it is hard not to be struck by the number of wave-like events that appear after fertilization. There are, for example, both chemical and mechanical waves which propagate on the surface of many vertebrate eggs. In developing living systems there is almost continual interchange of information at both the inter- and intra-cellular level. Such communication is necessary for the sequential development and generation of the required pattern and form. Propagating wave forms of varying biochemical concentrations are one means of transmitting such biochemical information. Customarily, a travelling wave is taken to be a wave which travels without change of shape, in fact, the shape of the solution will be the same for all time and the speed of propagation of this shape is a constant Fig.(1.14). A mathematical way of saying this is that if the solution

$$u(x, t) = u(x - ct) = u(z), \quad \& z = x - ct, \quad (1.14)$$

where $u(x, t)$ is a travelling wave, and it moves at constant speed c in the positive x – *direction*.

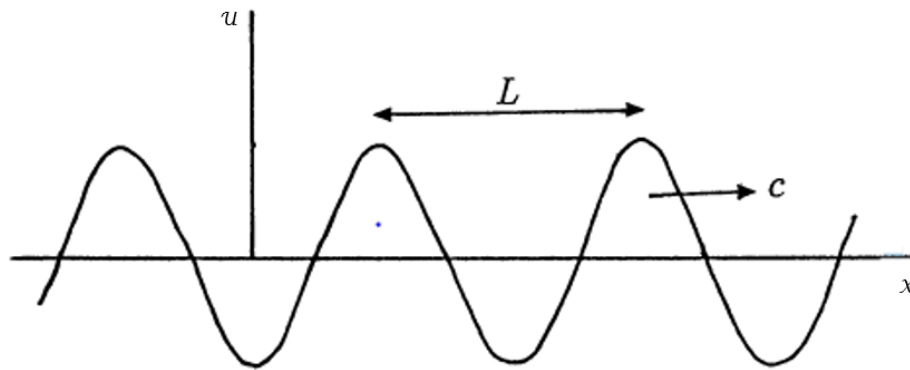


Figure 1.14: Small amplitude of travelling wave solution [81].

1.6 Conclusion

In this chapter, we have point out some generalities about protein molecules and also provided the background of the MARCKS protein models and the soliton theory. The major cellular substrate for protein kinase C appears as an spectacular regulator of the homeostasis of body fluids, blood coagulation, cell motility and as important players in cells regeneration. The model which mainly describes the dynamic of this protein through a non-linear reaction diffusion equations, known as the Sergio and Markus model, has been addressed. The exploration of this model will be of great interest in the rest of the thesis.

MATHEMATICAL BACKGROUND AND METHODOLOGY

2.1 Introduction

The previous chapter highlights the crucial role that MARCKS protein plays in the living world. The experimental study of the interactions between MARCKS protein, and other molecules such as: phospholipids and PKC was carried out *in vitro* and *in vivo*. However, mathematical modelling is an important means to analyzing the spread and control of diseases, determining dominant parameters. It can also be employed to predict the future behaviors or measure the outcomes of experiments that cannot be performed in reality. This chapter is a review of the MARCKS mathematical models and the methods used throughout this dissertation. These methods, include analytical and numerical methods, that are: methods for stability analysis, methods for reduction to a discrete nonlinear Schrödinger (DNLS) equation, methods for reduction to the complex cubic Ginzburg-Landau (CCGL) equation, and methods for building exact traveling wave and weakly nonlinear solutions. In this chapter, we present the general frameworks for MARCKS models under several circumstances, and we also present the tools used to analyze those models.

2.2 Reaction Diffusion model

The formation of patterns in chemical reactions has been the subject of multiple research papers [16, 106–108]. A family of models that have been extensively used to analyse patterns observed in chemical processes are reaction-diffusion systems [16, 106, 107, 109]. These models consist of a reaction part describing the chemical kinetics and a diffusion part representing transport processes. Models of reaction-diffusion type have received much attention in the literature, reflected in the plethora of research papers on this subject. Some representative reviews and introductory books that treat this topic are [16, 32, 106, 110–112]. Reaction-diffusion models are systems of coupled partial differential equations (PDEs) that can be written in the following way:

$$\frac{\partial V(x, t)}{\partial t} = \underbrace{g(V(x, t))}_{\text{reaction}} + \underbrace{D\nabla^2 V}_{\text{Diffusion}}, \quad (2.1)$$

where V is a (column) vector field. In the context of chemical reactions, the elements of this field represent the concentrations of different reactants. The functions in the vector $g(V(x, t))$ are typically nonlinear and the diffusion matrix, D , is square and typically diagonal. In this Thesis we will concentrate on cases where the physical space on which the reactants diffuse is one-dimensional, that means that we will substitute the Laplacian operator ∇^2 by a one dimensional spatial (second) derivative $\frac{\partial^2}{\partial x^2}$, since proteins are essentially one-dimensional [113].

Reaction-diffusion models have been also applied to other fields like, biology and ecology [25–28]. In this thesis, it will be applied to the field of biology, since the spatiotemporal evolution of protein in living cell constitute our main topic. In fact, the number of components in metabolic networks is usually very large. To model the relations among the components, the interactions are simplified and the pathways are described by ordinary differential equations of the component concentrations in the cell. However, some molecules and reactions are restricted to particular compartments of the cell. As a result, the spatiotemporal distribution of proteins in the cell is important [114]. The communication between steps of the pathways restricted to different compartments is typically achieved by diffusion and active transport of the involved molecules. For sufficiently high molecular concentrations, the spatial distribution can be modeled by reaction-diffusion equations. These equations permit also the implementation of spatially inhomogeneous conditions.

2.2.1 MARCKS dynamics diagram

Here, we consider a spatial domain formation of the unfolded protein myristoylated alanine-rich C kinase substrate (MARCKS) which interacts electrostatically with the acidic phospholipids and binds to the membrane. MARCKS proteins lose their affinity to membranes when they are phosphorylated by protein kinase C. The phosphates reduce the positive charge of the protein and cause the unbinding from the membrane to the cytoplasm. In the cytoplasm, phosphatases remove the phosphates again from the protein. Consequently, MARCKS can bind again at the membrane. The processes of binding, phosphorylation and dephosphorylation constitute the so called myristoyl-electrostatic switch and give rise to a cyclic dynamics powered by the consumption of ATP. Phosphorylation and dephosphorylation of proteins are mechanisms of activation and deactivation which regulate many cellular processes. There exist a cyclical set of reactions between three states of the proteins:

$M \rightarrow P \rightarrow C \rightarrow M$, where M , P and C denote membrane-bound, phosphorylated and free

cytosolic proteins, respectively. Membrane-bound proteins (M) sequester acidic phospholipids and perform diverse functions [115]. Phosphorylation of the membrane bound proteins by PKC in the presence of ATP produces the translocation to the cytosol (P).

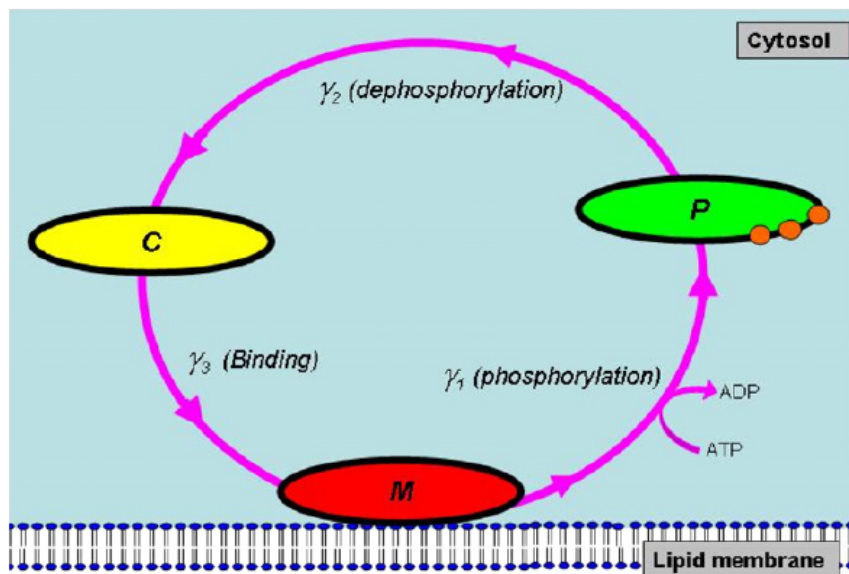


Figure 2.1: Sketch of the myristoyl-electrostatic switch. The red objects represent membrane proteins (M), green objects phosphorylated proteins (P) and yellow objects free cytosolic proteins (C). Reaction rates are correspondingly noted [18].

In Fig.(2.1), we notice that MARCKS is phosphorylated by protein kinase C under consumption of adenosine tri-phosphate. The phosphorylated proteins translocate rapidly to the cytosol because of the loss of electric charges, responsible for the interaction with the membrane. The enzyme PKC also interacts with the phospholipids and translocates to the membrane and the rate of MARCKS phosphorylation is controlled by the concentration of active membrane-bound PKC. instead, the activation of PKC is regulated by calcium and the phospholipids at the membrane.

2.2.2 MARCKS protein model with homogenous diffusion coefficients

The model that we study here is a PDE that was proposed in [18]. It describes the spatio-temporal evolution of the concentration of the MARCKS protein at biomembrane involving: binding, phos-

phorylation and dephosphorylation of the MARCKS protein when the total number of proteins is conserved. This model take the form:

$$\frac{\partial m}{\partial t} = \gamma_3 c(1 - m) - \gamma_1(1 - m) \frac{m}{k_m + m} + D_m \frac{\partial^2 m}{\partial x^2}, \quad (2.2)$$

$$\frac{\partial c}{\partial t} = -\gamma_3 c(1 - m) + \gamma_2 p + D \frac{\partial^2 c}{\partial x^2}, \quad (2.3)$$

$$\frac{\partial p}{\partial t} = \gamma_1(1 - m) \frac{m}{k_m + m} - \gamma_2 p + D \frac{\partial^2 p}{\partial x^2}, \quad (2.4)$$

where the three dimensionless variables m , c and p represent the concentrations of MARCKS protein in the membrane, cytosol and phosphorylated site, respectively. The rates γ_1 , γ_2 and γ_3 refer to phosphorylation, dephosphorylation and binding, respectively. Parameters D_m and D account for membrane and cytosolic diffusion coefficients of MARCKS. The term $(1 - m)$ represents the coverage of the membrane by MARCKS proteins which locally prevents the activation of PKC at the membrane. This model is applied to the description of gradient sensing of cells.

2.2.3 MARCKS protein model with the inhomogeneity effect

Intracellular protein-protein interactions are dynamics events that require tightly regulated spatiotemporal control points. The process of regulating these dynamics produces highly specific molecular response patterns that are based on the ephemeral localization and activity of various coordinating proteins that direct the function of the organism Fig.(2.2). One of the regulating proteins is the myristoylated alanine-rich C-kinase substrate which emerged as an important component of cellular map, governing a wide variety of proteins interactions in all types of brain cells [116]. However, biological processes in the nature are carried out in a setting of inhomogeneities. For example, proteins and enzymes catalyze millions of chemical reactions that occur every moment in biological systems, but this occurs in a crowded molecular environment and not as isolated entities [117].

Therefore, it is important to take into account the inhomogeneity effect to model the MARCKS diffusion through cytoplasmic membrane. Doing so, the discreteness model of EqS.(2.3-2.4) reads:

$$\begin{aligned} \frac{\partial m_n}{\partial t} + \alpha_0 m_n &= \gamma_3 c_n - \gamma_3 c_n m_n + \alpha_1 m_n^2 + \alpha_2 m_n^3 + D(m_n)(m_{n+1} - 2m_n + m_{n-1}), \\ \frac{\partial c_n}{\partial t} + \gamma_3 c_n &= \gamma_2 p_n + \gamma_3 c_n m_n + D(c_{n+1} - 2c_n + c_{n-1}), \\ \frac{\partial p_n}{\partial t} + \gamma_2 p_n &= \alpha_0 m_n - \alpha_1 m_n^2 - \alpha_2 m_n^3 + D(p_{n+1} - 2p_n + p_{n-1}), \end{aligned} \quad (2.5)$$

with : $\alpha_0 = \frac{\gamma_1}{k_m}$; $\alpha_1 = (1 + \frac{1}{k_m}) \frac{\gamma_1}{k_m}$; $\alpha_2 = -\frac{\gamma_1}{k_m^2}$. The discrete variables m_n , c_n and p_n represent the concentrations of membrane proteins, phosphorylated proteins and free cytosolic proteins, respectively of node n . The function $D(m_n)$ accounts for a self diffusion quadratic law, and

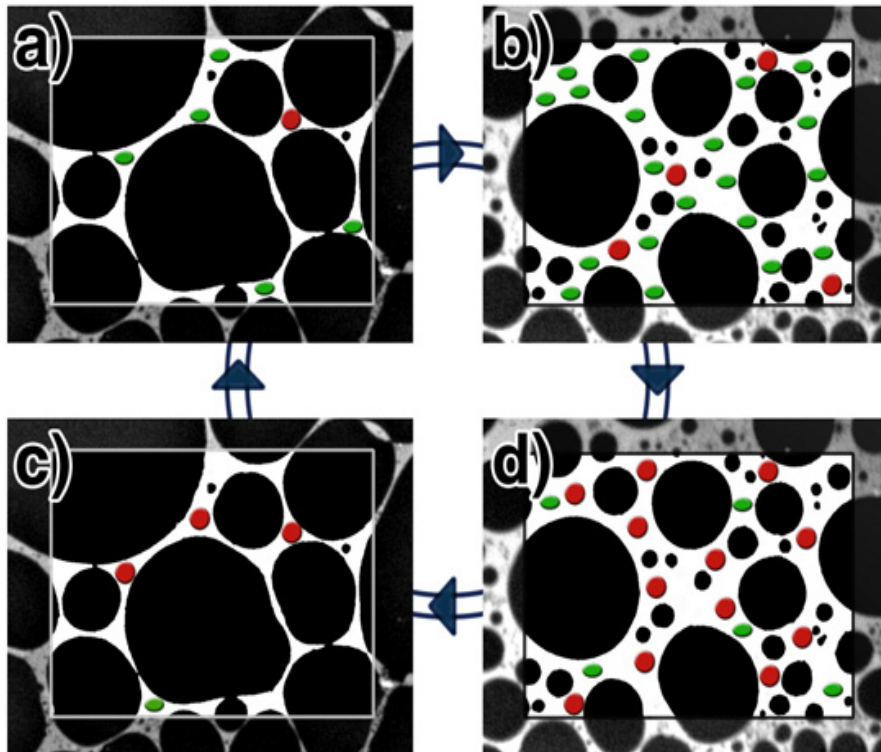


Figure 2.2: The membrane structure and protein attachment during different phases ($a - d$) of the oscillation. The bright parts of the background symbolize the disordered phase of the membrane and the dark parts the ordered phase. The green dots indicate MARCKS molecules while the red dots stand for PKC. The right figure shows the membrane associated variables amount of membrane bound MARCKS in green, the amount of membrane bound PKC in red [47].

defined by $D(m_n) = D_0 + D_1 m_n + D_2 m_n^2$ as in [36]. This means that the diffusion of MARCKS protein at the level of cytoplasmic membrane is not homogeneous, rather, the diffusion term is inhomogeneous.

2.3 Analytical methods

The subject of partial differential equations (PDEs) is enormous. At the same time, it is very important, since so many phenomena in nature and technology find their mathematical formulation through such equations. Knowing how to solve at least some PDEs is therefore of great importance to physicians.

2.3.1 The reductive perturbation method

The reductive perturbation method (or multiscale analysis) follows the concept of approximating the dynamics of a system by exploiting the existence of multiple temporal and spatial scales in its dynamics. Some natural processes have more than one characteristic length or time scales

associated with them, for example, the turbulent flow consists of various length scales of the turbulent eddies along with the length scale of the objects over which the fluid flows. The failure to recognize a dependence on more than one space/time scale is a common source of non- uniformity in perturbation expansions. The method of multiple scales comprises techniques used to construct uniformly valid approximations to the solutions of perturbation problems in which the solutions depend simultaneously on widely different scales. This is done by introducing fast-scale and slow-scale variables for an independent variable, and subsequently treating these variables, fast and slow, as if they are independent.

This method allowing the deduction of simplified equations from a basic model without losing its characteristic features [117]. The success of the method relies mainly on the nice property that the resulting reduced models are simple (allowing for useful information), representative (they illustrate effectively real processes) [118, 119] and often integrable (they carry an infinite set of conserved quantities) [120]. There are three different approaches to multiscale analysis for a discrete evolution. The first is obviously to go to the continuous limit right in the starting system, for which discreteness effects are wiped out; The second is the semi-discrete approach which consists in having a discrete carrier wave modulated by a continuous envelope and the third stems from the adiabatic approximation. Let us assume that the models to be solved are given by Eqs.(2.3-2.4). Then the application of this methods requires the introduction of the fast spatial variables $\xi = \epsilon(x - v_g t)$, and the slow temporal variable $\tau = \epsilon^2 t$. ϵ measures nonlinearity order, v_g being the group velocity. Furthermore, we expand solutions of Eqs.(2.3-2.4) around a reference state m_0, c_0, p_0 , hence the consideration of the finite sums [36]

$$\begin{aligned}
 m(x, t) &= \sum_{n=1}^{\infty} \epsilon^n \sum_{l=-n}^n m_n^{(l)}(\xi, \tau) A^{(l)}(x, t), \\
 c(x, t) &= \sum_{n=1}^{\infty} \epsilon^n \sum_{l=-n}^n c_n^{(l)}(\xi, \tau) A^{(l)}(x, t), \\
 p(x, t) &= \sum_{n=1}^{\infty} \epsilon^n \sum_{l=-n}^n p_n^{(l)}(\xi, \tau) A^{(l)}(x, t),
 \end{aligned} \tag{2.6}$$

where, of course, $A^{(l)}(x, t) = \exp il(kx - \omega t)$, $\xi = \epsilon(x - v_g t)$, $\tau = \epsilon^2 t$, and where the reality condition results in $m_n^{(-l)} = (m_n^{(l)})^*$ and $c_n^{(-l)} = (c_n^{(l)})^*$, with asterisk denoting the complex conjugate. The quantities ω and v_g represent, respectively the angular frequency and the group velocity, while k denotes the wavenumber of the carrier wave $A^{(l)}(x, t)$.

Illustration of the method of multiple scales analysis using the Sergio and Markus model (2010)

The reaction-diffusion system described by Eqs.(2.3-2.4) appears more complicated to find their analytical solutions. However, some technical approaches allow to simplify it into partial derivative equations with well-known properties. Among these approaches, we will adopt the multiple-scale approximation in the reductive perturbation method (RPM). To further, the whole system is firstly linearized by reducing Eq.2.3 and Eq.2.4 in the same denominator. Then we differentiate Eq.2.4 over the time, following by the substitution of variables \dot{m} and \dot{p} by their respective expressions into the obtained second-order ODE in c . This allows to definitively eliminate the variable p which is extracted from Eq.2.4 as $p = \frac{1}{\gamma_2}[\frac{\partial c}{\partial t} + \gamma_3 c(1 - m) - D\frac{\partial^2 c}{\partial x^2}]$. Therefore, we obtain the following reduced system.

$$\begin{aligned}
(k_m + m)\frac{\partial m}{\partial t} &= -\mu_1 m + \mu_2 c + \mu_1 m^2 + \mu_3 m c + \mu_4 m^2 c + [d_0 + d_1 m]\frac{\partial^2 m}{\partial x^2}, \\
(k_m + m)\frac{\partial^2 c}{\partial t^2} + \Omega_0^2 c + \lambda_1 c^2 + \lambda_2 m^2 + \lambda_3 m c + \lambda_4 m^2 c + \lambda_5 m c^2 + \lambda_6 m \\
+ [\sigma_0 + \sigma_1 m + \sigma_2 m^2]\frac{\partial c}{\partial t} &= [D_0 + D_1 m + D_2 m^2]\frac{\partial^2 c}{\partial x^2} + [D_3 c + D_4 m c]\frac{\partial^2 m}{\partial x^2} \\
+ [D_5 + D_6 m]\frac{\partial m}{\partial x}\frac{\partial c}{\partial x} + [D_7 + D_8 m]\frac{\partial^2 c}{\partial x^2}\left(\frac{\partial c}{\partial t}\right) + [D_9 + D_{10} m]\frac{\partial^4 c}{\partial x^4}, \tag{2.7}
\end{aligned}$$

where the auxiliary coefficients of Eq.(2.7) are given in **Appendix A₁**. We can now apply the RPM which requires the introduction of a small parameter $\epsilon \ll 1$ while the medium is supposed to be weakly dissipative. We will also consider parameters σ_0 , λ_6 and D_7 to be perturbed at order ϵ^2 , i.e., $\sigma_0 \leftarrow \epsilon^2 \sigma_0$, $\lambda_6 \leftarrow \epsilon^2 \lambda_6$, $D_7 \leftarrow \epsilon^2 D_7$. By inserting solutions 2.6 into Eq.2.7, we obtain the following system:

$$\begin{aligned}
 & \left(k_m + \sum_{n=1}^{\infty} \epsilon^n \sum_{l=-n}^n m_n^{(l)} A^{(l)} \right) \times \sum_{p=1}^{\infty} \epsilon^n \sum_{l=-n}^n \left[-\epsilon v_g \frac{\partial m_n^{(l)}}{\partial \xi} + \epsilon^2 \frac{\partial m_n^{(l)}}{\partial \tau} - i l \omega m_n^{(l)} \right] A^{(l)} = \\
 & - \mu_1 \sum_{n=1}^{\infty} \epsilon^n \sum_{l=-n}^n m_n^{(l)} A^{(l)} + \mu_2 \sum_{n=1}^{\infty} \epsilon^n \sum_{l=-n}^n c_n^{(l)} A^{(l)} + \mu_1 \left(\sum_{n=1}^{\infty} \epsilon^n \sum_{l=-n}^n m_n^{(l)} A^{(l)} \right)^2 \\
 & + \mu_3 \sum_{n=1}^{\infty} \epsilon^n \sum_{l=-n}^n m_n^{(l)} A^{(l)} \sum_{n=1}^{\infty} \epsilon^n \sum_{l=-n}^n c_n^{(l)} A^{(l)} + \mu_4 \left(\sum_{n=1}^{\infty} \epsilon^n \sum_{l=-n}^n m_n^{(l)} A^{(l)} \right)^2 \sum_{n=1}^{\infty} \epsilon^n \sum_{l=-n}^n c_n^{(l)} A^{(l)} \\
 & + \left(d_0 + d_1 \sum_{n=1}^{\infty} \epsilon^n \sum_{l=-n}^n m_n^{(l)} A^{(l)} \right) \times \sum_{n=1}^{\infty} \epsilon^n \sum_{l=-n}^n \left[\epsilon^2 \frac{\partial^2 m_n^{(l)}}{\partial \xi^2} + 2 i l k \epsilon \frac{\partial m_n^{(l)}}{\partial \xi} - l^2 k^2 m_n^{(l)} \right] A^{(l)} \\
 & \left(k_m + \sum_{n=1}^{\infty} \epsilon^n \sum_{l=-n}^n m_n^{(l)} A^{(l)} \right) \times \sum_{n=1}^{\infty} \epsilon^n \sum_{l=-n}^n \left[\epsilon^2 v_g^2 \frac{\partial^2 c_n^{(l)}}{\partial \xi^2} + 2 i l \omega v_g \epsilon \frac{\partial c_n^{(l)}}{\partial \xi} - 2 i l \omega \epsilon^2 \frac{\partial c_n^{(l)}}{\partial \tau} \right. \\
 & \left. - l^2 \omega^2 c_n^{(l)} \right] A^{(l)} + \Omega_0^2 \sum_{n=1}^{\infty} \epsilon^n \sum_{l=-n}^n c_n^{(l)} A^{(l)} + \lambda_1 \left(\sum_{n=1}^{\infty} \epsilon^n \sum_{l=-n}^n c_n^{(l)} A^{(l)} \right)^2 + \lambda_2 \left(\sum_{n=1}^{\infty} \epsilon^n \sum_{l=-n}^n m_n^{(l)} A^{(l)} \right)^2 \\
 & + \lambda_3 \sum_{n=1}^{\infty} \epsilon^n \sum_{l=-n}^n m_n^{(l)} A^{(l)} \sum_{n=1}^{\infty} \epsilon^n \sum_{l=-n}^n c_n^{(l)} A^{(l)} + \lambda_4 \left(\sum_{n=1}^{\infty} \epsilon^n \sum_{l=-n}^n m_n^{(l)} A^{(l)} \right)^2 \sum_{n=1}^{\infty} \epsilon^n \sum_{l=-n}^n c_n^{(l)} A^{(l)} \\
 & + \lambda_5 \sum_{n=1}^{\infty} \epsilon^n \sum_{l=-n}^n m_n^{(l)} A^{(l)} \left(\sum_{n=1}^{\infty} \epsilon^n \sum_{l=-n}^n c_n^{(l)} A^{(l)} \right)^2 + \lambda_6 \sum_{n=1}^{\infty} \epsilon^n \sum_{l=-n}^n m_n^{(l)} A^{(l)} \\
 & + \left(\sigma_0 + \sigma_1 \sum_{n=1}^{\infty} \epsilon^n \sum_{l=-n}^n m_n^{(l)} A^{(l)} + \sigma_2 \left(\sum_{n=1}^{\infty} \epsilon^n \sum_{l=-n}^n c_n^{(l)} A^{(l)} \right)^2 \right) \times \sum_{p=1}^{\infty} \epsilon^n \sum_{l=-n}^n \left[-\epsilon v_g \frac{\partial m_n^{(l)}}{\partial \xi} + \epsilon^2 \frac{\partial m_n^{(l)}}{\partial \tau} \right. \\
 & \left. - i l \omega m_n^{(l)} \right] A^{(l)} = \left(D_0 + D_1 \sum_{n=1}^{\infty} \epsilon^n \sum_{l=-n}^n m_n^{(l)} A^{(l)} + D_2 \left(\sum_{n=1}^{\infty} \epsilon^n \sum_{l=-n}^n c_n^{(l)} A^{(l)} \right)^2 \right) \times \sum_{n=1}^{\infty} \epsilon^n \sum_{l=-n}^n \left[\epsilon^2 \frac{\partial^2 c_n^{(l)}}{\partial \xi^2} \right. \\
 & \left. + 2 i l k \epsilon \frac{\partial c_n^{(l)}}{\partial \xi} - l^2 k^2 c_n^{(l)} \right] A^{(l)} \left[D_3 \sum_{n=1}^{\infty} \epsilon^n \sum_{l=-n}^n c_n^{(l)} A^{(l)} D_4 \sum_{n=1}^{\infty} \epsilon^n \sum_{l=-n}^n m_n^{(l)} A^{(l)} \sum_{n=1}^{\infty} \epsilon^n \sum_{l=-n}^n c_n^{(l)} A^{(l)} \right] \\
 & \times \sum_{n=1}^{\infty} \epsilon^n \sum_{l=-n}^n \left[\epsilon^2 \frac{\partial^2 m_n^{(l)}}{\partial \xi^2} - 2 i l k \epsilon \frac{\partial m_n^{(l)}}{\partial \xi} - l^2 k^2 m_n^{(l)} \right] A^{(l)} \left[D_5 + D_6 \sum_{n=1}^{\infty} \epsilon^n \sum_{l=-n}^n m_n^{(l)} A^{(l)} \right] \\
 & \times \sum_{n=1}^{\infty} \epsilon^n \sum_{l=-n}^n \left[\epsilon \frac{\partial m_n^{(l)}}{\partial \xi} A^{(l)} i l k m_n^{(l)} A^{(l)} \right] \times \sum_{n=1}^{\infty} \epsilon^n \sum_{l=-n}^n \left[\epsilon \frac{\partial c_n^{(l)}}{\partial \xi} A^{(l)} + i l k c_n^{(l)} A^{(l)} \right] \\
 & + \left[D_7 + D_8 \sum_{n=1}^{\infty} \epsilon^n \sum_{l=-n}^n m_n^{(l)} A^{(l)} \right] \times \sum_{n=1}^{\infty} \epsilon^n \sum_{l=-n}^n \left[\epsilon^2 \frac{\partial^2 m_n^{(l)}}{\partial \xi^2} - 2 i l k \epsilon \frac{\partial m_n^{(l)}}{\partial \xi} - l^2 k^2 m_n^{(l)} \right] A^{(l)} \\
 & + \left[D_9 + D_{10} \sum_{n=1}^{\infty} \epsilon^n \sum_{l=-n}^n m_n^{(l)} A^{(l)} \right] \times \sum_{n=1}^{\infty} \epsilon^n \sum_{l=-\infty}^{+\infty} -\epsilon^2 6 l^4 k^4 \frac{\partial^2 c_l^{(n)}}{\partial \xi^2} A^l \\
 & \times \sum_{n=1}^{\infty} \epsilon^n \sum_{l=-\infty}^{+\infty} -\epsilon 4 i l^3 k^3 \frac{\partial c_l^{(n)}}{\partial \xi} A^l + \sum_{n=1}^{\infty} \epsilon^n \sum_{l=-\infty}^{+\infty} l^4 k^4 c_l^{(n)} A^l
 \end{aligned}$$

Now we proceed by collecting and solving different orders (p, l) in above system.

Order (1,1)

At this order, we obtain the following system

$$\begin{aligned}
 - \sum_{l=-1}^1 il\omega k_m m_1^{(l)} A^{(l)} &= -\mu_1 \sum_{l=-1}^1 m_1^{(l)} A^{(l)} + \mu_2 \sum_{l=-1}^1 c_1^{(l)} A^{(l)} - \sum_{l=-1}^1 l^2 k^2 d_0 m_1^{(l)} A^{(l)}, \\
 - \sum_{l=-1}^1 k_m l^2 \omega^2 c_1^{(l)} A^{(l)} + \Omega_0^2 \sum_{l=-1}^1 c_1^{(l)} A^{(l)} &= - \sum_{l=-1}^1 D_0 l^2 k^2 c_1^{(l)} A^{(l)} + \sum_{l=-1}^1 D_9 l^4 k^4 c_1^{(l)} A^{(l)},
 \end{aligned}$$

Thus, at the order $(1, 0)$, we obtain $m_1^{(0)} = c_1^{(0)} = 0$.

The order $(1, 1)$ gives raise to the following nonlinear dispersion relation:

$$\omega^2 = \frac{\Omega_0^2 + D_0 k^2 - D_9 k^4}{k_m}, \quad (2.8)$$

along with the following solutions: $\psi \equiv c_1^{(1)}$, $m_1^{(1)} = (\alpha_1 + i\alpha_2)\psi$, with

$$\alpha_1 = \frac{\mu_2(d_0 k^2 + \mu_1)}{(d_0 k^2 + \mu_1)^2 + (\omega k_m)^2}, \quad \alpha_2 = \frac{\omega \mu_2 k_m}{(d_0 k^2 + \mu_1)^2 + (\omega k_m)^2},$$

where ψ is an arbitrary function.

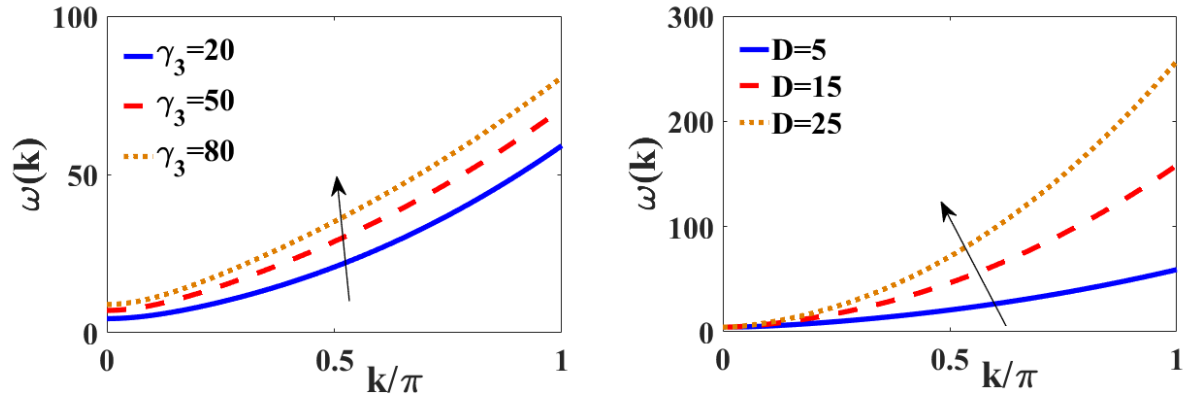


Figure 2.3: The dispersion relation of Eq.2.8. Parameters are chosen as $k_m = 0.1$, $D_m = 0.5\mu m^2 s^{-1}$, $D = 10.0\mu m^2 s^{-1}$, $\gamma_1 = 6.0s^{-1}$, $\gamma_2 = 1.0s^{-1}$, $\gamma_3 = 5.0s^{-1}$.

In Fig.(2.3), we plot The dispersion relation of Eq.2.8 in function of the wave number K . This deviation from the linear dispersion relation is, of course, generated by the nonlinearity [121]. A very important use of the dispersion relation is that it shows immediately whether patterns can grow and if so, what the size of the patterns are. Thus the dispersion curve shows that while

the spatially homogeneous state is stable, the system will amplify patterns of a particular spatial extent, should they be excited by random fluctuations, which are always present in a biological system.

Order (2,1)

This order leads to the following system

$$\begin{aligned}
 & - k_m \sum_{l=-1}^1 v_g \frac{\partial m_1^{(l)}}{\partial \xi} A^{(l)} - k_m \sum_{l=-2}^2 i l \omega m_2^{(l)} A^{(l)} - i \omega (m_1^{(1)})^2 A^2 = -\mu_1 \sum_{l=-2}^2 m_2^{(l)} A^{(l)} + \mu_2 \sum_{l=-2}^2 c_2^{(l)} A^{(l)} \\
 & + \mu_1 [(m_1^{(1)})^2 A^2 + 2|m_1^{(1)}|^2 A^0] + \mu_3 \left[(m_1^{(1)} c_{-1}^{(1)} + m_{-1}^{(1)} c_1^{(1)}) A^{(0)} + m_1^{(1)} c_1^{(1)} A^2 \right] + d_0 \sum_{l=-1}^1 2i l k \frac{\partial m_1^{(l)}}{\partial \xi} A^{(l)} \\
 & - d_0 \sum_{l=-2}^2 l^2 k^2 m_2^{(l)} A^{(l)} - d_1 k^2 [(m_1^{(1)})^2 A^2 + 2|m_1^{(1)}|^2 A^0], \\
 & k_m \sum_{l=-1}^1 2i l \omega v_g \frac{\partial c_1^{(l)}}{\partial \xi} A^{(l)} - k_m \sum_{l=-2}^2 l^2 \omega^2 c_2^{(l)} A^{(l)} + [-\omega^2 (m_{-1}^{(1)} c_1^{(1)} + m_1^{(1)} c_{-1}^{(1)}) A^{(0)} - \omega^2 m_1^{(1)} c_1^{(1)} A^2] \\
 & + \Omega_0^2 \sum_{l=-2}^2 c_2^{(l)} A^{(l)} + \lambda_1 [(c_1^{(1)})^2 A^2 + 2|c_1^{(1)}|^2 A^0] + \lambda_2 \left[(m_1^{(1)})^2 A^2 + 2|m_1^{(1)}|^2 A^0 \right] \\
 & + \lambda_3 \left[(m_1^{(1)} c_{-1}^{(1)} + m_{-1}^{(1)} c_1^{(1)}) A^{(0)} + m_1^{(1)} c_1^{(1)} A^2 \right] - \sigma_1 [-i \omega (-m_1^{(1)} c_{-1}^{(1)} + m_{-1}^{(1)} c_1^{(1)}) A^{(0)} + i \omega m_1^{(1)} c_1^{(1)} A^2] \\
 & = D_0 \left[\sum_{l=-1}^1 2i l k \frac{\partial c_1^{(l)}}{\partial \xi} A^{(l)} - \sum_{l=-2}^2 l^2 k^2 c_2^{(l)} A^{(l)} \right] + D_1 k^2 \left[m_1^{(1)} c_1^{(1)} A^2 + (m_1^{(1)} c_{-1}^{(1)} + m_{-1}^{(1)} c_1^{(1)}) A^{(0)} \right] \\
 & - D_3 k^2 \left[m_1^{(1)} c_1^{(1)} A^2 + (m_1^{(1)} c_{-1}^{(1)} + m_{-1}^{(1)} c_1^{(1)}) A^{(0)} \right] + D_5 k^2 \left[(m_1^{(1)} c_{-1}^{(1)} + m_{-1}^{(1)} c_1^{(1)}) A^{(0)} + m_1^{(1)} c_1^{(1)} A^2 \right] \\
 & - D_8 k^2 i \omega \left[m_1^{(1)} c_1^{(1)} A^2 + (m_{-1}^{(1)} c_1^{(1)} - m_1^{(1)} c_{-1}^{(1)}) A^{(0)} \right] + D_9 \left[\sum_{l=-1}^1 -4i l^3 k^3 \frac{\partial c_1^{(l)}}{\partial \xi} A^{(l)} - \sum_{l=-2}^2 l^4 k^4 c_2^{(l)} A^{(l)} \right] \\
 & + D_{10} k^4 \left[m_1^{(1)} c_1^{(1)} A^2 + (m_1^{(1)} c_{-1}^{(1)} + m_{-1}^{(1)} c_1^{(1)}) A^{(0)} \right], \\
 & .
 \end{aligned}$$

Solutions at order (2, 0) are given by

$$\begin{aligned}
 c_0^{(2)} &= \frac{2}{\Omega_0^2} (\alpha_1 (\omega^2 + D_1 k^2 - D_3 k^2 - \lambda_3 + D_5 k^2 + D_{10} k^4) - \lambda_1 - \lambda_2 (\alpha_1^2 + \alpha_2^2) - \alpha_2 \sigma_1 \omega - D_8 k^2 \alpha_2 \omega) |\psi|^2, \\
 m_0^{(2)} &= \frac{1}{\mu_1} (\mu_2 a_1 - 2d_1 k^2 (\alpha_1^2 + \alpha_2^2) + 2\mu_1 (\alpha_1^2 + \alpha_2^2) + 2\mu_3 \alpha_1) |\psi|^2 \\
 &, \text{ That can be write in the form below: } c_0^{(2)} = a_1 |\psi|^2, \quad m_0^{(2)} = a_2 |\psi|^2
 \end{aligned}$$

At the order (2, 1), the group velocity is found as:

$$v_g = \frac{D_0 k - 2D_9 k^3}{k_m \omega}, \quad (2.9)$$

which is known to verify the Fredholm solvability condition.

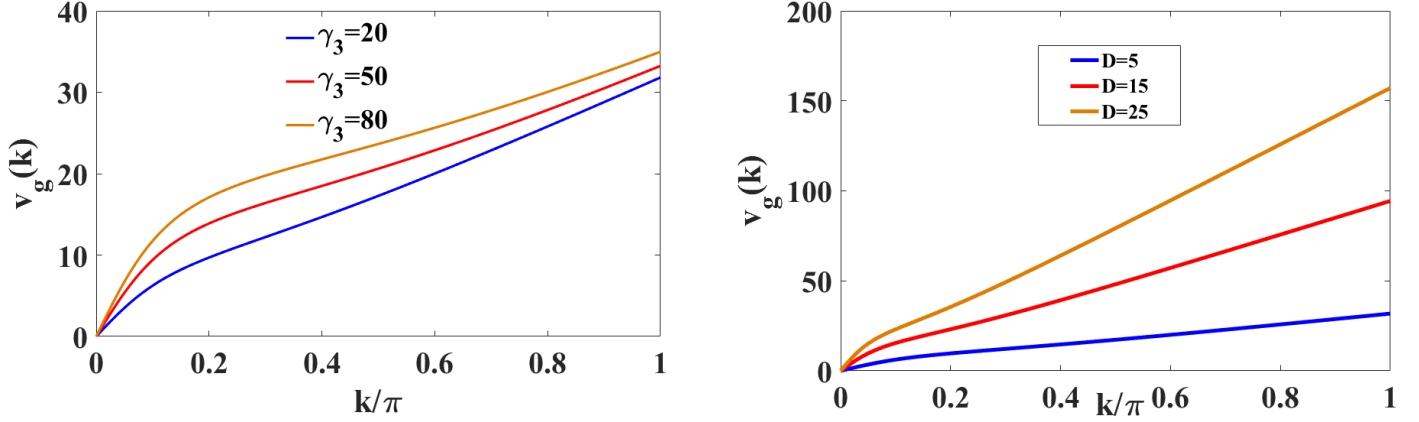


Figure 2.4: The group velocity of Eq.2.9. Parameters are chosen as $k_m = 0.1$, $D_m = 0.5\mu m^2 s^{-1}$, $D = 10.0\mu m^2 s^{-1}$, $\gamma_1 = 6.0s^{-1}$, $\gamma_2 = 1.0s^{-1}$, $\gamma_3 = 5.0s^{-1}$.

The group velocity of Eq.2.9 is represented in Fig.(2.4). It is the velocity with which the overall envelope shape of the wave amplitude, known as the modulation or envelope of the wave propagate through space.

while the non-trivial solutions are expressed by $m_2^{(1)} = \chi$, (χ being another arbitrary function), with:

$$\begin{aligned} c_1^2 = & \left(\frac{1}{(d_0 k^2 + \mu_1)^2 + (\omega k_m)^2} ((d_0 k^2 + \mu_1) \mu_2) \chi + \frac{1}{(d_0 k^2 + \mu_1)^2 + (\omega k_m)^2} [(d_0 k^2 + \mu_1) (\alpha_1 v_g - 2d_0 k \alpha_2) \right. \\ & - \omega (2\alpha_1 d_0 k + \alpha_2 v_g)] \frac{\partial c_1^1}{\partial \xi} \Big) + i \left(\frac{1}{(d_0 k^2 + \mu_1)^2 + (\omega k_m)^2} \omega \mu_2 \chi + \frac{1}{(d_0 k^2 + \mu_1)^2 + (\omega k_m)^2} [(d_0 k^2 + \mu_1) (2\alpha_1 d_0 k \right. \\ & + \alpha_2 v_g) + \omega (\alpha_1 v_g - 2d_0 k \alpha_2)] \frac{\partial c_1^1}{\partial \xi} \Big). \end{aligned}$$

Finally, the order (2, 2) yields the following solutions:

$$\begin{aligned}
 c_2^{(2)} &= \frac{1}{\Omega_0^2 + 4D_0k^2 - 16D_9k^4 - 4k_m\omega^2} (\alpha_1(\omega^2 - \lambda_3 + D_1k^2 - D_3k^2 - D_5k^2 + D_{10}k^4) + \lambda_1 \\
 &+ \lambda_2(\alpha_1^2 - \alpha_2^2) + \omega\alpha_2(-\sigma_1 + D_8k^2)) + i \left[\frac{1}{\Omega_0^2 + 4D_0k^2 - 16D_9k^4 - 4k_m\omega^2} (\alpha_2(\omega^2 - \lambda_3 + k^2D_1 - D_3k^2 \right. \\
 &+ k^4D_{10}) + 2\lambda_2\alpha_1\alpha_2 + \alpha_1\omega(\sigma_1 - D_8k^2)) \left. \right] \psi^2 \\
 m_2^{(2)} &= \frac{1}{(\mu_1 + 4k^2d_0)^2 + (2\omega k_m)^2} + \lambda_1 + ((\mu_1 + 4k^2d_0)(-2\omega\alpha_1\alpha_2 + \mu_2b_1 + \mu_1(\alpha_1^2 - \alpha_2^2) \\
 &+ \mu_3\alpha_1 - d_1k^2(\alpha_1^2 - \alpha_2^2)) - 2\omega \times k_m(\omega(\alpha_1^2 - \alpha_2^2) + \mu_2b_2 + 2\alpha_1\alpha_2\mu_1 + \mu_3\alpha_2 - 2d_1k^2\alpha_1\alpha_2) \\
 &+ i \left[\frac{1}{(\mu_1 + 4k^2d_0)^2 + (2\omega k_m)^2} ((\mu_1 + 4k^2d_0)(\omega(\alpha_1^2 - \alpha_2^2) + \mu_2b_2 + 2\alpha_1\alpha_2\mu_1 + \mu_3\alpha_2 - 2d_1k^2\alpha_1\alpha_2) + 2\omega k_m \right. \\
 &\times (-2\omega\alpha_1\alpha_2 + \mu_2b_1 + \mu_1(\alpha_1^2 - \alpha_2^2) + \mu_3\alpha_1 - d_1k^2(\alpha_1^2 - \alpha_2^2))) \left. \right] \psi^2,
 \end{aligned}$$

This can be writing to simplify the equation in the form below: $c_2^{(2)} = (b_1 + ib_2)\psi^2 m_2^{(2)} = (b_3 + ib_4)\psi^2$

Order (3,1)

The last order (3, l) which will lead to the Cubic Complex Ginzburg-Landau (CCGL) equation in the case $l \leq 1$ gives the system

$$\begin{aligned}
 & \sum_{l=-1}^1 k_m v_g^2 \frac{\partial^2 c_1^{(l)}}{\partial \xi^2} A^{(l)} + \sum_{l=-2}^2 2ilk_m \omega v_g \frac{\partial c_2^{(l)}}{\partial \xi} A^{(l)} - \sum_{l=-1}^1 2ilk_m \omega \frac{\partial x_1^{(l)}}{\partial \tau} A^{(l)} - \omega^2 [m_2^{(0)} c_1^{(1)} + m_2^{(2)} c_1^{(-1)} \\
 & + 4m_1^{(-1)} c_2^{(2)+m_1^{(1)} c_2^{(0)}] + \sum_{l=-3}^3 l^2 \Omega^2 c_3^{(l)} A^{(l)} + 2\lambda_1 [c_1^{(1)} c_2^{(0)} + c_1^{(-1)} c_2^{(2)}] A^1 + \lambda_2 [m_1^{(1)} m_2^{(0)} + m_1^{(-1)} m_2^{(2)}] A^1 \\
 & + \lambda_3 [m_1^{(1)} c_2^{(0)} + m_1^{(-1)} c_2^{(2)} + m_2^{(2)} c_1^{(-1)} + m_2^{(0)} c_1^{(1)}] + \lambda_4 [(m_1^{(1)})^2 c_1^{(-1)} + 2|m_1^{(1)}|^2 c_1^{(1)}] A^1 \\
 & + \lambda_5 [(c_1^{(1)})^2 m_1^{(-1)} + 2|c_1^{(1)}|^2 m_1^{(-1)}] A^1 + \lambda_6 m_1^{(1)} - i\omega \sigma_0 c_1^{(1)} - i\omega \sigma_1 [2m_1^{(-1)} c_2^{(2)} - c_1^{(-1)} m_2^{(2)} + m_2^{(0)} c_1^{(1)}] A^1 \\
 & + i\omega \sigma_2 [(m_1^{(1)})^2 c_1^{(-1)} - 2|m_1^{(1)}|^2 c_1^{(1)}] A^1 = D_0 \left[- \sum_{l=-1}^1 \frac{\partial^2 c_1^{(l)}}{\partial \xi^2} A^{(l)} + \sum_{l=-1}^1 2ilk \frac{\partial c_2^{(l)}}{\partial \xi} A^{(l)} - \sum_{l=-3}^3 l^2 k^2 c_3^{(l)} A^{(l)} \right] \\
 & - D_1 k^2 [4m_1^{(-1)} c_2^{(2)} + c_1^{(-1)} m_2^{(2)} + m_2^{(0)} c_1^{(1)}] A^1 - D_2 k^2 [(m_1^{(1)})^2 c_1^{(-1)} + 2|m_1^{(1)}|^2 c_1^{(1)}] A^1 \\
 & + D_3 k^2 [4c_1^{(-1)} m_2^{(2)} - m_1^{(-1)} c_2^{(2)} - c_2^{(0)} m_1^{(1)}] A^1 + D_4 k^2 [(m_1^{(1)})^2 c_1^{(-1)} + |m_1^{(1)}|^2 c_1^{(1)}] A^1 + D_5 k^2 [c_2^{(2)} m_1^{(-1)} \\
 & + m_2^{(2)} c_1^{(-1)}] A^1 + D_6 k^2 [2|m_1^{(1)}|^2 c_1^{(1)} + (m_1^{(1)})^2 c_1^{(-1)} +] A^1 + D_7 i\omega k^2 c_1^{(1)} - D_8 k^2 i\omega [4m_1^{(-1)} c_2^{(2)} \\
 & - c_1^{(-1)} m_2^{(2)} + m_2^{(0)} c_1^{(1)}] A^1 - D_9 \left[- \sum_{l=-1}^1 6k^4 l^4 \frac{\partial^2 c_1^{(l)}}{\partial \xi^2} A^{(l)} + \sum_{l=-1}^1 4il^3 k^3 \frac{\partial c_2^{(l)}}{\partial \xi} A^{(l)} - \sum_{l=-3}^3 l^4 k^4 c_3^{(l)} A^{(l)} \right] \\
 & - k^4 D_{10} [16m_1^{(-1)} c_2^{(2)} + m_2^{(2)} c_1^{(-1)} + m_2^{(0)} c_1^{(1)}].
 \end{aligned}$$

To further, the order (3, 0) allows to derive $c_3^{(0)} = 0$ and

$$m_3^{(0)} = \frac{1}{\mu_1} (\mu_1 a_1 (\alpha_1 + i\alpha_2) + \mu_3 a_2 (\alpha_1 + i\alpha_2) + 2\mu_4 (\alpha_1^2 + \alpha_2^2)) |\psi|^2 \psi.$$

with:

$$\alpha_1 = \frac{\mu_2 (d_0 k^2 + \mu_1)}{(d_0 k^2 + \mu_1)^2 + (\omega k_m)^2}, \quad \alpha_2 = \frac{\omega \mu_2 k_m}{(d_0 k^2 + \mu_1)^2 + (\omega k_m)^2},$$

$$\begin{aligned}
 a_1 &= \frac{2}{\Omega_0^2} (\alpha_1 (\omega^2 + D_1 k^2 - D_3 k^2 - \lambda_3 + D_5 k^2 + D_{10} k^4) - \lambda_1 - \lambda_2 (\alpha_1^2 + \alpha_2^2) - \alpha_2 \sigma_1 \omega - D_8 k^2 \alpha_2 \omega) \\
 a_2 &= \frac{1}{\mu_1} (\mu_2 a_1 - 2d_1 k^2 (\alpha_1^2 + \alpha_2^2) + 2\mu_1 (\alpha_1^2 + \alpha_2^2) + 2\mu_3 \alpha_1)
 \end{aligned}$$

At the order (3, 1) the terms in $x_3^{(1)}$ and the terms in $\frac{\partial x_2^{(1)}}{\partial \xi}$ cancel out simultaneous due to the dispersion relation on the one hand and the solvability condition on the other hand. Therefore,

after taking into account the previous relations we obtain

$$\begin{aligned}
& 2i\omega k_m \frac{\partial \psi}{\partial \tau} + \frac{(D_0 - 6D_9 k^4 - k_m v_g^2)}{2\omega k_m} \frac{\partial^2 \psi}{\partial \xi^2} + \left[\frac{1}{2\omega k_m} \left(\omega^2 (a_2 + b_3 + 4b_1 \alpha_1 + 4b_2 \alpha_2 + a_1 \alpha_1) - 2\lambda_1 (a_1 + b_1) \right. \right. \\
& - \lambda_2 (\alpha_1 a_2 + \alpha_1 b_3 + \alpha_2 + b_4) - \lambda_3 (\alpha_1 a_1 + \alpha_1 b_1 + \alpha_2 b_2 + \alpha_1 b_3 + \alpha_2 b_4 + a_2) - \lambda_4 (3\alpha_1^2 + \alpha_2^2) - 3\lambda_5 \alpha_1 \\
& + \sigma_1 \omega (-2b_2 \alpha_1 + 2b_1 \alpha_2 + b_4) + 2\sigma_2 \omega \alpha_1 \alpha_2 - D_1 k^2 (4(\alpha_1 b_1 + \alpha_2 b_2) + b_3 + a_2) - D_2 k^2 (3\alpha_1^2 + \alpha_2^2) \\
& + D_3 k^2 (4b_3 - \alpha_1 b_1 - \alpha_2 b_2 - a_1 \alpha_1) + 2D_4 \alpha_1 k^2 + D_5 k^2 (b_1 \alpha_1 + b_2 \alpha_2 + b_3) + D_6 k^2 (3\alpha_1^2 + \alpha_2^2) \\
& \left. \left. - D_8 k^2 \omega (-8\alpha_1 b_2 + 8\alpha_2 b_1 + \alpha_2) + D_{10} k^4 (16(b_1 \alpha_1 + b_2 \alpha_2) + \alpha_1 + a_2) \right) \right] \\
& + i \left(\frac{1}{2\omega k_m} \left(\omega^2 (b_4 + 4\alpha_1 b_2 - 4\alpha_2 b_1 + \alpha_2 a_1) - 2\lambda_1 b_2 - \lambda_2 (\alpha_2 a_2 + \alpha_1 b_4 - \alpha_2 b_3) \right. \right. \\
& - \lambda_3 (\alpha_2 a_1 + \alpha_1 b_2 - \alpha_2 b_1 + \alpha_1 b_4 - \alpha_2 b_3) - 2\lambda_4 \alpha_1 \alpha_2 - \lambda_5 \alpha_2 + \omega \sigma_1 (2\alpha_1 b_1 \\
& + 2\alpha_2 b_2 - b_3 + a_2) + \omega \sigma_2 (\alpha_1^2 + 3\alpha_2^2) - D_1 k^2 (4(\alpha_1 b_2 - \alpha_2 b_1) + b_4) - 2D_2 k^2 \alpha_1 \alpha_2 \\
& + D_3 k^2 (4b_4 - \alpha_1 b_2 + \alpha_2 b_1 - a_1 \alpha_2) + 2D_4 k^2 \alpha_1 \alpha_2 + D_5 k^2 (-b_1 \alpha_2 + b_2 \alpha_1 + b_4) + 2D_6 k^2 \alpha_1 \alpha_2 \\
& \left. \left. - D_8 k^2 \omega (8\alpha_1 b_1 - 8\alpha_2 b_2 - \alpha_1 + a_2) + D_{10} k^4 (16(b_2 \alpha_1 - b_1 \alpha_2) + \alpha_2) \right) \right) \right] \times |\psi|^2 \psi \\
& = \left[\frac{1}{2\omega k_m} (\lambda_6 \alpha_2 - \omega \sigma_0 - D_7 k^2 \omega) + i \left(\frac{-\lambda_6 \alpha_1}{2\omega k_m} \right) \right] \psi
\end{aligned}$$

In short, the equation for envelope solution $\psi \equiv c_1^{(1)}$ reads

$$i \frac{\partial \psi}{\partial \tau} + P \frac{\partial^2 \psi}{\partial \xi^2} + Q |\psi|^2 \psi = iR \psi, \quad (2.10)$$

whit $R = (R_r + iR_i)$ and $Q = (Q_r + iQ_i)$. Where the dispersion coefficient P , the real and imaginary parts Q_r and Q_i of the nonlinearity coefficient, the real and imaginary part R_r and R_i of the dissipation coefficient are given are given in **Appendix A3**.

Equation Eq.(2.10) describes the spatiotemporal evolution of envelop soliton $\psi(\xi, \tau)$ associated to the concentration of MARCKS protein in the cytosol. In this equation, the dispersion coefficient P is real, while the nonlinearity coefficient Q and the dissipative coefficient R are both complex with Q_r and R_r theirs real parts and Q_i and R_i theirs imaginary parts, respectively. Therefore, Eq.(2.10) is well-known as the 1D-CCGL equation which is one of the most-studied nonlinear equations in the physics community. Similar equation was previously found by Moukam *et al.* [122] in the context of propagation and transmission of action membrane potential through neural networks. Here it will be useful to seek the domains of parameter space where transport of MARCKS protein from cytoplasmic membrane into cytosol is modulationally unstable. Thus, involving soliton-like wave known as the best candidate in information transport within biological cells [123].

2.3.2 The Hirota Bilinear Method (HBM)

The bilinear, or Hirota's direct, method was invented in the early 1970s as an elementary means of constructing soliton solutions that avoided the use of the heavy machinery of the inverse scattering transform and was successfully used to construct the multisoliton solutions of many new equations. This approach provided a direct method for finding N-soliton solutions to non-linear evolutionary equations. The author applied this method to the Korteweg-deVries (KdV) equation [124]. Over the last two decades this method has been shown to be applicable to a large class of nonlinear evolution equations, including difference-differential and integro-differential equations [125]. Hirota bilinear method, which is usually applied to completely integrable equations, is well suited for partially integrable equations as well [126]. In this section, we explain how to transform a nonlinear differential equation into a type of a bilinear differential equation, often called the Hirota form, and discuss how to find an exact solution by a perturbation method. Let us consider

$$G \left(u, \frac{\partial u}{\partial t}, \frac{\partial u}{\partial x}, \frac{\partial^2 u}{\partial x \partial t}, \frac{\partial^2 u}{\partial t^2}, \frac{\partial^2 u}{\partial x^2}, \frac{\partial^3 u}{\partial t^2 \partial x}, \frac{\partial^3 u}{\partial t \partial x^2} \dots \right) = 0, \quad (2.11)$$

as the model to be solved, where $u(x, t)$ depends on how the equation is built. The bilinearization of Eq.(2.11) requires to consider $u(x, t)$ in a specific form For example, if Eqs.(2.3- 2.4) is reduced to the nonlinear Schrödinger equation, then we must set $u(x, t) = \frac{H(x,t)}{F(x,t)}$, and if Eqs.(2.3- 2.4) is reduced to a cubic complex Ginzburg-Landau equation, then $u(x, t) = \frac{H(x,t)}{F^{1+i\delta}(x,t)}$. In all these cases, $H(x, t)$ and $F(x, t)$ are, respectively complex and real functions. As part of Hirota's analysis he introduced a bilinear form defined as:

$$D_{x,\alpha}(F \cdot H) = \left(\frac{\partial}{\partial x_1} - \alpha \frac{\partial}{\partial x_2} \right) F(x_1)H(x_2)|_{x_1=x_2}, \quad (2.12)$$

or, more generally

$$D_{x,\alpha}^m(F \cdot H) = \left(\frac{\partial}{\partial x_1} - \alpha \frac{\partial}{\partial x_2} \right)^m \left(\frac{\partial}{\partial t_1} - \alpha \frac{\partial}{\partial t_2} \right)^n F(x_1)H(x_2)|_{x_1=x_2, t_1=t_2}, \quad (2.13)$$

$m, n \in \mathbb{N}$,

Where D is a binary operator (because it operates on a pair of functions) and is called the Hirota derivative. Some examples of bilinear operations follow.

$$\begin{aligned} D_x(F \cdot H) &= F_x H - F H_x = -D_x(H \cdot F), \\ D_x^2(F \cdot H) &= F_{xx} H - 2F_x H_x + F H_{xx} = D_x^2(H \cdot F), \\ D_x D_t(F \cdot F) &= 2(F F_x - F_x F_t) \end{aligned} \quad (2.14)$$

Then, Eq.(2.11) is factorized in a polynomial form hence:

$$P(D_t, D_x, D_x \cdot D_t, D_{xx} \dots) F \cdot F = 0. \quad (2.15)$$

Eq.(2.15) is the generic class of bilinear equations. The perturbation method consists of expanding F with respect to a small parameter ϵ to obtain.

$$F(x, t) = f_0 + \epsilon f_1(x, t) + \epsilon^2 f_2(x, t) + \epsilon^3 f_3(x, t) + \epsilon^4 f_4(x, t) + \dots \quad (2.16)$$

The first order solution of Eq.(2.15) is obtained by truncating the expansion Eq.(2.16) at the first order, hence Eq.(2.15) becomes,

$$P(D_x, D_t, D_x \cdot D_t, D_{xx} \dots) [f_0 \cdot f_0 + \epsilon (f_0 \cdot f_1 + f_1 \cdot f_0) + \epsilon^2 (f_1 \cdot f_1)] = 0, \quad (2.17)$$

Eq.(2.17) is solved recursively at each order of ϵ . The first and second order of ϵ yield

$$(\epsilon) : P \left(\frac{\partial}{\partial t}, \frac{\partial}{\partial x}, \frac{\partial^2}{\partial x \partial t}, \frac{\partial^2}{\partial x^2} \dots \right) f_1(x, t) = 0, \quad (2.18a)$$

$$(\epsilon^2) : P(D_x, D_t, D_x \cdot D_t, D_{xx} \dots) f_1 \cdot f_1 = 0, \quad (2.18b)$$

Eq.(2.18a) is linear, hence its solutions may be taken as

$$f_1(x, t) = e^{px+qt+p_0}. \quad (2.19)$$

p , q , and p_0 are constant that may be determined by inserting the solution Eq.(2.19) into Eq.(2.18b), hence are constructed analytical solutions of Eq.(2.10)

Illustration of the Hirota Bilinear Method to solve the 1D-CCGL equation

In order to specify spatiotemporal evolutions of weak order protein concentration, solutions of Eq.(2.10) should be constructed. The singularity analysis of this equation that starts by adopting the ansatz:

$$\psi = \frac{G \exp(Kx - \Omega t)}{F^{1+i\alpha}}, \quad (2.20)$$

where K , Ω , α and $F(x, t)$ are assume to be real, with G a complex function. By inserting Eq.(2.20) into Eq.(2.10), and decoupling the obtained relation, we arrive at the following bilinear equation:

$$\begin{aligned} & \frac{G^*F}{Q} [\Omega - K^2P - \lambda + iD_{\alpha,t} + 2iKPD_{\alpha,x} + PD_{\alpha,x}^2](GF) \\ = & |G|^2 \left[\frac{P(1+i\alpha)(2+i\alpha)D_{1,x}^2}{2Q} + \left(\frac{iR}{2} - \lambda\right)(FF) - |G|^2 \right], \end{aligned} \quad (2.21)$$

where the complex constant parameters $\lambda = \lambda_r + i\lambda_i$ were introduced as the decoupling parameters. According to Hirota method [127], the bilinear operator $D_{\alpha,x}$ is defined by:

$$\begin{aligned} D_{\alpha,x}(GF) &= \left[\frac{\partial}{\partial x} - (1+i\alpha)\frac{\partial}{\partial x'} G(x)F(x') \right]_{x=x'} \\ D_{\alpha,x}^2(GF) &= \left[\left(\frac{\partial}{\partial x} - (1+i\alpha)\frac{\partial}{\partial x'} \right)^2 G(x,t)G(x',t') \right]_{x=x',t=t'} \\ D_x^2(FF) &= \left[\left(\frac{\partial}{\partial x} - (1+i\alpha)\frac{\partial}{\partial x'} \right) F(x,t)F(x',t') \right]_{x=x',t=t'} \end{aligned}$$

the functions F and G take the form:

$G = G_0 \exp(\theta)$ and $F = 1 + \exp(\theta + \theta^*)$, where $K = K_r + iK_i$ and $\Omega = \Omega_r + i\Omega_i$, being a complex constant. A complex constant λ and α are determined so that the right hand side of Eq.(2.21) becomes real, thus those parameters are subject to constraints:

$Q_i(R_i + \lambda_r) = Q_r(R_r + \lambda_i)$, with , where $|G_0|^2 = \frac{4k_r}{A}$, $Imk = k_i = \alpha k_r$, $Re\omega = \omega_r = 0$, $Im\omega = \omega_i = [(\alpha^2 - 1)P]k_r^2 - R_i$, $k_r^2 = \frac{3AR_r}{2Q_i}$ and A can be always taken positive so that $|G_0|^2 > 0$. Setting $K = \Omega = 0$, the general soliton solution can then be written:

$$\psi(x,t) = \frac{G_0 \exp(\theta)}{[1 + \exp(\theta + \theta^*)]^{1+i\alpha}}. \quad (2.22)$$

With: $|G_0|^2 = \frac{-3R_r}{Q_r}$, $\beta = \frac{3Q_r}{2Q_i}$, $\Omega = PK^2 - Q_r|G_0|^2 - R_i$, $\alpha = -\beta \pm (2 + \beta^2)^{\frac{1}{2}}$, $A = \frac{Q_r}{P(2-\alpha^2)}$, $\theta = kx - vt$, $\theta^* = k^*x - \omega t$, $k = k_r + ik_i$, $k_r = \sqrt{\frac{-3AR_r}{4Q_i}}$, $k_i = \alpha k_r$, $v = v_r + iv_i$, with $v_r = 0$ and $v_i = \frac{1}{2}[R_i - \frac{3APR_r}{4Q_i}(\alpha^2 - 1)]$

Therefore, based on all above relations, in particular,Eq.(2.6) , solutions of Eqs.(2.3-(2.4)) are given by

$$\begin{aligned}
 m(x, t) &= 2\epsilon [(\alpha_1\psi_r - \alpha_2\psi_i) \cos \theta \\
 &\quad - (\alpha_2\psi_r + \alpha_1\psi_i) \sin \theta] + O(\epsilon^2), \\
 c(x, t) &= 2\epsilon(\psi_r \cos \theta - \psi_i \sin \theta) + O(\epsilon^2), \\
 p(x, t) &= \frac{2\epsilon}{\gamma_2} [\omega(\psi_r \sin \theta + \psi_i \cos \theta) \\
 &\quad + (\gamma_3 + Dk^2)(\psi_r \cos \theta - \psi_i \sin \theta)] + O(\epsilon^2),
 \end{aligned} \tag{2.23}$$

where ψ_r and ψ_i denote real and imaginary parts of ψ , $\theta = kx - \omega t$, k and ω being the wave number and angular frequency of the carrier wave.

2.3.3 Leon and Manna method

This method rely on the definition of a large grid scale via the comparison of the magnitude of the related difference operator, and on the expansion of the wavenumber in powers of frequency variations due to nonlinearity [121]. According to the multiple scale expansion analysis, the MARCKS protein is considered to be excited with the natural frequency Ω , which depends on the actual frequency ω and the wavenumber q . The relationship between both angular frequency is giving by: $\omega = \Omega_0 + \epsilon\lambda$, while the actual wavenumber is expressed by: $q = q_0 + \epsilon\frac{\lambda}{v_g} + \epsilon^2 c_g \lambda^2 + \dots$, where $v_g = \frac{\partial\Omega}{\partial q}$ represents the group velocity and $2c_g = \frac{\partial^2 q}{\partial \Omega^2}$ represents the group velocity dispersion. Parameter λ is a small deviation from the natural frequency Ω . For $\epsilon = 0$, the frequency ω can be reduced to the natural frequency Ω of the system. Solutions of Eq.(2.5) can be summarized in terms of the state vector $v_n(t) = (m_n(t), c_n(t), p_n(t))$, whose the generalized form of the unperturbed expressions can be taken in the form:

$$v_n(t) = \int d\omega \hat{V}(\omega) \exp i(\omega t + q_0 n), \tag{2.24}$$

where $\hat{V}(\omega) = (\hat{M}_n(\omega), \hat{C}_n(\omega), \hat{P}_n(\omega))$. After including the derivation of ω and q , the generalized solutions take the form:

$$\begin{aligned}
 m_n(t) &= A(n, t)\psi(\zeta_n, \tau_n), \\
 c_n(t) &= A(n, t)\theta(\zeta_n, \tau_n), \\
 p_n(t) &= A(n, t)\chi(\zeta_n, \tau_n),
 \end{aligned} \tag{2.25}$$

where $A(n, t) = \exp i(qn + \omega t)$, $\tau_n = \epsilon(t + \frac{n}{v_g})$, $\zeta_n = \epsilon^2 n$ and $c_g = 1$. The small parameter can be taken as $\epsilon^2 = \frac{1}{N}$. In order to support a large grid, we have introduced a new lattice m . Thus, for a

given lattice number n , only a set of lattice points can be constructed at each $N = \epsilon^{-2}$. Therefore, we can index ζ_n by m so that $(n - N) \rightarrow (m - 1), n \rightarrow m, (n + N) \rightarrow (m + 1)$. More precisely, $\zeta_n - N = (m - 1), \zeta_n = m, \zeta_n + N = (m + 1)$. All the above implies that the slow modulations $v(\zeta_n, \tau_n)$ of the plane wave $A(n, t)$ can be replaced by the functions $v(m, \tau)$ of the variables m and $\tau = \tau_n$. While the second discrete derivative of $v_n(t) = A(n, t)\psi(\zeta_n, \tau_n)$ is given by:

$$\begin{aligned} v_{n+1} - 2v_n + v_{n-1} &= [A_{n+1} - 2A_n + A_{n-1}]\psi_m + \frac{\epsilon}{v_g}[A_{n+1} - A_{n-1}]\frac{\partial\psi_m}{\partial\tau} \\ &+ (\epsilon/v_g)^2 \frac{1}{2}[A_{n+1} + A_{n-1}]\frac{\partial^2\psi_m}{\partial\tau^2} + \frac{\epsilon^2}{2}[A_{n+1} - A_{n-1}][\psi_{n+1} - \psi_{n-1}] \end{aligned}$$

Following all the above, the solutions for the set of Eq.(2.5) can be investigated in the form of the Fourier series, in power of the small parameter ϵ :

Illustration of the Leon and Manna method using the inhomogeneous reaction-diffusion model (2010)

According to the multiple scale expansion analysis, the MARCKS protein is considered to be excited with the natural frequency Ω which depends on the actual frequency ω and the wavenumber q . The relationship between both angular frequency is giving by: $\omega = \Omega_0 + \epsilon\lambda$, while the actual wavenumber is expressed by: $q = q_0 + \epsilon\frac{\lambda}{v_g} + \epsilon^2 c_g \lambda^2 + \dots$, where $v_g = \frac{\partial\Omega}{\partial q}$ represents the group velocity and $2c_g = \frac{\partial^2 q}{\partial\Omega^2}$ represents the group velocity dispersion. Parameter λ is a small deviation from the natural frequency Ω . For $\epsilon = 0$, the frequency ω can be reduced to the natural frequency Ω of the system. Solutions of Eq.(2.5) can be summarized in terms of the state vector $v_n(t) = (m_n(t), c_n(t), p_n(t))$, whose the generalized form of the unperturbed expressions can be taken in the form:

$$v_n(t) = \int d\omega \hat{V}(\omega) \exp i(\omega t + q_0 n), \quad (2.26)$$

where $\hat{V}(\omega) = (\hat{M}_n(\omega), \hat{C}_n(\omega), \hat{P}_n(\omega))$. After including the derivation of ω and q , the generalized solutions take the form:

$$\begin{aligned} m_n(t) &= A(n, t)\psi(\zeta_n, \tau_n), \\ c_n(t) &= A(n, t)\theta(\zeta_n, \tau_n), \\ p_n(t) &= A(n, t)\chi(\zeta_n, \tau_n), \end{aligned} \quad (2.27)$$

where $A(n, t) = \exp i(qn + \omega t)$, $\tau_n = \epsilon(t + \frac{n}{v_g})$, $\zeta_n = \epsilon^2 n$ and $c_g = 1$. The small parameter can be taken as $\epsilon^2 = \frac{1}{N}$. In order to support a large grid, we have introduced a new lattice m .

Thus, for a given lattice number n , only a set of lattice points can be constructed at each $N = \epsilon^{-2}$. Therefore, we can index ζ_n by m so that $(n - N) \rightarrow (m - 1), n \rightarrow m, (n + N) \rightarrow (m + 1)$. More precisely, $\zeta_n - N = (m - 1), \zeta_n = m, \zeta_n + N = (m + 1)$. All the above implies that the slow modulations $v(\zeta_n, \tau_n)$ of the plane wave $A(n, t)$ can be replaced by the functions $v(m, \tau)$ of the variables m and $\tau = \tau_n$. This approach based on discrete multi-scale analysis has been studied in [128–130]. Following all the above, the solutions for the set of Eq.(2.5) can be investigated in the form of the following Fourier series, in power of the small parameter ϵ :

$$\begin{aligned} m_n(t) &= \sum_{s=1}^{\infty} \epsilon^s \sum_{l=-s}^s \psi_s^{(l)}(\zeta_n, \tau_n) A^{(l)}(n, t), \\ c_n(t) &= \sum_{s=1}^{\infty} \epsilon^s \sum_{l=-s}^s \theta_s^{(l)}(\zeta_n, \tau_n) A^{(l)}(n, t), \\ p_n(t) &= \sum_{s=1}^{\infty} \epsilon^s \sum_{l=-s}^s \chi_s^{(l)}(\zeta_n, \tau_n) A^{(l)}(n, t), \end{aligned} \quad (2.28)$$

with $\psi_s^{-l}(m, \tau) = (\psi_s^l(m, \tau))^*$, $\theta_s^{-l}(m, \tau) = (\theta_s^l(m, \tau))^*$, and $\chi_s^{-l}(m, \tau) = (\chi_s^l(m, \tau))^*$, where the asterisk (*) represents the complex conjugate of the preceding term. Inserting the above solutions into Eq.(2.5) leads to a set of coupled equations to be solved at different orders of the small parameter ϵ , with the corresponding harmonics l .

At the leading order $(1, l)$, with $l = 0$, we obtain $\psi_1^{(0)}(m, \tau) = \theta_1^{(0)}(m, \tau) = \chi_1^{(0)}(m, t) = 0$. For $l = 1$, the dispersion relation :

$$\begin{aligned} &(i\omega)^3 + (i\omega)^2(\gamma_2 - 8D \sin^2 \frac{q}{2} + \gamma_3 + \alpha_0 - 4D_0 \sin^2 \frac{q}{2}) \\ &+ (i\omega)[(\gamma_3 - 4D \sin^2 \frac{q}{2})(\gamma_2 - 4D \sin^2 \frac{q}{2}) + (\alpha_0 - 4D_0 \sin^2 \frac{q}{2}) \\ &\times (\gamma_2 + \gamma_3 - 8D \sin^2 \frac{q}{2})] + (\alpha_0 - 4D_0 \sin^2 \frac{q}{2})(\gamma_3 - 4D \sin^2 \frac{q}{2}) \\ &\times (\gamma_2 - 4D \sin^2 \frac{q}{2}) - \alpha_0 \gamma_3 \gamma_2 = 0, \end{aligned} \quad (2.29)$$

should be satisfied for the system to admit non-trivial solutions in the form: $\psi_1^{(1)}(m, \tau) = \varphi(m, \tau), \chi_1^{(1)} = a\varphi(m, \tau), \theta_1^{(1)} = b\varphi(m, \tau)$. The coefficients a and b are obtained as:

$$a = \frac{\alpha_0}{i\omega + \gamma_2 - 4D \sin^2 \frac{q}{2}}, \quad b = \frac{a\alpha_0}{i\omega + \gamma_3 - 4D \sin^2 \frac{q}{2}}.$$

. At the order (2, 0) the following solutions

$$\begin{aligned}\psi_2^{(0)} &= \frac{-2\alpha}{\alpha_0} |\psi_1^{(1)}|^2, \\ \theta_2^{(0)} &= \left(\frac{-2\alpha_1}{\gamma_3} + \frac{2\gamma_2 a(\gamma_3 - 4D \sin^2 \frac{q}{2})}{(\gamma_3 - 4D \sin^2 \frac{q}{2}) + \omega^2} \right) |\psi_1^{(1)}|^2, \\ \chi_2^{(0)} &= \left(\frac{-2\alpha_1}{\gamma_2} + \frac{2\gamma_3 a(\gamma_3 - 4D \sin^2 \frac{q}{2})}{(\gamma_3 - 4D \sin^2 \frac{q}{2}) + \omega^2} \right) |\psi_1^{(1)}|^2,\end{aligned}$$

are found. While at the order (2, 1), the group velocity which satisfies the Fredholm solvability condition is expressed by:

$$v_g = \frac{i \sin q \left(D_0(i\omega + \gamma_2)(i\omega + \gamma_3) + D\gamma_3 b(i\omega + \gamma_2) + D\gamma_2 \gamma_3 a \right)}{(i\omega + \gamma_2)(i\omega + \gamma_3) + \gamma_3 b(i\omega + \gamma_2) + \gamma_3 \gamma_2 a}. \quad (2.30)$$

At the same order, solutions should be found in the form:

$$\begin{aligned}\psi_2^{(1)} &= \delta, \quad \chi_2^{(1)} = \frac{1}{i\omega + \gamma_2} \left(\alpha_0 \delta + \frac{2iDa \sin q}{v_g} - 1 \right) \frac{\partial \psi_1^{(1)}}{\partial \tau}, \\ \theta_2^{(1)} &= \frac{1}{(i\omega + \gamma_2)(i\omega + \gamma_3)} \left(\alpha_0 \gamma_2 \delta + a \left(\frac{2iD \sin q}{v_g} - 1 \right) + b \left(\frac{2iD \sin q}{v_g} - 1 \right) \right) \frac{\partial \psi_1^{(1)}}{\partial \tau},\end{aligned}$$

where $\delta(m, \tau)$ is an arbitrary function. Still at the same order ($s = 2$), for $l = 2$, solutions are giving in the form $\psi_2^{(2)} = a_2(\psi_1^{(1)})^2$, $\theta_2^{(2)} = a_3(\psi_1^{(1)})^2$, $\chi_2^{(2)} = a_4(\psi_1^{(1)})^2$, while the coefficients a_2 , a_3 and a_4 are given in **Appendix B**.

At the order ϵ^3 , the differential-difference equation investigated is derived for the case $l = 1$. Considering the fact that the coefficients of the terms $\chi_3^{(1)}(m, \tau)$, $\frac{\partial \psi_1^{(1)}(m, \tau)}{\partial \tau}$ are cancelled out due to the dispersion relation and the group velocity, the amplitude equation in $\varphi(m, \tau) \equiv \varphi_m$ reads:

$$iP[\varphi_{m+1} - \varphi_{m-1}] + Q \frac{\partial^2 \varphi_m}{\partial \tau^2} + R |\varphi_m|^2 \varphi_m = 0, \quad (2.31)$$

with:

$$\begin{aligned}
 P &= \sin q \left(D_0(i\omega + \gamma_2)(i\omega + \gamma_3) + D\gamma_3(i\omega + \gamma_2) + D\gamma_2\gamma_3 \right), \\
 Q &= \frac{\cos q}{v_g^2} \left[D_0(i\omega + \gamma_2)(i\omega + \gamma_3) + D\gamma_3(i\omega + \gamma_2) + D\gamma_2\gamma_3 \right], \\
 R &= (i\omega + \gamma_2)(i\omega + \gamma_3) \left[3\alpha_2 + 2\alpha_1 a_2 - (\gamma_3 b_2 a_2 + \gamma_3 a_2 + 4a_2 D_1 \sin^2 \frac{q}{2} + 4D_2 \sin^2 \frac{q}{2}) \right] \\
 &\quad + \gamma_3(i\omega + \gamma_2)(\gamma_3 a_3 + \gamma_2 a_2 b_2) - \gamma_2 \gamma_3 (2\alpha_1 a_2 + 3\alpha_2).
 \end{aligned}$$

The coefficients P , Q and R depend on the starting model equation and on the frequency of the carrier wave.

Eq.(2.31) represents the discrete nonlinear Schrödinger (DNLS) equation. The global form of such equation has already been obtained in some biological context including, DNA nonlinear dynamics [131], blood flow [132] or nonlinear dynamics of membrane potential in the central nervous system [133, 134].

2.4 Numerical schemes

In real physical experiments, there are some imperfections that shall perturb the system under consideration. These imperfections shall induce a small amount of perturbation that may destroy exact unstable solutions, which will not be observed in experiments. For these reasons, an approximate analytical solutions are compared with exact numerical solutions of the nonlinear partial differential equation under study. In this thesis, we have used different numerical methods in order to integrate the model equations of Eqs.(2.3-2.4).

2.4.1 Finite difference Method

We know how to solve ordinary differential equations, so in a way we are able to deal with the time derivative. Very often in mathematics, a new problem can be solved by reducing it to a series of problems we know how to solve. In the present case, it means that we must do something with the spatial derivative $\frac{\partial^2}{\partial x^2}$ in order to reduce the partial differential equation to ordinary differential equations. One important technique for achieving this, is based on finite difference discretization of spatial derivatives. To Reduce a PDE to a System of ODEs, we introduce a spatial mesh in the domain Ω with mesh points: $x_0 = 0 < x_1 < x_2 < \dots < x_N = L$. The space between two mesh points x_i and x_{i+1} *i.e.* the interval $[x_i, x_{i+1}]$, is called a cell. We shall here, for simplicity, assume that each cell has the same length $\Delta x = x_{i+1} - x_i, i = 0, \dots, N - 1$. The partial differential equation is valid at all spatial points $x \in \Omega$, but this condition is fulfilled at the internal mesh points only,

x_1, \dots, x_{N-1} :

$$\frac{\partial u(x_i, t)}{\partial t} = \beta \frac{\partial^2 u(x_i, t)}{\partial x^2} + g(x_i, t), i = 1, \dots, N - 1. \quad (2.32)$$

Now, at any point x_i we can approximate the second-order derivative by a finite difference as:

$$\left(\frac{\partial^2 u(x_i, t)}{\partial x^2} \right)_i \approx \frac{u(x_{i+1}, t) - 2u(x_i, t) + u(x_{i-1}, t)}{\Delta x^2}, \quad (2.33)$$

Where the first-order derivative by a finite difference is given as:

$$\left(\frac{\partial u_i(t)}{\partial t} \right)_i = \frac{u_{i+1} - u_i}{\Delta x} + 0(\Delta x)$$

It is common to introduce a short notation $u_i(t)$ for $u(x_i, t)$. With this new notation we can, after inserting (2.30) in (2.29), write an approximation to the partial differential equation at mesh point (x_i, t) as:

$$\frac{u_{i+1} - u_i}{\Delta x} = \beta \frac{u_{i+1}(t) - 2u_i(t) + u_{i-1}(t)}{\Delta x^2} + g_i(t), i = 1, \dots, N - 1. \quad (2.34)$$

Application of the finite difference method into Eqs.(2.3-2.4)

$$\begin{aligned} \frac{m_{i+1} - m_i}{h} &= \gamma_3 c_i (1 - m_i) - \frac{\gamma_1 m_i (1 - m_i)}{k_m + m_i} + D_m \frac{m_{i+1} - 2m_i + m_{i-1}}{h^2}, i = 1, \dots, N - 1. \\ \frac{c_{i+1} - c_i}{h} &= -\gamma_3 c_i (1 - m_i) + \gamma_2 p + D \frac{c_{i+1} - 2c_i + c_{i-1}}{h^2}, \\ \frac{p_{i+1} - p_i}{h} &= \frac{\gamma_1 m_i (1 - m_i)}{k_m + m_i} - \gamma_2 p + D_m \frac{m_{i+1} - 2m_i + m_{i-1}}{h^2}, \end{aligned} \quad (2.35)$$

2.4.2 The fourth order Runge-Kutta method (RK4)

The fourth order Runge-Kutta (RK4) is an integration technique used to numerically approximate solutions of ordinary linear and nonlinear differential equations. The 4th-order Runge-Kutta method (RK4) is clearly the most widely used method to solve ODEs. Its power comes from high accuracy even with not so small time steps. Assuming that the equation to solve takes the form of Eqs. (2.2- 2.4), the first step to apply the RK4 methods consists of writing Eqs.(2.3-2.4) in the form of an ordinary differential equation. One way of doing that consists of discretizing all the spatial derivatives embedded in Eqs.(2.3-2.4) using a centered finite difference. At a precise point

of the grid space, Eqs.(2.3-2.4) becomes

$$\frac{du_j}{dt} = F(t, u_j(t)), \quad u_j(t=0) = u_{j0}, \quad t > 0, \quad \text{where} \quad u_j(t) = u(x = j \cdot dx, t). \quad (2.36)$$

Then integrating Eqs.(2.3-2.4) using the RK4 scheme requires to calculate the intermediary variables and used the latter ones to extract the values of $u(x,t)$. The algorithm reads

$$\begin{aligned} K_{1j} &= F(t, u_j(t)), \\ K_{2j} &= F(t + dt/2, u_j(t) + K_{1j}/2), \\ K_{3j} &= F(t + dt/2, u_j(t) + K_{2j}/2), \\ K_{4j} &= F(t + dt, u_j(t) + K_{3j}), \\ u_j(t + dt) &= \frac{1}{6} (K_{1j} + 2 \cdot K_{2j} + 2 \cdot K_{3j} + K_{4j}). \end{aligned} \quad (2.37)$$

2.5 Conclusion

In this chapter we have reviewed both the MARCKS protein model with homogenous spatial diffusion coefficients and with inhomogeneity effects. We reviewed the main methods (analytical and numerical) applied to both models in this dissertation. The reductive perturbation method, Leon and Manna method, underpinning most of this dissertation was reviewed in this chapter as well as corresponding methods allowing for the reduction of the dynamics of the MARCKS protein models. A brief review of a few relevant analytical methods in constructing exact solutions was also conducted.

RESULTS AND DISCUSSION

3.1 Introduction

In this chapter, we use the latter approaches to investigate MARCKS protein models derived in the previous. Base on the Sergio Alonso model, we have derived a new equation which take into account the inhomogeneous diffusion effect in MARCKS protein dynamic at the level of mambrane bound. In fact, enzymes catalyze millions of chemical reactions that occur every moment in biological systems, but this occurs in a crowded molecular environment and not as isolated entities [46]. In order to achieve our objectives, we have highlighted some analytical methods. To confirm the different results obtained from the analytical methods, we also make use of numerical study. This chapter is based on our results. Since the suggestion of the nonlinear solitons mechanism for the localization and transport of vibrational energy and charges in proteins by Davydov and Kislukha [135], their study in biomolecules has become very active. MI is considered, to some extent, to be a precursor of soliton formation [136]. Recently, the behavior of nonlinear systems has received considerable attention in areas such as biophysics, Bose-Einstein condensates, hydrodynamics, and magnetostatic waves in optics [26–28, 137] just to cite a few. In general case, MI is the direct way through which localized patterns emerge in nonlinear systems. It has been widely shown in recent contributions that it gives more generalized solitonic structures and is the best mechanism by which energy can be localized and transported in biological molecules such as DNA and proteins [29,30].

3.2 Multisolitons-like patterns in homogeneous MARCKS protein cyclic model

3.2.1 Domain formation of MARCKS protein through modulational instability

Modulational instability (MI) is the phenomenon of formation of localized patterns in excitable media due to the interplay between dispersion and nonlinearity. Here the coupling between the diffusion of the proteins and the myristoyl-electrostatic switch can be considered as the precursor

of the MI phenomenon [18]. In practice, MI is based on the linear stability analysis of a periodic wave trains in a nonlinear dispersive systems. Indeed, the procedural analysis consists to injecting a slightly perturbed plane wave into the dynamical system like Eq.(2.10). As a result, if the perturbation grows exponentially, then the plane wave becomes unstable and breaks into a localized structures, if not it remains stable. The former case translates the onset of MI within the system.

MI is analyzed in the framework of the 1D-CCGL Eq.(2.10) by considering a first-order perturbation of harmonic waves whose stability/instability condition is sought. Plane wave solutions for Eq.(2.10) are considered in the general form: $\psi(\xi, \tau) = \psi_0 \exp i(\lambda\xi - \varpi\tau)$, where λ and ϖ are respectively, the wave number and the angular frequency of the plane wave. Parameter ψ_0 denotes the unperturbed amplitude of the plane wave. The dispersion relation associated with the above plane wave, after separating the real and the imaginary parts, is given by:

$$\varpi = P\lambda^2 - R_i - Q_r\psi_0^2. \quad (3.1)$$

$$Q_i\psi_0^2 - R_r = 0. \quad (3.2)$$

Equation Eq.(3.2) defines the nonlinear dispersion relation of the plane wave of a real constant amplitude ψ_0 , an angular frequency μ and a wavenumber λ . However, Eq.(3.2) allows to find the plane wave amplitude as $\psi_0 = \sqrt{\frac{R_r}{Q_i}}$. This implies that the product $Q_i \times R_r$ must remain positive to obey to the existence condition of ψ_0 . The linear stability analysis of the plane wave solutions is carried out by considering small perturbations χ and θ in amplitude and in phase, respectively, i.e., $\psi(\xi, \tau) = (\psi_0 + \chi(\xi, \tau)) \exp i(\lambda\xi - \varpi\tau + \theta(\xi, \tau))$. Inserting the corresponding solution into Eq.(2.10) and separating again the real and imaginary parts, and retaining only linear terms around the unperturbed solution, we find the following coupled linear differential equations for $\chi(\xi, \tau)$ and $\theta(\xi, \tau)$

$$\begin{aligned} -\psi_0\theta_\tau + P\chi_{\xi\xi} - 2P\lambda\psi_0\theta_\xi + 2Q_r\psi_0^2\chi &= 0, \\ \chi_\tau + P\psi_0\theta_{\xi\xi} + 2P\lambda\chi_\xi - R_r\chi &= 0, \end{aligned} \quad (3.3)$$

whose solutions are assumed to be

$\chi(\xi, \tau) = \chi_0 \exp i(K\xi - \nu\tau) + c.c.$ and

$\theta(\xi, \tau) = \theta_0 \exp(K\xi - \nu\tau) + c.c.$, with K and ν being, respectively, the perturbation wave number and the angular frequency of the perturbations and c.c. stands for the complex conjugate. Making use of these solutions, one obtains a homogeneous system for χ_0 and θ_0 in the form

$$\begin{pmatrix} 2Q_r\psi_0^2 - PK^2 & i\psi_0(\nu - 2P\lambda K) \\ -2R_r + i(\nu - 2P\lambda K) & PK^2\psi_0 \end{pmatrix} \begin{pmatrix} \chi_0 \\ \theta_0 \end{pmatrix} = \begin{pmatrix} 0 \\ 0 \end{pmatrix} \quad (3.4)$$

whose 2x2 matrix admits two possible eigenvalues as the dispersion relation for the perturbation, i.e.,

$$\nu_{\pm} = 2P\lambda K + i(-R_r \pm \sqrt{-\Delta}), \quad (3.5)$$

with $\Delta = P^2 K^4 (1 - \frac{2Q_r \psi_0^2}{PK^2}) - R_r^2$. The plane wave will then be modulationally unstable under the condition that at least one of the eigenvalues of the system matrix possesses a non-nil imaginary part. From this, one deduces the MI growth rate as $\Gamma(K, \delta) = 2Im(\nu(K, \delta))$, which is explicitly given by

$$\Gamma(K) = \left[R_r + \sqrt{P^2 Q^4 \left(\frac{2Q_r \psi_0^2}{PK^2} - 1 \right) + R_r^2} \right]. \quad (3.6)$$

The domain of the perturbation wavenumber K for which the Γ -function exists as a function of K is given by $K < \psi_0 \sqrt{\frac{2Q_r}{P}}$, while MI growth rate becomes maximal for $K = \psi_0 \sqrt{\frac{Q_r}{P}}$. The corresponding maximal MI growth rate is given by

$$\Gamma_{max} = \left[R_r + |Q_r| \psi_0^2 \sqrt{1 + \frac{R_r^2}{Q_r^2 \psi_0^4}} \right]. \quad (3.7)$$

To qualitatively characterize the MI onset through Eq.(2.10), the followings instability criteria

$$P \times Q_r > 0, \text{ and } Q_i \times R_r > 0, \quad (3.8)$$

must simultaneous be fulfilled according to the values of parameter space. Above conditions allow to find the appropriate values range of parameter space where a plane wave becomes unstable, thus leading to the formation of localized structures. In this framework, we attempt to find appropriate values range of nonlinearity parameters γ_1 and γ_3 , as well as of the cytosolic diffusion coefficient D , for which MARCKS-like patterns are expected in the cyclic model described in Eqs.(2.3 - 2.4). According to the previous reports [18], the long wavelength instability is responsible for patterns formation of MARCKS protein. To be convinced, the instability criteria of Eq.(3.8) is numerically solved in two-dimensional parameter space as shown in Fig.(3.1). In the corresponding figure, the left column depicts the variations of the product $P \times Q_r$, while the right column displays the variations of the product $Q_i \times R_r$. Both products are plotted: in $k - \gamma_1$ plane on the top row, in $k - \gamma_3$ plane on the middle row and in $k - D$ plane on the bottom row. These panels allow to find the instability regions where relations of Eq.(3.8) are simultaneous fulfilled. Observably, the instability regions in $k - \gamma_1$ plane correspond to the interplay between the purple regions of panel (a_1) and the red regions of panel (b_1). In $k - \gamma_3$ plane, the instability regions are the interplay of yellow regions of panel (a_2) and blue regions of panel (b_2). Finally, in $k - D$ plane, the instability

regions are the interplay of red regions of panel (a_3) and orange regions of panel (b_3). In each panel, the invariant parameters are fixed as: $k_m = 0.1$, $D_m = 0.5\mu m^2 s^{-1}$, $D = 10.0\mu m^2 s^{-1}$, $\gamma_1 = 10.0s^{-1}$, $\gamma_2 = 1.0s^{-1}$ and $\gamma_3 = 25.0s^{-1}$. It is found that apart from the long wavelength instability predicted in Ref. [18], dynamics of Marcks protein can also be expert from the mean wavelength instability. For instance, in the case of long wavelength instability, *i.e.*, $k = 0.05\pi$, MI occurs when $3.5 \leq \gamma_1 \leq 50.0$ by fixing γ_3 and D or when $15.0 \leq \gamma_3 \leq 100.0$ by fixing γ_1 and D or when $0.0 \leq D \leq 50.0$ by fixing γ_1 and γ_3 . However, in the case of mean wavelength instability, *i.e.*, $k = 0.25\pi$, MI occurs in the following cases: $2.5 \leq \gamma_1 \leq 50.0$ by fixing γ_3 and D or when $15.0 \leq \gamma_3 \leq 100.0$ by fixing γ_1 and D or when $4.5 \leq D \leq 50.0$ by fixing γ_1 and γ_3 . To reinforce these predictions we need to quantitatively characterize the real manifestation of MI through the maximal MI growth rate given in Eq.(3.7).

In reminder, MI growth rate is a state function (Γ) which accounts for the quantitative manifestation of MI in a given excitable system. Indeed, when $\Gamma = 0$, system does not yields MI and therefore supports only propagation of periodic wave trains. In contrast, when $\Gamma \neq 0$, system becomes sensitive to MI phenomenon and thenceforth can admit nonlinear localized excitations-like solutions. Additionally, the greater the magnitude of MI growth rate, the greater the magnitude of localized excitation, and vice-versa. Likewise, the spatial expansion (reduction) of MI growth rate is generally associated to the spacial spread (localization) of the excitation.

Results of Fig.(3.2) show the variations of the maximal MI growth rate Γ_{max} versus γ_1 in panels a_j , versus γ_3 in panels (b_j) and versus D in panels (c_j) (see figure caption for explicit readability). It is observed that the Γ_{max} -function are increase-and-decrease function of γ_1 . This suggests that when the mechanism of phosphorylation of MARCKS protein is accentuated, MARCKS protein concentration goes down-and-up (and vice-versa) from membrane-bound to cytosol. On the other hand, the Γ_{max} -function exponentially decreases when γ_3 increases in the case of the long wavelength instability. However, in the case of mean wavelength instability, the Γ_{max} -function decreases first, then increases with γ_3 . This predicts that, in the case of long wavelength instability, the binding process of MARCKS protein could induce the decreasing in MARCKS concentration. But in the case of mean wavelength instability, the binding process favors first the diminution of MARCKS concentration, then the increasing of the latter thereby leading the maximum molecules towards the membrane and preserving their conservation. Now regarding Fig.(3.2) (c_j), the maximal MI growth rate still increases with the diffusion coefficient D regardless of the type of instability. Consequently, the diffusion process of MARCKS protein from the cytosol to the membrane can enhance MI phenomenon which could yield the saturation phenomenon of MARCKS protein at the membrane. All these results support that the cyclic transport of MARCKS protein from membrane to cytosol may be done by means of nonlinear localized excitations for a suited values of parameter space. Unfortunately, these analytical results based only on the linear stability analysis of the plane wave do not highlight nor nature or the longtime spatiotemporal evolution of such localized excitations. It is therefore important to give a particular attention on this by looking for

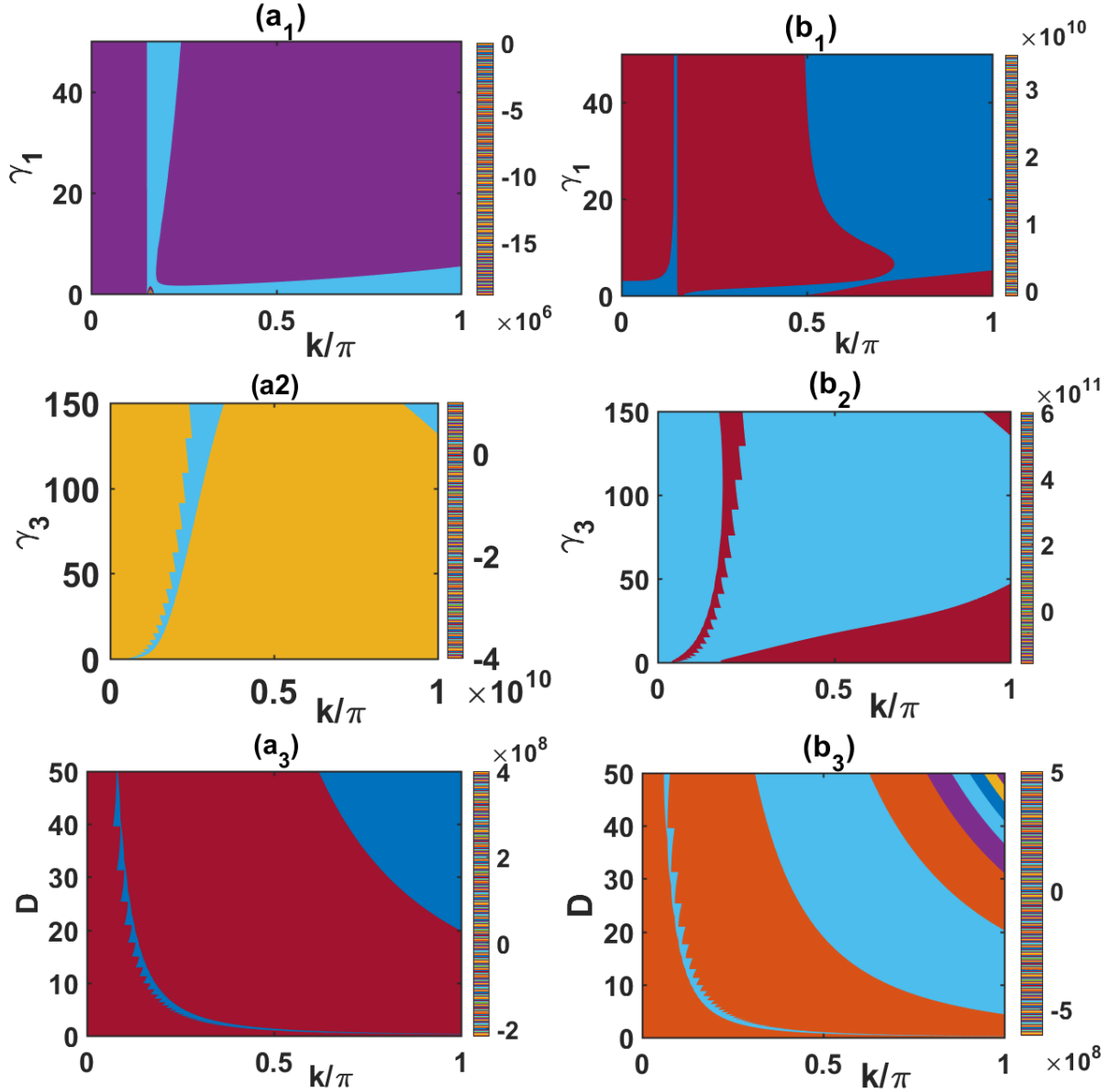


Figure 3.1: Qualitative characterization of MI through 3D view of stability/instability regions according to the criteria given in Eq.(3.8). The products $P \times Q_r$ on the left columns and $Q_i \times R_r$ on the right columns are plotted in: $k - \gamma_1$ plane in the first row while taking $\gamma_3 = 25s^{-1}$ and $D = 10\mu m^2 s^{-1}$; $k - \gamma_3$ plane in the second row while taking $\gamma_1 = 10s^{-1}$ and $D = 10.0$; $k - D$ plane in the third row while taking $\gamma_1 = 10s^{-1}$ and $\gamma_3 = 25s^{-1}$. The other parameters are $k_m = 0.1$, $D_m = 0.5\mu m^2 s^{-1}$, $\gamma_2 = 1.0s^{-1}$. Instability regions appear when both products are simultaneous positive.

the class of nonlinear excitation along with their spatiotemporal properties.

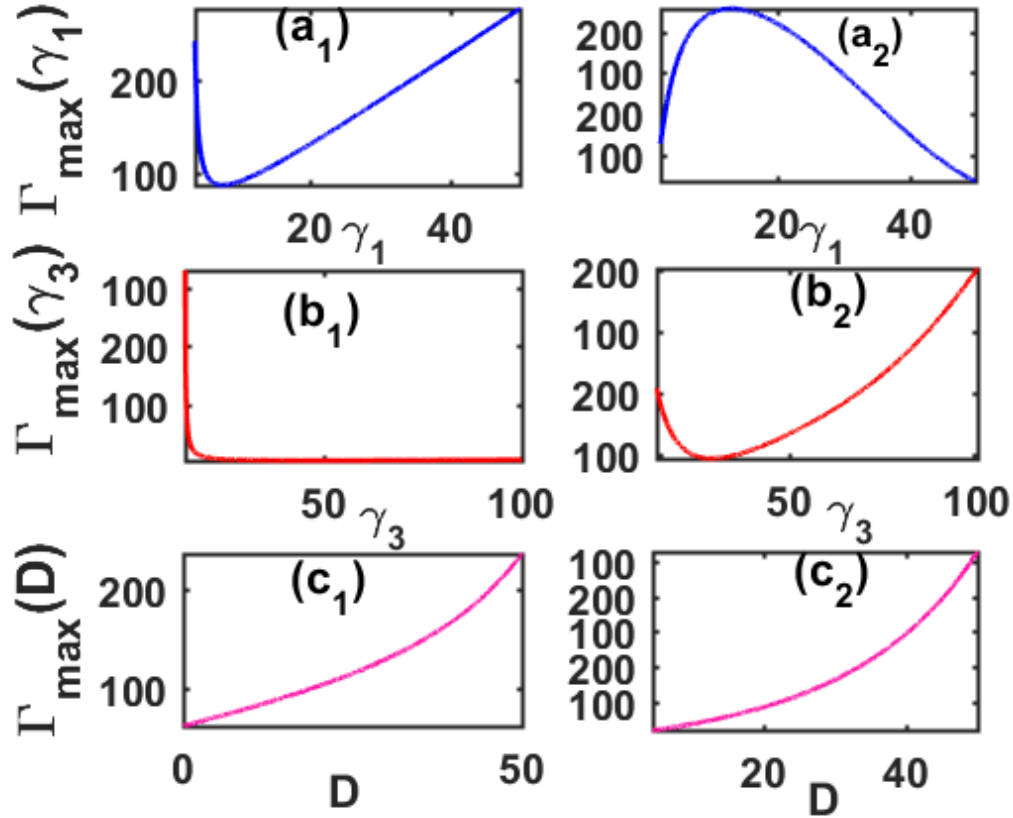


Figure 3.2: Quantitative characterization of MI through features of the maximal MI growth rate Γ_{max} . In panels (a_j), Γ_{max} is plotted versus γ_1 while fixing $\gamma_3 = 25.0s^{-1}$ and $D = 10.0\mu m^2s^{-1}$. In panels (b_j), Γ_{max} is plotted versus γ_3 while fixing $\gamma_1 = 10.0s^{-1}$ and $D = 10.0\mu m^2s^{-1}$. In panels (c_j), Γ_{max} is plotted versus D while fixing $\gamma_1 = 10.0s^{-1}$ and $\gamma_3 = 25.0s^{-1}$. The left panels correspond to the long wavelength instability ($k = 0.05\pi$), while the right panels correspond to the mean wavelength instability ($k = 0.25\pi$). The other parameters are: $k_m = 0.1$, $D_m = 0.5\mu m^2s^{-1}$, $\gamma_2 = 1.0s^{-1}$.

3.2.2 Multisolitons-like MARCKS patterns based on analytical predictions

Analytical solutions described in Eq.(2.23) are displayed in Fig.(3.3). On the top panels, the concentrations of MARCKS protein in membrane bound [see panel (a₁)], in phosphorylated site [see panel (b₁)] and in cytosol [see panel (c₁)] are surfed in $x - t$ parameter space. These solutions have the profiles of localized structures which are propagated over the time at specific domains. This suggests that the processes of transport and transfer of MARCKS protein in the cyclic model are done by means of multisolitons-like patterns. The features on the bottom in Fig.(3.4) show the evolution of MARCKS concentration along the x -direction at different times. These 2D-views show the propagation of a trisolitons-like wave which is involved in MARCKS dynamics. In order to confirm that the generic model can support above structures, it is convenient to point out the numerical simulations.

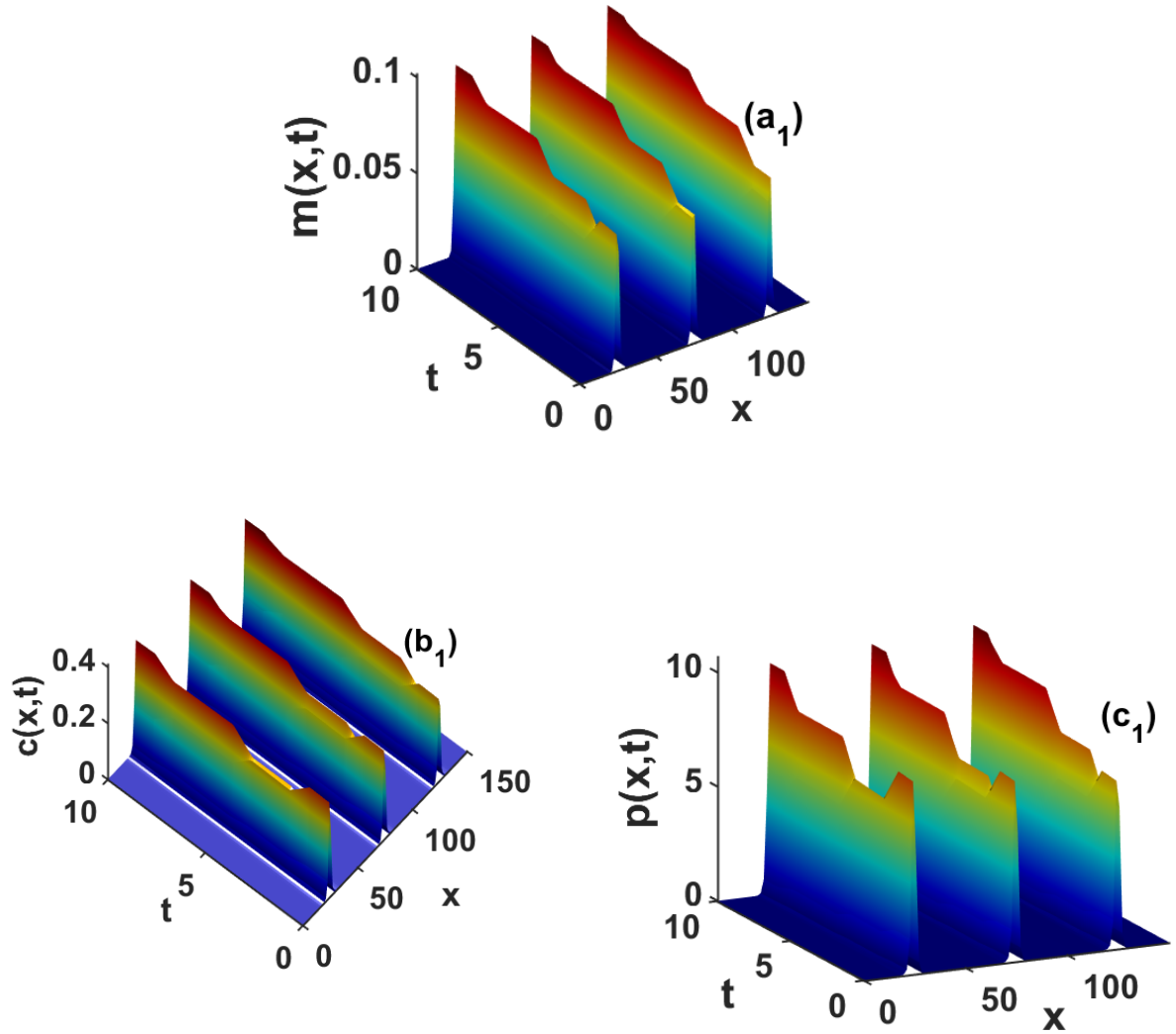


Figure 3.3: The spatiotemporal dynamics of MARCKS protein obtained from analytical solutions of Eq.(2.23). Parameters are chosen as $k_m = 0.1$, $D_m = 0.5\mu m^2 s^{-1}$, $D = 10.0\mu m^2 s^{-1}$, $\gamma_1 = 10.0s^{-1}$, $\gamma_2 = 1.0s^{-1}$, $\gamma_3 = 25.0s^{-1}$ and $k = 0.05\pi\mu m^{-1}$.

3.2.3 Multisolitons-like MARCKS patterns based on numerical experiments

The stability analysis done in section 3.2.2 allowed to find appropriate parameters space that can stimulate modulated patterns-like waves in MARCKS protein system, since a such waves are believed to be involved in energy transfer process along most biological systems. Therefore, the numerical simulations will be carried out by applying the fourth order Runge-Kutta computation scheme using analytical solutions given in Eq.(2.23) as initial conditions. We chosen $0 \leq x(\mu m) \leq 150$ as the spatial coordinate, $0 \leq t(ms) \leq 10$ as the integration duration, $\Delta x = 0.25\mu m$ as the space step and $\Delta t = 10\mu s$ as the time step. The constant parameters remain unchangeable as above, while the control parameters γ_1 , γ_3 and D are selected in instability regions, accordingly.

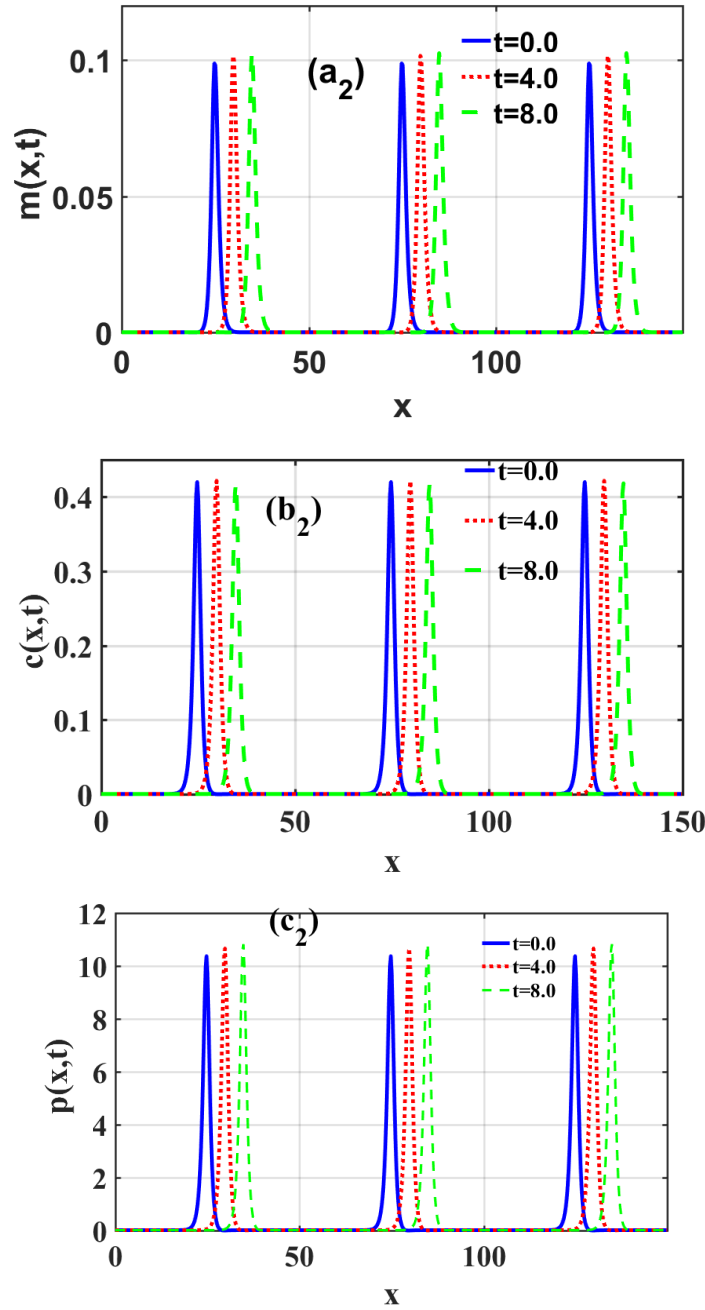


Figure 3.4: The spatiotemporal dynamics of MARCKS protein obtained from analytical solutions of Eq.(2.23). Parameters are chosen as $k_m = 0.1$, $D_m = 0.5\mu m^2 s^{-1}$, $D = 10.0\mu m^2 s^{-1}$, $\gamma_1 = 10.0s^{-1}$, $\gamma_2 = 1.0s^{-1}$, $\gamma_3 = 25.0s^{-1}$ and $k = 0.05\pi\mu m^{-1}$.

It is worth noticing that, here we only present the results on the long wavelength instability case by fixing $k = 0.05\pi$, μm^{-1} .

The features of Fig.(3.5) obtained from numerical simulations show the spatiotemporal dynamics on top panels and spatial dynamics on bottom panels, of MARCKS protein. As shown, the localized patterns are similar to those obtained analytically, thus suggesting that the generic

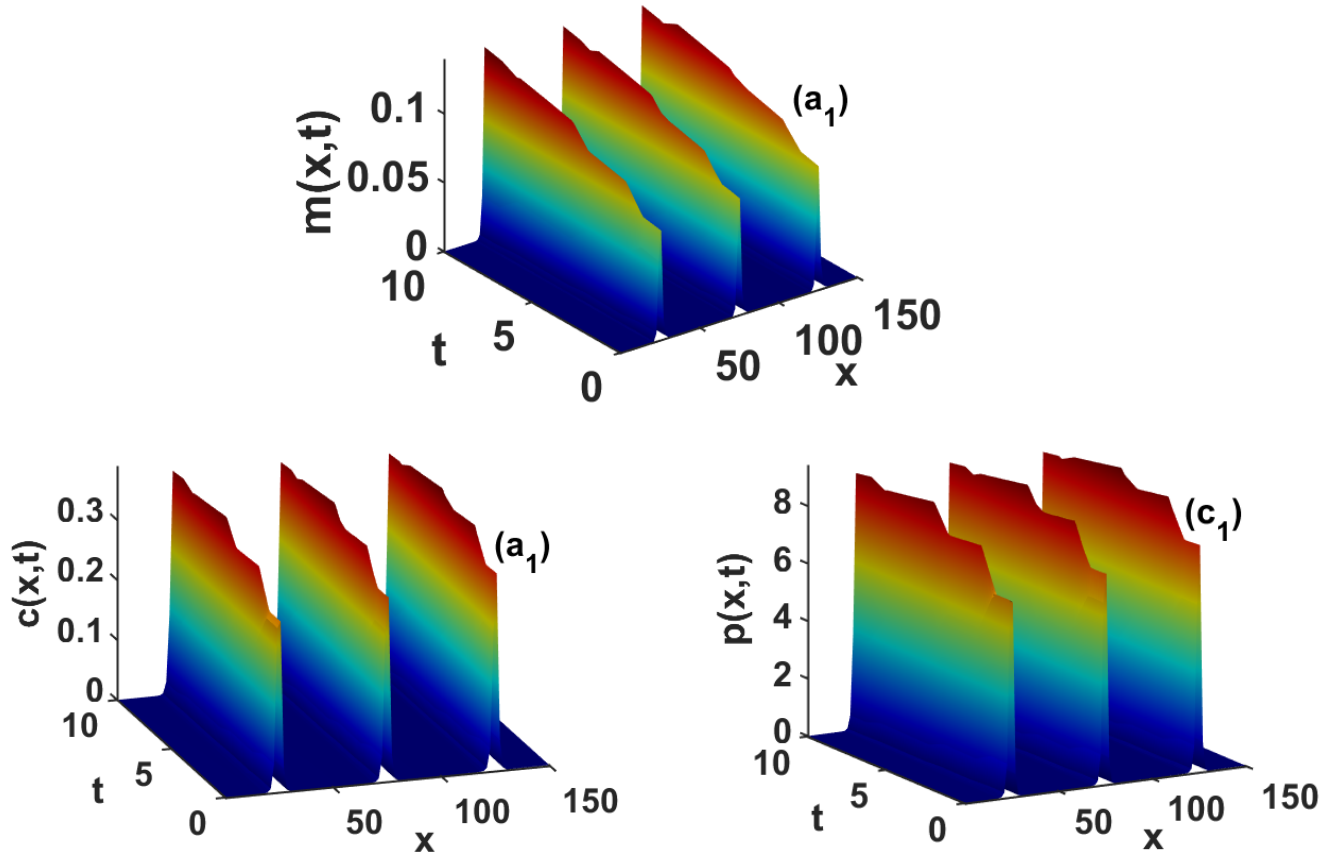


Figure 3.5: The spatiotemporal dynamics of MARCKS protein obtained from numerical simulations of Eqs.(2.3 - 2.4). Parameters are chosen as $k_m = 0.1$, $D_m = 0.5\mu m^2 s^{-1}$, $D = 10.0\mu m^2 s^{-1}$, $\gamma_1 = 10.0s^{-1}$, $\gamma_2 = 1.0s^{-1}$, $\gamma_3 = 25.0s^{-1}$ and $k = 0.05\pi\mu m^{-1}$.

model of Eqs.(2.3 - 2.4) may effectively support the propagation of multi-solitons-like patterns known as the best tool in transport and transfer of MARCKS protein from cytoplasmic membrane to cytosol. Interestingly, we notice that the wave amplitude increases over the time at the membrane and decreases at the cytosol. This suggests that the reorganization of the membrane after the binding of protein is not an instantaneous phenomenon. We also notice that the wave propagates in space with an almost constant width. This constitutes the main properties of wave-like soliton. In Fig.(3.7) the spatial multisoliton-like patterns of MARCKS protein are displayed under the variation of, the phosphorylation rate, where the effect of binding rate is displayed in Fig.(3.8) and the variation of diffusion coefficient is represented in Fig.(3.9) at time $t = 5ms$. We can see that under the increasing of γ_1 , the concentrations of MARCKS protein decreases in the cytoplasmic membrane and increases in the cytosol. However, under the increasing of γ_3 , the MARCKS concentration slowly decreases both in the membrane and in the cytosol. On the other hand, the increase in diffusion coefficient induces increasing in MARCKS protein concentration at in each site. Interestingly, these numerical findings are in perfect correlation with the analytical predictions and suggest that the phenomena of cyclic transport and transfer of MARKS protein

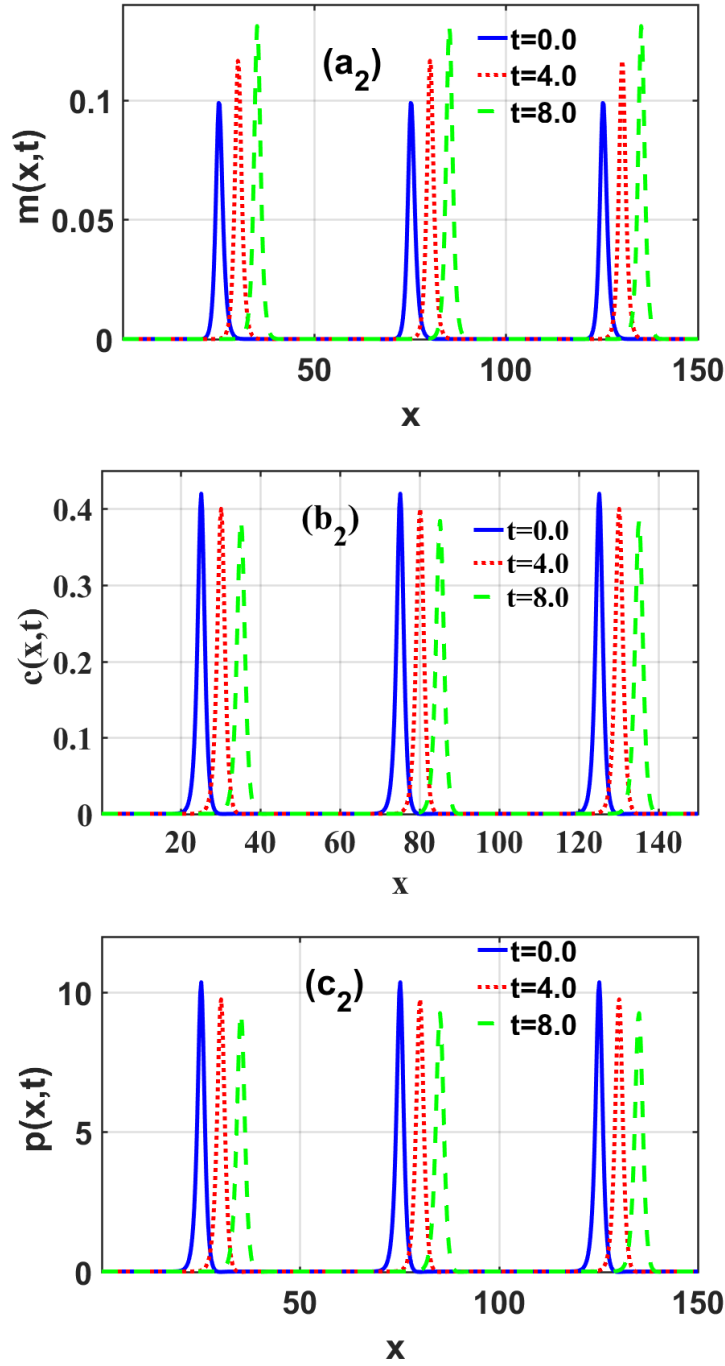


Figure 3.6: The spatiotemporal dynamics of MARCKS protein obtained from numerical simulations of Eqs.(2.3 - 2.4). Parameters are chosen as $k_m = 0.1$, $D_m = 0.5\mu\text{m}^2\text{s}^{-1}$, $D = 10.0\mu\text{m}^2\text{s}^{-1}$, $\gamma_1 = 10.0\text{s}^{-1}$, $\gamma_2 = 1.0\text{s}^{-1}$, $\gamma_3 = 25.0\text{s}^{-1}$ and $k = 0.05\pi\mu\text{m}^{-1}$.

from membrane to cytosol are highly influenced by phosphorylation and binding rates on the one hand and by the diffusion coefficient on the other hand.

In Fig.(3.10), the time series of the MARCKS protein for $x = 75\mu\text{m}$ are plotted. Panels (a),(b),(c) represent, respectively the concentration of the MARCKS protein at the membrane,

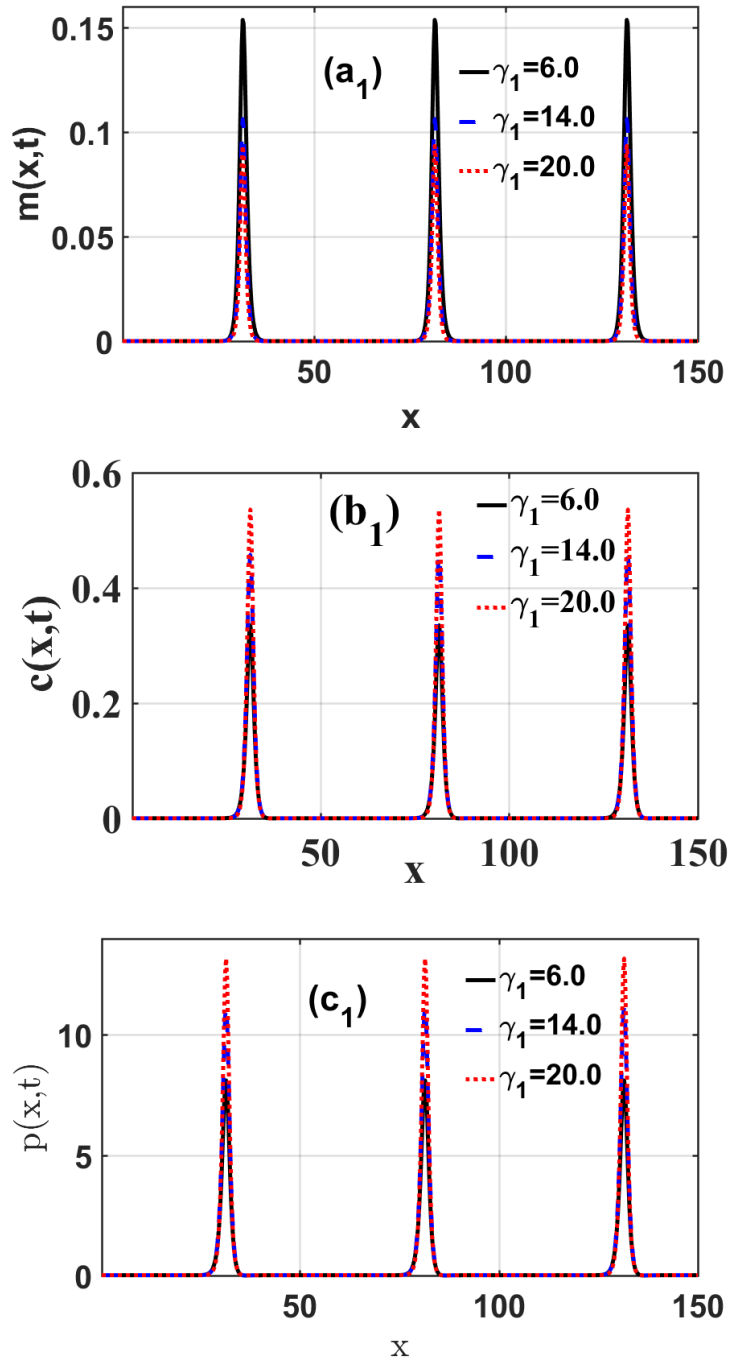


Figure 3.7: The spatial multisolitons-like patterns of MARCKS protein obtained from numerical simulations of Eqs.(2.3 - 2.4) using solutions of Eq.(2.23) as initial conditions. The increasing of phosphorylation rate γ_1 for $k_m = 0.1$, $D_m = 0.5\mu m^2 s^{-1}$, $D = 10.0\mu m^2 s^{-1}$, $\gamma_2 = 1.0s^{-1}$ is observed. This feature is depicted at $t = 5ms$ in the long wavelength instability case, i.e., $k = 0.05\pi \mu m^{-1}$.

phosphorylated and dephosphorylated cytosol. We observe a very fast decrease of the amplitude at the membrane level and a low decrease in the cytosol while the width of the wave being almost constant in the three cases. This informs us that the MARCKS protein at the membrane level is

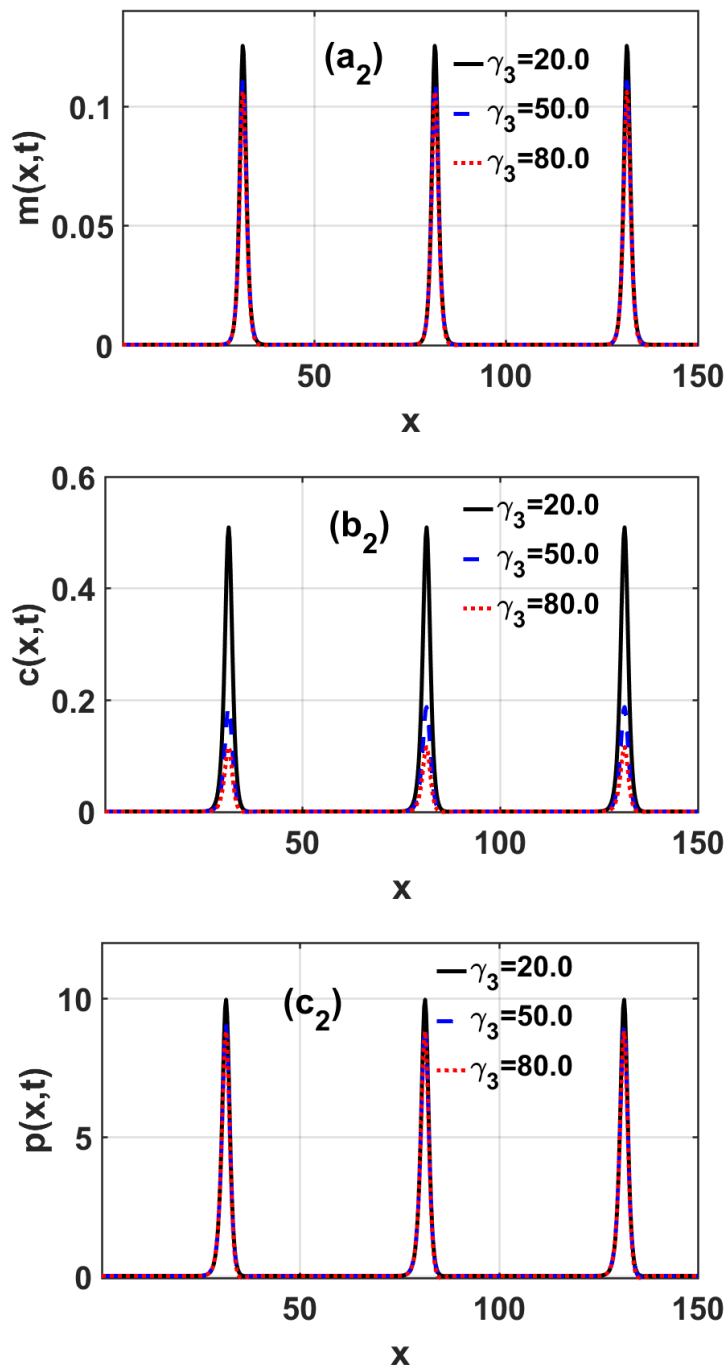


Figure 3.8: The spatial multisolitons-like patterns of MARCKS protein obtained from numerical simulations of Eqs.(2.3 - 2.4). The increasing of binding rate γ_3 is observed while $k_m = 0.1$, $D_m = 0.5 \mu m^2 s^{-1}$, $D = 10.0 \mu m^2 s^{-1}$, $\gamma_1 = 10.0 s^{-1}$ and $\gamma_2 = 1.0 s^{-1}$. This feature is depicted at $t = 5ms$ in the long wavelength instability case, i.e., $k = 0.05\pi \mu m^{-1}$.

the activating and inhibiting substance in the cytosol.

We used a reaction diffusion model describing the dynamics of MARCKS proteins concentration between cytosol and membrane-bound proposed by Sergio Alonso and Markus Bär [18]. They

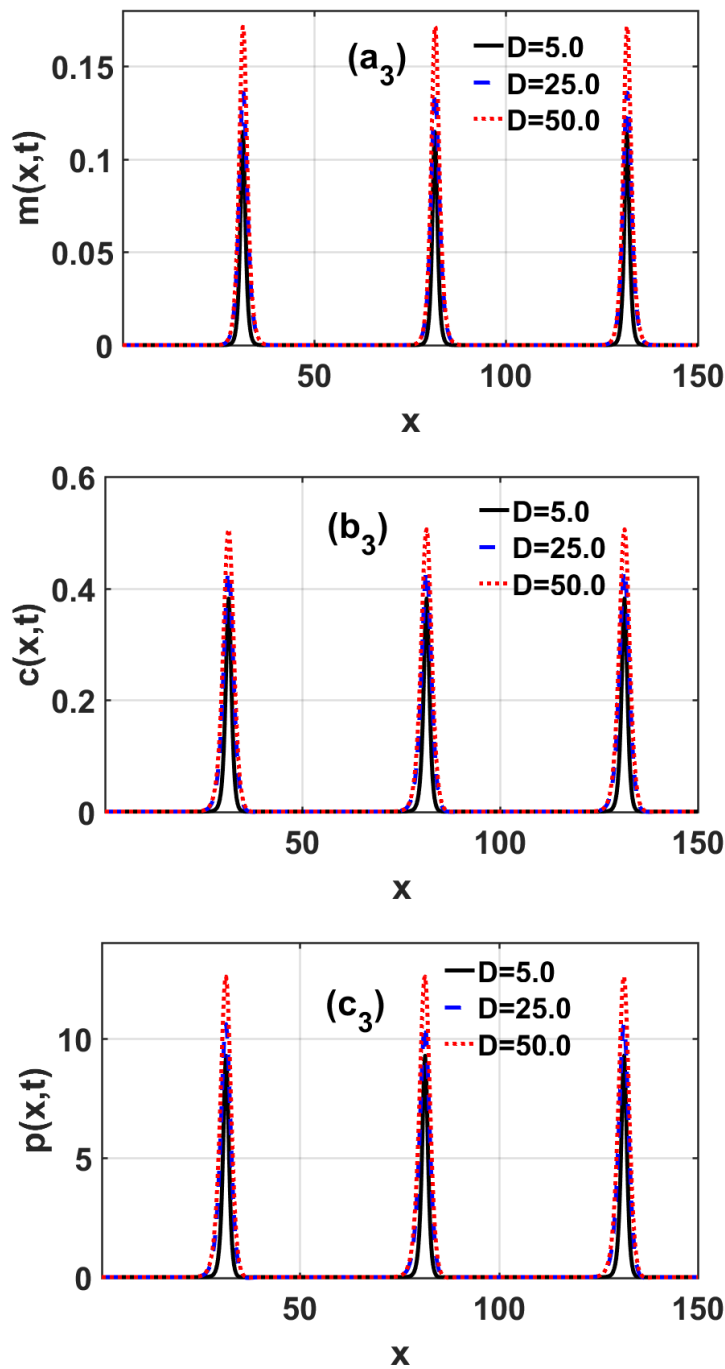


Figure 3.9: The spatial multisolitons-like patterns of MARCKS protein obtained from numerical simulations of Eqs.(2.3 - 2.4). The increasing of the cytosolic diffusion coefficient D is observed while $k_m = 0.1$, $D_m = 0.5 \mu m^2 s^{-1}$, $\gamma_1 = 10.0 s^{-1}$, $\gamma_2 = 10 s^{-1}$ and $\gamma_3 = 25.0 s^{-1}$. This feature is depicted at $t = 5ms$ in the long wavelength instability case, i.e., $k = 0.05\pi \mu m^{-1}$.

studied the spatio-temporal dynamics of MARCKS proteins and their interactions with enzymes. However, they did not propose either a full analytical investigations or the analytical solution of the system. In the present work we propose a complete analytical and numerical solution of the

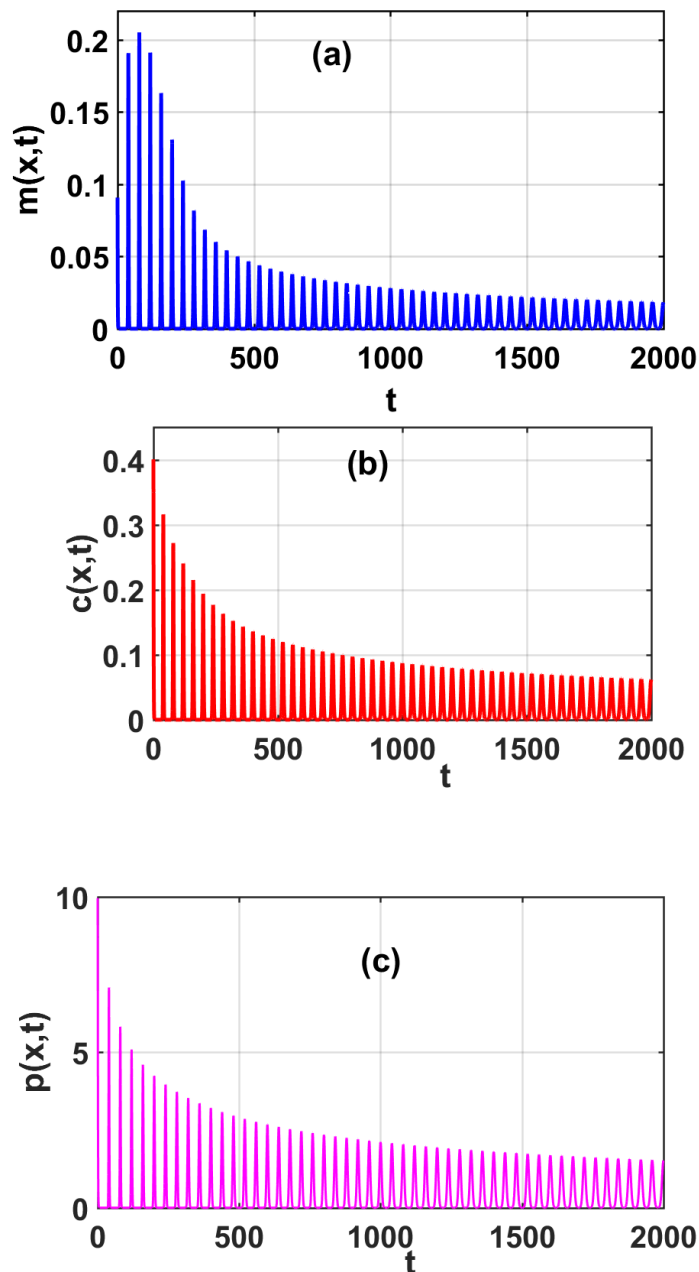


Figure 3.10: Time series for MARCKS protein at the position $x = 75 \mu m$. Panels (a), (b) and (c) correspond, respectively to the concentration of MARCKS in membrane bound, in cytosol and in phosphorylated site. Space parameters are given by $k_m = 0.1$, $D_m = 0.5 \mu m^2 s^{-1}$, $\gamma_1 = 10.0 s^{-1}$, $\gamma_2 = 1.0 s^{-1}$, $\gamma_3 = 25.0 s^{-1}$, $D = 10.0 \mu m^2 s^{-1}$.

system. we adopted the multiscale approximation in the reductive perturbation method (RPM). The medium is supposed to be weakly dissipative [117] which allowed to obtain the CCGL equation whose solutions forms were constructed. The CCGL equation is often used as a description of a system close to a bifurcation point and it is well known that the CCGL equation can produce space-time chaos in the form of defects. The CCGL equation is a universal model for predicting

pattern formation pattern formation in reaction-diffusion models [138]. The coefficients of this equation allowed us to qualitatively characterize the MI in order to determine the stability and instability zones of the MARCKS protein as a function of the phosphorylation rate, the parameters that significantly affect the stability zone are the binding rate and the diffusion coefficient in the cytosol. In order to predict the existence of the localized structures in the model, the maximal growth rate of MI is represented.

Hirota's method led to the multisolitons-like patterns in our system for a suitable modulational instability parameters. This type of wave corresponds to spatially broadened impulses and they are ubiquitous in excitable media such as neurons and cell membranes [139,140]. In the heart, for example, they are responsible for triggering harmonic contractions, the failure of which can lead to significant physiological perturbations [141,142]. Additionally, the multisoliton-like solutions have already been obtained by Issa *et al.* [143] in a biexciton molecular chain with saturable nonlinearity effects. Theoretically, the rate of phosphorylation leads to an increase in the non-linearity of the system. The above simulations demonstrate that three-species reaction-diffusion systems with spatially constant parameters can give rise to complex steady-state patterns and travelling peak waves. Such patterns were obtained in [37] through the study of embryonic development in a spatially heterogeneous background.

3.3 Traveling wave with inhomogeneous diffusion effect in MARCKS protein dynamic

Inhomogeneity in this model is due to defects caused by the presence of additional molecules at the level of cytoplasmic membrane. The process of phosphorylation which is an alteration of the protein can induce modification of the protein's structure. similar but not identical properties, we would be called upon to purify them, and this will be done only if there are inhomogeneities in the medium.

3.3.1 Linear stability analysis

The study of the stability of solutions of Eq.(2.31) is not usually easy, and in many cases has not yet been done. Because of the simplicity of the plane wave solutions in their cartesian form and for finite amplitude of wave, nonlinearities of the system give rise to the generation of higher harmonics. The linear analysis however is a good predictor for the finite amplitude patterns formed by the full nonlinear system [23] . In order to perform the stability/instability effect, we consider a plane wave solution of Eq.(2.31) in the form $\varphi_m(\tau) = \varphi_0 \exp i(\lambda m - \Gamma\tau)$, where λ represents the wavenumber and Γ the angular frequency of the plane wave. Inserting the plane wave solution in

Eq.(2.31), we obtain

$$\Gamma^2 = \frac{R}{Q} \left(|\varphi_0|^2 - \frac{2P}{R} \sin \lambda \right).$$

Unstable waves will then appear in the model and modulated wave patterns will be expected if $\Gamma^2 < 0$. This condition is fulfilled if $\frac{R}{Q} < 0$ and $|\varphi_0|^2 > \frac{2P \sin \lambda}{R}$. $\sin \lambda$ being a bounded function, the latter condition becomes

$$|\varphi_0|^2 > \frac{2P}{R} = \varphi_{0,cr}^2.$$

In Fig. 3.4, the critical amplitude $\varphi_{0,cr}$ is plotted versus the wavenumber q , while fixing $D_0 = 1.1$, $D_1 = 0.09$ and $D_2 = 0.05$. Therein, the stable and unstable regions of MI are clearly displayed. As shown, nonlinear patterns are expected in the system in the instability domain, *i.e.*, $0 \leq q \leq q_{cr}$, with $q_{cr} = 0.12\pi$. This means that when $q > q_{cr}$ the plane wave remains stable under any modulation. The instability curves displayed in Fig. 3.11 are similar to those obtained by Takembo and Ekobena [?]. The panels of Fig. 3.12 highlight the effect of phosphorylation rate γ_1 in (a) and inhomogeneous diffusion coefficients in (b). In Fig. 3.12 (a), we fixed $D_0 = 0.1$, $D_1 = 0.05$, $D_2 = 0.01$ and increased the phosphorylation rate γ_1 . It is observed that, the increase of γ_1 induces decrease of critical amplitude and reduction of instability region. As a result, the nonlinear patterns of MARCKS proteins are expected in the model for the small value of the phosphorylation rate. However, the panel of Fig. 3.12 (b) where $\gamma_1 = 0.1$ shows that the increase of the diffusion coefficients induces the increasing of critical amplitude and expansion of instability regions. In short, we found that nonlinear patterns are favorable in the MARCKS proteins dynamics for the short wavelength ($0 \leq q \leq q_{cr}$). Additionally, inhomogeneity effects significantly contribute to the formation of such patterns.

3.3.2 Weakly nonlinear solutions

Linear stability analysis is limited because it can only detect the onset of instability and therefore does not tell us anything about what kind of dynamical patterns one might obtain in the system when the instability grows for a longtime. In order to solve analytically Eq.(2.31) we first transform the DNLS equation into the continuous nonlinear Schrödinger equation using Taylor expansion method at the first order [121].

$$\varphi_{m+1} - \varphi_{m-1} = 2l \frac{\partial \varphi_m}{\partial z}, \quad (3.9)$$

with $z = ml$. Inserting Eq.(3.9) into Eq.(2.31) and taking $Z = zz_0$, $l = 1$, $T = \tau T_0$, $\varphi^* = \varphi_0 \varphi$, $z_0 = \frac{QT_0^2}{Pl}$, $\varphi_0 = \frac{1}{T_0} \sqrt{\frac{R}{2Q}}$, we obtain:

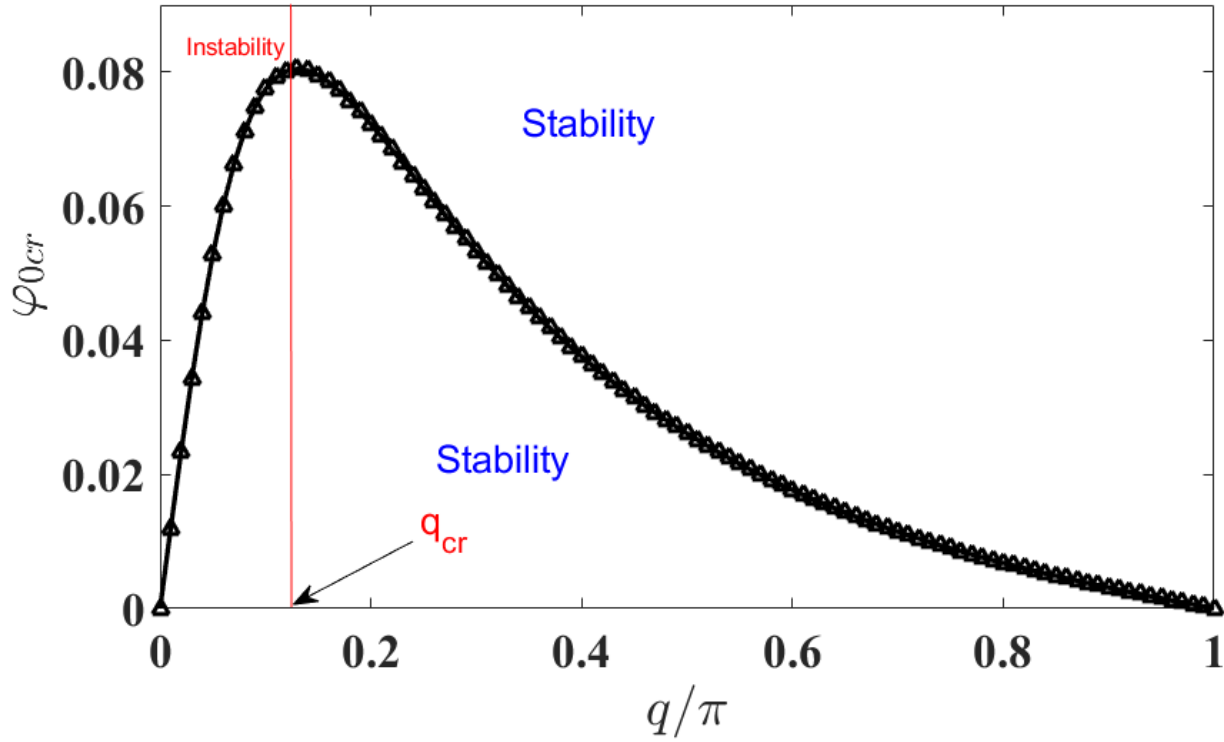


Figure 3.11: The plot of the critical amplitude versus the wave number q of the carrier wave. We have fixed $D_0 = 1.1, D_1 = 0.09, D_2 = 0.05, \gamma_1 = 2, \gamma_2 = 10, \gamma_3 = 50, k_m = 0.1, D = 10$ as the model parameters.

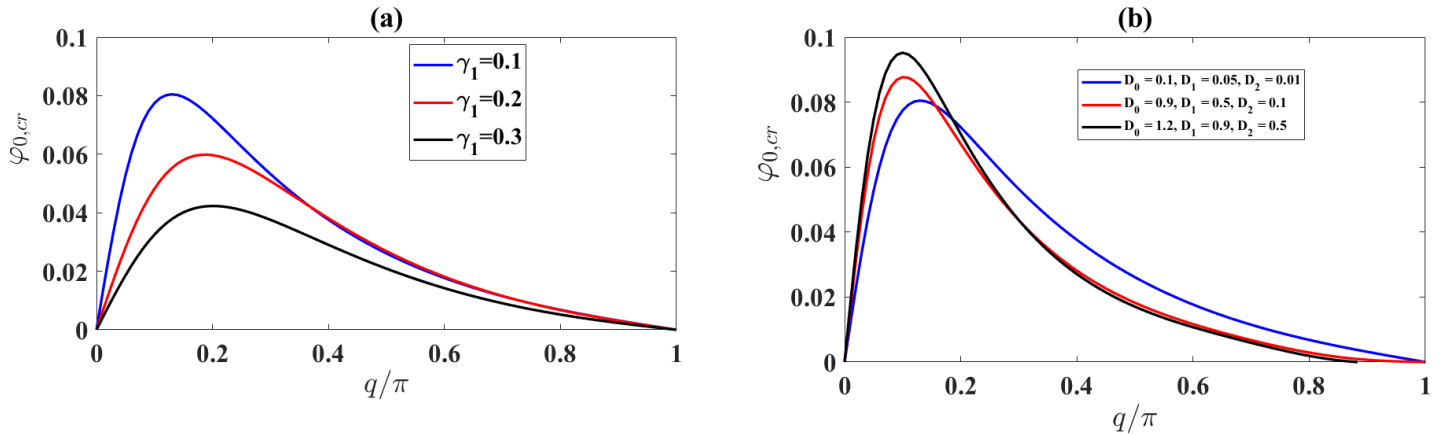


Figure 3.12: The panels show the critical amplitude versus the wave number q . In panel (a) we have fixed $D_0 = 1.1, D_1 = 0.09, D_2 = 0.05$ and increase γ_1 . In panel (b) we fixed $\gamma_1 = 2.0$ and increased the diffusion coefficients (see legend for more readability). The remaining parameters of the model are: $\gamma_2 = 10.0, \gamma_3 = 50.0, k_m = 0.1, D = 10$.

$$i \frac{\partial \varphi}{\partial Z} + e_0 \frac{\partial^2 \varphi}{\partial T^2} + e_1 |\varphi|^2 \varphi = 0, \quad (3.10)$$

with $e_0 = \frac{1}{2}$, $e_1 = 1$. Solutions of Eq.(3.10) at the first order has been suggested in [?] and read as follow:

$$\varphi(Z, T) = \left[4 \left(\frac{1 + 2iT}{1 + 4T^2 + 4Z^2} \right) - 1 \right] \exp(iZ). \quad (3.11)$$

Thus, combining Eq.(3.11) and Eq.(2.28) we derive the solutions of Eq.(2.5) as :

$$\begin{aligned} m_n(x, t) &= \left[4 \left(\frac{1+2iT}{1+4T^2+4Z^2} \right) - 1 \right] \exp(iZ) \exp(i\theta) + cc \\ c_n(x, t) &= a \left[4 \left(\frac{1+2iT}{1+4T^2+4Z^2} \right) - 1 \right] \exp(iZ) \exp(i\theta) + cc \\ p_n(x, t) &= b \left[4 \left(\frac{1+2iT}{1+4T^2+4Z^2} \right) - 1 \right] \exp(iZ) \exp(i\theta) + cc, \end{aligned} \quad (3.12)$$

3.4 Conclusion

In this section, we have investigated the generation of localized structures in the reaction-diffusion system describing the spatiotemporal evolution of myristoylated alanine-Rich C-kinase substrate from membrane to cytosol and from cytosol to membrane. Firstly, we have make use of the reductive perturbation approach to transformed the set of three coupled reaction-diffusion equation into a complex cubic Ginzburg-Landau equation in homogeneous media. Then, modulational instability (MI) is carried out thanks to the linear stability analysis which leads to the derivation of MI criteria. On the basis of these criteria, we find the domains of some parameter space where nonlinear patterns are expected in the model. Using the HB method, the analytical results on the MI growth rate predict that phosphorylation and binding rates affect MARCKS dynamics in opposite way. In second hand we have take into consideration the effect of inhomogeneity at the level of membrane. The Leon and Manna method leads us to transformed the nonlinear generic model into a one-dimensional discrete nonlinear Schrödinger equation. Through the linear stability analysis, we have established the instability criterion and it has been revealed that the model could be subjected to MI. The obtained results deal with the cyclic transport of MARCKS protein from membrane to cytosol that may be done by means of multisolitons-like patterns. These result seem relevant to reach a better understanding of the biological problem.

GENERAL CONCLUSION AND OUTLOOKS

In this thesis, we have studied the Nonlinear dynamics of MARCKS protein between membrane-bound and cytosol, taking into account the inhomogeneity effect. Our study was based on the mathematical model proposed by Alonso and Mbär. In fact, a mathematical model is a representation of a real-world system. The thesis was organized in three parts: In Chapter 1, we presented a literature review on PKC and traveling waves. The second Chapter was devoted to the mathematical background and methodology, where we presented the mathematical models, analytical and numerical methods used to achieve our goals. The last chapter has been devoted to the results of our investigations. We investigated the Alonso and Mbär model which allows predictions regarding the interaction of MARCKS with a lipid monolayer. We used the reductive perturbation method to construct a new families of exact soliton solutions for the MARCKS protein reaction-diffusion model. Thereafter, an exact analytical solutions of MARCKS patterns were derived by using the Hirota Bilinear method. These analytical solutions were using as initial conditions to compute the numerical solutions of the generic model. It was found that the transport of MARCKS from cytoplasmic membrane to the cytosol could be achieved by a tri-solitonic wave whose properties are considerable modified either by the phosphorylation and binding rate, on the one hand, and diffusion coefficient on the order hand. Our numerical results are found to be in perfect agreement with our analytical predictions. This gives more insight on the formation of domain patterns of MARCKS protein at the biomembrane.

We also used the Leon and Manna method in inhomogeneous media and showed that inhomogeneity effect do not alter the velocity and the amplitude of the soliton during propagation. By means of linear stability analysis, the modulational instability (MI) phenomenon has been explored. Then, we derived the condition for which the plane wave to become unstable along with the critical amplitude for the best characterization for the MI phenomenon. It was found that unstable patterns are expected in the short wavelength domain, *i.e.*, $0 \leq q \leq q_{cr}$. Additionally, the increase of phosphorylation rate induced a decrease in critical amplitude and reduction of instability regions. However, the increase of inhomogeneous diffusion coefficients induced a increasing in

critical amplitude and expansion of instability regions. In order to know what kind of dynamical patterns one might obtain in the system when the instability grows for a longtime, we found the exact analytical solutions. The results of this Thesis are applicable to cytoplasmic membranes in the brain, in the regulation of the homeostasis of body fluids, blood coagulation, cell motility, vesicular traffic, secretion as well as mediation of the inflammatory response and in hematological malignancies. Recombinant human proteins (MARCKS) can also be used for: Native antigens for optimized antibody production Positive controls in ELISA and other antibody assays.

However, there still remain unanswered questions that we aim at pursuing in a near future.

- As the required conditions are not exceptional, we will see how to apply these mechanisms to other proteins with similar properties like the proteins *GAP43*, F52 Protein and *CAP23* at membranes;
- A generic feature of the mechanism studied here is that any synthesis of proteins by the cell is not considered;
- We have limited the study of inhomogeneity effect to the level of cytoplasmic membrane, where it will be very interesting to consider this effect in the cytosol;
- We have limited the study in one dimensional approach, where it will be very interest to consider the two dimensional case;
- Previous authors subject that the low dephosphorylation rate produces a delay in the increase of free MARCKS proteins on the cytoplasm, so in future we will take into account the effect of delay in phosphorylation and dephosphorylation process.

Appendices: Derivation of the cubic complex Ginzburg-Landau Equation Eq. (3.6) and the discrete nonlinear Schrödinger (DNLS) equation Eq. (3.23)

Appendix A: Derivation of the cubic complex Ginzburg-Landau Equation Eq. (3.6)

3.4.1 Appendix A₁: Coefficients of Eqs.(3.1)

$$\begin{aligned}
\mu_1 &= \gamma_1, \mu_2 = \gamma_3 k_m, \mu_3 = \gamma_3(1 - k_m), \mu_4 = -\gamma_3, d_0 = D_m k_m d_1 = D_m, \Omega_0^2 = \gamma_2 \gamma_3 k_m, \\
\lambda_1 &= -\gamma_3^2 k_m, \lambda_2 = \gamma_1 \gamma_2, \lambda_3 = \gamma_1 \gamma_3 + \gamma_2 \gamma_3 - \gamma_2 \gamma_3 k_m, \lambda_4 = -(\gamma_1 \gamma_3 + \gamma_2 \gamma_3), \\
\lambda_5 &= -\gamma_3^2(1 - k_m), \lambda_6 = -\gamma_1 \gamma_2, \sigma_0 = \gamma_2 k_m + \gamma_3 k_m, \sigma_1 = \gamma_2 + \gamma_3(1 - k_m), \\
\sigma_2 &= -\gamma_3, D_0 = D\gamma_2 + k_m + D\gamma_3 k_m, D_1 = D\gamma_2 - D\gamma_3 k_m + D\gamma_3 D_2 = -D\gamma_3, \\
D_3 &= D_m \gamma_3 k_m - D\gamma_3 k_m, D_4 = D_m \gamma_3 - D\gamma_3, D_5 = -2D\gamma_3 k_m, \\
D_6 &= -2D\gamma_3, D_7 = 2D + k_m D, D_8 = D, D_9 = -D^2 k_m, D_{10} = -D^2.
\end{aligned} \tag{A.1}$$

3.4.2 Appendix A₂: Coefficients of Eq.(3.5)

$$\begin{aligned}
 \alpha_1 &= \frac{\mu_2(d_0k^2 + \mu_1)}{(d_0k^2 + \mu_1)^2 + (\omega k_m)^2}, \quad \alpha_2 = \frac{\omega\mu_2k_m}{(d_0k^2 - \mu_1)^2 + (\omega^2k_m)^2}, \\
 a_1 &= \frac{2}{\Omega_0^2}(\alpha_1(\omega^2 + D_1k^2 - D_3k^2 - \lambda_3 + D_5k^2 + D_{10}k^4) - \lambda_1 \\
 &\quad - \lambda_2(\alpha_1^2 + \alpha_2^2) - \alpha_2\sigma_1\omega - D_8k^2\alpha_2\omega), \\
 a_2 &= \frac{1}{\mu_1}(\mu_2a_1 - 2d_1k^2(\alpha_1^2 + \alpha_2^2) + 2\mu_1(\alpha_1^2 + \alpha_2^2) + 2\mu_3\alpha_1) \\
 b_1 &= \frac{1}{\Omega_0^2 + 4D_0k^2 - 16D_9k^4 - 4k_mk_m\omega^2}(\alpha_1(\omega^2 - \lambda_3 + D_1k^2 - D_3k^2 - D_5k^2 + D_{10}k^4) \\
 &\quad + \lambda_1 + \lambda_2(\alpha_1^2 - \alpha_2^2) + \omega\alpha_2(-\sigma_1 + D_8k^2)) \\
 b_2 &= \frac{1}{\Omega_0^2 + 4D_0k^2 - 16D_9k^4 - 4k_mk_m\omega^2}(\alpha_2(\omega^2 - \lambda_3 + k^2D_1 - D_3k^2 + k^4D_{10}) \\
 &\quad + 2\lambda_2\alpha_1\alpha_2 + \alpha_1\omega(\sigma_1 - D_8k^2)), \\
 b_3 &= \frac{1}{(\mu_1 + 4k^2d_0)^2 + (2\omega k_m)^2}((\mu_1 + 4k^2d_0)(-2\omega\alpha_1\alpha_2 + \mu_2b_1 + \mu_1(\alpha_1^2 - \alpha_2^2) + \mu_3\alpha_1 \\
 &\quad - d_1k^2(\alpha_1^2 - \alpha_2^2)) - 2\omega \times k_m(\omega(\alpha_1^2 - \alpha_2^2) + \mu_2b_2 + 2\alpha_1\alpha_2\mu_1 + \mu_3\alpha_2 - 2d_1k^2\alpha_1\alpha_2) \\
 b_4 &= \frac{1}{(\mu_1 + 4k^2d_0)^2 + (2\omega k_m)^2}((\mu_1 + 4k^2d_0)(\omega(\alpha_1^2 - \alpha_2^2) + \mu_2b_2 + 2\alpha_1\alpha_2\mu_1 + \mu_3\alpha_2 \\
 &\quad - 2d_1k^2\alpha_1\alpha_2) + 2\omega k_m \times (-2\omega\alpha_1\alpha_2 + \mu_2b_1 + \mu_1(\alpha_1^2 - \alpha_2^2) \\
 &\quad + \mu_3\alpha_1 - d_1k^2(\alpha_1^2 - \alpha_2^2))). \tag{A.2}
 \end{aligned}$$

3.4.3 Appendix A₃: Coefficients of Eq.(3.6)

$$\begin{aligned}
P &= \frac{D_0 - 6D_9k^4 - k_m v_g^2}{2\omega k_m}, \quad R_i = \frac{-\lambda_6 \alpha_1}{2\omega k_m}, \quad R_r = \frac{1}{2\omega k_m} (\lambda_6 \alpha_2 - \omega \sigma_0 - D_7 k^2 \omega), \\
Q_r &= \frac{1}{2\omega k_m} \left(\omega^2 (a_2 + b_3 + 4b_1 \alpha_1 + 4b_2 \alpha_2 + a_1 \alpha_1) - 2\lambda_1 (a_1 + b_1) \right. \\
&\quad - \lambda_2 (\alpha_1 a_2 + \alpha_1 b_3 + \alpha_2 + b_4) - \lambda_3 (\alpha_1 a_1 + \alpha_1 b_1 + \alpha_2 b_2 + \alpha_1 b_3 + \alpha_2 b_4 + a_2) \\
&\quad - \lambda_4 (3\alpha_1^2 + \alpha_2^2) - 3\lambda_5 \alpha_1 + \sigma_1 \omega (-2b_2 \alpha_1 + 2b_1 \alpha_2 + b_4) \\
&\quad + 2\sigma_2 \omega \alpha_1 \alpha_2 - D_1 k^2 (4(\alpha_1 b_1 + \alpha_2 b_2) + b_3 + a_2) - D_2 k^2 (3\alpha_1^2 + \alpha_2^2) + \\
&\quad D_3 k^2 (4b_3 - \alpha_1 b_1 - \alpha_2 b_2 - a_1 \alpha_1) + 2D_4 \alpha_1 k^2 + D_5 k^2 (b_1 \alpha_1 + b_2 \alpha_2 + b_3) \\
&\quad + D_6 k^2 (3\alpha_1^2 + \alpha_2^2) - D_8 k^2 \omega (-8\alpha_1 b_2 + 8\alpha_2 b_1 + \alpha_2) \\
&\quad \left. + D_{10} k^4 (16(b_1 \alpha_1 + b_2 \alpha_2) + \alpha_1 + a_2) \right), \\
Q_i &= \frac{1}{2\omega k_m} \left(\omega^2 (b_4 + 4\alpha_1 b_2 - 4\alpha_2 b_1 + \alpha_2 a_1) - 2\lambda_1 b_2 - \lambda_2 (\alpha_2 a_2 + \alpha_1 b_4 - \alpha_2 b_3) \right. \\
&\quad - \lambda_3 (\alpha_2 a_1 + \alpha_1 b_2 - \alpha_2 b_1 + \alpha_1 b_4 - \alpha_2 b_3) - 2\lambda_4 \alpha_1 \alpha_2 - \lambda_5 \alpha_2 + \omega \sigma_1 (2\alpha_1 b_1 \\
&\quad + 2\alpha_2 b_2 - b_3 + a_2) + \omega \sigma_2 (\alpha_1^2 + 3\alpha_2^2) - D_1 k^2 (4(\alpha_1 b_2 - \alpha_2 b_1) + b_4) - 2D_2 k^2 \alpha_1 \alpha_2 \\
&\quad + D_3 k^2 (4b_4 - \alpha_1 b_2 + \alpha_2 b_1 - a_1 \alpha_2) + 2D_4 k^2 \alpha_1 \alpha_2 + D_5 k^2 (-b_1 \alpha_2 + b_2 \alpha_1 + b_4) \\
&\quad + 2D_6 k^2 \alpha_1 \alpha_2 - D_8 k^2 \omega (8\alpha_1 b_1 - 8\alpha_2 b_2 - \alpha_1 + a_2) \\
&\quad \left. + D_{10} k^4 (16(b_2 \alpha_1 - b_1 \alpha_2) + \alpha_2) \right).
\end{aligned} \tag{A.3}$$

Appendix B: Coefficients at other order (2, 2) of the the discrete nonlinear Schrödinger (DNLS) equation Eq. (3.22)

$$\begin{aligned}
A &= (\alpha_1 - \gamma_3 b + 4D_0 \sin^2 \frac{q}{2}) (2i\omega + \gamma_3) (2i\omega + \gamma_2) \\
&\quad + \gamma_3 (2i\omega + \gamma_2) (\gamma_3 b + 4D \sin^2 \frac{q}{2}) + \gamma_2 \gamma_3 (-\alpha_1 + 4D \sin^2 \frac{q}{2}) \\
A_1 &= (2i\omega + \alpha_0 + 4D_1 \sin^2 q) (2i\omega + \gamma_3) (2i\omega + \gamma_2) - \gamma_2 \gamma_3 \alpha_0, \quad a_2 = \frac{A}{A_1} \\
B &= (\gamma_3 b + 4D \sin^2 \frac{q}{2}) (2i\omega + \gamma_2) (2i\omega - \alpha_0 - 4D_1 \sin^2 q) + \gamma_2 ((2i\omega - \alpha_0 - 4D_1 \sin^2 q) \\
&\quad (4D \sin^2 \frac{q}{2} - \alpha_1) + \gamma_2 \alpha_0 (\alpha_1 - \gamma_3 b + 4D_0 \sin^2 \frac{q}{2})), \quad a_3 = \frac{B}{A_1} \\
C &= (2i\omega - \alpha_0 - 4D_1 \sin^2 q) (2i\omega + \gamma_3) (-\alpha_1 + 4D \sin^2 \frac{q}{2}) + \gamma_3 \alpha_0 (\gamma_3 b + 4D \sin^2 \frac{q}{2}) \\
&\quad + \alpha_0 (2i\omega + \gamma_3) (\alpha_1 - \gamma_3 b + 4D_0 \sin^2 \frac{q}{2}), \quad a_4 = \frac{C}{A_1}.
\end{aligned}$$

Bibliography

- [1] Mohamed El Amri, Una Fitzgerald and Gerhard Schlosser, *MARCKS and MARCKS-like proteins in development and regeneration*, *Journal of Biomedical Science*, **Vol.25: 43**, (2018).
- [2] Arbuzova A, Wang J, Murray D, Jacob J, Cafiso D S, McLaughlin S, *Kinetics of interaction of the Myristoylated alanine-rich C kinase substrate, membranes, and calmodulin*, *J Biol Chem*, **Vol.272: 27167-21177**, (1997).
- [3] Wang J, Gambhir A, Mihalyne G, Murray D, Golebiewska U, McLaughlin S, *Lateral sequestration of phosphatidylinositol4,5- bisphosphate by the basic effector domain of Myristoylated alanine-rich C kinase substrate is due to non specific electrostatic interactions*, *J Biol Chem*, **Vol.277: 34401-34412**, (2002).
- [4] Rusu L, Gambhir A, McLaughlin S, Rädler J, *Fluorescence correlation spectroscopy studies of peptide and protein binding to phospholipid vesicles*, *Biophys J*, **Vol.87: 1044-1053**, (2004).
- [5] Verghese G M, Johnson J D, Vasulka C, Haupt D M, Stumpo D J, Blackshear P J, *Protein kinase C-mediated phosphorylation and calmodulin binding of recombinant Myristoylated alanine-rich C kinase substrate (MARCKS) and MARCKS-related protein*, *J Biol Chem*, **Vol.269: 9361-9367**, (1994).
- [6] Blackshear P J, Verghese G M, Johnson J D, Haupt D M, Stumpo D J, *Characteristics of the F52 protein, a MARCKS homologue*, *J Biol Chem*, **Vol.267:13540-13546**, (1992).
- [7] Rebecchi M, Boguslavsky V, Boguslavsky L, McLaughlin S, *Phosphoinositide-specific phospholipase C- δ 1 effect of monolayer surface pressure and electrostatic surface potentials on activity*, *Biochemistry*, **Vol.31: 12748-12753**, (1992).
- [8] Wang J, Arbuzova A, Hangyás-Mihályné G, McLaughlin S, *The effector domain of myristoylated alanine-rich C kinases substrate binds strongly to phosphatidylinositol4,5-Bisphosphate*. *J Biol Chem*, **Vol.276: 5012-5019**, (2001).
- [9] Dietrich U, Krüger P, Gutberlet T, Käs J .A, *Interaction of the MARCKS peptide with PIP2 in phospholipid monolayers*, *Biochim Biophys Acta*, **Vol.557: 1474-1481**, (2009).
- [10] Alonso S, Dietrich U, Händel C, Käs J A, Bär M, *Oscillations in the lateral pressure of lipid monolayers induced by nonlinear chemical dynamics of the second messengers MARCKS and protein kinase C*, *Biophysical J*, **Vol.100: 939-947**, (2011).

- [11] Ohmori S, Sakai N, Shirai Y, Yamamoto H, Miyamoto E, Shimizu N, Saito N, *Importance of protein kinase C targeting for the phosphorylation of its substrate, myristoylated alanine rich C-kinase substrate*, *J Biol Chem*, **Vol.275: 26449-26457**, (2000).
- [12] Mogami H, Zhang H, Suzuki Y, Urano T, Saito N, Kojima I, Petersen O H, *Decoding of short-lived Ca^{2+} in flux signals in to long term substrate phosphorylation through activation of two distinct classes of protein kinase C*, *J Biol Chem* , **Vol.278: 9896-9904**, (2003).
- [13] Uchino M, Sakai N, Kashiwagi K, Shirai Y, Shinohara Y, Hirose K, Iino M, Yamamura T, Saito N, *Isoform-specific phosphorylation of metabotropic glutamate receptor 5 by Protein Kinase C(PKC) blocks Ca^{2+} oscillation and oscillatory translocation of Ca^{2+} -dependent PKC*, *J Biol Chem* , **Vol.279: 2254-2261**, (2004).
- [14] Sawano A, Hama H, Saito N, Miyawaki A, *Multicolor imaging of Ca^{2+} and protein kinase C signals using novel epifluorescence microscopy*, *Biophys J*, **Vol.82: 1076-1085**, (2002).
- [15] Laux T, Fukami K, Thelen M, Golub T, Frey D and Caroni P, *GAP43, MARCKS, and CAP23 modulate $PI(4,5)P_2$ at plasmalemmal rafts, and regulate cell cortex actin dynamics through a common mechanism*, *J. Cell Biol.*, **Vol.149: 1455-72** , (2000).
- [16] R Kapral, K Showalter, *Chemical Waves and Patterns*, Kluwer, Dordrecht, (1994).
- [17] J Keener and J Sneyd, *Mathematical Physiology*, Springer, New York. **Vol.8**, (2009).
- [18] Alonso S, Markus B, *Phase separation and bistability in a three-dimensional model for protein domain formation at biomembranes*, *Phys. Biol*, **7: 046012**, (2010).
- [19] John K and Bär M, *Alternative mechanisms of structuring biomembranes: self-assembly versus self-organization*, *PLoS Comput. Biol*, **95: 198101**, (2005).
- [20] Otsuji M, Ishihara S, Co C, Kaibuchi K, Mochizuki A and Kuroda S, *A mass conserved reaction-diffusion system captures properties of cell polarity*, *Biophys J*, **3: 1044-1053**, (2007).
- [21] Mori Y, Jilkine A and Edelstein-Keshet L, *Wave-pinning and cell polarity from a bistable reaction-diffusion system*, *Biophys J*, **94: 3684-3697**, (2008).
- [22] Huang K C, Meir Y and Wingreen N S, *Dynamic structures in Escherichia coli: spontaneous formation of MinE rings and MinD polar zones*, *Proc. Natl Acad. Sci. USA* ,**100: 12724-12728**, (2003).
- [23] James O. Murray, *Mathematical Biology.*, Library of Congress Cataloging-in-Publication Data., **Vol.19**, (1989).
Chem. Rev **Vol.101: 2353-64**, (2001).
- [24] Davydov, A.S, Kislukha, N.I, *Solitary excitations in onedimensional molecular chains*, *Phys.Stat.Solidi(b)*, **Vol.59: 465** (1973).
- [25] Davydov, A.S, *Bisoliton mechanism of high-temperature superconductivity*, *Phys. Stat. Solidi (b)*, **Vol.146: 619**, (1988).
- [26] Brizhik, L.S, *Bisoliton mechanism of electron transport in biological systems*, *J. Biol. Phys*, **Vol.19: 123-131** (1993).

- [27] Brizhik, L.S, Eremko, A.A, *Role of bisolitons and their correlations in charge transfer processes*, *J. Biol. Phys.*, **Vol.24:** **233**, (1999).
- [28] Brizhik, L, *Delayed luminescence of biological systems arising from correlated many-soliton states*, *Phys. Rev. E*, **Vol.64:** **031902**, (2011).
- [29] Eremko, A.A, *Peierls-Frohlich problem in the continuum approximation*, *Phys. Rev. B*, **Vol.46:** **3721**, (1992).
- [30] Simo,E, Kofané,T.C, *Influence of the fuctuations of polarization in molecular chains*, *Phys. Rev. E*, **Vol.56:** **4751**, (1997)
- [31] Scott, A.C, *Davydov's soliton*, *Phys. Rev. Lett*, **Vol.1:** **217**, (1992).
- [32] Kuramoto, Y, *Chemical Oscillations, Waves and Turbulence*, Springer, Berlin, (1984).
- [33] Aranson, I.S, Kramer L, *The world of the complex Ginzburg-Landau equation*, *Rev. Mod. Phys.*, **Vol.74:** **99**, (2002).
- [34] Alain Mvogo, Germain Hubert Ben-Bolie, and Timoléon Crépin Kofané, *Solitary waves of a-helix propagation in media with arbitrary inhomogeneities*, *The European Physicaljournal B*, **Vol.86:** **217**, (2013).
- [35] Alain Mvogo, Germain Hubert Ben-Bolie, and Timoléon Crépin Kofané, *Solitary waves in an inhomogeneous chain of a-helical proteins*, *International Journal of Modern Physics B* . **Vol.28:** **17**, (2014)
- [36] A. Gizzi, A. Loppini, R. Ruiz-Baier, A. Ippolito, A. Camassa, A. La Camera, E. Emmi, L. Di Perna, V. Garofalo, C. Cherubini, and S. Filippi, *Nonlinear diffusion and thermo-electric coupling in a two-variable model of cardiac action potential*, *Chaos*. **Vol.27:** **093919**, (2017).
- [37] Karen M. Pagea, Philip K. Mainib, Nicholas A.M. Monk, *Complex pattern formation in reaction-diffusion systems with spatially varying parameters*, *Physica D*, **Vol.202:** **95115**, (2005).
- [38] T. Alarcon, H.M. Byrneb, P.K. Maini, *A cellular automaton model for tumour growth in inhomogeneous environment.*, *Journal ofTheoretical biology*, **Vol.225:** **257274**, (2003).
- [39] Philip K. Maini, Debbie L. Benson, Jonathan A. Sherratt, *Pattern formation in reaction-diffusion models with spatially inhomogeneous diffusion coefficients*, *IMA Journal of Mathematics Applied in Medicine and Biology.*, **Vol.9:** **197213**, (1992).
- [40] Wikipedia, *Proteins*, **23: 10-2023** , (2023).
- [41] Alan Mathison Turing, *The chemical basis of morphogenesis*, *Biological Sciences*, **Vol.237(641):** **37-72**, (1952).
- [42] Philip Cohen, *The origins of protein phosphorylation* , *Nature cell biology*, **Vol.4**, (2002).
- [43] Burnett, G. Kennedy, *The enzymatic phosphorylation of proteins*, *E. P. J. Biol. Chem.*, **Vol.211:** **969-980**, (1954).

- [44] Fischer, E. H, Krebs, *Conversion of phosphorylase b to phosphorylase a in muscle extracts*, *E. G. J. Biol. Chem*, **Vol.216**: 121-132, (1955).
- [45] Sutherland E. W, Wosilait, *Inactivation and activation of liver phosphorylase*, *W. D. Nature*, **Vol.175**: 169-170 , (1955).
- [46] Newton A C, *Protein kinase C: structural and spatial regulation by phosphorylation, cofactors, and macromolecular interactions*, *Chem. Rev.* **Vol.101**: 2353-64, (2001).
- [47] Glaser M, Wanaski S, Buser C A, Boguslavsky V, Rashidzada W, Morris A, Rebecchi M, Scarlata S F, Runnels L W, Prestwich G D, Chen J, Aderemi A, Ahni J, McLaughlin S, *Myristoylated alanine-rich C kinase substrate(MARCKS) produces reversible inhibition of phospholipase C by sequestering phosphatidylinositol4,5-Bisphosphate in lateral domains*, *J Biol Chem* , **Vol.271**: 26187-26193 , (1996).
- [48] U. Salli, N. Saito, and F. Stormshak, *Spatiotemporal Interactions of Myristoylated Alanine-Rich C Kinase Substrate (MARCKS) Protein with the Actin Cytoskeleton and Exocytosis of Oxytocin upon Prostaglandin F_{2α} Stimulation of Bovine Luteal Cells*, *BIOLOGY OF REPRODUCTION*, **Vol.69**: 2053-2058, (2003).
- [49] George M. Verghese, J. David Johnson, Charles Vasulkag, Dale M. Haupts, Deborah J. Stumpo, and Perry J. Blackshear Sn , *Protein Kinase C-mediated Phosphorylation and Calmodulin Binding of Recombinant Myristoylated Alanine-rich Kinase Substrate (MARCKS) and RIARCKS-related Protein*, *J. Biol. Chem*, **Vol.269**: 9361-9367, (1994).
- [50] Kim, J., T. Shishido, X. Jiang, A. Aderem, and S. McLaughlin, *Phosphorylation, high ionic strength, and calmodulin reverse the binding of MARCKS to phospholipid vesicles*, *J. Biol. Chem*, **Vol.269**: 28214-28219, (1994).
- [51] Wu, W.C, Walaas, S.I, Nairn, A.C, and Greengard, P, *Calcium/phospholipid regulates phosphorylation of a Mr 87k substrate protein in brain synaptosomes.*, *Proc. Natl. Acad. Sci. USA*, **Vol.79**: 5249-5253, (1982).
- [52] Weimer, J.M, Yokota, Y, Stanco, A, Stumpo, D.J, Blackshear, P.J, and Anton, E.S, *MARCKS modulates radial progenitor placement, proliferation and organization in the developing cerebral cortex*, *Development*, **Vol.136**: 2965-2975, (2009).
- [53] J. Lippoldt, C. Händel, U. Dietrich, J.A. Käs, *Dynamic membrane structure induces temporal pattern formation*, *Biochimica et Biophysica Acta*, **Vol.1838**: 2380-2390, (2014).
- [54] Damera G, Jester WF, Jiang M, Zhao H, Fogle HW, Mittelman M, et al, *Inhibition of myristoylated alanine-rich C kinase substrate (MARCKS) protein inhibits ozone-induced airway neutrophilia and inflammation*, *Exp Lung Res*, **Vol.36(2)**: 75-84, (2010).
- [55] Takashi S, Park J, Fang S, Koyama S, Parikh I, Adler KB, *A peptide against the N-terminus of myristoylated alanine-rich C kinase substrate inhibits degranulation of human leukocytes in vitro*, *Am J Respir Cell Mol Biol*, **Vol.34(6)**: 647-652, (2006).
- [56] Li J, D'Annibale-Tolhurst MA, Adler KB, Fang S, Yin Q, Birkenheuer AJ, et al, *A myristoylated alanine-rich C kinase substrate-related peptide suppresses cytokine mRNA and protein expression in LPS-activated canine neutrophils*, *Am J Respir Cell Mol Biol*, **Vol.48(3)**: 314-321, (2013).

- [57] Sheats MK, Sung EJ, Adler KB, Jones SL, *In vitro neutrophil migration requires protein kinase C-Delta (delta-PKC)-mediated Myristoylated alaninerich C-kinase substrate (MARCKS) phosphorylation, Inflammation*, **Vol.38(3): 1126-1141**, (2015).
- [58] Alli AA, Bao HF, Liu BC, Yu L, Aldrugh S, Montgomery DS, et al, *Calmodulin and CaMKII modulate ENaC activity by regulating the association of MARCKS and the cytoskeleton with the apical membrane, Am J Physiol Renal Physiol*, **Vol.309(5): 456-463**, (2015).
- [59] Alli AA, Bao HF, Aldrugh Y, Song JZ, Ma HP, et al, *Phosphatidylinositol phosphate-dependent regulation of Xenopus ENaC by MARCKS protein, Am J Physiol Renal Physiol*, **Vol.303(6): 800-811**, (2012).
- [60] Chen X, Rotenberg SA, *Phospho MARCKS drives motility of mouse melanoma cells, Cell Signal*, **Vol.22(7): 1097-1103**, (2010).
- [61] Estrada-Bernal A, Gatlin JC, Sunpaweravong S, Pfenninger KH, *Dynamic adhesions and MARCKS in melanoma cells, J Cell Sci*, **Vol.122(13): 2300-2310**, (2009).
- [62] Mohapatra P, Yadav V, Toftdahl M, Andersson T, *WNT5A-induced activation of the protein Kinase C Substrate MARCKS is required for Melanoma Cell Invasion, Cancers*, **Vol.12(2): 346**, (2020).
- [63] Eustace NJ, Anderson JC, Langford CP, Trummell HQ, Hicks PH, Jarboe JS, et al, *Myristoylated alanine-rich C-kinase substrate effector domain phosphorylation regulates the growth and radiation sensitization of glioblastoma, Int J Oncol*, **Vol.54(6): 3039-2053**, (2019).
- [64] Micallef J, Taccone M, Mukherjee J, Croul S, Busby J, Moran MF, et al, *Epidermal growth factor receptor variant III-induced Glioma invasion is mediated through Myristoylated alanine-rich protein kinase C substrate overexpression, Cancer Res*, **Vol.69(19): 7548-7556**, (2009).
- [65] Jarboe JS, Anderson JC, Duarte CW, Mehta T, Newsheer S, Hicks PH, et al, *MARCKS regulates growth and radiation sensitivity and is a novel prognostic factor for Glioma, Clin Cancer Res*, **Vol.18(11): 3030-3041**, (2012).
- [66] Chen CH, Fong LWR, Yu E, Wu R, Trott JF, Weiss RH, *Up regulation of MARCKS in kidney cancer and its potential as a therapeutic target, Oncogene*, **Vol.36(25): 3588-3598**, (2017).
- [67] Liang WJ, Gao RC, Yang MX, Wang XH, Cheng KW, Shi XJ, et al, *MARCKSL1 promotes the proliferation, migration and invasion of lung adenocarcinoma cells, Oncol Lett*, **Vol.19(3): 2272-2280**, (2020).
- [68] Rao GH, Pierobon M, Kim IK, Hsu WH, Deng JH, Moon YW, et al, *Inhibition of AKT1 signaling promotes invasion and metastasis of non-small cell lung cancer cells with K-RAS or EGFR mutations, Sci Rep*, **Vol.7: 1-2**, (2017).
- [69] Bickeboller M, Tagscherer KE, Kloor M, Jansen L, Chang-Claude J, Brenner H, et al, *Functional characterization of the tumor-suppressor MARCKS in colorectal cancer and its association with survival, Oncogene*, **Vol.34(9): 1150-1159**, (2015).
- [70] Wenzel T, Buch T, Urban N, Weirauch U, Schierle K, Aigner A, et al, *Restoration of MARCK enhances chemosensitivity in cancer, J Cancer Res Clin*, **Vol.146(4): 843-858**, (2020).

- [71] Techasen A, Loilome W, Namwat N, Takahashi E, Sugihara E, Puapairoj A, et al, *Myristoylated alanine-rich C kinase substrate phosphorylation promotes cholangiocarcinoma cell migration and metastasis via the protein kinase C-dependent pathway*, *Cancer Sci*, **Vol.101(3): 658-665**, (2010).
- [72] Song JJ, Wang Q, Luo YY, Yuan P, Tang CF, Hui YF, et al, *miR-34c-3p inhibits cell proliferation, migration and invasion of hepatocellular carcinoma by targeting MARCKS*, *Int J Clin Exp Pathol*, **Vol.8(10): 12728-12737**, (2015).
- [73] Manai M, Thomassin-Piana J, Gamoudi A, Finetti P, Lopez M, Eghozzi R, et al, *MARCKS protein overexpression in inflammatory breast cancer*, *Oncotarget*, **Vol.8(4): 6246-6257**, (2017).
- [74] Chen CH, Cheng CT, Yuan Y, Zhai J, Arif M, Fong LWR, et al, *Elevated MARCKS phosphorylation contributes to unresponsiveness of breast cancer to paclitaxel treatment*, *Oncotarget*, **Vol.6(17): 15194-15203**, (2015).
- [75] Manai M, Abdeljaoued S, Goucha A, Adouni O, Bettaieb I, Bouzaïen H, et al, *MARCKS protein overexpression is associated with poor prognosis in male breast cancer*, *Cancer Biomark*, **Vol.26(4): 513-522**, (2019).
- [76] Lebedev TD, Vagapova ER, Popenko VI, Leonova OG, Spirin PV, Prassolov VS, *Two receptors, two isoforms, Two Cancers: Comprehensive Analysis of KIT and TrkA Expression in Neuroblastoma and Acute Myeloid Leukemia*, *Front Oncol*, **Vol.9: 1046**, (2019).
- [77] Yang Y, Chen Y, Saha MN, Chen J, Evans K, Qiu L, et al, *Targeting phospho- MARCKS overcomes drug-resistance and induces antitumor activity in preclinical models of multiple myeloma*, *Leukemia*, **Vol.29(3): 715-726**, (2015).
- [78] Zhang L, Rastgoo N, Wu J, Zhang M, Pourabdollah M, Zacksenhaus E, et al, *Targeting phospho- MARCKS inhibition cooperates with autophagy antagonists to potentiate the effect of standard therapy against drug-resistant multiple myeloma*, *Cancer Lett*, **Vol.480: 29-38**, (2020).
- [79] Zhang L, Abdi J, Wang MJ, Rastgoo N, Chang H, *Marcks peptide inhibitor displays Synergistic Cytotoxicity with Bortezomib in drug resistant multiple Myeloma cells but enhances Autophagic effect*, *Blood*, **Vol.128**, (2016).
- [80] Alain Mvogo, Germain Hubert Ben-Bolie, and Timoléon Crépin Kofané, *Solitary waves of α -helix propagation in media with arbitrary inhomogeneities*, *The European Physical Journal B*. **Vol.86, 217**, (2013).
- [81] Stumpo, D.J, Bock,C.B, Tuttle,J.S, and Blackshear,P.J, *MARCKS deficiency in mice leads to abnormal brain development and perinatal death*, *Proc. Natl.Acad.Sci.USA*, **Vol.92: 944-948**, (1995).
- [82] Iglesias P A, Levchenko A, *Models of eukaryotic gradient sensing: application to chemotaxis of amoebae and neutrophils*, *Phil. Trans, Biophys. J*, **Vol. 50-82**, (2002).
- [83] Blackshear P J, *The MARCKS family of cellular protein kinase C substrates*, *J. Biol. Chem*, **Vol.268: 1501**, (1993).

- [84] K. Nishinari, K. Abe, J. Satsuma, *A new-type of soliton behavior in a two dimensional plasma system*, *J. Phys, Soc. Japan*, **Vol.62(6): 2021-2029**, (1993).
- [85] Rusu L, Gambhir A, McLaughlin S, Rädler J, *Fluorescence correlation spectroscopy studies of peptide and protein binding to phospholipid vesicles*, *Biophys J*, **Vol.87: 1044-1053**, (2004).
- [86] Sergio Alonso, Undine Dietrich, Chris Händel, Josef A. Käs and Markus Bär , *Oscillations in the Lateral Pressure of Lipid Monolayers Induced by Nonlinear Chemical Dynamics of the Second Messengers MARCKS and Protein Kinase C*, *Biophysical journal*, **Vol.100: 939-947**, (2011).
- [87] Goldbeter A, Koshland D.E, *An amplified sensitivity arising from covalent modification in biological systems*, *Proc Nati Acad Sci USA.*, **Vol.78: 6840-6844. 11**, (1981).
- [88] Sergio Alonso, Undine Dietrich, Chris Händel, Josef A. Käs and Markus Bär , *Oscillations in the Lateral Pressure of Lipid Monolayers Induced by Nonlinear Chemical Dynamics of the Second Messengers MARCKS and Protein Kinase C*, *Biophysical journal .*, **Vol.100: 939-947** , (2011).
- [89] John K and Bär M, *Travelling lipid domains in a dynamic model for protein-induced pattern formation in biomembranes*, *Phys. Biol*, **Vol.2: 123-32**, (2005).
- [90] Sergio Alonso and Markus Bär, *Modeling domain formation of MARCKS and protein kinase C at cellular membranes*, *EPJ nonlinear bio,edical physics.*, **Vol.2: 1**, (2014).
- [91] McLaughlin S, Wang J, Gambhir A, Murray D, *The electrostatic properties of membranes*, *Annu Rev Biophys Biomol Struct*, **Vol.31: 151-175**, (2002).
- [92] Mogami H, Zhang H, Suzuki Y, Urano T, Saito N, Kojima I, Petersen OH, *Decoding of short-lived Ca₂ influx signals into long term substrate phosphorylation through activation of two distinct classes of protein kinase C*, *J Biol Chem*, **Vol.278: 9896-9904**, (2003).
- [93] Brown GC, Kholodenko BN, *Spatial gradients of cellular phospho-proteins*, *FEBS Lett*, **Vol.457:452-454**, (1999).
- [94] Bhat NR, *Phosphorylation of MARCKS (80-kDa) protein, a major substrate for protein kinase C in oligodendroglial progenitors*, *J Neurosci Res*, **Vol.308: 447-454**, (1991).
- [95] Verghese GM, Johnson JD, Vasulka C, Haupt DM, Stumpo DJ, Blackshear PJ, *Protein kinase C-mediated phosphorylation and calmodulin binding of recombinant Myristoylated alanine-rich C kinase substrate (MARCKS) and MARCKS-related protein*, *J Biol Chem*, **Vol.269: 9361-9367**, (1994).
- [96] Valdez-taubas J, Pelham RB, *PSlow diffusion of proteins in the yeast plasma membrane allows polarity to be maintained by endocytic cycling*, *Curr Biol*, **Vol.13: 1636-1640**, (2003).
- [97] Bhalla US, Iyengar R, *Emergent properties of networks of biological signaling pathways*, *Science*, **Vol.283: 381-387**, (1999).
- [98] Arrio-Dupont M, *Mobility of creatine phosphokinase and \hat{a} -Enolase in cultured muscle cells*, *Biophys J*, **Vol.73:2667-2673**, (1997).

- [99] Rüdiger S, Shuai JW, Huisinga W, Nagaiah C, Warnecke G, Parker I, Falcke M, *Hybrid stochastic and deterministic simulations of calcium blips*, *Biophys J*, **Vol.93**: 1847-1857, (2007).
- [100] Bhalla US, Iyengar R, *Emergent properties of networks of biological signaling pathways*, *Science*, **Vol.283**:381-387,(1999).
- [101] Luby-Phelps K, *Cytoarchitecture and physical properties of cytoplasm: volume, viscosity, diffusion, intracellular surface area*, *Int Rev Cytol*, **Vol.192**:189-221,(1997).
- [102] Christina Kuttler, *Reaction-Diffusion equations with applications*, *Sommer semester*, (2011).
- [103] Michel Peyrard, Thierry Dauxois, *Physique des solitons*, *EDP Sciences*, (2004).
- [104] Davydov, A. S. and Kislukha, N. I , *Solitary excitations in one-dimensional molecular chains*, *Phys. Stat. Sol. B.*, **Vol.59**: 465-470, (1973).
- [105] Loose, M. E, Fischer-Friedrich, P. Schwille, *Spatial regulators for bacterial cell division self-organize into surface waves in vitro.*, *Science* **Vol.320**: 789-792, (2006).
- [106] Nicolis. G, *Introduction to Nonlinear Sciences*, *Cambridge University Press*, Cambridge, (1995).
- [107] Scott S.K, *Oscillation, waves, and chaos in chemical kinetics*, (*Oxford University Press*, Oxford), (1994).
- [108] Walgraef D, *Spatio-temporal pattern formation: with examples from physics, chemistry and materials science.*, *Springer-Verlag*, New York, (1996).
- [109] Tyson J.J, J.P Keener, *Singular Perturbation-Theory of Travelling Waves in Excitable Media*, *Physica D*, **Vol.32**: 327-361, (1988).
- [110] Murray, J.D, *Mathematical Biology*, (*Springer-Verlag*, Berlin), (1989).
- [111] Mikhailov, A.S, *Foundations of Synergetics I: Distributed Active Systems*, (*Springer-Verlag*, Berlin), (1991).
- [112] Mori H, and Y Kuramoto, *Dissipative Structures and Chaos*, (*Springer-Verlag*, Berlin), (1998).
- [113] Michel Peyrard, Thierry Dauxois, *Physique des solitons*, *EDP Sciences*, (2004).
- [114] Kholodenko BN, *Cell-signalling dynamics in time and space*, *Nat Rev Mol Cell Biol*, **Vol.7**: 165-176, (2006).
- [115] McLaughlin S and Murray D. *Plasma membrane phosphoinositide organization by protein electrostatics* , *Nature*. **Vol.438**: 605-611 (2005).
- [116] Jon J. Brudvig, and Jill M. Weimer, *X MARCKS the spot: myristoylated alanine-rich C kinase substrate in neuronal function and disease*, *Frontiers in cellular neuroscience.*, **Vol.9**: 407, (2015).

- [117] Taniuti T, *Reductive perturbation method and far fields of wave equations*, *Prog. Theor. Phys. Suppl.*, **Vol.55: 1**, (1974).
- [118] Kraenkel R, Manna M and Pereira J G, *The Korteweg-de Vries hierarchy and long water-waves*, *J. Math. Phys.*, **Vol.36: 307** (1995).
- [119] Kodama Y and Mikhailov A V, *Obstacles to asymptotic integrability Algebraic Aspects of Integrability*, Boston: Birkäuser, **173-204**, (1996).
- [120] Calogero F C, *What is Integrability ed V E Zakharov*, Berlin: Springer, **pp 1-61**, (1991).
- [121] J Leon and M Manna, *Multiscale analysis of discrete nonlinear evolution equations*, *J. Phys. A: Math. Gen.*, **Vol.32: 2845-2869**, (1999).
- [122] G. Fongang Achu, F. M. Moukam Kakmeni, and A. M. Dikande, *Breathing pulses in the damped-soliton model for nerves*, *PHYSICAL REVIEW E*, **Vol.97: 012211**, (2018).
- [123] Garc I Morales, V., Krischer, K, *The complex Ginzburg- Landau equation: an introduction*, *Contemp. Phys*, **Vol.53: 79-95**, (2012).
- [124] Hirota, R, *Exact solution of the Korteweg-de Vries equation for multiple collisions of solitons*, *Phys. Review Letters*, **Vol.27: 1192-1194**, (1971).
- [125] Y. Matsuno, *Bilinear Transformation Method*, Academic Press, **Orlando**, (1984).
- [126] E.Yomba, T. C Kofané and F.B.Pelap, *on exact solutions of the generalized modifies Ginzburg-landau Equation using hirota S method*, *journal of physical society in japan* **Vol.65: 2337-2338** , (1996).
- [127] R. Hirota, *The Direct Method in Soliton Theory*, Cambridge University Press, New York, (2004).
- [128] Armand S. Etémé, Conrad B. Tabi, Alidou Mohamadou, Timoléon C. Kofané, *Long-range memory effects in a magnetized Hindmarsh-Rose neural network*, *Commun Nonlinear Sci Numer Simulat.*, **Vol.84: 105208** , (2020).
- [129] Armand S. Etémé, Conrad B. Tabi, Alidou Mohamadou, Timoléon C. Kofané, *Unstable discrete modes in HindmarshRose neural networks under magnetic flow effect*, *Chaos, Solitons and Fractals*, **Vol.123: 116123** , (2019).
- [130] Tabi C B, Maïna I, Mohamadou A, Ekobena HPF, Kofané T C, *Fractional unstable patterns of energy in alpha- helix proteins with long-range interactions*, *Chaos, Solitons and Fractal*, **Vol.116: 386391** , (2018).
- [131] A.D. Koko, C.B. Tabi, H.P.F. Ekobena, A. Mohamadou, T.C. Kofané , *Nonlinear charge transport in the helicoidal DNA molecule*, *Chaos.*, **Vol.22: 043110** , (2012).
- [132] G.R.Y. Mefire, C.B. Tabi, A. Mohamadou, H.P.F. Ekobena, T.C. Kofané, *Modulated pressure waves in large elastic tubes*, *Chaos*, **Vol. 23: 033128**, (2013).
- [133] Armand Sylvain Etémé, Conrad Bertrand Tabi, Alidou Mohamadou, *Long-range patterns in Hindmarsh-Rose networks*, *Commun Nonlinear Sci Numer Simulat.*, **Vol.43: 211-219**, (2017).

- [134] Armand S. Etémé, Conrad B. Tabi, Alidou Mohamadou, Timoléon C. Kofané, *Long-range memory effects in a magnetized Hindmarsh-Rose neural network*, *Commun Nonlinear Sci Numer Simulat.* **Vol.84**, **105208**, (2020).
- [135] Davydov, A.S, Kislukha, N.I, *Solitary excitations in onedimensional molecular chains*, *Phys.Stat.Solidi(b)*, **Vol.59**: **465**, (1973).
- [136] S. Issa, C.B. Tabi, H.P. Ekobena Fouda, T.C. Kofané, *Three excitons states in nonlinear saturation α -helix protein*, *Eur. Phys. J. Plus.* **Vol.133**: **233**, (2018).
- [137] Davydov, A.S, *Bisoliton mechanism of high-temperature superconductivity*, *Phys. Stat. Solidi (b)*, **Vol.146**: **619**, (1988).
- [138] Cross, M.C., Hohenberg, P.C, *Pattern formation outside of equilibrium* *Rev. Mod. Phys.***Vol.65**: **851**, (1993).
- [139] Takembo C.N, Nyifeh P, Fouda H.E, Kofane T, *Modulated wave pattern stability in chain neural networks under high-low frequency magnetic radiation*, *Physica A* .**Vol.65**: **126891**, (2022).
- [140] Takembo C.N.*Information pattern stability in memristive Izhikevich neural networks*, *Mod Phys Lett B*, (2022).
- [141] Takembo C.N, Ekobena H.P.*Effect of temperature fluctuation on the localized pattern of action potential in cardiac tissue*, *Sci Rep* .**Vol.10(1)**: **15087**, (2020).
- [142] Mvogo A, Takembo C.N, Ekobena H.P, Kofane T.C.*Pattern formation in diffusive excitable systems under magnetic flow effects*, *Phys Lett A* **71**: **3812264**, (2017)
- [143] Issa Sali, C. B. Tabi, H. P. Ekobena and T. C. Kofané, *Modulational instability in a biexciton molecular chain with saturable nonlinearity effects*, *International Journal of Modern Physics B*, **Vol.30**, (2017).

List of publications

1. **Chenceline Fouedji**, Armand Sylvain Etémé, Conrad Bertrand Tabi, Henri Paul Ekobena Fouda , "*Pattern formation in a one-dimensional MARCKS protein cyclic model with spatially inhomogeneous diffusion coefficients*" Eur. Phys. J. Plus, **Vol.138:987**.(2023)
2. **Chenceline Fouedji**, Armand Sylvain Etémé, Conrad Bertrand Tabi, Henri Paul Ekobena Fouda, Timoléon Crépin Kofané, "*Multisolitons-like patterns in a one-dimensional MARCKS protein cyclic model*" journal of theoretical biology ,**Vol.579:111702**. (2024)



Pattern formation in a one-dimensional MARCKS protein cyclic model with spatially inhomogeneous diffusion coefficients

Chenceline Fouedji^{1,a} , Armand Sylvain Etémé^{1,b}, Conrad Bertrand Tabi^{2,c}, Henri Paul Ekobena Fouda^{1,d}

¹ Laboratory of Biophysics, Department of Physics, Faculty of Science, University of Yaounde I, P.O. Box 812, Yaounde, Cameroon

² Botswana International University of Science and Technology, P/Bag 16, Palapye, Botswana

Received: 13 June 2023 / Accepted: 9 October 2023

© The Author(s), under exclusive licence to Società Italiana di Fisica and Springer-Verlag GmbH Germany, part of Springer Nature 2023

Abstract We analytically investigate the conditions for the wave instability in a reaction-diffusion system describing the nonlinear dynamics of the myristoylated alanine-rich C kinase substrate (MARCKS) between cytosol and cytoplasmic membrane. Taking into account the effect of spatial inhomogeneous diffusion coefficients, and by applying the discrete multiple scale expansion method, we show that the nonlinear generic model can be transformed into a one-dimensional discrete nonlinear Schrödinger equation. We perform a linear stability analysis on the plane wave solutions to derive the criterion of the modulational instability (MI) phenomenon. This analysis reveals that the critical amplitude of the plane wave is highly influenced by the phosphorylation rate and weakly influenced by the inhomogeneous diffusion coefficients. The exact analytical solutions show that the system exhibits traveling waves and periodic array of patterns. The results seem to indicate the features of synchronization in the collective dynamics. In homogenous state, we obtained a spatial pattern of horizontal stripes. By considering the spatial inhomogeneity effect, we obtain a spatial pattern of oblique stripes. We also notice that an increase in wavenumber induces the increase in the number of stripes in the model.

1 Introduction

Embryology is that part of biology which is concerned with the formation and development of an embryo from fertilization until birth. Morphogenesis, a part of embryology, is the development of pattern and form. The myristoylated alanine-rich C kinase substrate (MARCKS) is a peripheral membrane protein, particularly abundant in the nervous system. It plays an important role in embryonic development, adult brain plasticity, regeneration, and the inflammatory response. In adult vertebrates, MARCKS proteins are very important for multiple regenerative processes, including the regeneration of peripheral nerves in the appendages and tail [1]. This implies that the ability to detect and analyze spatiotemporal patterns is essential for understanding how neural circuits function.

Understanding the formation of spatiotemporal patterns in biological systems is relevant for regulatory processes in cells. The role of MARCKS proteins in this process has been the focus of several experimental studies (see Refs. [2–7]). The first theoretical model describing the nonlinear dynamics of MARCKS proteins concentrations, between cytosol and cytoplasmic membrane in the brain, was proposed by Alonso and Bär [8]. The authors studied the spatiotemporal dynamic of MARCKS with homogeneous protein coverage. However, biological processes in nature are carried out in the presence of inhomogeneities [9]. Thus, the impact of spatial inhomogeneity on MARCKS proteins patterns formation constitutes the main motivation of this work. These inhomogeneities are due to defects caused by the presence of additional molecules in the cytoplasmic membrane and in the cytosol.

During the last decades, the effects of inhomogeneity on the regulation of some biological processes have been increasingly studied in different biological systems such as alpha-helix proteins [9, 10], cardiac tissue [11], embryonic development [12], cellular automaton model for tumor [13], and Turing model [14]. However, it is well known that degenerative diseases are caused by incorrect protein folding. Also, biological processes in nature are carried out in a medium full of inhomogeneities.

The pattern formation in an excitable media is due to the modulational instability phenomenon (MI) which result to the interplay between the dispersion and nonlinearity of media. Over the last years, MI phenomenon has intensively studied in many areas of physics including neural networks [15–18], alpha helix protein [19], DNA molecules [20] or Bose-Einstein condensates [21, 22] just to cite a few. Indeed, Etémé has recently demonstrated that energy localization is tightly correlated with MI phenomenon in time-delay-memristive neural network [18]. On the other hand, Tabi et al. [21, 22] have study matter-wave formation using MI in 2D

^a e-mail: fhenceline@yahoo.fr (corresponding author)

^b e-mail: etemearmand@yahoo.fr

^c e-mail: tabic@biust.ac.bw

^d e-mail: hpekobena@gmail.com

dissipative open Bose-Einstein condensate under the competitive effect of Rashba, Dresselhaus, and helicoidal spin-orbit couplings. They found that the interplay between the spin coupling gives rise to dissipative solitons known as localized patterns. In this work, we will evaluate the impacts of the phosphorylation rate on the one hand and the impact of the inhomogeneous diffusion on the other hand on the pattern formation of MARCKS proteins in biomolecule membrane.

This paper is organized as follows: In Sect. 2, we introduce a spatiotemporal MARCKS proteins model with the effect of inhomogeneities. Furthermore by means of the discrete multiple scale method, we derive a discrete nonlinear Schrödinger (DNLS) equation. In Sect. 3, we perform the modulational instability phenomenon by means of the linear stability analysis and find the stability/instability regions where MARCKS proteins patterns are expected. In Sect. 4, we derive the exact solution of the generic model and present a series of analytical solutions to reveal the impact of the spatial inhomogeneity on the spatiotemporal dynamics of MARCKS. Finally, Sect. 5 summarizes the findings.

2 Model description and multiple scale expansion

2.1 Reaction-diffusion model with inhomogeneity effect

The model which is explored here was proposed in [8]. It describes the spatiotemporal evolution of the concentration of the MARCKS protein at biomembrane involving: binding, phosphorylation and dephosphorylation of the MARCKS protein. This model reads:

$$\begin{aligned}\frac{\partial m}{\partial t} &= \gamma_3 c(1-m) - \gamma_1(1-m)\frac{m}{k_m+m} + D_m \frac{\partial^2 m}{\partial x^2}, \\ \frac{\partial c}{\partial t} &= -\gamma_3 c(1-m) + \gamma_2 p + D \frac{\partial^2 c}{\partial x^2}, \\ \frac{\partial p}{\partial t} &= \gamma_1(1-m)\frac{m}{k_m+m} - \gamma_2 p + D \frac{\partial^2 p}{\partial x^2},\end{aligned}\quad (1)$$

where the variables m , c and p represent the concentrations of MARCKS protein in the membrane, cytosol and phosphorylated site, respectively. The rates γ_1 , γ_2 and γ_3 refer to phosphorylation, dephosphorylation and binding, respectively. The term $(1-m)$ represents the coverage of the membrane by MARCKS proteins which locally prevents the activation of protein kinase C (PKC) at the membrane. Parameters D_m and D account for membrane and cytosolic diffusion coefficients of MARCKS.

Intracellular protein-protein interactions are dynamic events that require tightly regulated spatiotemporal control points. The process of regulating these dynamics produces highly specific molecular response patterns that are based on the ephemeral localization and activity of various coordinating proteins that direct the function of the organism. One of the regulating proteins is the myristoylated alanine-rich C kinase substrate which emerged as an important component of cellular map, governing a wide variety of protein interactions in all types of brain cells [23]. However, biological processes in nature are carried out in a setting of inhomogeneities. For example, proteins and enzymes catalyze millions of chemical reactions that occur every moment in biological systems, but this occurs in a crowded molecular environment and not as isolated entities [24]. Therefore, it is important to take into account the spatial inhomogeneity effect to model the MARCKS diffusion through cytoplasmic membrane. Doing so, the discreteness model of Eq.(1) reads:

$$\begin{aligned}\frac{\partial m_n}{\partial t} + \alpha_0 m_n &= \gamma_3 c_n - \gamma_3 c_n m_n + \alpha_1 m_n^2 + \alpha_2 m_n^3 + D(m_n)(m_{n+1} - 2m_n + m_{n-1}), \\ \frac{\partial c_n}{\partial t} + \gamma_3 c_n &= \gamma_2 p_n + \gamma_3 c_n m_n + D(c_{n+1} - 2c_n + c_{n-1}), \\ \frac{\partial p_n}{\partial t} + \gamma_2 p_n &= \alpha_0 m_n - \alpha_1 m_n^2 - \alpha_2 m_n^3 + D(p_{n+1} - 2p_n + p_{n-1}),\end{aligned}\quad (2)$$

with: $\alpha_0 = \frac{\gamma_1}{k_m}$; $\alpha_1 = (1 + \frac{1}{k_m})\frac{\gamma_1}{k_m}$; $\alpha_2 = -\frac{\gamma_1}{k_m^2}$. The discrete variables m_n , c_n and p_n represent the concentrations of membrane proteins, phosphorylated proteins and free cytosolic proteins, respectively of node n . The function $D(m_n)$ accounts for a self diffusion quadratic law, and defined by $D(m_n) = D_0 + D_1 m_n + D_2 m_n^2$ as in [26]. This means that the diffusion of MARCKS protein at the level of cytoplasmic membrane is not homogeneous, rather, the distribution is inhomogeneous in space.

2.2 Multiple scale expansion

According to the multiple scale expansion analysis, the MARCKS protein is considered to be excited with the natural frequency Ω which depends on the actual frequency ω and the wavenumber q . The relationship between both angular frequency is given by: $\omega = \Omega_0 + \epsilon \lambda$, while the actual wavenumber is expressed by: $q = q_0 + \epsilon \frac{\lambda}{v_g} + \epsilon^2 c_g \lambda^2 + \dots$, where $v_g = \frac{\partial \Omega}{\partial q}$ represents the group velocity and $2c_g = \frac{\partial^2 \Omega}{\partial q^2}$ represents the group velocity dispersion. Parameter λ is a small deviation from the natural frequency Ω . For

$\epsilon = 0$, the frequency ω can be reduced to the natural frequency Ω of the system. Solutions of Eq. (2) can be summarized in terms of the state vector $v_n(t)=(m_n(t), c_n(t), p_n(t))$, whose the generalized form of the unperturbed expressions can be taken in the form:

$$v_n(t) = \int d\omega \hat{V}(\omega) \exp i(\omega t + q_0 n), \tag{3}$$

where $\hat{V}(\omega) = (\hat{M}_n(\omega), \hat{C}_n(\omega), \hat{P}_n(\omega))$. After including the derivation of ω and q , the generalized solutions take the form:

$$\begin{aligned} m_n(t) &= A(n, t)\psi(\zeta_n, \tau_n), \\ c_n(t) &= A(n, t)\theta(\zeta_n, \tau_n), \\ p_n(t) &= A(n, t)\chi(\zeta_n, \tau_n), \end{aligned} \tag{4}$$

where $A(n, t) = \exp i(qn + \omega t)$, $\tau_n = \epsilon(t + \frac{n}{v_g})$, $\zeta_n = \epsilon^2 n$ and $c_g = 1$. The small parameter can be taken as $\epsilon^2 = \frac{1}{N}$. In order to support a large grid, we have introduced a new lattice m . Thus, for a given lattice number n , only a set of lattice points can be constructed at each $N = \epsilon^{-2}$. Therefore, we can index ζ_n by m so that $(n - N) \rightarrow (m - 1)$, $n \rightarrow m$, $(n + N) \rightarrow (m + 1)$. More precisely, $\zeta_n - N = (m - 1)$, $\zeta_n = m$, $\zeta_n + N = (m + 1)$. All the above implies that the slow modulations $v(\zeta_n, \tau_n)$ of the plane wave $A(n, t)$ can be replaced by the functions $v(m, \tau)$ of the variables m and $\tau = \tau_n$. This approach based on discrete multi-scale analysis has been studied in [15, 16, 19]. Following all the above, the solutions for the set of Eq. (2) can be investigated in the form of the following Fourier series, in power of the small parameter ϵ :

$$\begin{aligned} m_n(t) &= \sum_{s=1}^{\infty} \epsilon^s \sum_{l=-s}^s \psi_s^{(l)}(\zeta_n, \tau_n) A^{(l)}(n, t), \\ c_n(t) &= \sum_{s=1}^{\infty} \epsilon^s \sum_{l=-s}^s \theta_s^{(l)}(\zeta_n, \tau_n) A^{(l)}(n, t), \\ p_n(t) &= \sum_{s=1}^{\infty} \epsilon^s \sum_{l=-s}^s \chi_s^{(l)}(\zeta_n, \tau_n) A^{(l)}(n, t), \end{aligned} \tag{5}$$

with $\psi_s^{-l}(m, \tau) = (\psi_s^{(l)}(m, \tau))^*$, $\theta_s^{-l}(m, \tau) = (\theta_s^{(l)}(m, \tau))^*$, and $\chi_s^{-l}(m, \tau) = (\chi_s^{(l)}(m, \tau))^*$, where the asterisk (*) represents the complex conjugate of the preceding term. Inserting the above solutions into Eq. (2) leads to a set of coupled equations to be solved at different orders of the small parameter ϵ , with the corresponding harmonics l .

At the leading order (1, l), with $l = 0$, we obtain $\psi_1^{(0)}(m, \tau) = \theta_1^{(0)}(m, \tau) = \chi_1^{(0)}(m, t) = 0$. For $l = 1$, the dispersion relation:

$$\begin{aligned} &(i\omega)^3 + (i\omega)^2 \left(\gamma_2 - 8D \sin^2 \frac{q}{2} + \gamma_3 + \alpha_0 - 4D_0 \sin^2 \frac{q}{2} \right) \\ &+ (i\omega) \left[\left(\gamma_3 - 4D \sin^2 \frac{q}{2} \right) \left(\gamma_2 - 4D \sin^2 \frac{q}{2} \right) + \left(\alpha_0 - 4D_0 \sin^2 \frac{q}{2} \right) \right. \\ &\times \left. \left(\gamma_2 + \gamma_3 - 8D \sin^2 \frac{q}{2} \right) \right] + \left(\alpha_0 - 4D_0 \sin^2 \frac{q}{2} \right) \left(\gamma_3 - 4D \sin^2 \frac{q}{2} \right) \\ &\times \left(\gamma_2 - 4D \sin^2 \frac{q}{2} \right) - \alpha_0 \gamma_3 \gamma_2 = 0, \end{aligned} \tag{6}$$

should be satisfied for the system to admit non-trivial solutions in the form: $\psi_1^{(1)}(m, \tau) = \varphi(m, \tau)$, $\chi_1^{(1)} = a\varphi(m, \tau)$, $\theta_1^{(1)} = b\varphi(m, \tau)$. The coefficients a and b are given in "Appendix A". At the order (2, 0) the following solutions

$$\begin{aligned} \psi_2^{(0)} &= \frac{-2\alpha}{\alpha_0} |\psi_1^{(1)}|^2, \\ \theta_2^{(0)} &= \left(\frac{-2\alpha_1}{\gamma_3} + \frac{2\gamma_2 a \left(\gamma_3 - 4D \sin^2 \frac{q}{2} \right)}{\left(\gamma_3 - 4D \sin^2 \frac{q}{2} \right) + \omega^2} \right) |\psi_1^{(1)}|^2, \\ \chi_2^{(0)} &= \left(\frac{-2\alpha_1}{\gamma_2} + \frac{2\gamma_3 a \left(\gamma_3 - 4D \sin^2 \frac{q}{2} \right)}{\left(\gamma_3 - 4D \sin^2 \frac{q}{2} \right) + \omega^2} \right) |\psi_1^{(1)}|^2, \end{aligned}$$

are found. At the order (2, 1), the group velocity which satisfies the Fredholm solvability condition is expressed by:

$$v_g = \frac{i \sin q \left(D_0(i\omega + \gamma_2)(i\omega + \gamma_3) + D\gamma_3b(i\omega + \gamma_2) + D\gamma_2\gamma_3a \right)}{(i\omega + \gamma_2)(i\omega + \gamma_3) + \gamma_3b(i\omega + \gamma_2) + \gamma_3\gamma_2a} \tag{7}$$

At the same order, solutions should be found in the form:

$$\begin{aligned} \psi_2^{(1)} &= \delta, \quad \chi_2^{(1)} = \frac{1}{i\omega + \gamma_2} \left(\alpha_0\delta + \frac{2iDa \sin q}{v_g} - 1 \right) \frac{\partial \psi_1^{(1)}}{\partial \tau}, \\ \theta_2^{(1)} &= \frac{1}{(i\omega + \gamma_2)(i\omega + \gamma_3)} \left(\alpha_0\gamma_2\delta + a \left(\frac{2iD \sin q}{v_g} - 1 \right) + b \left(\frac{2iD \sin q}{v_g} - 1 \right) \right) \frac{\partial \psi_1^{(1)}}{\partial \tau}, \end{aligned}$$

where $\delta(m, \tau)$ is an arbitrary function. Still at the same order ($s = 2$), for $l = 2$, solutions are giving in the form $\psi_2^{(2)} = a_2(\psi_1^{(1)})^2$, $\theta_2^{(2)} = a_3(\psi_1^{(1)})^2$, $\chi_2^{(2)} = a_4(\psi_1^{(1)})^2$, while the coefficients a_2, a_3 and a_4 are given in "Appendix B".

At the order ϵ^3 , the differential-difference equation investigated is derived for the case $l = 1$. Considering the fact that the coefficients of the terms $\chi_3^{(1)}(m, \tau), \frac{\partial \psi_1^{(1)}(m, \tau)}{\partial \tau}$ are cancelled out due to the dispersion relation and the group velocity, the amplitude equation in $\varphi(m, \tau) \equiv \varphi_m$ reads:

$$iP[\varphi_{m+1} - \varphi_{m-1}] + Q \frac{\partial^2 \varphi_m}{\partial \tau^2} + R |\varphi_m|^2 \varphi_m = 0, \tag{8}$$

with:

$$\begin{aligned} P &= \sin q \left(D_0(i\omega + \gamma_2)(i\omega + \gamma_3) + D\gamma_3(i\omega + \gamma_2) + D\gamma_2\gamma_3 \right), \\ Q &= \frac{\cos q}{v_g^2} \left[D_0(i\omega + \gamma_2)(i\omega + \gamma_3) + D\gamma_3(i\omega + \gamma_2) + D\gamma_2\gamma_3 \right], \\ R &= (i\omega + \gamma_2)(i\omega + \gamma_3) \left[3\alpha_2 + 2\alpha_1a_2 - \left(\gamma_3b_2a_2 + \gamma_3a_2 + 4a_2D_1 \sin^2 \frac{q}{2} + 4D_2 \sin^2 \frac{q}{2} \right) \right] \\ &\quad + \gamma_3(i\omega + \gamma_2)(\gamma_3a_3 + \gamma_2a_2b_2) - \gamma_2\gamma_3(2\alpha_1a_2 + 3\alpha_2). \end{aligned}$$

Equation (8) represents the discrete nonlinear Schrödinger (DNLS) equation. The global form of such equation has already been obtained in some biological context including, DNA nonlinear dynamics [20], blood flow [2527] or nonlinear dynamics of membrane potential in the central nervous system [15, 26, 27].

3 Linear stability analysis

The study of the stability of solutions of Eq. (8) is not usually easy and in many cases has not yet been done. Because of the simplicity of the plane wave solutions in their cartesian form and for finite amplitude of wave, nonlinearities of the system give rise to the generation of higher harmonics. In order to perform the stability/instability effect, we consider a plane wave solution of Eq. (8) in the form $\varphi_m(\tau) = \varphi_0 \exp i(\lambda m - \Gamma \tau)$, where λ represents the wavenumber and Γ the angular frequency of the plane wave. Inserting the plane wave solution in Eq. (8), we obtain

$$\Gamma^2 = \frac{R}{Q} \left(|\varphi_0|^2 - \frac{2P}{R} \sin \lambda \right).$$

Unstable waves will then appear in the model and modulated wave patterns will be expected if $\Gamma^2 < 0$. This condition is fulfilled if $\frac{R}{Q} < 0$ and $|\varphi_0|^2 > \frac{2P \sin \lambda}{R}$. $\sin \lambda$ being a bounded function, the latter condition becomes

$$|\varphi_0|^2 > \frac{2P}{R} = \varphi_{0,cr}^2.$$

In Fig. 1, the critical amplitude $\varphi_{0,cr}$ is plotted versus the wavenumber q , while fixing $D_0 = 1.1, D_1 = 0.09$ and $D_2 = 0.05$. Therein, the stable and unstable regions of MI are clearly displayed. As shown, nonlinear patterns are expected in the system in the instability domain, i.e., $0 \leq q \leq q_{cr}$, with $q_{cr} = 0.12\pi$. This means that when $q > q_{cr}$ the plane wave remains stable under any modulation. The instability curves displayed in Fig. 1 are similar to those obtained by Takembo and Ekobena [17]. The panels of Fig. 2 highlight the effect of phosphorylation rate γ_1 in (a) and inhomogeneous diffusion coefficients in (b). In Fig. 2a, we fixed $D_0 = 0.1, D_1 = 0.05, D_2 = 0.01$ and increased the phosphorylation rate γ_1 . It is observed that the increase in γ_1 induces decrease of critical amplitude and reduction of instability region. As a result, the nonlinear patterns of MARCKS proteins are expected in the model for the small value of the phosphorylation rate. However, the panel of Fig. 2b where $\gamma_1 = 0.1$ shows that the increase in the

Fig. 1 The plot of the critical amplitude versus the wavenumber q of the carrier wave. We have fixed $D_0 = 1.1, D_1 = 0.09, D_2 = 0.05, \gamma_1 = 2, \gamma_2 = 10, \gamma_3 = 50, k_m = 0.1, D = 10$ as the model parameters

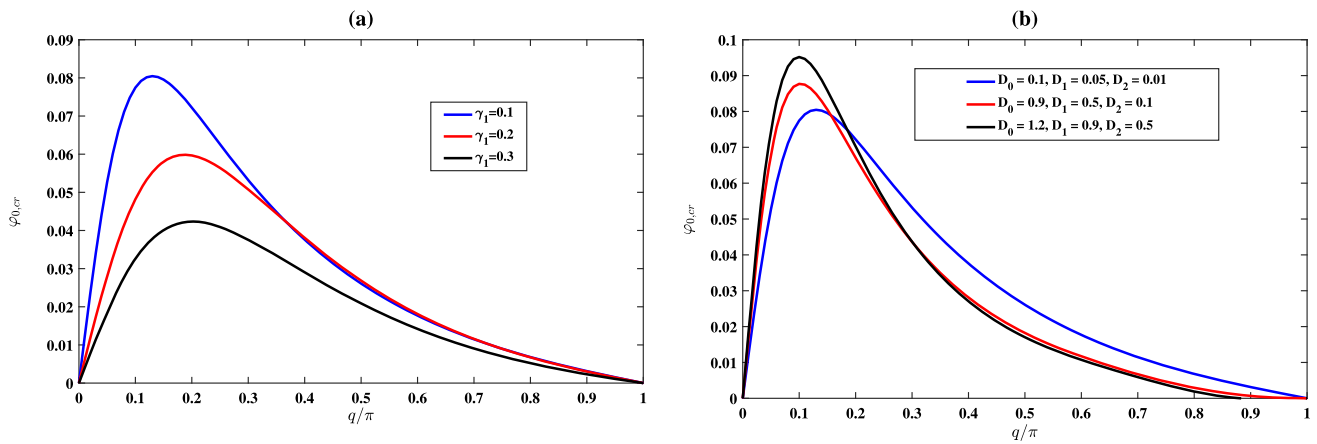
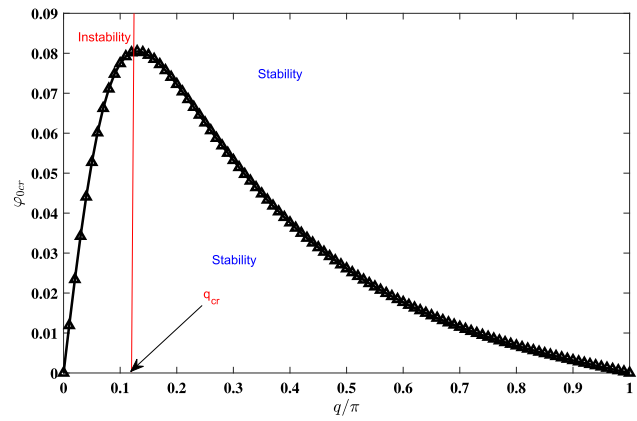


Fig. 2 The panels show the critical amplitude versus the wavenumber q . In panel **a** we have fixed $D_0 = 1.1, D_1 = 0.09, D_2 = 0.05$ and increase γ_1 . In panel **b** we fixed $\gamma_1 = 2.0$ and increased the diffusion coefficients (see legend for more readability). The remaining parameters of the model are: $\gamma_2 = 10.0, \gamma_3 = 50.0, k_m = 0.1, D = 10$

diffusion coefficients induces the increasing critical amplitude and expansion of instability regions. In short, we found that nonlinear patterns are favorable in the MARCKS proteins dynamics for the short wavelength ($0 \leq q \leq q_{cr}$). Additionally, inhomogeneity effects significantly contribute to the formation of such patterns.

4 Weakly nonlinear solutions

Linear stability analysis is limited because it can only detect the onset of instability and therefore does not tell us anything about what kind of dynamical patterns one might obtain in the system when the instability grows for a longtime. In order to solve analytically Eq. (8), we first transform the DNLS equation into the continuous nonlinear Schrödinger equation using Taylor expansion method at the first order [28].

$$\varphi_{m+1} - \varphi_{m-1} = 2l \frac{\partial \varphi_m}{\partial z}, \tag{9}$$

with $z = ml$. Inserting Eq. (9) into Eq. (8) and taking $Z = zz_0, l = 1, T = \tau T_0, \varphi^* = \varphi_0 \varphi, z_0 = \frac{QT_0^2}{Pl}, \varphi_0 = \frac{1}{T_0} \sqrt{\frac{R}{2Q}}$, we obtain:

$$i \frac{\partial \varphi}{\partial Z} + e_0 \frac{\partial^2 \varphi}{\partial T^2} + e_1 |\varphi|^2 \varphi = 0, \tag{10}$$

with $e_0 = \frac{1}{2}, e_1 = 1$. Solutions of Eq.(10) at the first order has been suggested in [29] and read as follows:

$$\varphi(z, T) = \left[4 \left(\frac{1 + 2iT}{1 + 4T^2 + 4z^2} \right) - 1 \right] \exp(iz). \tag{11}$$

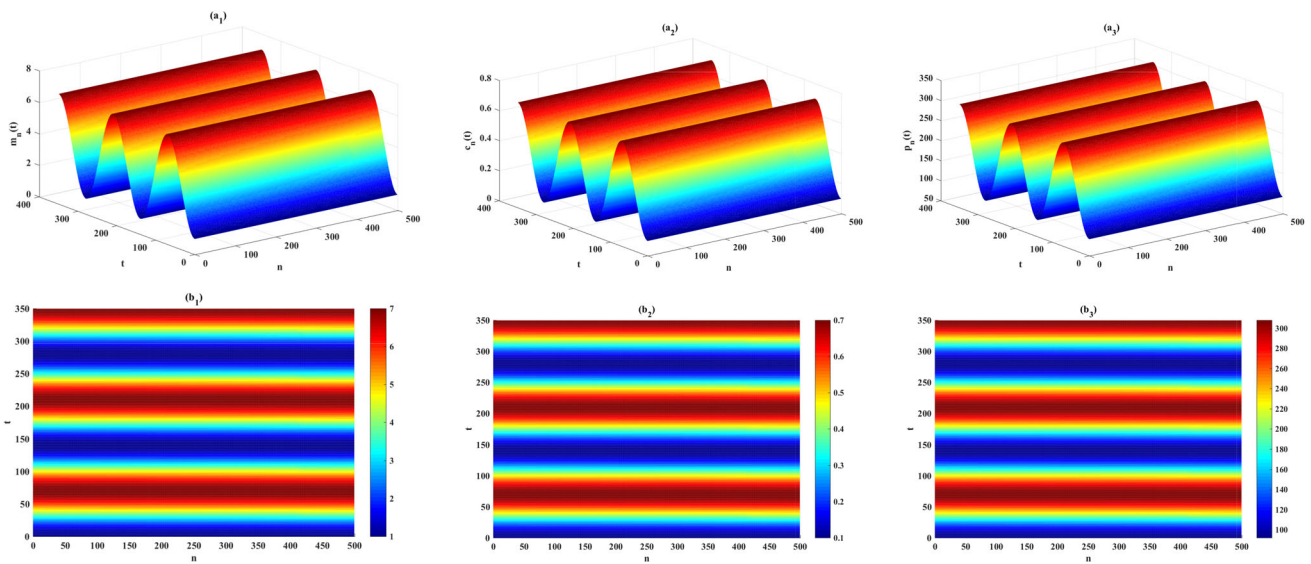


Fig. 3 Spatiotemporal evolution of solutions (12) is displayed on top and their corresponding density plots on down. The concentration of membrane proteins, phosphorylated proteins and free cytosolic proteins with inhomogeneity effect are represented in left, center and right, respectively. We have fixed $q = 0.005\pi$, $D_0 = 0.1$, $D_1 = 0.05$, $D_2 = 0.01$, $\gamma_1 = 1$, $\gamma_2 = 10$, $D = 10$, $\gamma_3 = 50$, $k_m = 0.1$

Thus, combining Eqs. (11) and (5), we derive the solutions of Eq. (2) as:

$$\begin{aligned}
 m_n(x, t) &= \left[4 \left(\frac{1 + 2iT}{1 + 4T^2 + 4Z^2} \right) - 1 \right] \exp(im) \exp(i(\omega t + qn)) \\
 c_n(x, t) &= a \left[4 \left(\frac{1 + 2iT}{1 + 4T^2 + 4Z^2} \right) - 1 \right] \exp(im) \exp(i(\omega t + qn)) \\
 p_n(x, t) &= b \left[4 \left(\frac{1 + 2iT}{1 + 4T^2 + 4Z^2} \right) - 1 \right] \exp(im) \exp(i(\omega t + qn)), \tag{12}
 \end{aligned}$$

The corresponding solutions of membrane-bound, phosphorylated and free cytosolic proteins are represented in Fig. 3, while fixing $q = 0.005\pi$ as the wavenumber. In Fig. 3, we represent the spatiotemporal dynamics of MARCKS between cytosol and membrane bound without inhomogeneity effect. In this case we obtain horizontal stripes. In Fig. 4, we depict the solution for the same wavenumber by taking into account inhomogeneity effect. Here we obtain oblique stripes. Figure 5 shows the solutions when $q = 0.01\pi$ without inhomogeneity effect, and Fig. 6 is obtained for the same wavenumber with inhomogeneity effect. Travelling waves are obtained for a sustainable parameters and homogeneous patterns are observed in both cases. We notice that the increasing wavenumber leads to an increases in the number of stripes, and sweet values of inhomogeneous diffusion rate give rise to oblique stripes. Localized structures consist of alternate bright and blue bands. It is important to notify that, the nonlinear structures of Fig. 3 and Fig. 5 have the future of synchronization patterns. This was previously observed in [26] and translate the fact that all cells of MARCKS proteins share the same dynamics at the same time. Travelling waves trains are known to play several roles in different biological systems. This was experimentally verified in the context of Belousov- Zhabotinskii reaction by Zaikin and Zhabotinskii [30] and by Tyson and Fife in the context of target patterns [31]. Figure 7 shows the spatial evolution of MARCKS dynamics at the time $t = 50$ ms while fixing $D_0 = 0.1$, $D_1 = 0.05$, $D_2 = 0.01$, $\gamma_1 = 0.1$, $\gamma_2 = 10$, $\gamma_3 = 36$, $D = 10$ and $k_m = 0.1$ as the system parameters. Therein, periodic structures are clearly showed in all cases. This is in agreement with the literature review because, according to Alonso et al. [32], the dynamics of unbinding modulated by protein kinase C leads to periodic oscillations in the lateral pressure of lipid monolayers. The nonlinearities of Eq. (1) are responsible for pattern formation and may give rise to oscillations and complex dynamics in membranes [33]. Pattern formation has been extensively study in protein model [34]. Therein, the saturable nonlinearity effects in a biexciton molecular chain reveal that the system exhibits incoherent periodic array of patterns and train of pulses. Dynamic membrane structure induces temporal pattern formation using phase space an unexpected intermediate state prior to the oscillations for high amounts of MARCKS in the system [35]. It was also shown that the onset of oscillatory behavior is independent of diffusion and consumption of reactants [35].

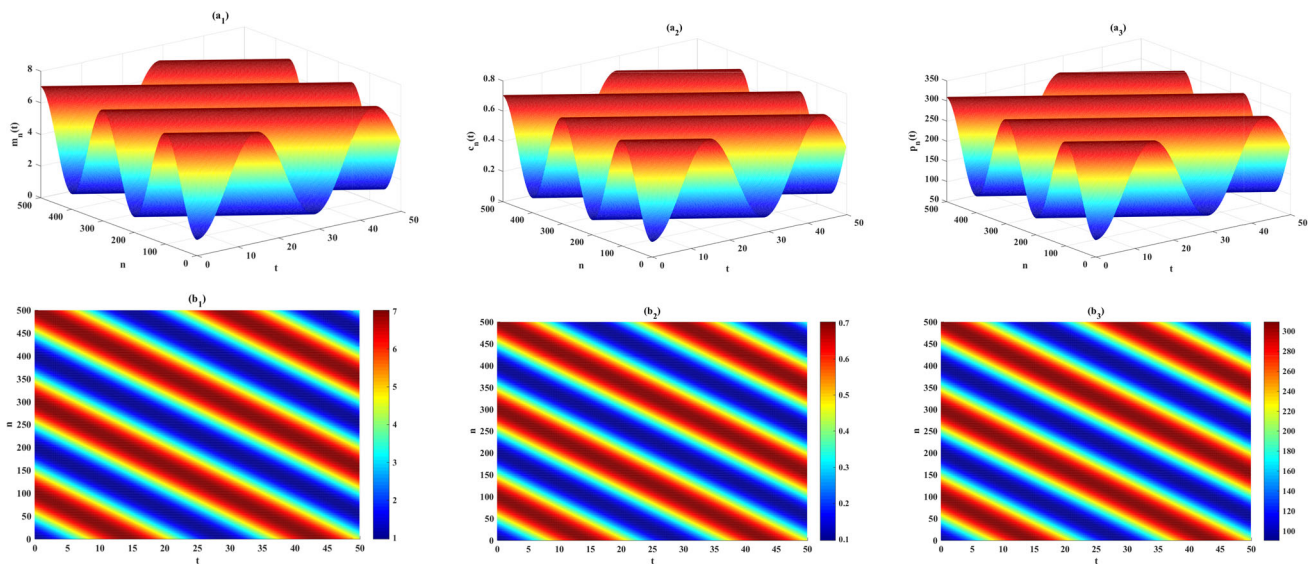


Fig. 4 Spatiotemporal evolution of solutions (12) is displayed on top and their corresponding density plots on down. The concentration of membrane proteins, phosphorylated proteins and free cytosolic proteins with inhomogeneity effect are represented in left, center and right, respectively. We have fixed $q = 0.005\pi$, $D_0 = 500$, $D_1 = 100$, $D_2 = 50$, $\gamma_1 = 1$, $\gamma_2 = 10$, $D = 10$, $\gamma_3 = 50$, $km = 0.1$

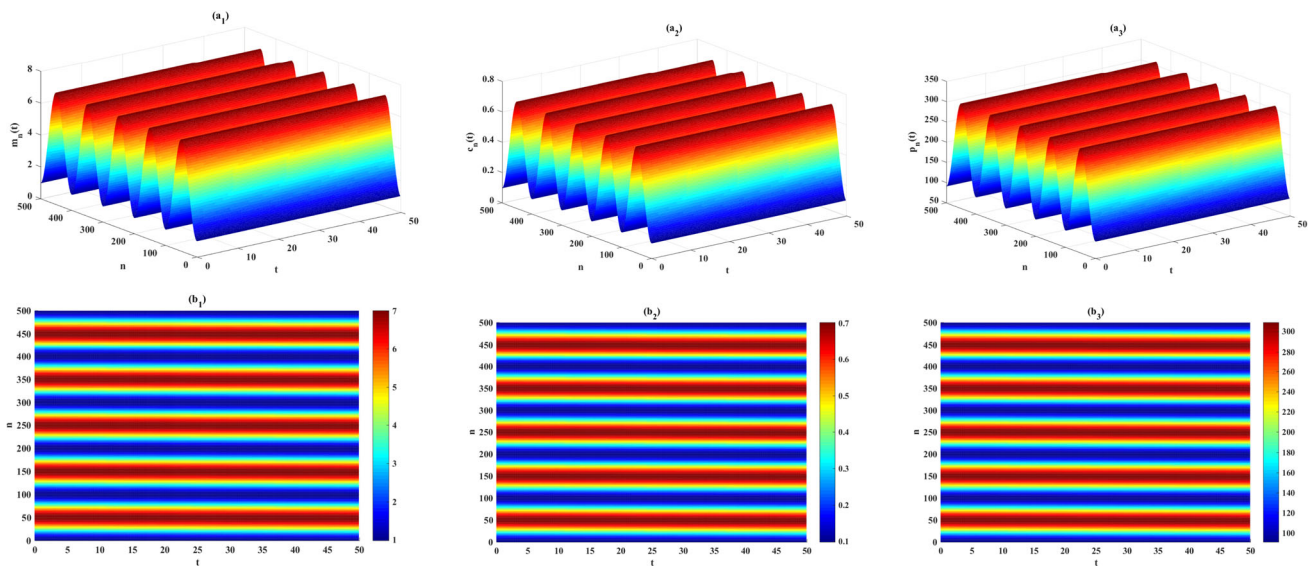


Fig. 5 Spatiotemporal evolution of solutions (12) is displayed on top and their corresponding density plots on down. The concentration of membrane proteins, phosphorylated proteins and free cytosolic proteins with inhomogeneity effect are represented in left, center and right, respectively. We have fixed $q = 0.01\pi$, $D_0 = 0.1$, $D_1 = 0.05$, $D_2 = 0.01$, $\gamma_1 = 1$, $\gamma_2 = 10$, $D = 10$, $\gamma_3 = 36$, $km = 0.1$

5 Conclusion

In this paper, we have studied the effect of inhomogeneities in MARCKS proteins models in the brain at the level of cytoplasmic membrane and cytosol. Applying the multiple scale expansion method, we have derived the discrete nonlinear Schrödinger equation whose coefficients are impacted by inhomogeneity effect. By means of linear stability analysis, the modulational instability (MI) phenomenon has been explored. Then, we have derived the condition for which the plane wave become unstable along with the critical amplitude for the best characterization for the MI phenomenon. It was found that unstable patterns are expected in the short wavelength domain, i.e., $0 \leq q \leq q_{cr}$. Additionally, the increase in phosphorylation rate has induced the decrease of critical amplitude and reduction of instability regions. However, the increase in inhomogeneous diffusion coefficients has induced the increasing critical amplitude and expansion of instability regions. In order to know what kind of dynamical patterns one might obtain in the system when the instability grows for a longtime, we found the exact analytical solutions, and showed that the MARCKS dynamic can be

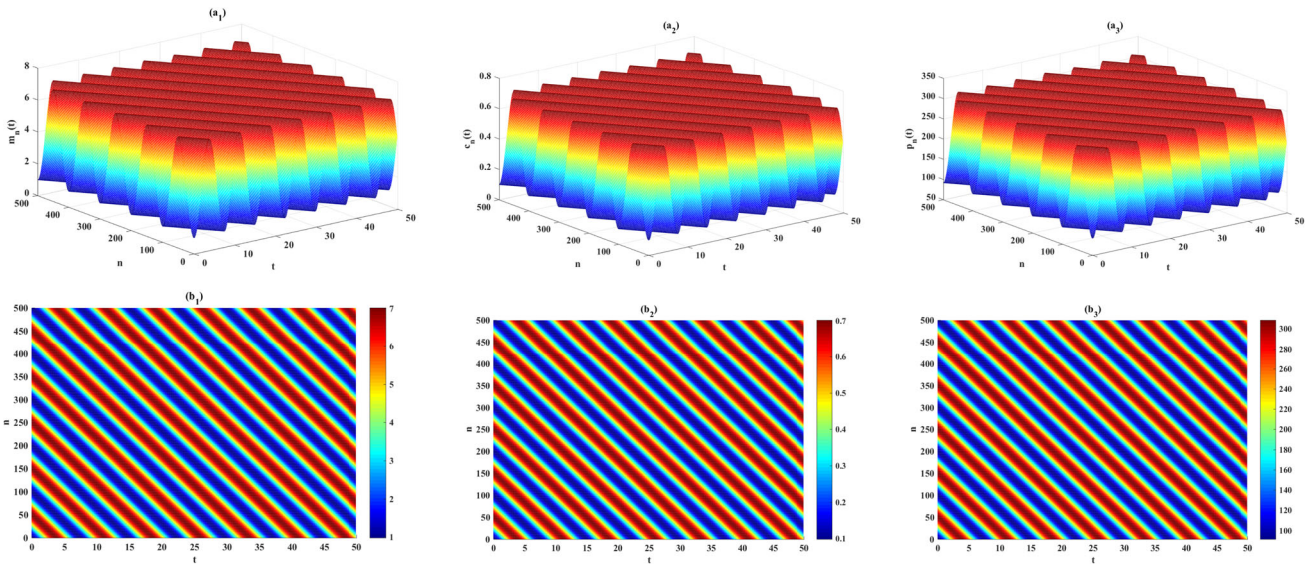


Fig. 6 Spatiotemporal evolution of solutions (12) is displayed on top and their corresponding density plots on down. The concentration of membrane proteins, phosphorylated proteins and free cytosolic proteins with inhomogeneity effect are represented in left, center and right, respectively. We have fixed $q = 0.01\pi$, $D_0 = 500$, $D_1 = 100$, $D_2 = 50$, $\gamma_1 = 1$, $\gamma_2 = 10$, $D = 10$, $\gamma_3 = 50$, $km = 0.1$

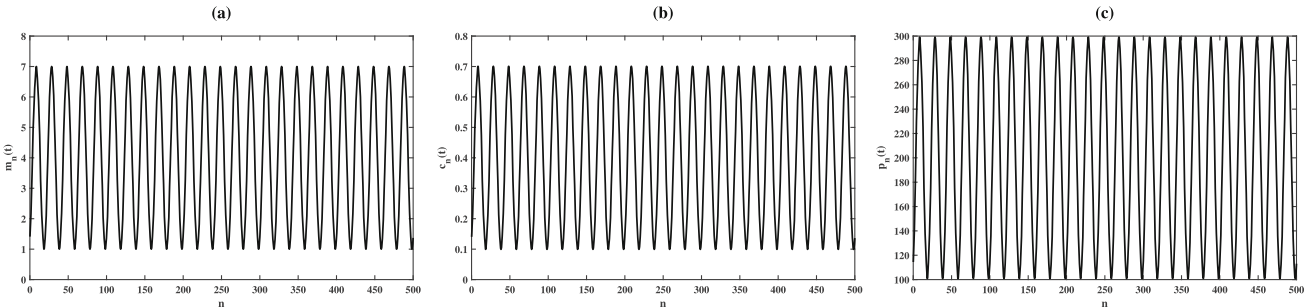


Fig. 7 The panels show space evolution of the traveling waves solutions of (12). We have fixed $t = 50ms$ at the wavenumber $q = 0.01\pi$. Parameters are chosen as $D_0 = 0.1$, $D_1 = 0.05$, $D_2 = 0.01$, $\gamma_1 = 1$, $\gamma_2 = 10$, $D = 10$, $\gamma_3 = 36$, $km = 0.1$

governed by traveling waves. We investigated the effect of the wavenumber and demonstrated a novel form of moving patterns. The results of this work are applicable to cytoplasmic membranes in the brain.

Acknowledgements The corresponding authors (Chenceline Fouedji) is very grateful to Blaise Tabi Dzou for stimulating discussions.

Data availability This manuscript has no data associated.

Declarations

Conflict of interest The authors declare that they have no conflict of interest.

Appendix A

Coefficients at other order (1, l)

$$a = \frac{\alpha_0}{i\omega + \gamma_2 - 4D \sin^2 \frac{q}{2}}, b = \frac{a\alpha_0}{i\omega + \gamma_3 - 4D \sin^2 \frac{q}{2}}.$$

Appendix B

Coefficients at other order (2, 2)

$$\begin{aligned}
 A &= \left(\alpha_1 - \gamma_3 b + 4D_0 \sin^2 \frac{q}{2} \right) \left(2i\omega + \gamma_3 \right) \left(2i\omega + \gamma_2 \right) \\
 &\quad + \gamma_3 \left(2i\omega + \gamma_2 \right) \left(\gamma_3 b + 4D \sin^2 \frac{q}{2} \right) + \gamma_2 \gamma_3 \left(-\alpha_1 + 4D \sin^2 \frac{q}{2} \right) \\
 A_1 &= (2i\omega + \alpha_0 + 4D_1 \sin^2 q)(2i\omega + \gamma_3)(2i\omega + \gamma_2) - \gamma_2 \gamma_3 \alpha_0, \quad a_2 = \frac{A}{A_1} \\
 B &= \left(\gamma_3 b + 4D \sin^2 \frac{q}{2} \right) \left(2i\omega + \gamma_2 \right) \left(2i\omega - \alpha_0 - 4D_1 \sin^2 q \right) + \gamma_2 \left(2i\omega - \alpha_0 - 4D_1 \sin^2 q \right) \\
 &\quad \left(4D \sin^2 \frac{q}{2} - \alpha_1 \right) + \gamma_2 \alpha_0 \left(\alpha_1 - \gamma_3 b + 4D_0 \sin^2 \frac{q}{2} \right), \quad a_3 = \frac{B}{A_1} \\
 C &= \left(2i\omega - \alpha_0 - 4D_1 \sin^2 q \right) \left(2i\omega + \gamma_3 \right) \left(-\alpha_1 + 4D \sin^2 \frac{q}{2} \right) + \gamma_3 \alpha_0 \left(\gamma_3 b + 4D \sin^2 \frac{q}{2} \right) \\
 &\quad + \alpha_0 \left(2i\omega + \gamma_3 \right) \left(\alpha_1 - \gamma_3 b + 4D_0 \sin^2 \frac{q}{2} \right), \quad a_4 = \frac{C}{A_1}.
 \end{aligned}$$

References

1. M. El Amri, U. Fitzgerald, G. Schlosser, MARCKS and MARCKS-like proteins in development and regeneration. *J. Biomed. Sci.* **25**, 43 (2018)
2. A. Arbuzova, J. Wang, D. Murray, J. Jacob, D.S. Cafiso, S. Mc Laughlin, Kinetics of interaction of the Myristoylated alanine-rich C kinase substrate, membranes, and calmodulin. *J. Biol. Chem.* **272**, 27167–27177 (1997)
3. J. Wang, A. Gambhir, G. Mihalyne, D. Murray, U. Golebiewska, S. McLaughlin, Lateral sequestration of phosphatidylinositol4,5- bisphosphate by the basic effector domain of Myristoylated alanine-rich C kinase substrate is due to non specific electrostatic interactions. *J. Biol. Chem.* **277**, 34401–34412 (2002)
4. L. Rusu, A. Gambhir, S. McLaughlin, J. Rdlar, Fluorescence correlation spectroscopy studies of peptide and protein binding to phospholipid vesicles. *Biophys. J.* **87**, 1044–1053 (2004)
5. G.M. Verghese, J.D. Johnson, C. Vasulka, D.M. Haupt, D.J. Stumpo, P.J. Blackshear, protein kinase C-mediated phosphorylation and calmodulin binding of recombinant Myristoylated alanine-rich C kinase substrate (MARCKS) and MARCKS-related protein. *J. Biol. Chem.* **269**(12), 9361–9367 (1994)
6. P.J. Blackshear, G.M. Verghese, J.D. Johnson, D.M. Haupt, D.J. Stumpo, Characteristics of the F52 protein, a MARCKS homologue. *J. Biol. Chem.* **267**, 13540–13546 (1992)
7. M. Glaser, S. Wanaski, A. Buser, V. Boguslavsky, W. Rashidzada, A. Morris, M. Rebecchi, S.F. Scarlata, L.W. Runnels, G.D. Prestwich, J. Chen, A. Aderemi, J. Ahni, S. McLaughlin, Myristoylated alanine-rich C kinase substrate(MARCKS) produces reversible inhibition of phospholipase C by sequestering phosphatidylinositol4, 5-Bisphosphate in lateral domains. *J. Biol. Chem.* **271**, 26187–26193 (1996)
8. S. Alonso, M. Bär, Phase separation and bistability in a three-dimensional model for protein domain formation at biomembranes. *Phys. Biol.* **7**, 046012 (2010)
9. A. Mvogo, Germain Hubert Ben-Bolie, and Timoléon Crépin Kofané, Solitary waves of a-helix propagation in media with arbitrary inhomogeneities. *Eur. Phys. J. B* **86**, 217 (2013)
10. A. Mvogo, G.H. Ben-Bolie, T.C. Kofané, Solitary waves in an inhomogeneous chain of a-helical proteins. *Int. J. Modern Phys. B* **28**, 17 (2014)
11. A. Gizzi, A. Loppini, R. Ruiz-Baier, A. Ippolito, A. Camassa, A. La Camera, E. Emmi, L. Di Perna, V. Garofalo, C. Cherubini, S. Filippi, Nonlinear diffusion and thermo-electric coupling in a two-variable model of cardiac action potential. *Chaos* **27**, 093919 (2017)
12. K.M. Pagea, P.K. Mainib, N.A.M. Monk, Complex pattern formation in reaction-diffusion systems with spatially varying parameters. *Phys. D* **202**(1–2), 95–115 (2005)
13. T. Alarcon, H.M. Byrne, P.K. Maini, A cellular automaton model for tumour growth in inhomogeneous environment. *J. Theor. Biol.* **225**(2), 257–274 (2003)
14. P.K. Maini, D.L. Benson, J.A. Sherratt, Pattern formation in reaction-diffusion models with spatially inhomogeneous diffusion coefficients. *IMA J. Math. Appl. Med. Biol.* **9**, 197–213 (1992)
15. A.S. Etémé, C.B. Tabi, A. Mohamadou, T.C. Kofané, Long-range memory effects in a magnetized Hindmarsh-Rose neural network. *Commun. Nonlinear Sci. Numer. Simul.* **84**, 105208 (2020)
16. A.S. Etémé, C.B. Tabi, A. Mohamadou, T.C. Kofané, Unstable discrete modes in Hindmarsh-Rose neural networks under magnetic flow effect. *Chaos Solitons Fractals* **123**, 116123 (2019)
17. C.N. Takembo, H.P.E. Fouda, Effect of temperature fluctuation on the localized pattern of action potential in cardiac tissue. *Sci. Rep.* **10**, 15087 (2020)
18. A.S. Etémé, Consistency between modulational instability and energy localization in time-delay-memristive neural network. *Europhys. Lett.* **143**, 42002 (2023)
19. C.B. Tabi, I. Maïna, A. Mohamadou, H.P.F. Ekobena, T.C. Kofané, Fractional unstable patterns of energy in alpha-helix proteins with long-range interactions. *Chaos Solitons Fractal* **116**, 386391 (2018)
20. A.D. Koko, C.B. Tabi, H.P.F. Ekobena, A. Mohamadou, T.C. Kofané, Nonlinear charge transport in the helicoidal DNA molecule. *Chaos* **22**, 043110 (2012)
21. C.B. Tabi, S. Veni, E. Wamba, T.C. Kofané, Modulational instability and droplet formation in Bose-Bose mixtures with Lee-Huang-Yang correction and polaron-like impurity. *Phys. Lett. A* **485**, 129087 (2023)
22. C.B. Tabi, P. Otaadisa, T.C. Kofané, Modulational instability in two-dimensional dissipative open Bose-Einstein condensates with mixed helicoidal and Rashba-Dresselhaus spin-orbit couplings. *Phys. Lett. A* **481**, 129004 (2023)

23. J.J. Brudvig, J.M. Weimer, X MARCKS the spot: myristoylated alanine-rich C kinase substrate in neuronal function and disease. *Front. Cell. Neurosci.* **9**, 407 (2015)
24. J. Herrera, M.A. Maza, A.A. Minzoni, N.F. Smyth, A.L. Worthy, Davydov soliton evolution in temperature gradients driven by hyperbolic waves. *Phys. D* **191**, 156–177 (2004)
25. G.R.Y. Mefire, C.B. Tabi, A. Mohamadou, H.P.F. Ekobena, T.C. Kofané, Modulated pressure waves in large elastic tubes. *Chaos* **23**, 033128 (2013)
26. A.S. Etémé, C.B. Tabi, A. Mohamadou, Long-range patterns in Hindmarsh-Rose networks. *Commun. Nonlinear Sci. Numer. Simul.* **43**, 211–219 (2017)
27. C.B. Tabi, A.S. Etémé, A. Mohamadou, T.C. Kofané, Unstable discrete modes in Hindmarsh-Rose neural networks under magnetic flow effect. *Chaos Solitons Fractals* **123**, 116–123 (2019)
28. J. Leon, M. Manna, Multiscale analysis of discrete nonlinear evolution equations, *physique mathématique et théorique*. CNRS-UMR. **5825**, (1999)
29. N. Akhmediev, J.M. Soto-Crespo, A. Ankiewicz, Extreme waves that appear from nowhere: on the nature of rogue waves. *Phys. Lett. A* **373**, 2137–2145 (2009)
30. A.N. Zaikin, A.M. Zhabotinsky, Concentration wave propagation in two-dimensional liquid-phase self-oscillating system. *Nature* **225**, 535–537 (1970)
31. J.J. Tyson, P.C. Fife, Target patterns in a realistic model of the Belousov-Zhabotinskii reaction. *J. Chem. Phys.* **73**, 2224–2237 (1980)
32. S. Alonso, U. Dietrich, C. Händel, J.A. Käs, M. Bär, Oscillations in the lateral pressure of lipid monolayers induced by nonlinear chemical dynamics of the second messengers MARCKS and Protein Kinase C. *Biophys. J.* **100**, 939–947 (2011)
33. K. John, M. Bär, Travelling lipid domains in a dynamic model for protein induced pattern formation in biomembranes. *Phys. Biol.* **B2**, 23–32 (2005)
34. I. Sali, C.B. Tabi, H.P. Ekobena, T.C. Kofané, Modulational instability in a biexciton molecular chain with saturable nonlinearity effects. *Int. J. Modern Phys. B* **30**, 1550244 (2016)
35. J. Lippoldt, C. Händel, U. Dietrich, J.A. Käs, Dynamic membrane structure induces temporal pattern formation. *Biochim. Biophys. Acta* **1838**, 2380–2390 (2014)

Springer Nature or its licensor (e.g. a society or other partner) holds exclusive rights to this article under a publishing agreement with the author(s) or other rightsholder(s); author self-archiving of the accepted manuscript version of this article is solely governed by the terms of such publishing agreement and applicable law.



Multisolitons-like patterns in a one-dimensional MARCKS protein cyclic model

Chenceline Fouedji^a, Armand Sylvain Etémé^{a,*}, Conrad Bertrand Tabi^b,
Henri Paul Ekobena Fouda^a, Timoléon Crépin Kofané^c

^a Laboratory of Biophysics, Department of Physics, Faculty of Science, University of Yaounde I, P.O. Box 812, Yaounde, Cameroon

^b Botswana International University of Science and Technology, P/Bag 16 Palapye, Botswana

^c Laboratory of Mechanics, Department of Physics, Faculty of Science, University of Yaounde I, P.O. Box 812, Yaounde, Cameroon

ARTICLE INFO

Keywords:

MARCKS protein
Long wavelength instability
Patterns formation
Multisolitons

ABSTRACT

In this paper, we study the nonlinear dynamics of the MARCKS protein between cytosol and cytoplasmic membrane through the modulational instability phenomenon. The reaction–diffusion generic model used here is firstly transformed into a cubic complex Ginzburg–Landau equation. Then, modulational instability (MI) is carried out in order to derive the MI criteria. We find the domains of some parameter space where nonlinear patterns are expected in the model. The analytical results on the MI growth rate predict that phosphorylation and binding rates affect MARCKS dynamics in opposite way: while the phosphorylation rate tends to support highly localized structures of MARCKS, the binding rate in turn tends to slow down such features. On the other hand, self-diffusion process always amplifies the MI phenomenon. These predictions are confirmed by numerical simulations. As a result, the cyclic transport of MARCKS protein from membrane to cytosol may be done by means of multisolitons-like patterns.

1. Introduction

The myristoylated alanine-rich C kinase substrate (MARCKS) protein is the *in vivo* major substrate of protein kinase C (PKC) in the brain. It is a rod-shaped protein with a mass of 35 kDa (Ito et al., 2001), consisting of three functional domains (Blackshear, 1992; Kato et al., 1998) namely: the effector domain (ED) rich in positively charged lysine residues located in the center of the protein; the MARCKS 2 homology domain (MH2) (Kozma et al., 1997) and finally the N-terminal domain containing a myristoylation site. In its non-phosphorylated state, positively charged ED attaches to the negatively charged cytosolic side of the plasma membrane (Blackshear, 1992). As a result, the N-terminal myristoylation site reversibly inserts into the plasma membrane, serving as a lipid anchor to the protein (Meller and Gebhart, 1993; Muratani et al., 2002). Once ED is phosphorylated, it loses its affinity for the plasma membrane, displacing MARCKS into the cytoplasm (Blackshear, 1992). This translocation, called an “electrostatic switch” (Muratani et al., 2002), can also be achieved through increased levels of Ca²⁺, which allows calmodulin to bind to MARCKS ED (Nagumo et al., 2001).

MARCKS plays an important role in the living world: it is involved in the regulation of the homeostasis of body fluids, blood coagulation,

cell motility, vesicular traffic, secretion as well as mediation of the inflammatory response. Phosphorylated MARCKS has been reported to induce thrombin-induced release of serotonin in platelets (Elzagallaai et al., 2001), trafficking in synaptic vesicles and release of neurotransmitters from neuronal cells (Sasaki, 2003; Robinson, 1991), secretion of mucin in blood cells and human respiratory tract. In addition, phosphorylated MARCKS has a recognized role in the migration of inflammatory leukocytes such as neutrophils and macrophages (Damera et al., 2010; Takashi et al., 2006; Li et al., 2013; Sheats et al., 2015). Phosphorylated by PKC in macrophages, it regulates phagocytosis through the formation, maturation and translocation of actin-dependent phagosomes (Allen and Aderem, 1995). MARCKS is a charged and unfolded protein that appears in living cells at high concentrations of the order of 10 μM (McLaughlin, 1989).

The experimental study of the interactions between the MARCKS protein, phospholipids and PKC was carried out at three levels: *in vitro* experiments where MARCKS interacts with vesicles composed of neutral and acid phospholipids (Arbuzova et al., 1997; Wang et al., 2022; Rusu et al., 2004; Verghese et al., 1994; Blackshear et al., 1992; Glaser et al., 1996), *in vitro* experiments where MARCKS and PKC

* Corresponding author.

E-mail addresses: fhenceline@yahoo.fr (C. Fouedji), etemearmand@yahoo.fr (A.S. Etémé), tabic@biust.ac.bw (C.B. Tabi), hekobena@gmail.com (H.P.E. Fouda), tckofane@yahoo.com (T.C. Kofané).

<https://doi.org/10.1016/j.jtbi.2023.111702>

Received 30 July 2023; Received in revised form 16 November 2023; Accepted 8 December 2023

Available online 12 December 2023

0022-5193/© 2023 Published by Elsevier Ltd.

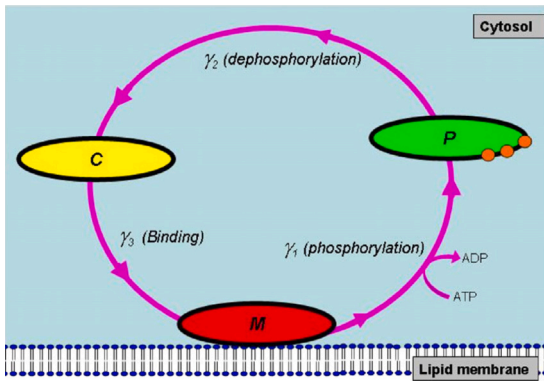


Fig. 1. Sketch of the myristoyl-electrostatic switch. The red objects represent membrane proteins (M), green objects phosphorylated proteins (P) and yellow objects free cytosolic proteins (C). Reaction rates are correspondingly noted (Alonso and Markus, 2010).

interact with a monolayer Langmuir formed from a mixture of acidic and neutral phospholipids (Rebecchi et al., 1992; Wang et al., 2021; Dietrich et al., 2009; Alonso et al., 2011), and in vivo experiments with living cells subjected to external disturbances (Ohmori et al., 2000; Mogami et al., 2003; Uchino et al., 2004; Sawano et al., 2022). In vitro experiments make it possible to monitor the distributions of phospholipids on vesicles and in Langmuir monolayers and the concentrations of proteins. They allow the characterization of the protein response to different concentrations of acid phospholipids and the performance of dynamic experiments by the introduction of activated PKC (Verghese et al., 1994; Alonso et al., 2011). A recent study for the interaction of MARCKS and PKC with a Langmuir monolayer (Alonso et al., 2011) shows oscillations based on the nonlinear nature of protein–phospholipid interactions. In vivo experiments are more realistic, however, additional components in the cell can alter the dynamics. Due to the sufficiently high concentration of this protein, the spatial distribution can be modeled by reaction–diffusion equations.

The model that we study here was proposed in Alonso and Markus (2010). It describes the spatio-temporal evolution of the concentration of the MARCKS protein at biomembrane involving: binding, phosphorylation and dephosphorylation of the MARCKS protein when the total number of proteins is conserved. Fig. 1 imported from Alonso and Markus (2010) shows an explanatory diagram for the cyclic translocation of MARCKS. The corresponding model reads

$$\frac{\partial m}{\partial t} = \gamma_3 c(1 - m) - \gamma_1(1 - m) \frac{m}{k_m + m} + D_m \frac{\partial^2 m}{\partial x^2}, \quad (1)$$

$$\frac{\partial c}{\partial t} = -\gamma_3 c(1 - m) + \gamma_2 p + D \frac{\partial^2 c}{\partial x^2}, \quad (2)$$

$$\frac{\partial p}{\partial t} = \gamma_1(1 - m) \frac{m}{k_m + m} - \gamma_2 p + D \frac{\partial^2 p}{\partial x^2}, \quad (3)$$

where the three dimensionless variables m , c and p represent the concentrations of MARCKS protein in the membrane, cytosol and phosphorylated site, respectively. The rates γ_1 , γ_2 and γ_3 refer to phosphorylation, dephosphorylation and binding, respectively. Parameters D_m and D account for membrane and cytosolic diffusion coefficients of MARCKS. The term $(1 - m)$ represents the coverage of the membrane by MARCKS proteins which locally prevents the activation of PKC at the membrane (Newton, 2001). The pioneers have shown by using numerical simulations that the model presents two qualitatively different mechanisms of protein domain formation namely: phase separation linked to long wavelength instability of a membrane state with homogeneous protein coverage and stable coexistence of two states with protein coverage different homogeneous in bistable media (Alonso and Markus, 2010).

However, given the complexity of this model to be analytically solved, no analytical study has been proposed up to date to compare the previous results. This paper contributes to unveil the implication of multisolitons in the process of the transport of MARCKS protein from the membrane to cytosol. Since the suggestion of the nonlinear solitons mechanism for the localization and transport of vibrational energy and charges in proteins by Newton (2001), their study in biomolecules has become very active. Modulational instability (MI) is considered, to some extent, to be a precursor of soliton formation (Davydov and Kislukha, 1973). Recently, the behavior of nonlinear systems has received considerable attention in areas such as biophysics, Bose–Einstein condensates, hydrodynamics, and magnetostatic waves in optics (Davydov, 1988; Brizhik, 1993; Brizhik and Eremko, 1999; Brizhik et al., 2001), just to cite a few. In general case, MI is the direct way through which localized patterns emerge in nonlinear and dispersive media. It has been widely shown in recent contributions that it gives more generalized solitonic structures and is the best mechanism by which energy can be localized and transported in biological molecules such as DNA and proteins (Eremko, 1992; Simo and Kofané, 1997). This constitutes another motivation for our study. Generally, in continuous media, multi-solitons appear as a solution of coupled nonlinear equations. It was shown by Kuramoto (1984) that all reaction–diffusion systems with a reaction dynamic close to the start of oscillations, can be reduced to an universal envelope equation, with a great predictive power, which is the cubic complex Ginzburg–Landau (CCGL) equation. This equation has therefore become an appropriate setup for the search and characterization of patterns in oscillatory media (Scott, 1992; Aranson and Kramer, 2002). For instance, the two-dimensional CCGL equations have been derived to study: high- and low-frequency dynamical regimes of nonlinear patterns in Hindmarsh–Rose neural networks (Tabi et al., 2017), the formation of Ca^{2+} -spiral waves in cell networks with bidirectional paracrine coupling (Tabi et al., 2021), flow-driven formation of unstable patterns of cyclic adenosine monophosphate (cAMP) in the Martiel–Goldbeter model (Zaoro et al., 2020) or frequency regimes in a two-dimensional RosenzweigMacArthur ecological network (Legoya et al., 2022). On the other hand, Etémé et al. (2017), Etémé (2023) found that the nonlinear dynamics of membrane potential in neural networks can be governed by a one-dimensional CCGL equations, thus proving the great significance of such equation in the understanding of some nonlinear and dispersive dynamic systems. Here, we will show that the dynamics of the MARCKS protein described by the Eqs. (1)–(3) can be governed by a one-dimensional CCGL equation.

The rest of the paper is structured as follows: in Section 2 we make use of the multiple scales method to show that the dynamics of the system can be fully described by the CCGL equation. In Section 3, linear stability analysis of the plane wave is performed and we discuss the possibility of common regions of instability between phosphorylation, dephosphorylation, binding rates and diffusion coefficient. Analytical and numerical solutions are computed in Section 4, where we discuss their different characteristics with respect to different oscillation regimes. Some concluding remarks are given in Section 5.

2. MARCKS dynamics and equation of envelope soliton

The reaction–diffusion system described by Eqs. (1)–(3) appears more complicated to find their analytical solutions. However, some technical approaches allow to simplify it into a partial derivative equations with well-known properties. Among these approaches, we will adopt the multiple scales approximation in the reductive perturbation method (RPM). Indeed, the MARCKS protein, like any other protein, is made up of a large number of elementary motifs which obviously significantly affect its overall dynamics. The underlying dynamics of an elementary pattern can be studied at small space-and time-scales, while the overall dynamics of the protein or any motifs cluster can be studied at large space-and time-scales. It is therefore appropriate to apply the multiple scales method in order to better understand the

dynamics behavior of proteins in general and of the MARCKS protein in particular. To further, the whole system is firstly linearized by reducing Eq. (1) and Eq. (3) in the same denominator. Then, we differentiate Eq. (2) over the time, following by the substitution of variables m and \dot{p} by their respective expressions into the obtained second-order ODE in c . This allows to definitively eliminate the variable p which is extracted from Eq. (2) as $p = \frac{1}{\gamma_2} [\frac{\partial c}{\partial t} + \gamma_3 c(1-m) - D \frac{\partial^2 c}{\partial x^2}]$. Therefore, we obtain the following reduced system

$$(k_m + m) \frac{\partial m}{\partial t} = -\mu_1 m + \mu_2 c + \mu_1 m^2 + \mu_3 mc + \mu_4 m^2 c + [d_0 + d_1 m] \frac{\partial^2 m}{\partial x^2},$$

$$(k_m + m) \frac{\partial^2 c}{\partial t^2} + \Omega_0^2 c + \lambda_1 c^2 + \lambda_2 m^2 + \lambda_3 mc + \lambda_4 m^2 c + \lambda_5 m c^2 + \lambda_6 m$$

$$+ [\sigma_0 + \sigma_1 m + \sigma_2 m^2] \frac{\partial c}{\partial t} \tag{4}$$

$$= [D_0 + D_1 m + D_2 m^2] \frac{\partial^2 c}{\partial x^2} + [D_3 c + D_4 mc] \frac{\partial^2 m}{\partial x^2} + [D_5 + D_6 m] \frac{\partial m}{\partial x} \frac{\partial c}{\partial x}$$

$$+ [D_7 + D_8 m] \frac{\partial^2 c}{\partial x^2} \left(\frac{\partial c}{\partial t} \right) + [D_9 + D_{10} m] \frac{\partial^4 c}{\partial x^4}, \tag{5}$$

where the auxiliary coefficients of Eqs. (4)–(5) are given in Appendix A. We can now apply the RPM which requires the introduction of a small parameter $\epsilon \ll 1$ while the medium is supposed to be weakly dissipative. As we are looking for the envelope soliton equation with a small damping term, parameters σ_0 , λ_6 and D_7 will be perturbed at order ϵ^2 , i.e., $\sigma_0 \leftarrow \epsilon^2 \sigma_0$, $\lambda_6 \leftarrow \epsilon^2 \lambda_6$, $D_7 \leftarrow \epsilon^2 D_7$. Solutions of above system can be found in the following form (Tabi et al., 2020)

$$m(x, t) = \sum_{n=1}^{\infty} \epsilon^n \sum_{l=-n}^n m_n^{(l)}(\xi, \tau) A^{(l)}(x, t),$$

$$c(x, t) = \sum_{n=1}^{\infty} \epsilon^n \sum_{l=-n}^n c_n^{(l)}(\xi, \tau) A^{(l)}(x, t), \tag{6}$$

where, of course, $A^{(l)}(x, t) = \exp il(kx - \omega t)$, $\xi = \epsilon(x - v_g t)$, $\tau = \epsilon^2 t$. The reality condition results in $m_n^{(-l)} = (m_n^{(l)})^*$ and $c_n^{(-l)} = (c_n^{(l)})^*$, with asterisk denoting the complex conjugate. The quantities ω , k and v_g represent the angular frequency, the wavenumber of the carrier wave $A^{(l)}$ and the group velocity of the envelope soliton, respectively.

Inserting solutions (6) into Eqs. (4)–(5) and solving the obtained system at different orders ($\epsilon^n, A^{(l)}$), we get the following solutions:

$$c_1^{(0)} = m_1^{(0)} = 0, \quad \omega^2 = \frac{\Omega_0^2 + D_0 k^2 - D_9 k^4}{k_m}, \quad c_1^{(1)} = \psi,$$

$$m_1^{(1)} = (\alpha_1 + i\alpha_2)\psi, \quad c_2^{(0)} = a_1 |\psi|^2, \quad m_2^{(0)} = a_2 |\psi|^2,$$

$$v_g = \frac{D_0 k - 2D_9 k^3}{k_m \omega}, \quad c_2^{(2)} = (b_1 + ib_2)\psi^2,$$

$$m_2^{(2)} = (b_3 + ib_4)\psi^2, \tag{7}$$

where the new auxiliary parameters α_1 , α_2 , a_1 , a_2 , b_1 , b_2 , b_3 and b_4 are given in Appendix B. In above Eq. (7), the nonlinear dispersion relation is given by $\omega^2 = \frac{\Omega_0^2 + D_0 k^2 - D_9 k^4}{k_m}$, while the group velocity that is known to verify the Fredholm solvability condition is expressed as $v_g = \frac{D_0 k - 2D_9 k^3}{k_m \omega}$. It is worth noticing that above dispersion relation and group velocity are found at the order ($\epsilon^1, A^{(1)}$) for the former and at the order ($\epsilon^2, A^{(1)}$) for the latter.

Finally, the order ($\epsilon^3, A^{(1)}$) leads to a nonlinear inhomogeneous system in $m_3^{(1)}$ and $c_3^{(1)}$. The determinant of the obtained system vanishes due to the dispersion relation. Consequently, such a system admits non-trivial solutions if the Fredholm solvability condition is fulfilled.

This leads to a nonlinear PDE in which the terms in $c_3^{(1)}$ and in $\frac{\partial c_2^{(1)}}{\partial \xi}$ cancel out due to the dispersion relation and the Fredholm solvability condition, respectively. Using now the previous results accompanied by intensive computations, we arrive at a nonlinear dispersive and dissipation partial derivative equation in $\psi \equiv c_1^{(1)}$ which reads

$$i \frac{\partial \psi}{\partial \tau} + P \frac{\partial^2 \psi}{\partial \xi^2} + (Q_r + iQ_i) |\psi|^2 \psi = i(R_r + iR_i) \psi, \tag{8}$$

where the k -dependent coefficients of Eq. (8) are given in Appendix C.

Eq. (8) describes the spatiotemporal evolution of envelope soliton $\psi(\xi, \tau)$ associated to the concentration of MARCKS protein in the cytosol. In this equation, the dispersion coefficient P is real, while the nonlinearity coefficient Q and the dissipative coefficient R are both complex with Q_r and R_r their real parts and Q_i and R_i their imaginary parts, respectively. Therefore, Eq. (8) is well-known as the 1D-CCGL equation. Similar equation was previously found in Etémé (2023), Achu et al. (2018) in the context of propagation and transmission of action membrane potential through neural networks. Here it will be useful to seek the domains of parameter space where transport of MARCKS protein from cytoplasmic membrane into cytosol is modulationally unstable, thus, involving soliton-like wave known as the best candidate in information transport within biological cells (Etémé, 2023; Tabi et al., 2020; Achu et al., 2018; Vladimir and Katharina, 2012; Tabi et al., 2008).

3. Domain formation of MARCKS protein through modulational instability

Modulational instability is the phenomenon of formation of localized patterns in excitable media due to the interplay between dispersion and nonlinearity. Here the coupling between the diffusion of the proteins and the myristoyl-electrostatic switch can be considered as the precursor of the MI phenomenon (Alonso and Markus, 2010). In practice, MI is based on the linear stability analysis of a periodic wave trains in a nonlinear dispersive systems. Indeed, the procedural analysis consists to injecting a slightly perturbed plane wave into the dynamical system like Eq. (8). As a result, if the perturbation grows exponentially, then the plane wave becomes unstable and breaks into a localized structures, if not it remains stable. The former case translates the onset of MI within the system.

MI is analyzed in the framework of the 1D-CCGL Eq. (8) by considering a first-order perturbation of harmonic waves whose stability/instability condition is sought. Plane wave solutions for (8) are considered in the general form: $\psi(\xi, \tau) = \psi_0 \exp i(\lambda \xi - \varpi \tau)$, where λ and ϖ are respectively, the wavenumber and the angular frequency of the plane wave. Parameter ψ_0 denotes the constant amplitude of the plane wave. Inserting above plane wave solution into Eq. (8) followed by the separation of the real and the imaginary parts, we get:

$$\varpi = P \lambda^2 - R_i - Q_r \psi_0^2, \tag{9}$$

$$Q_i \psi_0^2 - R_r = 0. \tag{10}$$

Eq. (9) defines the nonlinear dispersion relation of the plane wave of a real constant amplitude ψ_0 , an angular frequency ϖ and a wavenumber λ . However, Eq. (10) allows to find the plane wave amplitude as $\psi_0 = \sqrt{\frac{R_r}{Q_i}}$. This implies that the product $Q_i \times R_r$ must remain positive to obey to the existence condition of ψ_0 . The linear stability analysis of the plane wave solutions is carried out by considering small perturbations χ and θ in amplitude and in phase, respectively, i.e., $\psi(\xi, \tau) = (\psi_0 + \chi(\xi, \tau)) \exp i(\lambda \xi - \varpi \tau + \theta(\xi, \tau))$. Inserting the corresponding solution into Eq. (8) and separating again the real and imaginary parts, and retaining only linear terms around the unperturbed solution, we find the following coupled linear partial differential equations for $\chi(\xi, \tau)$ and $\theta(\xi, \tau)$

$$-\psi_0 \theta_\tau + P \chi_{\xi\xi} - 2P \lambda \psi_0 \theta_\xi + 2Q_r \psi_0^2 \chi = 0,$$

$$\chi_\tau + P \psi_0 \theta_{\xi\xi} + 2P \lambda \psi_\xi + 2R_r \chi = 0, \tag{11}$$

whose solutions are assumed to be $\chi(\xi, \tau) = \chi_0 \exp i(K \xi - \nu \tau) + c.c.$ and $\theta(\xi, \tau) = \theta_0 \exp(K \xi - \nu \tau) + c.c.$, with K and ν being, respectively, the perturbation wavenumber and the angular frequency of the perturbations while c.c. stands for the complex conjugate. Making use of these

solutions, one obtains an homogeneous system for χ_0 and θ_0 in the form

$$\begin{pmatrix} 2Q_r\psi_0^2 - PK^2 & i\psi_0(v - 2P\lambda K) \\ -2R_r + i(v - 2P\lambda K) & PK^2\psi_0 \end{pmatrix} \begin{pmatrix} \chi_0 \\ \theta_0 \end{pmatrix} = \begin{pmatrix} 0 \\ 0 \end{pmatrix} \quad (12)$$

Above 2×2 matrix admits non-trivial solutions if the following non-linear dispersion relation for the perturbations is verified.

$$\begin{aligned} &v^2 + 2(2P\lambda K - iQ_i\psi_0^2)v + P^2(4\lambda^2 K^2 - K^4) \\ &+ 2PQ_r K^2\psi_0^2 - 4iP\lambda K Q_i\psi_0^2 = 0. \end{aligned} \quad (13)$$

Solving Eq. (13), we get $v_{\pm} = 2P\lambda K + i(-R_r \pm \sqrt{-\Delta})$, with $\Delta = P^2 K^4 (1 - \frac{2Q_r\psi_0^2}{PK^2}) - R_r^2$. The plane wave will then be modulationally unstable if the discriminant $\Delta < 0$. From this, one deduces the MI growth rate as $\Gamma(K) = |Im(v(K))|$, which is explicitly given by

$$\Gamma(K) = \left[R_r + \sqrt{P^2 Q^4 \left(\frac{2Q_r\psi_0^2}{PK^2} - 1 \right) + R_r^2} \right]. \quad (14)$$

The domain of the perturbation wavenumber K for which the Γ -function exists as a function of K is given by $K < \psi_0 \sqrt{\frac{2Q_r}{P}}$, while MI growth rate becomes maximal for $K = \psi_0 \sqrt{\frac{Q_r}{P}}$. The corresponding maximal MI growth rate is given by

$$\Gamma_{max} = \left[R_r + |Q_r|\psi_0^2 \sqrt{1 + \frac{R_r^2}{Q_r^2\psi_0^4}} \right]. \quad (15)$$

To qualitatively characterize the MI onset through Eq. (8), the following instability criteria (Etémé, 2023)

$$P \times Q_r > 0; \quad Q_i \times R_r > 0, \quad (16)$$

must simultaneous be fulfilled according to the values of parameter space. Above conditions allow to find the appropriate values range of parameter space where a plane wave becomes unstable, thus leading to the formation of localized structures. In this framework, we attempt to find appropriate values range of nonlinearity parameters γ_1 and γ_3 , as well as of the cytosolic diffusion coefficient D , for which MARCKS-like patterns are expected in the cyclic model described in Eqs. (1)–(3). According to the previous reports (Alonso and Markus, 2010), the long wavelength instability is responsible for patterns formation of MARCKS protein. To be convinced, the instability criteria of Eq. (16) is numerically solved in two-dimensional parameter space as shown in Fig. 2. In the corresponding figure, the left column depicts the variations of the product $P \times Q_r$, while the right column displays the variations of the product $Q_i \times R_r$. Both products are plotted: in $k - \gamma_1$ plane on the top row, in $k - \gamma_3$ plane on the middle row and in $k - D$ plane on the bottom row. These panels allow to find the instability regions where relations of Eq. (16) are simultaneous fulfilled. Observably, the instability regions in $k - \gamma_1$ plane correspond to the interplay between the purple regions of panel (a₁) and the red regions of panel (b₁). In $k - \gamma_3$ plane, the instability regions are the interplay of yellow regions of panel (a₂) and blue regions of panel (b₂). Finally, in $k - D$ plane, the instability regions are the interplay of red regions of panel (a₃) and orange regions of panel (b₃). In each panel, the invariant parameters are fixed as: $k_m = 0.1$, $D_m = 0.5 \mu\text{m}^2\text{s}^{-1}$, $D = 10.0 \mu\text{m}^2\text{s}^{-1}$, $\gamma_1 = 10.0 \text{ s}^{-1}$, $\gamma_2 = 1.0 \text{ s}^{-1}$ and $\gamma_3 = 25.0 \text{ s}^{-1}$. It is found that apart from the long wavelength instability predicted in Alonso and Markus (2010), dynamics of MARCKS protein can also experience mean wavelength instability. For instance, in the case of long wavelength instability, i.e., $k = 0.05\pi$, MI occurs when $3.5 \leq \gamma_1 \leq 50.0$ by fixing γ_3 and D or when $15.0 \leq \gamma_3 \leq 100.0$ by fixing γ_1 and D or when $0.0 \leq D \leq 50.0$ by fixing γ_1 and γ_3 . However, in the case of mean wavelength instability, i.e., $k = 0.25\pi$, MI occurs in the following cases: $2.5 \leq \gamma_1 \leq 50.0$ by fixing γ_3 and D or when $15.0 \leq \gamma_3 \leq 100.0$ by fixing γ_1 and D or when $4.5 \leq D \leq 50.0$ by fixing γ_1 and γ_3 . To reinforce these predictions we need to quantitatively characterize the

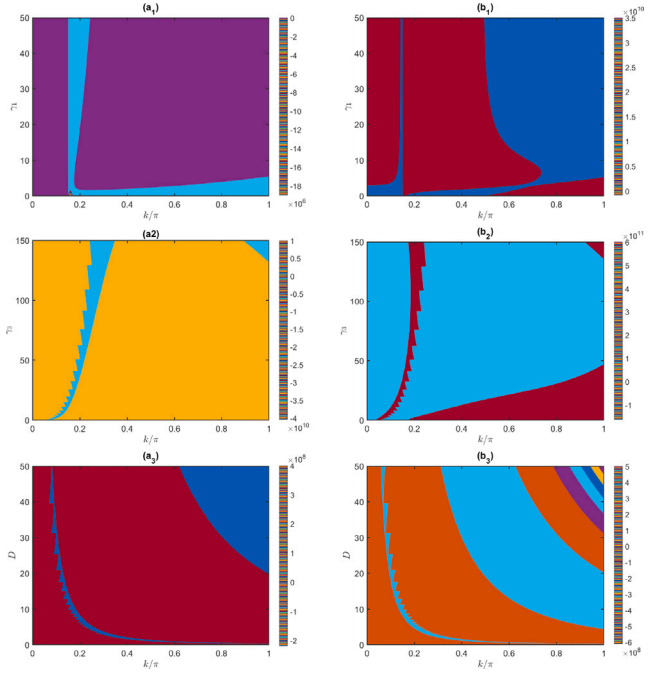


Fig. 2. Qualitative characterization of MI through 3D view of stability/instability regions according to the criteria given in Eq. (16). The products $P \times Q_r$ on the left columns and $Q_i \times R_r$ on the right columns are plotted in: $k - \gamma_1$ plane in the first row while taking $\gamma_3 = 25 \text{ s}^{-1}$ and $D = 10 \mu\text{m}^2\text{s}^{-1}$; $k - \gamma_3$ plane in the second row while taking $\gamma_1 = 10 \text{ s}^{-1}$ and $D = 10.0 \mu\text{m}^2\text{s}^{-1}$; $k - D$ plane in the third row while taking $\gamma_1 = 10 \text{ s}^{-1}$ and $\gamma_3 = 25 \text{ s}^{-1}$. The other parameters are $k_m = 0.1$, $D_m = 0.5 \mu\text{m}^2\text{s}^{-1}$, $\gamma_2 = 1.0 \text{ s}^{-1}$. Instability regions appear when both products are simultaneous positive.

real manifestation of MI through the maximal MI growth rate given in Eq. (15). In reminder, MI growth rate is a state function Γ which accounts for the quantitative manifestation of MI in a given excitable system. Indeed, when $\Gamma = 0$, system does not yields MI and therefore supports only propagation of periodic wave trains. In contrast, when $\Gamma \neq 0$, system becomes sensitive to MI phenomenon and thenceforth can admit nonlinear localized excitations-like solutions. Additionally, the greater the magnitude of MI growth rate, the greater the magnitude of localized excitation, and vice-versa. Likewise, the spatial expansion (reduction) of MI growth rate is generally associated to the spacial spread (localization) of the excitation.

Results of Fig. 3 show the variations of the maximal MI growth rate Γ_{max} versus γ_1 in panels (a_j)_{j=1,2}, versus γ_3 in panels (b_j)_{j=1,2} and versus D in panels (c_j)_{j=1,2} (see figure caption for explicit readability). It is observed that the Γ_{max} -function is an increased/decreased function of γ_1 . This suggests that when the mechanism of phosphorylation of MARCKS protein is accentuated, MARCKS protein concentration goes down-and-up (and vice-versa) from membrane-bound to cytosol. On the other hand, the Γ_{max} -function exponentially decreases when γ_3 increases in the case of the long wavelength instability. However, in the case of mean wavelength instability, the Γ_{max} -function decreases first, then increases with γ_3 . This predicts that, in the case of long wavelength instability, the binding process of MARCKS protein could induce the decreasing in MARCKS concentration. But in the case of mean wavelength instability, the binding process favors first the diminution of MARCKS concentration, then the increasing of the latter thereby leading the maximum molecules towards the membrane and preserving their conservation. Now regarding Fig. 3(c_j)_{j=1,2}, the maximal MI growth rate still increases with the diffusion coefficient D regardless of the type of instability. Consequently, the diffusion process of MARCKS protein from the cytosol to the membrane can enhance MI phenomenon which could yield the saturation phenomenon of MARCKS protein at the membrane. All these results support the fact that the cyclic transport of

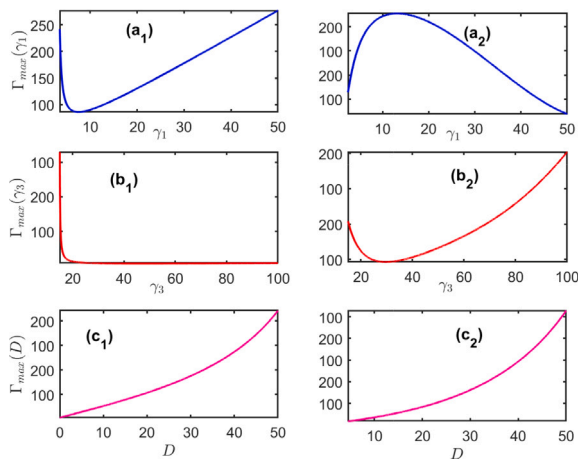


Fig. 3. Quantitative characterization of MI through features of the maximal MI growth rate Γ_{max} . In panels (a_j), Γ_{max} is plotted versus γ_1 while fixing $\gamma_3 = 25.0 \text{ s}^{-1}$ and $D = 10.0 \mu\text{m}^2\text{s}^{-1}$. In panels (b_j), Γ_{max} is plotted versus γ_3 while fixing $\gamma_1 = 10.0 \text{ s}^{-1}$ and $D = 10.0 \mu\text{m}^2\text{s}^{-1}$. In panels (c_j), Γ_{max} is plotted versus D while fixing $\gamma_1 = 10.0 \text{ s}^{-1}$ and $\gamma_3 = 25.0 \text{ s}^{-1}$. The left panels correspond to the long wavelength instability ($k = 0.05\pi$), while the right panels correspond to the mean wavelength instability ($k = 0.25\pi$). The other parameters are: $k_m = 0.1$, $D_m = 0.5 \mu\text{m}^2\text{s}^{-1}$, $\gamma_2 = 1.0 \text{ s}^{-1}$.

MARCKS protein from membrane to cytosol may be done by means of nonlinear localized excitations for a suited values of parameter space. Unfortunately, these analytical results based only on the linear stability analysis of the plane wave do not highlight nor the nature or the longtime spatiotemporal evolution of such localized excitations. It is therefore important to give a particular attention on this by looking for the class of nonlinear excitation along with their spatiotemporal properties.

4. Multisolitons-like Marcks patterns based on analytical predictions

4.1. Analytical solutions

The aim of this subsection is to find exact soliton-like spatiotemporal solutions of MARCKS protein model described in Eqs. (1)–(3). These solutions are closely related to the envelope soliton solution of Eq. (8) whose exact solutions are well-established in Yomba et al. (1996) and given by

$$\psi(\xi, \tau) = \frac{g \exp(\Theta)}{[1 + \exp(\Theta + \Theta^*)]^{1+i\alpha}}, \quad (17)$$

where after some computations,

$$g = \sqrt{\frac{6R_r}{Q_i}}, \quad \beta = \frac{3Q_r}{2Q_i}, \quad \alpha = -\beta \pm (2 + \beta^2)^{1/2},$$

$$\Theta = \kappa\xi - \varpi\tau, \quad \kappa = \kappa_r + i\kappa_i, \quad \tau = e^2 t$$

$$\kappa_r = \sqrt{\frac{3R_r Q_r}{2PQ_i(2 - \alpha^2)}}, \quad \kappa_i = \alpha\kappa_r, \quad \varpi = \varpi_r + i\varpi_i,$$

$$\varpi_r = 0, \quad \varpi_i = \frac{3Q_r R_r (\alpha^2 - 1)}{2Q_i(2 - \alpha^2)} - R_i, \quad \xi = \epsilon(x - v_g t). \quad (18)$$

Therefore, based on all above relations, in particular, Eqs. (6), (17) and (18), solutions of Eqs. (1)–(3) are given by

$$m(x, t) = 2\epsilon [(\alpha_1 \psi_r - \alpha_2 \psi_i) \cos \theta - (\alpha_2 \psi_r + \alpha_1 \psi_i) \sin \theta] + O(\epsilon^2),$$

$$c(x, t) = 2\epsilon (\psi_r \cos \theta - \psi_i \sin \theta) + O(\epsilon^2),$$

$$p(x, t) = \frac{2\epsilon}{\gamma_2} [\omega (\psi_r \sin \theta + \psi_i \cos \theta)$$

$$+ (\gamma_3 + Dk^2) (\psi_r \cos \theta - \psi_i \sin \theta)] + O(\epsilon^2), \quad (19)$$

where ψ_r and ψ_i denote real and imaginary parts of ψ , $\theta = kx - \omega t$, k and ω being the wavenumber and angular frequency of the carrier wave. It is relevant to mention that above solutions (19) are consistent with those found by Etémé (2023) while studying the close relationship between MI and energy localization in time-delay-memristive Hindmarsh–Rose neural networks. Analytical solutions described in Eq. (19) are displayed in Fig. 4. On the top panels, the concentrations of MARCKS protein in membrane bound [see panel (a₁)], in phosphorylated site [see panel (b₁)] and in cytosol [see panel (c₁)] are surfed in $x - t$ parameter space. These solutions have the profiles of localized structures which are propagated over the time at specific domains. This suggests that the processes of transport and transfer of MARCKS protein in the cyclic model maybe done by means of multisolitons-like patterns. The features on the bottom in Fig. 4 show the evolution of MARCKS concentration along the x -direction at different times. These 2D-views show the propagation of a trisolitons-like wave which is involved in MARCKS dynamics. In order to confirm that the generic model can support above structures, it is convenient to point out the numerical simulations.

4.2. Numerical experiments

The stability analysis done in Section 3 allowed to find appropriate parameter space that can sustainably stimulate modulated waves-like patterns in MARCKS protein system, since such waves are believed to be involved in energy transfer process along most biological systems. Therefore, the numerical simulations will be carried out by applying the fourth-order Runge–Kutta computation scheme using analytical solutions given in Eq. (19) as initial conditions. We chosen $0 \leq x(\mu\text{m}) \leq 150$ as the spatial coordinate, $0 \leq t(\text{ms}) \leq 10$ as the integration duration, $\Delta x = 0.25 \mu\text{m}$ as the space step and $\Delta t = 10 \mu\text{s}$ as the time step. The constant parameters remain unchangeable as above, while the control parameters γ_1 , γ_3 and D are selected in instability regions, accordingly. It is worth noticing that, here we only present the results on the long wavelength instability case by fixing $k = 0.05\pi \mu\text{m}^{-1}$.

The features of Fig. 5 obtained from numerical simulations show the spatiotemporal dynamics on top panels and spatial dynamics on bottom panels, of MARCKS protein. As shown, the localized patterns are similar to those obtained analytically, thus suggesting that the generic model of Eqs. (1)–(3) may effectively support the propagation of multisolitons-like patterns known as the best tool in transport and transfer of MARCKS protein from cytoplasmic membrane to cytosol. Interestingly, we notice that the wave amplitude increases over the time at the membrane level and decreases at the cytosol level. This suggests that the reorganization of the membrane after the binding of protein is not an instantaneous phenomenon. We also notice that the wave propagates in space with an almost constant width. This constitutes the main properties of soliton-like wave. In Fig. 6 the spatial multisolitons-like patterns of MARCKS protein are displayed under the variation of, the phosphorylation rate on top row, the binding rate on middle row and diffusion coefficient on bottom row at time $t = 5 \text{ ms}$. We can see that under the increasing of γ_1 , the concentrations of MARCKS protein decreases in the cytoplasmic membrane and increases in the cytosol. However, under the increasing of γ_3 , the MARCKS concentration slowly decreases both in the membrane and in the cytosol. On the other hand, the increase in diffusion coefficient induces increasing in MARCKS protein concentration at in each site. Interestingly, these numerical findings are in perfect correlation with the analytical predictions and suggest that the phenomena of cyclic transport and transfer of MARKS protein from membrane to cytosol are highly influenced by phosphorylation and binding rates on the one hand and by the diffusion coefficient on the other hand.

In Fig. 7, the time series of the MARCKS protein for $x = 75 \mu\text{m}$ are plotted. Panels (a),(b),(c) represent, respectively the concentration of

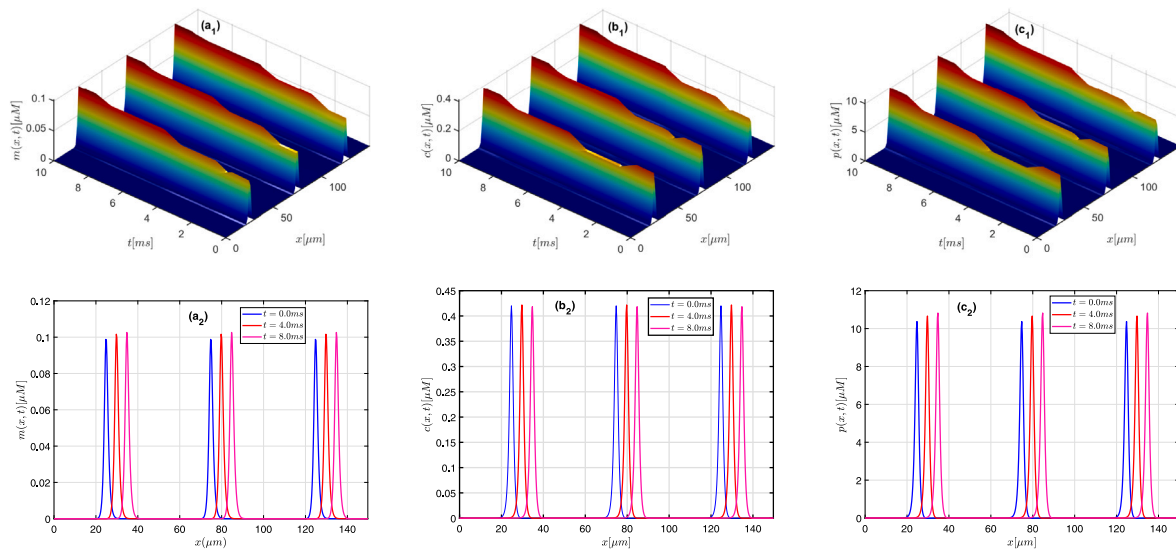


Fig. 4. The spatiotemporal dynamics of MARCKS protein obtained from analytical solutions of Eq. (19). Parameters are chosen as $k_m = 0.1$, $D_m = 0.5 \mu\text{m}^2\text{s}^{-1}$, $D = 10.0 \mu\text{m}^2\text{s}^{-1}$, $\gamma_1 = 10.0 \text{ s}^{-1}$, $\gamma_2 = 1.0 \text{ s}^{-1}$, $\gamma_3 = 25.0 \text{ s}^{-1}$ and $k = 0.05\pi \mu\text{m}^{-1}$.

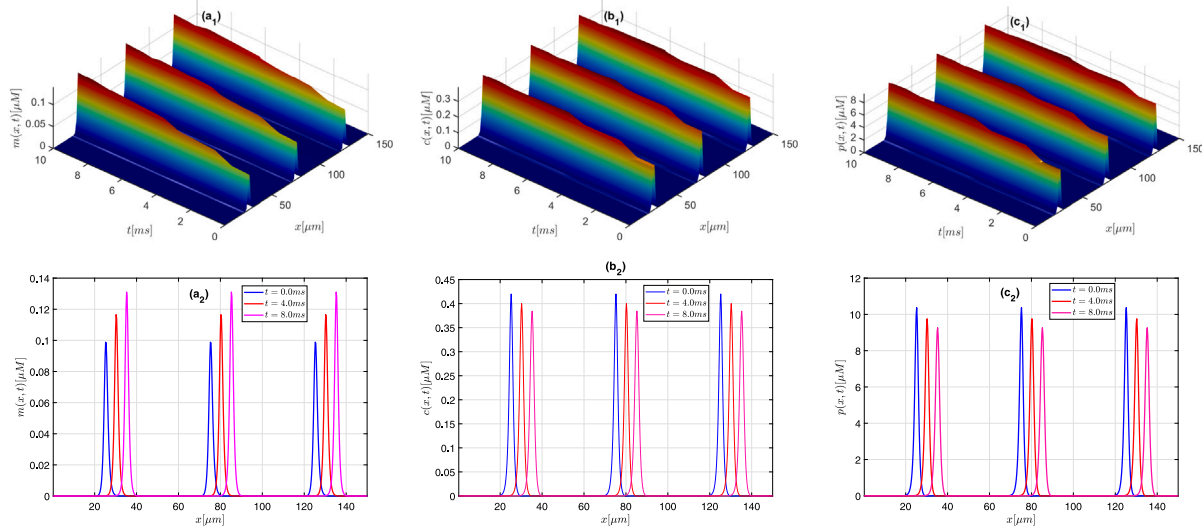


Fig. 5. The spatiotemporal dynamics of MARCKS protein obtained from numerical simulations of Eqs. (1)–(3) using solutions of Eq. (19) as initial conditions. Parameters are chosen as $k_m = 0.1$, $D_m = 0.5 \mu\text{m}^2\text{s}^{-1}$, $D = 10.0 \mu\text{m}^2\text{s}^{-1}$, $\gamma_1 = 10.0 \text{ s}^{-1}$, $\gamma_2 = 1.0 \text{ s}^{-1}$, $\gamma_3 = 25.0 \text{ s}^{-1}$ and $k = 0.05\pi \mu\text{m}^{-1}$.

the MARCKS protein at the membrane, phosphorylated and dephosphorylated cytosol. We observe a very fast decrease of the amplitude at the membrane level and a low decrease in the cytosol while the width of the wave being almost constant in the three cases. This informs us that MARCKS protein at the membrane level is the activating and inhibiting substance in the cytosol.

4.3. Discussion

We used a reaction–diffusion model describing the dynamics of MARCKS proteins concentration between cytosol and membrane-bound proposed by Alonso and Markus (2010). They studied the spatiotemporal dynamics of MARCKS proteins and their interactions with enzymes. However, they did not propose either a full analytical investigations or the analytical solution of the system. In the present work we propose a complete analytical and numerical solution of the system. To reduce the generic model into a CCGL equation, we have applied the multiple scales method, since the global dynamics of MARCKS protein viewed at the macroscopic scale is highly influenced by the underlying

dynamics of its components which is yielded at different space–time-scales. The medium is supposed to be weakly dissipative (Etémé, 2023; Achu et al., 2018) which allowed to obtain the CCGL equation whose solutions forms were constructed. The CCGL equation is often used as a description of a system close to a bifurcation point and it is well known that the CCGL equation can produce space–time chaos in the form of defects (Aranson and Kramer, 2002; Cross and Hohenberg, 1993). The CCGL equation is a universal model for predicting pattern formation in reaction–diffusion models (Cross and Hohenberg, 1993). The coefficients of this equation allowed us to qualitatively characterize the MI in order to determine the stability and instability zones of the MARCKS protein as a function of the phosphorylation rate, the parameters that significantly affect the stability zone are the binding rate and the diffusion coefficient in the cytosol. In order to predict the existence of the localized structures in the model, the maximal growth rate of MI is represented. Hirota’s method (Yomba et al., 1996) led to the multisolitons-like patterns in our system for a suitable modulational instability parameters. This type of wave corresponds to spatially broadened impulses and they are ubiquitous in excitable

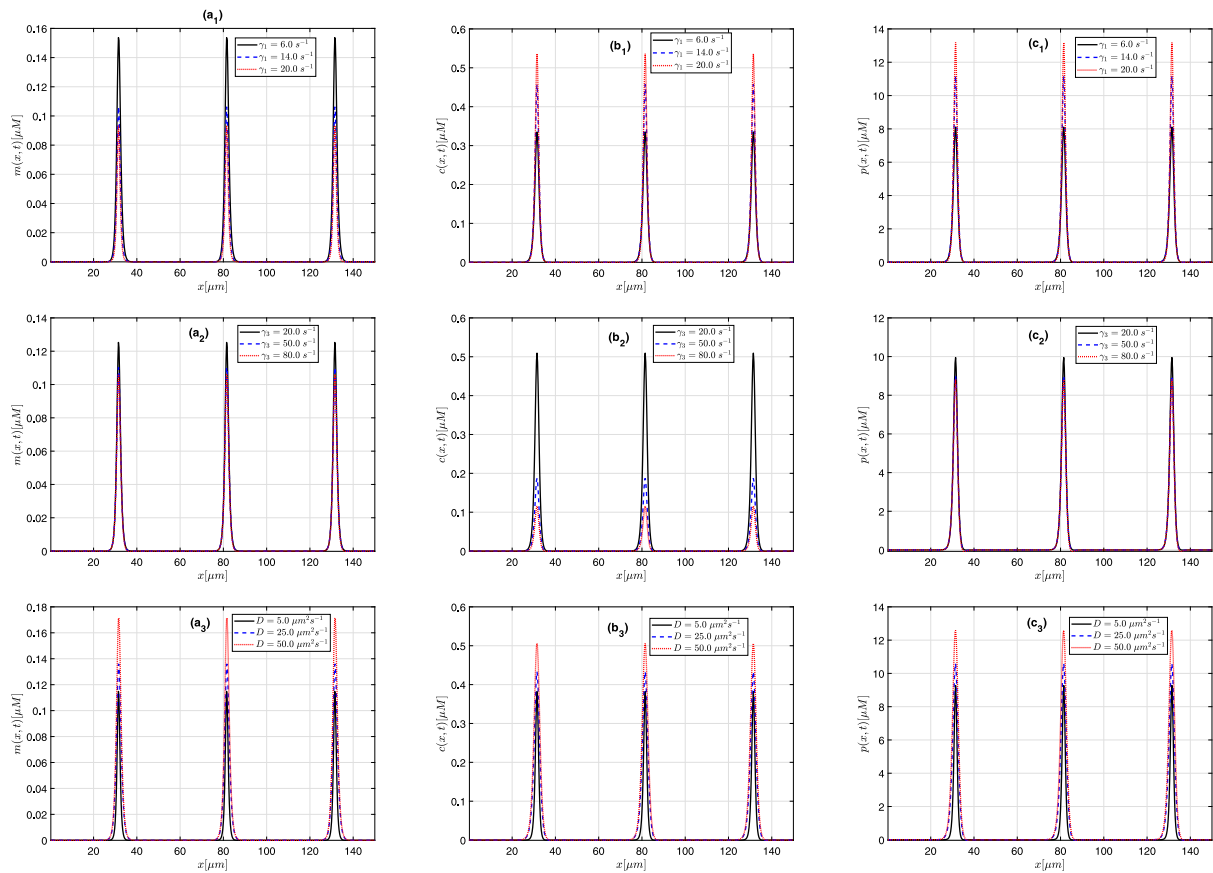


Fig. 6. The spatial multisolitons-like patterns of MARCKS protein obtained from numerical simulations of Eqs. (1)–(3) using solutions of Eq. (19) as initial conditions. Top row corresponds to the increasing of phosphorylation rate γ_1 for $k_m = 0.1$, $D_m = 0.5 \mu\text{m}^2\text{s}^{-1}$, $D = 10.0 \mu\text{m}^2\text{s}^{-1}$, $\gamma_2 = 1.0 \text{ s}^{-1}$ and $\gamma_3 = 25.0 \text{ s}^{-1}$. Middle row corresponds to the increasing of binding rate γ_3 while $k_m = 0.1$, $D_m = 0.5 \mu\text{m}^2\text{s}^{-1}$, $D = 10.0 \mu\text{m}^2\text{s}^{-1}$, $\gamma_1 = 10.0 \text{ s}^{-1}$ and $\gamma_2 = 1.0 \text{ s}^{-1}$. Finally, bottom row corresponds to the increasing of the cytosolic diffusion coefficient D while $k_m = 0.1$, $D_m = 0.5 \mu\text{m}^2 \text{ s}^{-1}$, $\gamma_1 = 10.0 \text{ s}^{-1}$, $\gamma_2 = 10 \text{ s}^{-1}$ and $\gamma_3 = 25.0 \text{ s}^{-1}$. All these features are depicted at $t = 5 \text{ ms}$ in the long wavelength instability case, i.e., $k = 0.05\pi \mu\text{m}^{-1}$.

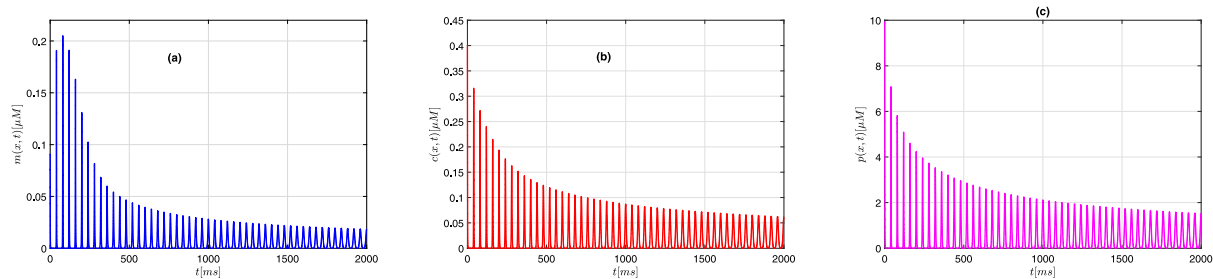


Fig. 7. Time series for MARCKS protein at the position $x = 75 \mu\text{m}$. Panels (a), (b) and (c) correspond, respectively to the concentration of MARCKS in membrane bound, in cytosol and in phosphorylated site. Space parameters are given by $k_m = 0.1$, $D_m = 0.5 \mu\text{m}^2\text{s}^{-1}$, $\gamma_1 = 10.0 \text{ s}^{-1}$, $\gamma_2 = 1.0 \text{ s}^{-1}$, $\gamma_3 = 25.0 \text{ s}^{-1}$, $D = 10.0 \mu\text{m}^2\text{s}^{-1}$.

media such as neurons and cell membranes (Takembo C.N et al., 2022; Takembo, 2022). In the heart, for example, they are responsible for triggering harmonic contractions, the failure of which can lead to significant physiological perturbations (Takembo and Ekobena Fouda, 2020; Mvogo et al., 2017). Additionally, the multisolitons-like solutions have already been obtained by Issa et al. (2016) in a biexciton molecular chain with saturable nonlinearity effects. Theoretically, the rate of phosphorylation leads to an increase in the nonlinearity of the system. The above simulations demonstrate that three-species reaction–diffusion systems with spatially constant parameters can give rise to complex steady-state patterns and traveling peak waves. Such patterns were obtained in Karen et al. (2005) through the study of embryonic development in a spatially heterogeneous background.

5. Conclusion

The main objective of this work was the analytical and numerical study of modulational instability in a three-dimensional model for protein domain formation at biomembranes (Alonso and Markus, 2010). By means of the reductive perturbation technique, we firstly reduced the generic model into a cubic complex Ginzburg–Landau equation. The existence of nonlinear patterns within the model was highlighted through the linear stability analysis of the plane wave injected into the CCGL equation. The domains of parameter space, where these nonlinear patterns are suspected were found, both in the long wavelength instability and in the mean wavelength instability. Thereafter, an exact analytical solutions of MARCKS patterns were derived by inspiring on the solutions proposed by Yomba and its collaborators (Yomba et al., 1996). These analytical solutions were using as initial

conditions to compute the numerical solutions of the generic model. It was found that the transport of MARCKS from cytoplasmic membrane to cytosol could be achieved by a tri-soliton wave whose properties are considerable modified either by the phosphorylation and binding rates on the one hand and the diffusion coefficient on the other hand. Our numerical results are found to be in perfect agreement with the analytical predictions. This work gives more insight on the formation of domain patterns of MARCKS protein at the biomembrane. It will be important to investigate by means of the modulational instability phenomenon, the formation of spiral-like waves patterns by extended the one-dimensional model studied here into a two-dimensional model.

CRedit authorship contribution statement

Chenceline Fouedji: Data curation, Investigation, Methodology, Writing – original draft, Writing – review & editing. **Armand Sylvain Etémé:** Conceptualization, Data curation, Formal analysis, Investigation, Methodology, Resources, Software, Validation, Writing – original draft, Writing – review & editing. **Conrad Bertrand Tabi:** Supervision, Validation, Visualization. **Henri Paul Ekobena Fouda:** Conceptualization, Supervision, Validation, Visualization. **Timoléon Crépin Kofané:** Supervision, Validation.

Declaration of competing interest

The authors declare that they have no known competing financial interests or personal relationships that could have appeared to influence the work reported in this paper.

Appendix A. Coefficients of Eqs. (4)–(5)

$$\begin{aligned} \mu_1 &= \gamma_1, \mu_2 = \gamma_3 k_m, \mu_3 = \gamma_3(1 - k_m), \mu_4 = -\gamma_3, \\ d_0 &= D_m k_m, d_1 = D_m, \Omega_0^2 = \gamma_2 \gamma_3 k_m, \lambda_1 = -\gamma_3^2 k_m, \\ \lambda_2 &= \gamma_1 \gamma_2, \lambda_3 = \gamma_1 \gamma_3 + \gamma_2 \gamma_3 - \gamma_2 \gamma_3 k_m, \\ \lambda_4 &= -(\gamma_1 \gamma_3 + \gamma_2 \gamma_3), \lambda_5 = -\gamma_3^2(1 - k_m), \lambda_6 = -\gamma_1 \gamma_2, \\ \sigma_0 &= \gamma_2 k_m + \gamma_3 k_m, \sigma_1 = \gamma_2 + \gamma_3(1 - k_m), \sigma_2 = -\gamma_3, \\ D_0 &= D\gamma_2 + k_m + D\gamma_3 k_m, D_1 = D\gamma_2 - D\gamma_3 k_m + D\gamma_3 \\ D_2 &= -D\gamma_3, D_3 = D_m \gamma_3 k_m - D\gamma_3 k_m, D_4 = D_m \gamma_3 - D\gamma_3, \\ D_5 &= -2D\gamma_3 k_m, D_6 = -2D\gamma_3, D_7 = 2D + k_m D, \\ D_8 &= D, D_9 = -D^2 k_m, D_{10} = -D^2. \end{aligned} \quad (20)$$

Appendix B. Coefficients of Eq. (7)

$$\begin{aligned} \alpha_1 &= \frac{\mu_2(d_0 k^2 + \mu_1)}{(d_0 k^2 + \mu_1)^2 + (\omega k_m)^2}, \alpha_2 = \frac{\omega \mu_2 k_m}{(d_0 k^2 - \mu_1)^2 + (\omega^2 k_m)^2}, \\ a_1 &= \frac{2}{\Omega_0^2} (\alpha_1(\omega^2 + D_1 k^2 - D_3 k^2 - \lambda_3 + D_5 k^2 + D_{10} k^4) \\ &\quad - \lambda_1 - \lambda_2(\alpha_1^2 + \alpha_2^2) - \alpha_2 \sigma_1 \omega - D_8 k^2 \alpha_2 \omega), \\ a_2 &= \frac{1}{\mu_1} (\mu_2 a_1 - 2d_1 k^2(\alpha_1^2 + \alpha_2^2) + 2\mu_1(\alpha_1^2 + \alpha_2^2) + 2\mu_3 \alpha_1) \\ b_1 &= \frac{1}{\Omega_0^2 + 4D_0 k^2 - 16D_9 k^4 - 4k_m \omega^2} (\alpha_1(\omega^2 - \lambda_3 + D_1 k^2 - D_3 k^2 \\ &\quad - D_5 k^2 + D_{10} k^4) + \lambda_1 + \lambda_2(\alpha_1^2 - \alpha_2^2) + \omega \alpha_2(-\sigma_1 + D_8 k^2)) \\ b_2 &= \frac{1}{\Omega_0^2 + 4D_0 k^2 - 16D_9 k^4 - 4k_m \omega^2} (\alpha_2(\omega^2 - \lambda_3 + k^2 D_1 - D_3 k^2 \\ &\quad + k^4 D_{10}) + 2\lambda_2 \alpha_1 \alpha_2 + \alpha_1 \omega(\sigma_1 - D_8 k^2)), \\ b_3 &= \frac{1}{(\mu_1 + 4k^2 d_0)^2 + (2\omega k_m)^2} + \lambda_1 + (\mu_1 + 4k^2 d_0)(-2\omega \alpha_1 \alpha_2 \\ &\quad + \mu_2 b_1 + \mu_1(\alpha_1^2 - \alpha_2^2) + \mu_3 \alpha_1 - d_1 k^2(\alpha_1^2 - \alpha_2^2)) - 2\omega \times \\ &\quad k_m(\omega(\alpha_1^2 - \alpha_2^2) + \mu_2 b_2 + 2\alpha_1 \alpha_2 \mu_1 + \mu_3 \alpha_2 - 2d_1 k^2 \alpha_1 \alpha_2) \end{aligned}$$

$$\begin{aligned} b_4 &= \frac{1}{(\mu_1 + 4k^2 d_0)^2 + (2\omega k_m)^2} ((\mu_1 + 4k^2 d_0)(\omega(\alpha_1^2 - \alpha_2^2) \\ &\quad + \mu_2 b_2 + 2\alpha_1 \alpha_2 \mu_1 + \mu_3 \alpha_2 - 2d_1 k^2 \alpha_1 \alpha_2) + 2\omega k_m \times \\ &\quad (-2\omega \alpha_1 \alpha_2 + \mu_2 b_1 + \mu_1(\alpha_1^2 - \alpha_2^2) + \mu_3 \alpha_1 \\ &\quad - d_1 k^2(\alpha_1^2 - \alpha_2^2))). \end{aligned} \quad (21)$$

Appendix C. Coefficients of Eq. (8)

$$\begin{aligned} P &= \frac{D_0 - 6D_9 k^4 - k_m v_g^2}{2\omega k_m}, R_i = \frac{-\lambda_6 \alpha_1}{2\omega k_m}, \\ R_r &= \frac{1}{2\omega k_m} (\lambda_6 \alpha_2 - \omega \sigma_0 - D_7 k^2 \omega), \\ Q_r &= \frac{1}{2\omega k_m} \left(\omega^2(a_2 + b_3 + 4b_1 \alpha_1 + 4b_2 \alpha_2 + a_1 \alpha_1) \right. \\ &\quad - 2\lambda_1(a_1 + b_1) - \lambda_2(\alpha_1 \alpha_2 + \alpha_1 b_3 + \alpha_2 + b_4) \\ &\quad - \lambda_3(\alpha_1 a_1 + \alpha_1 b_1 + \alpha_2 b_2 + \alpha_1 b_3 + \alpha_2 b_4 + a_2) \\ &\quad - \lambda_4(3\alpha_1^2 + \alpha_2^2) - 3\lambda_5 \alpha_1 + \sigma_1 \omega(-2b_2 \alpha_1 + \\ &\quad 2b_1 \alpha_2 + b_4) + 2\sigma_2 \omega \alpha_1 \alpha_2 \\ &\quad - D_1 k^2(4(\alpha_1 b_1 + \alpha_2 b_2) + b_3 + a_2) - D_2 k^2(3\alpha_1^2 + \alpha_2^2) + \\ &\quad D_3 k^2(4b_3 - \alpha_1 b_1 - \alpha_2 b_2 - a_1 \alpha_1) + 2D_4 \alpha_1 k^2 \\ &\quad + D_5 k^2(b_1 \alpha_1 + b_2 \alpha_2 + b_3) + D_6 k^2(3\alpha_1^2 + \alpha_2^2) \\ &\quad \left. - D_8 k^2 \omega(-8\alpha_1 b_2 + 8\alpha_2 b_1 + \alpha_2) + D_{10} k^4(16(b_1 \alpha_1 \right. \\ &\quad \left. + b_2 \alpha_2) + \alpha_1 + a_2) \right), \\ Q_i &= \frac{1}{2\omega k_m} \left(\omega^2(b_4 + 4\alpha_1 b_2 - 4\alpha_2 b_1 \right. \\ &\quad + \alpha_2 a_1) - 2\lambda_1 b_2 - \lambda_2(\alpha_2 a_2 + \alpha_1 b_4 - \alpha_2 b_3) \\ &\quad - \lambda_3(\alpha_2 a_1 + \alpha_1 b_2 - \alpha_2 b_1 + \alpha_1 b_4 - \alpha_2 b_3) \\ &\quad - 2\lambda_4 \alpha_1 \alpha_2 - \lambda_5 \alpha_2 + \omega \sigma_1(2\alpha_1 b_1 \\ &\quad + 2\alpha_2 b_2 - b_3 + a_2) + \omega \sigma_2(\alpha_1^2 + 3\alpha_2^2) \\ &\quad - D_1 k^2(4(\alpha_1 b_2 - \alpha_2 b_1) + b_4) - 2D_2 k^2 \alpha_1 \alpha_2 \\ &\quad + D_3 k^2(4b_4 - \alpha_1 b_2 + \alpha_2 b_1 - a_1 \alpha_2) + 2D_4 k^2 \alpha_1 \alpha_2 \\ &\quad + D_5 k^2(-b_1 \alpha_2 + b_2 \alpha_1 + b_4) + 2D_6 k^2 \alpha_1 \alpha_2 \\ &\quad - D_8 k^2 \omega(8\alpha_1 b_1 - 8\alpha_2 b_2 - \alpha_1 + a_2) \\ &\quad \left. + D_{10} k^4(16(b_2 \alpha_1 - b_1 \alpha_2) + a_2) \right), \end{aligned} \quad (22)$$

References

- Achu, G.F., Kakmeni, F.M.M., Dikande, A.M., 2018. Breathing pulses in the damped-soliton model for nerves. *Phys. Rev. E* 97, 012211.
- Allen, L.H., Aderem, A., 1995. A role for MARCKS, the alpha isozyme of protein kinase C and myosin I in zymosan phagocytosis by macrophages. *J. Exp. Med.* 182, 829–840.
- Alonso, S., Dietrich, U., Händel, C., Käs, J.A., Bär, M., 2011. Oscillations in the lateral pressure of lipid monolayers induced by nonlinear chemical dynamics of the second messengers MARCKS and protein kinase C. *Biophys. J.* 100, 939–947.
- Alonso, S., Markus, B., 2010. Phase separation and bistability in a three-dimensional model for protein domain formation at biomembranes. *Phys. Biol.* 7, 046012.
- Aronson, I.S., Kramer, L., 2002. The world of the complex Ginzburg–Landau equation. *Rev. Modern Phys.* 74, 99–143.
- Arbuzova, A., Wang, J., Murray, D., Jacob, J., Cafiso, D.S., McLaughlin, S., 1997. Kinetics of interaction of the myristoylated alanine-rich C kinase substrate, membranes, and calmodulin. *J. Biol. Chem.* 272, 27167–27177.
- Blackshear, P.J., 1992. The MARCKS family of cellular protein kinase C substrates. *J. Biol. Chem.* 268, 1501–1504.
- Blackshear, P.J., Verghese, G.M., Johnson, J.D., Haupt, D.M., Stumpo, D.J., 1992. Characteristics of the F52 protein, a MARCKS homologue. *J. Biol. Chem.* 267, 13540–13546.
- Brizhik, L.S., 1993. Bisoliton mechanism of electron transport in biological systems. *J. Biol. Phys.* 19, 123–131.
- Brizhik, L.S., Eremko, A.A., 1999. Role of bisolitons and their correlations in charge transfer processes. *J. Biol. Phys.* 24, 233–244.

- Brizhik, L., Scordino, A., Triglia, A., Musumeci, F., 2001. Delayed luminescence of biological systems arising from correlated many-soliton states. *Phys. Rev. E* 64, 031902.
- Cross, M.C., Hohenberg, P.C., 1993. Pattern formation outside of equilibrium. *Rev. Modern Phys.* 65, 851.
- Damera, G., Jester, W.F., Jiang, M., et al., 2010. Inhibition of myristoylated alanine-rich C kinase substrate (MARCKS) protein inhibits ozone-induced airway neutrophilia and inflammation. *Exp. Lung. Res.* 36, 75–84.
- Davydov, A.S., 1988. Bisoliton mechanism of high-temperature superconductivity. *Phys. Status Solidi. B* 146, 619–641.
- Davydov, A.S., Kislukha, N.I., 1973. Solitary excitons in one-dimensional molecular chains. *Phys. Status Solidi. B* 59, 465–470.
- Dietrich, U., Krüger, P., Gutberlet, T., Käs, J.A., 2009. Interaction of the MARCKS peptide with PIP2 in phospholipid monolayers. *Biochim. Biophys. Acta* 557, 1474–1481.
- Elzagallaai, A., Rosé, S.D., Brandan, N.C., Trifaró, J.M., 2001. Myristoylated alanine-rich C kinase substrate phosphorylation is involved in thrombin-induced serotonin release from platelets. *Br. J. Haematol.* 112, 593–602.
- Eremko, A.A., 1992. Peierls-Frohlich problem in the continuum approximation. *Phys. Rev. B* 46, 3721–3728.
- Etémé, A.S., 2023. Consistency between modulational instability and energy localization in time-delay-memristive neural network. *Europhys. Lett.* 143, 42002–42008.
- Etémé, A.S., Tabi, C.B., Mohamadou, A., 2017. Synchronized nonlinear patterns in electrically coupled Hindmarsh-Rose neural networks with long-range diffusive interactions. *Chaos Solitons Fractals* 104, 813–826.
- Glaser, M., Wanaski, S., Buser, C.A., et al., 1996. Myristoylated alanine-rich C kinase substrate (MARCKS) produces reversible inhibition of phospholipase C by sequestering phosphatidylinositol 4 5-bisphosphate in lateral domains. *J. Biol. Chem.* 271, 26187–26193.
- Issa, S., Tabi, C.B., Ekobena Fouda, H.P., Kofané, T.C., 2016. Modulational instability in a biexciton molecular chain with saturable nonlinearity effects. *Internat. J. Modern Phys. B* 30, 1550244.
- Ito, S., Okuda-Ashitak, E., Minami, T., 2001. Central and peripheral roles of prostaglandins in pain and their interactions with novel neuropeptides nociceptin and nocistatin. *Neurosci. Res.* 41, 299–332.
- Karen, M.P., Philip, K.M., Nicholas, A.M.M., 2005. Complex pattern formation in reaction–diffusion systems with spatially varying parameters. *Phys. D: Nonlinear Phenom* 202, 95–115.
- Katoh, H., Aoki, J., Ichikawa, A., Negishi, M., 1998. p160 RhoA-binding kinase ROKalpha induces neurite retraction. *J. Biol. Chem.* 273, 2489–2492.
- Kozma, R., Sarner, S., Ahmed, S., Lim, L., 1997. Rho family GTPases and neuronal growth cone remodelling: relationship between increased complexity induced by Cdc42Hs, Rac1, and acetylcholine and collapse induced by RhoA and lysophosphatidic acid. *Mol. Cell. Biol.* 17, 1201–1211.
- Kuramoto, Y., 1984. Chemical oscillations, waves and turbulence. In: *Springer Series in Synergetics*. vol. 19, pp. 1–4.
- Legoya, P.G., Etémé, A.S., Tabi, C.B., Mohamadou, A., Kofané, T.C., 2022. Frequency modes of unstable spiral waves in two-dimensional Rosenzweig-MacArthur ecological networks interactions. *Chaos Solitons Fractals* 164, 112599–112610.
- Li, J., D'Annibale-Tollhurst, M.A., Adler, K.B., et al., 2013. A myristoylated alanine-rich C kinase substrate-related peptide suppresses cytokine mRNA and protein expression in LPS-activated canine neutrophils. *Am. J. Respir. Cell Mol. Biol.* 48, 314–321.
- McLaughlin, S., 1989. The electrostatic properties of membranes. *Annu. Rev. Biophys. Chem.* 18, 113–136.
- Meller, S.T., Gebhart, G.F., 1993. Nitric oxide (NO) and nociceptive processing in the spinal cord. *Pain* 52, 127–136.
- Mogami, H., Zhang, H., Suzuki, Y., et al., 2003. Decoding of short-lived Ca^{2+} influx signals into long term substrate phosphorylation through activation of two distinct classes of protein kinase C. *J. Biol. Chem.* 278, 9896–9904.
- Muratani, T., Minami, T., Enomoto, U., Sakai, M., Okuda-Ashitaka, E., Kiyokane, K., Mori, H., Ito, S., 2002. Characterization of nociceptin/orphanin FQ-induced pain responses by the novel receptor antagonist N-(4-amino-2-methylquinolin-6-yl)-2-(4-ethylphenoxy)methyl benzamide monohydrochloride. *J. Pharmacol. Exp. Ther.* 303, 424–430.
- Mvogo, A., Takembo, C.N., Ekobena Fouda, H.P., Kofané, T.C., 2017. Pattern formation in diffusive excitable systems under magnetic flow effects. *Phys. Lett. A* 381, 2264–2271.
- Nagumo, H., Ikenoya, M., Sakurada, K., Furuya, K., Ikuhara, T., Hiraoka, H., Sasaki, Y., 2001. Rho-associated kinase phosphorylates MARCKS in human neuronal cells. *Biochem. Biophys. Res. Commun.* 280, 605–609.
- Newton, A.C., 2001. Protein kinase C: structural and spatial regulation by phosphorylation, cofactors, and macromolecular interactions. *Chem. Rev.* 101, 2353–2364.
- Ohmori, S., Sakai, N., Shirai, Y., Yamamoto, H., Miyamoto, E., Shimizu, N., Saito, N., 2000. Importance of protein kinase C targeting for the phosphorylation of its substrate, myristoylated alanine-rich C-kinase substrate. *J. Biol. Chem.* 275, 26449–26457.
- Rebecchi, M., Boguslavsky, V., Boguslavsky, L., McLaughlin, S., 1992. Phosphoinositide-specific phospholipase C-delta 1: effect of monolayer surface pressure and electrostatic surface potentials on activity. *Biochemistry* 31, 12748–12753.
- Robinson, P.J., 1991. The role of protein kinase C and its neuronal substrates dephosphin, B-50, and MARCKS in neurotransmitter release. *Mol. Neurobiol.* 5, 87–130.
- Rusu, L., Gambhir, A., McLaughlin, S., Rädler, J., 2004. Fluorescence correlation spectroscopy studies of peptide and protein binding to phospholipid vesicles. *Biophys. J.* 87, 1044–1053.
- Sasaki, Y., 2003. New aspects of neurotransmitter release and exocytosis: Rho-kinase-dependent myristoylated alanine-rich C-kinase substrate phosphorylation and regulation of neurofilament structure in neuronal cells. *J. Pharmacol. Sci.* 93, 35–40.
- Sawano, A., Hama, H., Saito, N., Miyawaki, A., 2022. Multicolor imaging of Ca^{2+} and protein kinase C signals using novel epifluorescence microscopy. *Biophys. J.* 82, 1076–1085.
- Scott, A., 1992. Davydov's soliton. *Phys. Rep.* 217, 1–67.
- Sheats, M.K., Sung, E.J., Adler, K.B., Jones, S.L., 2015. In vitro neutrophil migration requires protein kinase C-delta (δ -PKC)-mediated myristoylated alanine-rich C-kinase substrate (MARCKS) phosphorylation. *Inflammation* 38, 1126–1141.
- Simo, E., Kofané, T.C., 1997. Influence of the fluctuations of polarization in molecular chains. *Phys. Rev. E* 56, 4751–4756.
- Tabi, C.B., Etémé, A.S., Kofané, T.C., 2020. Unstable cardiac multi-spiral waves in a FitzHugh–Nagumo soliton model under magnetic flow effect. *Nonlinear Dyn.* 100, 3799–3814.
- Tabi, C.B., Etémé, A.S., Mohamadou, A., 2017. Frequency mode excitations in two-dimensional Hindmarsh-Rose neural networks. *Phys. A: Stat. Mech. Appl.* 474, 186–198.
- Tabi, C.B., Etémé, A.S., Mohamadou, A., T.C., Kofané, 2021. Oscillating two-dimensional Ca^{2+} waves in cell networks with bidirectional paracrine signaling. *Waves Random Complex Media* 31, 1028–1049.
- Tabi, C.B., Mohamadou, A., Kofané, T.C., 2008. Soliton excitation in the DNA double helix. *Phys. Scr.* 77, 045002.
- Takashi, S., Park, J., Fang, S., Koyama, S., Parikh, I., Adler, K.B., 2006. A peptide against the N-terminus of myristoylated alanine-rich C kinase substrate inhibits degranulation of human leukocytes in vitro. *Am. J. Respir. Cell Mol. Biol.* 34, 647–652.
- Takembo, C.N., 2022. Information pattern stability in memristive Izhikevich neural networks. *Modern Phys. Lett. B* 36, 2250006.
- Takembo, C.N., Ekobena Fouda, H.P., 2020. Effect of temperature fluctuation on the localized pattern of action potential in cardiac tissue. *Sci. Rep.* 10, 15087.
- Takembo C.N, P., Ekobena Fouda, H.P., Kofané, T.C., 2022. Modulated wave pattern stability in chain neural networks under high-low frequency magnetic radiation. *Phys. A: Stat. Mech. Appl.* 593, 126891.
- Uchino, M., Sakai, N., Kashiwagi, K., et al., 2004. Isoform-specific phosphorylation of metabotropic glutamate receptor 5 by protein kinase C (PKC) blocks Ca^{2+} oscillation and oscillatory translocation of Ca^{2+} -dependent PKC. *J. Biol. Chem.* 279, 2254–2261.
- Vergheze, G.M., Johnson, J.D., Vasulka, C., Haupt, D.M., Stumpo, D.J., Blackshear, P.J., 1994. Protein kinase C-mediated phosphorylation and calmodulin binding of recombinant myristoylated alanine-rich C kinase substrate (MARCKS) and MARCKS-related protein. *J. Biol. Chem.* 269, 9361–9367.
- Vladimir, G.-M., Katharina, K., 2012. The complex Ginzburg–Landau equation: an introduction. *Contemp. Phys.* 53, 79–95.
- Wang, J., Arbuzova, A., Hangyás-Mihályné, G., McLaughlin, S., 2021. The effector domain of myristoylated alanine-rich C kinase substrate binds strongly to phosphatidylinositol 4 5-bisphosphate. *J. Biol. Chem.* 276, 5012–5019.
- Wang, J., Gambhir, A., Mihalyne, G., Murray, D., Golebiewska, U., McLaughlin, S., 2022. Lateral sequestration of phosphatidylinositol 4 5-bisphosphate by the basic effector domain of Myristoylated alanine-rich C kinase substrate is due to non specific electrostatic interactions. *J. Biol. Chem.* 277, 34401–34412.
- Yomba, E., Kofané, T.C., Pelap, F.B., 1996. On exact solutions of the generalized modifies Ginzburg-landau Equation using Hirota's method. *J. Phys. Soc. Japan* 65, 2337–2338.
- Zaoro, N.R., Tabi, C.B., Etémé, A.S., Kofané, T.C., 2020. Unstable cAMP wave patterns during aggregation of Dictyostelium discoideum cells. *Phys. Lett. A* 384, 126133–126141.